UAB
Universitat Autònoma de Barcelona

Renormalization of Effective Field Theories with on-shell amplitude methods

Clara Fernández Castañer

Renormalization of Effective Field Theories with on-shell amplitude methods

A thesis submitted for the degree of Doctor in Physics by

Clara Fernández Castañer

Supervisor: Prof. Àlex Pomarol Clotet

July 2025

Abstract

This thesis explores the use of on-shell amplitude methods in the context of Effective Field Theories (EFTs), focusing on their application to renormalization. We begin by reviewing the construction of tree-level on-shell amplitudes from general principles, considering Lorentz invariance, locality, and dimensional analysis. These techniques are then applied to construct the amplitude structures of the Standard Model (SM) and the Standard Model Effective Field Theory (SMEFT). In the SMEFT, we include contact interactions at orders $1/\Lambda$ and $1/\Lambda^2$, which correspond to operators of mass dimension five and six, respectively. After that, we explore loop amplitudes via the generalized unitarity method. We show how on-shell methods can be used to extract the anomalous dimensions for the renormalization group mixing of higher-dimension operators. In particular, we obtain a formula for the anomalous dimensions at leading order, written as a product of tree-level amplitudes integrated over some phase-space. This simplifies the calculations by avoiding explicit loop computations. We apply this result to 1-loop and 2-loop anomalous dimensions for various SMEFT operators, including those relevant to dipole transitions and lepton flavor violating processes. Finally, we revisit the renormalization of EFTs by considering the angular momentum decomposition of amplitudes. In this way, we obtain a formula for the anomalous dimensions as a sum over products of partial-wave coefficients. Our results demonstrate the power of on-shell methods in simplifying renormalization and provide novel tools for precision phenomenology in searches for physics beyond the Standard Model.

Contents

Publications

The main ideas presented in this thesis have previously appeared in the following publications:

[1] Baratella, P., Fernandez, C., Pomarol, A. (2020). *Renormalization of higher-dimensional operators from on-shell amplitudes. Nuclear Physics B, 959*, 115155. arXiv:2005.07129 [hep-ph].

[2] Baratella, P., Fernandez, C., von Harling, B., Pomarol, A. (2021). *Anomalous dimensions of effective theories from partial waves. Journal of High Energy Physics, 2021*(3), 287. arXiv:2010.13809 [hep-ph].

[3] Elias Miro, J., Fernandez, C., Gümüş, M. A., Pomarol, A. (2022). *Gearing up for the next generation of LFV experiments, via on-shell methods. Journal of High Energy Physics, 2022*(6), 126. arXiv:2112.12131 [hep-ph].

Introduction

Scattering amplitudes play a central role in particle physics, quantifying the probabilities of specific outcomes in particle interactions. They are essential for understanding the dynamics of fundamental forces and for linking theoretical models to experimental observations. Among the modern approaches to scattering amplitudes, on-shell methods stand out as a powerful framework. Rather than relying on the traditional Lagrangian-based formulation, these techniques use basic amplitude properties to avoid some of its inherent complexities and redundancies.

This thesis explores applications of on-shell amplitude methods in Effective Field Theories (EFTs) and their renormalization. The motivation for our research is both phenomenological and theoretical. On one hand, searches for new physics Beyond the Standard Model (BSM) require precise calculations to match the experimental data, which can be performed using on-shell techniques. On the other hand, these methods may also reveal novel insights into the mathematical structure of scattering amplitudes, deepening our understanding of Quantum Field Theory (QFT).

On-shell amplitude methods

The study of scattering amplitudes has been developed since the early days of QFT. Formally, the S-matrix was introduced to describe the dynamics of fundamental particles. The transition probability from an initial multi-particle state $|i\rangle$ to a final state $|f\rangle$ is given by the matrix element

$$S_{fi} = \langle f|\hat{S}|i\rangle \ , \tag{1}$$

with $\hat{S}$ the S-matrix operator [4]. We define $\hat{S} = \mathbb{1} + i\hat{T}$, where $\mathbb{1}$ is the identity and $\hat{T}$ is the transition matrix. We can also write

$$S_{fi} = \delta_{fi} + i(2\pi)^4\delta^{(4)}(p_f - p_i)\mathcal{M}_{fi} \ , \tag{2}$$

where $\delta^{(4)}(p_f - p_i)$ ensures energy-momentum conservation and $\mathcal{M}_{fi}$ is the transition amplitude. Within perturbation theory, the S-matrix can be expressed as an expansion in terms of the interaction Lagrangian $\mathcal{L}_{\text{int}}$, according to

$$\hat{S} = \mathcal{T}\exp\left(-i\int d^4x\mathcal{L}_{\text{int}}(x)\right) \ , \tag{3}$$

with $\mathcal{T}$ the time-ordering operator. The scattering amplitude $\mathcal{M}_{fi}$ can be computed perturbatively using this expression. The usual prescription is to draw Feynman diagrams to visually

represent the different terms in the S-matrix expansion. Each diagram can be systematically translated into a mathematical expression by using the so-called Feynman rules. This approach is typically taught in introductory QFT courses, but it is mostly inconvenient for processes involving many particles or higher loop orders. For example, one can check [5] that the 4-gluon tree-level amplitude involves 4 Feynman diagrams, whereas the 6-gluon one already involves 220 diagrams. The scaling is such that the 10-gluon amplitude includes more than a million diagrams, making it computationally unwieldy.

The shortcomings of the Feynman perturbative method led to other approaches to the study of amplitudes. In the early 60s, the S-matrix bootstrap was first proposed as a way to use basic principles such as locality, causality and Lorentz invariance in order to derive amplitudes directly, without referencing a Lagrangian. This program was born with the goal to describe strong interactions and thus it was eventually overshadowed by the success of quantum chromodynamics (QCD) in the 70s. The bootstrap program has regained interest in recent years, using it to constrain and solve for scattering amplitudes in a variety of theories [6, 7]. As a simple example, see the bootstrapping of 3-point tree-level amplitudes in Section 1.1 of this dissertation. For more details on amplitude bootstrap, see [8].

A significant step forward in the study of scattering amplitudes was the development of the Parke-Taylor formula in the 80s [9]. As we have mentioned earlier, the scattering of n gluons generally involves a large number of Feynman diagrams. It turns out that, for on-shell gluons of definite helicity, the maximally helicity-violating (MHV) amplitude can be written in a surprisingly compact form. The all-incoming amplitude for two gluons of helicity $-$ and $n-2$ gluons of helicity $+$ is given by

$$A_n(1^-, 2^-, 3^+, \ldots, n^+) = i\,\frac{\langle 12\rangle^4}{\langle 12\rangle\,\langle 23\rangle\cdots\langle n1\rangle}\ , \tag{4}$$

where the angle and square brackets are functions of the gluon momenta defined in Appendix A. This formula reveals how the enormous complexity of Feynman diagrams gets simplified for the case of physical on-shell amplitudes. It suggests the existence of hidden structures in gauge theories, which are obscured in the off-shell Feynman diagram approach.

On-shell amplitude methods were further developed after the derivation of the Parke-Taylor formula. One of the most remarkable results came in the early 2000s with the BCFW recursion relations [10]. From the basic properties of analyticity and factorization, higher-point tree-level amplitudes can be expressed in terms of lower-point ones. This allows us to derive all n-point amplitudes of a theory from a few elementary building blocks. In Chapter 1 of this dissertation, we show how to construct 4-point amplitudes from 3-point ones. Another relevant cornerstone of on-shell amplitude methods is the treatment of loops with the generalized unitary method [11, 12]. This procedure relates loop amplitudes to tree-level ones, greatly simplifying loop calculations. See Chapter 3 for further details.

In recent years, on-shell amplitude methods have been applied in a variety of contexts, from QCD calculations to formal developments in theories like supergravity. The basics of modern amplitude methods and their most relevant applications are covered in reviews such as [13–16]. This dissertation focuses on the renormalization of EFTs, which plays an important role in the phenomenology of BSM physics.

The Standard Model Effective Field Theory

The Standard Model (SM) of particle physics is a QFT describing the electromagnetic, weak, and strong interactions of elementary particles. It constitutes the main cornerstone of particle physics and its predictions have been tested with extraordinary precision by a wide range of experiments, such as the Large Hadron Collider (LHC). Despite these successes, the SM fails to account for several important phenomena [17]: gravity, dark matter, dark energy, neutrino masses and the observed matter–antimatter asymmetry. These shortcomings have motivated the development of new theories for physics Beyond the Standard Model (BSM).

The SM can be understood as an Effective Field Theory (EFT), a low-energy approximation of a more general framework. EFTs allow us to describe physical phenomena in terms of the relevant degrees of freedom at low energies, without requiring a complete understanding of the underlying high-energy theory. The Standard Model Effective Field Theory (SMEFT) is particularly useful to describe deviations from the SM in a systematic, model-independent way [18]. The idea is to account for the effects of new particles, above the electroweak scale, through a series of non-renormalizable operators made of the SM fields. These operators are organized by increasing mass dimension and suppressed by powers of the high-energy scale or cut-off Λ. The SMEFT Lagrangian can be written as

$$\mathcal{L}_{\text{SMEFT}} = \mathcal{L}_{\text{SM}} + \frac{1}{\Lambda}\sum_{\mathcal{O}_5} C_{\mathcal{O}_5}\mathcal{O}_5 + \frac{1}{\Lambda^2}\sum_{\mathcal{O}_6} C_{\mathcal{O}_6}\mathcal{O}_6 + \dots \,, \tag{5}$$

where $\mathcal{L}_{\text{SM}}$ is the SM Lagrangian and $\mathcal{O}_n$ are non-renormalizable operators of mass dimension n for $n > 4$, also known as higher-dimension operators. The dimensionless coefficients $C_{\mathcal{O}_n}$ are the so-called Wilson coefficients.

The SMEFT is a valuable tool in searches for BSM physics, since higher-dimension operators can enter physical observables at low energies. By comparing the experimental measurements with theoretical predictions, we can derive bounds on different Wilson coefficients and the cut-off Λ. This is especially useful for observables that are suppressed in the SM, such as some lepton-flavor violating muon decays (see Chapter 5). In order to understand the various SMEFT operators contributing to a physical process, it is essential to consider the operator mixing induced by renormalization. At the loop level, Wilson coefficients run with the renormalization scale μ as follows,

$$\gamma_i \equiv \frac{d\, C_{\mathcal{O}_i}}{d \ln \mu} = \sum_j \gamma_{ij}\, C_{\mathcal{O}_j} \,, \tag{6}$$

where γ_{ij} is the so-called anomalous dimension matrix, which contains information on the mixing of operators of the same mass dimension. Computing γ_{ij} is a critical step in deriving robust bounds on the SMEFT parameter space.

In the early 2010s, the full 1-loop anomalous dimension matrix of dimension-six operators in the SMEFT was computed using traditional Feynman diagram techniques, see [19–25]. More recently, there have been several efforts to apply on-shell amplitude methods to determine anomalous dimensions in general EFTs, including [26–32]. This dissertation encompasses several contributions made in that direction.

This thesis is structured as follows:

- Chapter 1 explains how to build on-shell tree-level amplitudes from first principles and factorization, focusing on 3-point and 4-point amplitudes.
- Chapter 2 provides a review of the Standard Model and the Standard Model Effective Field Theory. It also lists the tree-level on-shell amplitudes associated with the SM interactions and SMEFT interactions at orders $1/\Lambda$ and $1/\Lambda^2$, which correspond to dimension-five and dimension-six operators.
- Chapter 3 introduces loop amplitudes and the effects of renormalization. We show how on-shell amplitude methods can be used to obtain the anomalous dimension matrix from a product of tree-level amplitudes integrated over a phase-space, without the need to consider loop integrals explicitly.
- Chapters 4, 5 and 6 present some applications of the main formula derived in Chapter 3. In Chapter 4, we explicitly compute the 1-loop anomalous dimension for the dimension-6 SMEFT dipole operator. In Chapter 5, we show examples of the calculation of 2-loop anomalous dimensions in the context of lepton flavor violating processes. We consider the experimental constraints on several observables and derive bounds on the energy scale of New Physics Λ. In Chapter 6, we consider the angular momentum decomposition of on-shell amplitudes and derive an expression for the anomalous dimensions in terms of products of partial wave coefficients.

Chapter 1

Building on-shell amplitudes

In this chapter we present the basics of constructing tree-level on-shell amplitudes. We show how these amplitudes can be directly derived from first principles, without defining a Lagrangian. Similar derivations can be found in on-shell amplitude reviews, such as [13–16, 33]. We use the following properties:

- Locality. Tree-level amplitudes are rational functions of the external momenta, with simple pole singularities corresponding to propagators of intermediate states. Amplitudes must have proper factorization properties, as we discuss in Section 1.3.
- Dimensional analysis. From [14], the mass dimension of an amplitude $\mathcal{A}_n$ obeys

$$[\mathcal{A}_n] = 4 - n \ , \tag{1.1}$$

  with n the number of scattered particles. Any amplitude can be written as a coupling constant C times some kinematic function. Once we establish the kinematic structure, Eq. (1.1) can be used to determine the mass dimensions of the coupling constant.
- Lorentz symmetry. Amplitudes must be invariant under Lorentz transformations. They must also be covariant under the little group, which is the subgroup of the Lorentz group that leaves a given momentum invariant. We refer to Section 1.2 for the details.

In Section 1.1 we construct 3-point on-shell amplitudes for the scattering of particles with spin-0, -1 and -2. In Section 1.2 we derive the general formula for the scattering of particles with any helicity using spinor-helicity variables. In Section 1.3 we explain how to construct 4-point (and higher-point) amplitudes and the role of factorization. We summarize our main results in Section 1.4.

1.1 3-point amplitudes: some examples

First, we present a simple yet enlightening derivation of some bosonic 3-point amplitudes. Our derivation is mostly based on the 2023 TASI Lectures on Scattering Amplitudes by C. Cheung that can be watched in [34]. A given 3-point amplitude $\mathcal{A}_3$ is fully determined by imposing locality, Lorentz invariance and dimensional analysis. The on-shell kinematics for massless particles imply that

$$p_1 + p_2 + p_3 = 0 \ , \ p_1^2 = p_2^2 = p_3^2 = 0 \quad \Longrightarrow \quad p_i p_j = 0 \ , \text{for } i,j = 1,2,3 \ . \tag{1.2}$$

Using Eq. (1.1), the amplitude must have dimension $[\mathcal{A}_3] = 1$. In general, we can write

$$\mathcal{A}_3 = C_d \times \text{ kinematic function} \ , \tag{1.3}$$

with C_d a coupling constant of mass dimension d. We remain agnostic about the mass dimensions of this constant, as long as the kinematic factor does not have negative powers of momenta. This is because 3-point amplitudes cannot have simple poles coming from propagators.

We must also take into account that, in general, scattering amplitudes are multilinear in the polarizations of the different particles [35]

$$\mathcal{A}(1^{h_1}, ..., n^{h_n}) = e^{h_1}_{\mu_1} ... e^{h_n}_{\mu_n} \mathcal{A}^{\mu_1 \cdots \mu_n} \ , \tag{1.4}$$

where the form of the polarization $e^{h_1}_{\mu_1}$ depends on the particle spin. Spin-0 particles have no polarization, spin-1 particles have polarization vectors, and spin-2 particles have polarization tensors.

1.1.1 3 scalars

We begin by considering the scattering of three identical scalar particles ϕ. In this case it turns out there is only one possible 3-point amplitude

$$\mathcal{A}(1_\phi, 2_\phi, 3_\phi) = C_{d=1} \ , \tag{1.5}$$

with $[C_{d=1}] = 1$. One would naively expect to have other amplitudes with higher powers of momenta in the kinematic function. However, the only option for scalars is to have even powers of momenta contracted among themselves ($p_i p_j$), which vanish due to Eq. (1.2).

The generalization to the case of scalars carrying flavor ϕ^a is straightforward,

$$\mathcal{A}(1_{\phi^a}, 2_{\phi^b}, 3_{\phi^c}) = C_{d=1} \delta_{abc} \ , \tag{1.6}$$

where δ_{abc} is a totally symmetric flavor tensor.

We can revisit the Lagrangian formulation to gain a deeper understanding of this result. The amplitudes in Eqs. (1.5, 1.6) arise from the following interaction Lagrangians,

$$\mathcal{L} \supset C_{d=1} \phi^3 \ , \qquad \mathcal{L} \supset C_{d=1} \delta_{abc} \ \phi^a \phi^b \phi^c \ . \tag{1.7}$$

We can write additional 3-scalar interaction terms with derivatives, such as $(\partial\phi)^2\phi$. However, now we know that all these terms do not contribute to the 3-point amplitude, since there are no valid amplitudes with higher powers of momenta. Indeed, at the level of the action, one can apply integration by parts to the derivative interactions and eliminate them by using field redefinitions of ϕ [33].

1.1.2 3 vector bosons

We now consider the scattering of three identical spin-1 particles. The 3-vector scattering amplitude is constructed from Lorentz-invariant products of the particle momenta $p_1^\mu, p_2^\mu, p_3^\mu$ and the polarization vectors $e_1^\mu, e_2^\mu, e_3^\mu$. From Eq. (1.2), the 3-particle on-shell kinematics enforce the conditions $p_i^2 = 0$ and $p_i p_j = 0$. Moreover, the fact that longitudinal polarizations are not physical implies that $p_i e_i = 0$ as well. Thus, one can prove there are only six independent vector products:

$$\{e_1e_2,\ e_2e_3,\ e_3e_1,\ p_1e_2,\ p_1e_3,\ p_2e_1\}\ . \tag{1.8}$$

We want to build amplitudes made of these vector products and having the proper powers of polarization vectors. For only one power of momenta, we obtain:

$$O(p^1): \qquad \mathcal{A}(1_V, 2_V, 3_V) = C_1(e_1e_3)(p_1e_2) + C_2(e_1e_2)(p_1e_3) + C_3(e_2e_3)(p_2e_1)\ , \tag{1.9}$$

where C_i are coupling constants. Two of the C_i can be eliminated by using the Ward-Takahashi identity [36, 37], which states that the amplitude vanishes if we replace any polarization vector e_i^μ by its corresponding momenta p_i^μ. In particular,

$$\begin{aligned} 0 &= \mathcal{A}(1_V, 2_V, 3_V)|_{e_1\to p_1} = (C_1 + C_2)(p_1e_2)(p_1e_3)\ , \\ 0 &= \mathcal{A}(1_V, 2_V, 3_V)|_{e_2\to p_2} = (C_2 - C_3)(p_2e_1)(p_1e_3)\ , \\ 0 &= \mathcal{A}(1_V, 2_V, 3_V)|_{e_3\to p_3} = (C_1 + C_3)(p_3e_1)(p_1e_2)\ , \end{aligned} \tag{1.10}$$

so we conclude that $C_1 = -C_2 = -C_3$. This fixes the amplitude up to an overall constant,

$$\mathcal{A}(1_V, 2_V, 3_V) = C_1\left[(e_1e_3)(p_1e_2) - (e_1e_2)(p_1e_3) - (e_2e_3)(p_2e_1)\right]\ . \tag{1.11}$$

One can check that this amplitude is antisymmetric under the exchange of any two vector bosons since, for example, $p_1e_2 = -p_3e_2$. It is convenient to make this antisymmetry explicit in the following way,

$$\mathcal{A}(1_V, 2_V, 3_V) = -\frac{C_1}{2}\left[e_1e_2(p_1e_3 - p_2e_3) + e_2e_3(p_2e_1 - p_3e_1) + e_3e_1(p_3e_2 - p_1e_2)\right]\ . \tag{1.12}$$

The antisymmetry of the amplitude poses a problem, as amplitudes must be symmetric under the exchange of identical vector bosons. This means that, by Bose-Einstein symmetry, we must fix the coupling constant C_1 to zero. Indeed, this is not a surprising result, since the 3-photon amplitude vanishes in QED by Furry's theorem [38]. For non-identical vector bosons carrying flavor, we can write a valid amplitude

$$\mathcal{A}(1_{V^a}, 2_{V^b}, 3_{V^c}) = C_{d=0} f_{abc}\left[e_1e_2(p_1e_3 - p_2e_3) + e_2e_3(p_2e_1 - p_3e_1) + e_3e_1(p_3e_2 - p_1e_2)\right]\ , \tag{1.13}$$

with f_{abc} a totally antisymmetric constant.

Up until now we have discussed 3-vector amplitudes with one power of momenta. The next possibility is having three powers of momenta,

$$O(p^3): \qquad \mathcal{A}(1_{V^a}, 2_{V^b}, 3_{V^c}) = C_{d=-2} f_{abc}(p_1e_2)(p_2e_3)(p_3e_1)\ . \tag{1.14}$$

In this case the kinematic factor is again antisymmetric under the exchange of vector bosons, so the amplitude is only valid for non-identical particles.

We could try to build amplitudes with, for example, five powers of momenta. However, since there are only three polarization vectors, we would have to include products of the momenta $p_i p_j$, which vanish by Eq. (1.2). We conclude that there are no allowed amplitudes for higher powers of momenta.

Let us connect these results for the 3-vector scattering amplitude with the Lagrangian formulation. The amplitude of $O(p^1)$ in Eq. (1.13) corresponds to a non-abelian gauge theory such as QCD, with an interaction term given by

$$\mathcal{L} \supset C_{d=0} f_{abc} (\partial^\mu G^{a,\nu} - \partial^\nu G^{a,\mu}) G^b_\mu G^c_\nu \ , \tag{1.15}$$

where $C_{d=0}$ is the gauge coupling, G^a_μ is the gauge field and f_{abc} is the structure constant of the Lie algebra. It is remarkable how we have derived the presence of the structure constant without using the notion of Lie groups.

Regarding the amplitude of $O(p^3)$ in Eq. (1.14), it corresponds to the following higher-dimension operator in a non-renormalizable theory

$$\mathcal{L} \supset C_{d=-2} f_{abc} \ \partial^\mu G^a_\nu \partial^\nu G^b_\rho \partial^\rho G^c_\mu \ . \tag{1.16}$$

There are no amplitudes with higher powers of momenta, which would come from operators with more derivatives. This is because such operators are proportional to $\partial^2 G$ and can be eliminated using the equations of motion for G^a_μ.

1.1.3 3 spin-2 particles

Next, we consider the scattering of three particles of spin-2. In this case, the amplitude must be proportional to the polarization tensor $e_i^{\mu\nu}$ of each particle. The polarization tensor can be expressed as a product of two polarization vectors $e_i^{\mu\nu} = e_i^\mu e_i^\nu$. Then we can construct all possible amplitudes using the vector products in Eq. (1.8). At the lowest order in momenta,

$$\begin{aligned} O(p^2): \qquad \mathcal{A}(1_T, 2_T, 3_T) = {} & C_1 (e_1 e_2)^2 (p_1 e_3)^2 + C_2 (e_2 e_3)^2 (p_2 e_1)^2 + C_3 (e_3 e_1)^2 (p_1 e_2)^2 \\ & + C_4 (e_1 e_2)(e_2 e_3)(p_1 e_3)(p_2 e_1) + C_5 (e_1 e_2)(e_3 e_1)(p_1 e_2)(p_1 e_3) \\ & + C_6 (e_2 e_3)(e_3 e_1)(p_1 e_2)(p_2 e_1) \ , \end{aligned} \tag{1.17}$$

where the C_i coefficients are determined using the Ward-Takahashi identity. We impose that the amplitude vanishes when we replace $e_i^\mu e_i^\nu \to \frac{1}{2}(p_i^\mu e_i^\nu + e_i^\mu p_i^\nu)$. This leads to

$$\begin{aligned} 0 = \mathcal{A}(1_T, 2_T, 3_T)|_{e_1 \to p_1} = {} & (p_1 e_2)(p_1 e_3) \left[(C_1 + \tfrac{C_5}{2})(e_1 e_2)(p_1 e_3) + (C_3 + \tfrac{C_5}{2})(e_3 e_1)(p_1 e_2) \right. \\ & \left. + (\tfrac{C_4}{2} + \tfrac{C_6}{2})(e_2 e_3)(p_2 e_1) \right] \ , \\ 0 = \mathcal{A}(1_T, 2_T, 3_T)|_{e_2 \to p_2} = {} & (p_2 e_1)(p_1 e_3) \left[(C_1 - \tfrac{C_4}{2})(e_1 e_2)(p_1 e_3) + (\tfrac{C_4}{2} - C_2)(e_2 e_3)(p_2 e_1) \right. \\ & \left. + (\tfrac{C_5}{2} - \tfrac{C_6}{2})(e_3 e_1)(p_1 e_2) \right] \ , \\ 0 = \mathcal{A}(1_T, 2_T, 3_T)|_{e_3 \to p_3} = {} & (p_3 e_2)(p_2 e_1) \left[(C_2 + \tfrac{C_6}{2})(e_2 e_3)(p_2 e_1) + (C_3 + \tfrac{C_6}{2})(e_3 e_1)(p_1 e_2) \right. \\ & \left. + (\tfrac{C_4}{2} + \tfrac{C_5}{2})(e_1 e_2)(p_1 e_3) \right] \ , \end{aligned} \tag{1.18}$$

so the coefficients obey $C_1 = C_2 = C_3 = C_4/2 = -C_5/2 = -C_6/2$. The amplitude can be written in a compact form,

$$\mathcal{A}(1_T, 2_T, 3_T) = C_{d=-1}\left[e_1e_2(p_1e_3 - p_2e_3) + e_2e_3(p_2e_1 - p_3e_1) + e_3e_1(p_3e_2 - p_1e_2)\right]^2 \ . \tag{1.19}$$

For amplitudes involving four powers of momenta, we have

$$\begin{aligned} O(p^4): \qquad \mathcal{A}(1_T, 2_T, 3_T) = {} & C_1(e_3e_1)(p_1e_3)(p_2e_1)(p_1e_2)^2 + C_2(e_1e_2)(p_2e_1)(p_1e_2)(p_1e_3)^2 \\ & + C_3(e_2e_3)(p_1e_3)(p_1e_2)(p_2e_1)^2 \ . \end{aligned} \tag{1.20}$$

Once more, the constants are determined by imposing the Ward-Takahashi identity,

$$\begin{aligned} 0 = \mathcal{A}(1_T, 2_T, 3_T)|_{e_1\to p_1} &= \tfrac{1}{2}(C_1 + C_2)(p_1e_2)^2(p_1e_3)^2(p_2e_1) \ , \\ 0 = \mathcal{A}(1_T, 2_T, 3_T)|_{e_2\to p_2} &= \tfrac{1}{2}(C_2 - C_3)(p_2e_1)^2(p_1e_3)^2(p_1e_2) \ , \\ 0 = \mathcal{A}(1_T, 2_T, 3_T)|_{e_3\to p_3} &= -\tfrac{1}{2}(C_1 + C_3)(p_1e_2)^2(p_2e_1)^2(p_1e_3) \ . \end{aligned} \tag{1.21}$$

The coefficients are related by $C_1 = -C_2 = -C_3$, so we obtain

$$\begin{aligned} \mathcal{A}(1_T, 2_T, 3_T) = C_{d=-3}(p_1e_3)(p_2e_1)(p_1e_2)\left[(e_1e_2)(p_1e_3 - p_2e_3) + (e_2e_3)(p_2e_1 - p_3e_1)\right. \\ \left. + (e_3e_1)(p_3e_2 - p_1e_2)\right] \ . \end{aligned} \tag{1.22}$$

Finally, the last amplitude we can write corresponds to six powers of momenta,

$$O(p^6): \qquad \mathcal{A}(1_T, 2_T, 3_T) = C_{d=-5}(p_1e_2)^2(p_2e_3)^2(p_3e_1)^2 \ . \tag{1.23}$$

We now associate these amplitudes with their corresponding Lagrangian formulations. Eq. (1.19) comes from the Einstein-Hilbert action,

$$S \supset C_{d=-1}\int \sqrt{-g}\ R\ d^4x \ , \tag{1.24}$$

where R is the Ricci scalar and g is the determinant of the metric tensor. Thus, Eq. (1.19) is the full tree-level 3-graviton scattering amplitude in General Relativity.

The amplitude in Eq. (1.22) arises from the Gauss-Bonnet [39] modified theory of gravity,

$$S \supset C_{d=-3}\int \sqrt{-g}\ (R^2 - 4R_{\mu\nu}R^{\mu\nu} + R_{\mu\nu\rho\sigma}R^{\mu\nu\rho\sigma})d^4x \ , \tag{1.25}$$

with $R_{\mu\nu}$ the Ricci tensor and $R_{\mu\nu\rho\sigma}$ the Riemann tensor.

The amplitude in Eq. (1.23) corresponds to a modified theory of gravity cubic in the Riemann tensor,

$$S \supset C_{d=-5}\int \sqrt{-g}\ R^3 d^4x \ . \tag{1.26}$$

It is worth mentioning that the amplitude Eq. (1.19) for the scattering of 3 gravitons at order $O(p^2)$ has the same kinematic structure as the square of the 3-vector amplitude Eq. (1.13). This feature is an example of the broader principle of color-kinematics duality, where graviton amplitudes can be obtained by squaring the kinematic component of gluon amplitudes. See [40] for a review on this topic.

1.2 General 3-point helicity amplitudes

Having examined the cases of spin-0, 1, and 2, we now consider 3-particle scattering amplitudes in a systematic framework. We have been working with generic polarization vectors and tensors, but these are redundant objects that obscure the amplitude structure. Instead, it is enlightening to consider the helicity basis for the particle polarizations [13].

According to Wigner's classification [41], particles are described as irreducible representations of the Poincaré group. Given some particle with momentum p, we define the little group as the group of Lorentz transformations that leave p invariant. Then, particle states can be defined by the momentum p and how they transform under the little group [42]. In the case of massless particles in 4 dimensions, the little group is $\mathrm{SO}(2) \simeq \mathrm{U}(1)$. The quantum number associated with this group is the helicity h, defined as the projection of the particle spin onto its direction of motion. Every massless particle can have two helicities $\pm h$.

Helicity amplitudes describe the scattering of particles with well-defined helicities. These amplitudes have the right transformation properties under the little group, and in many cases they show a surprisingly simple structure. Perhaps the most famous example of this is the Parke-Taylor formula for gluon scattering in a configuration of maximum helicity violation [9], which we mentioned in the introduction of this thesis.

When computing on-shell helicity amplitudes, we ideally want to replace the redundant momenta and polarization vectors by some objects that transform properly under the little group. This goal is accomplished using spinor-helicity variables. The details and conventions for these variables are specified in Appendix A.

After these considerations, we are ready to derive the general formula for 3-point helicity amplitudes. Expressing the 3-particle on-shell kinematics Eq. (1.2) in terms of spinor-helicity variables,

$$\begin{aligned} 0 = p_1^2 = (p_2 + p_3)^2 = \langle 23 \rangle [32] \ , \\ 0 = p_2^2 = (p_1 + p_3)^2 = \langle 13 \rangle [31] \ , \\ 0 = p_3^2 = (p_1 + p_2)^2 = \langle 12 \rangle [21] \ . \end{aligned} \tag{1.27}$$

For instance, the first line shows that either $\langle 23 \rangle \neq 0$ or $[32] \neq 0$. This leads to two different kinematic configurations for the 3-particle amplitude [33], as shown below.

- If $\langle 23 \rangle \neq 0$, then $[32] = [31] = [12] = 0$.
- If $[23] \neq 0$, then $\langle 32 \rangle = \langle 31 \rangle = \langle 12 \rangle = 0$.

This statement can be demonstrated as follows. If $\langle 23 \rangle \neq 0$, then $[32] = 0$. Since $\langle 23 \rangle [31] = -\langle 21 \rangle [11] - \langle 22 \rangle [21] = 0$, in this case $[31] = 0$ as well. Similarly, since $\langle 23 \rangle [21] = -\langle 13 \rangle [11] - \langle 33 \rangle [31] = 0$, we see that $[21] = 0$. The case $[23] \neq 0$ is exactly the same but interchanging angle and square brackets.

In the configuration where $[32] = [31] = [12] = 0$, the general expression for a 3-particle amplitude is given by

$$\mathcal{A}(1^{h_1}, 2^{h_2}, 3^{h_3}) = C \langle 12 \rangle^a \langle 23 \rangle^b \langle 31 \rangle^c \ , \tag{1.28}$$

where C is a constant and a, b, c are fixed when we take into account little group covariance. Under the little group, the amplitude transforms as

$$\begin{aligned} \mathcal{A}(1^{h_1}, 2^{h_2}, 3^{h_3}) &\longrightarrow t_1^{h_1} t_2^{h_2} t_3^{h_3}\ \mathcal{A}(1^{h_1}, 2^{h_2}, 3^{h_3}) \ , \\ \langle 12\rangle^a \langle 23\rangle^b \langle 31\rangle^c &\longrightarrow t_1^{(a+c)} t_2^{(a+b)} t_3^{(b+c)} \langle 12\rangle^a \langle 23\rangle^b \langle 31\rangle^c \ , \end{aligned} \tag{1.29}$$

with t some parameter. Equating the little group weights, the exponents are

$$a = h_3 - h_1 - h_2 \ , \qquad b = h_1 - h_2 - h_3 \ , \qquad c = h_2 - h_3 - h_1 \ . \tag{1.30}$$

Then the mass dimension of the kinematic part of the amplitude is

$$\left[\langle 12\rangle^a \langle 23\rangle^b \langle 31\rangle^c\right] = a + b + c = -h_1 - h_2 - h_3 \ , \tag{1.31}$$

As we mentioned before, this number cannot be negative by locality, because 3-point amplitudes do not have poles. Then, we must impose $-h_1 - h_2 - h_3 = -h \geq 0$, with $h = h_1 + h_2 + h_3$ the total helicity. If this condition on the particle helicities is not satisfied, then the amplitude cannot be written as in Eq. (1.28) and instead we have to use the configuration where $\langle 32\rangle = \langle 31\rangle = \langle 12\rangle = 0$. Overall, the most general expression for the 3-point amplitude is [33]

$$\mathcal{A}(1^{h_1}, 2^{h_2}, 3^{h_3}) = \begin{cases} C \langle 12\rangle^{h_3 - h_1 - h_2} \langle 23\rangle^{h_1 - h_2 - h_3} \langle 31\rangle^{h_2 - h_3 - h_1} & \text{if } h \leq 0 \\ \tilde{C}\, [12]^{h_1 + h_2 - h_3} [23]^{h_2 + h_3 - h_1} [31]^{h_3 + h_1 - h_2} & \text{if } h \geq 0 \end{cases} \ . \tag{1.32}$$

This formula is valid non-perturbatively, as it relies solely on Lorentz symmetry, locality and dimensional analysis. Using it, we can easily rederive the 3-point amplitudes for spin-0, -1 and -2.

- Spin 0: All the particles have helicity zero and the amplitude is just a constant, as we saw in Eq. (1.5),

$$\mathcal{A}(1, 2, 3) = C_{d=1} \ . \tag{1.33}$$

- Spin 1: Vector bosons have helicity $h = \pm 1$ and there are 4 non-vanishing amplitudes. The helicities choices $--+$ and $++-$ lead to

$$\mathcal{A}(1_a^-, 2_b^-, 3_c^+) = C_{d=0} f^{abc} \frac{\langle 12\rangle^3}{\langle 13\rangle \langle 32\rangle} \ , \quad \mathcal{A}(1_a^+, 2_b^+, 3_c^-) = C_{d=0} f^{abc} \frac{[12]^3}{[13]\,[32]} \ , \tag{1.34}$$

  which correspond to Eq. (1.13) written in terms of spinor-helicity variables. For the helicity choices $---$ and $+++$, we obtain

$$\begin{aligned} \mathcal{A}(1_a^-, 2_b^-, 3_c^-) &= C_{d=-2} f^{abc} \langle 12\rangle \langle 23\rangle \langle 31\rangle \ , \\ \mathcal{A}(1_a^+, 2_b^+, 3_c^+) &= C_{d=-2} f^{abc} [12]\,[23]\,[31] \ , \end{aligned} \tag{1.35}$$

  which correspond to Eq. (1.14).

- Spin 2: the particles have helicities $h = \pm 2$ and again there are 4 non-vanishing amplitudes. Helicities $--+$ and $++-$ correspond to Eq. (1.19) and can be written as

$$\mathcal{A}(1^{--}, 2^{--}, 3^{++}) = C_{d=-1} \frac{\langle 12\rangle^6}{\langle 13\rangle^2 \langle 32\rangle^2} \ , \quad \mathcal{A}(1^{++}, 2^{++}, 3^{--}) = C_{d=-1} \frac{[12]^6}{[13]^2 [32]^2} \ . \tag{1.36}$$

  The other helicity choices $---$ and $+++$ are associated to Eq. (1.23) and lead to

$$\begin{aligned} \mathcal{A}(1^{--}, 2^{--}, 3^{--}) &= C_{d=-5} \langle 12\rangle^2 \langle 23\rangle^2 \langle 31\rangle^2 \ , \\ \mathcal{A}(1^{++}, 2^{++}, 3^{++}) &= C_{d=-5} [12]^2 [23]^2 [31]^2 \ . \end{aligned} \tag{1.37}$$

  Remarkably, these are the only amplitudes we can write and Eq. (1.22) is missing. This is because now we are working with spinor-helicity variables in 4-dimensions and Eq. (1.22) vanishes in that case. Indeed, in 4-dimensions the Gauss-Bonnet is a total derivative [43] and does not contribute to graviton scattering.

  Notice as well how Eq. (1.36) and Eq. (1.37) are the square of the kinematic part of Eq. (1.34) and Eq. (1.35), as expected due to color-kinematics duality.

These examples illustrate the scattering of three particles with the same spin. However, the general expression Eq. (1.32) enables the derivation of any 3-point amplitude. In Section 2.1 we will use it to build all the 3-point amplitudes in the Standard Model.

1.3 4-point amplitudes and factorization

We now extend our discussion to on-shell amplitudes for higher-point interactions. Let us consider the scattering of four massless particles with momenta p_i. In this configuration, we define the following kinematic variables

$$\begin{aligned} s \equiv s_{12} &= (p_1 + p_2)^2 = (p_3 + p_4)^4 = \langle 12\rangle [12] = \langle 34\rangle [34] \ , \\ t \equiv s_{13} &= (p_1 + p_3)^2 = (p_2 + p_4)^4 = \langle 13\rangle [13] = \langle 24\rangle [24] \ , \\ u \equiv s_{14} &= (p_1 + p_4)^2 = (p_2 + p_3)^4 = \langle 14\rangle [14] = \langle 23\rangle [23] \ . \end{aligned} \tag{1.38}$$

These are the well-known Mandelstam variables, which obey $s + t + u = 0$. It is also helpful to remember that the mass dimension of a 4-point amplitude is $[\mathcal{A}_4] = 0$.

At tree level, we can construct two classes of 4-point amplitudes: contact amplitudes and amplitudes with propagators. In general we have to consider both of these terms, and locality fixes the 4-point amplitude structure to be the following:

$$\mathcal{A}_4 = \mathcal{A}_4^{\text{contact}} + \mathcal{A}_4^s + \mathcal{A}_4^t + \mathcal{A}_4^u \ , \tag{1.39}$$

where $\mathcal{A}_4^{\text{contact}}$ is the contact amplitude and $\mathcal{A}_4^s$, $\mathcal{A}_4^t$, $\mathcal{A}_4^u$ have poles corresponding to the exchange of a particle in the s-, t- or u- channels. We will study the two classes of amplitudes separately.

1.3.1 Contact amplitudes

Contact amplitudes originate from 4-particle interactions and have no momentum poles. The recipe for constructing them is to write down all possible terms with the proper little group weights and no negative powers of momenta. This must be done on a case-by-case basis, as there is no analog of Eq. (1.32) for n-point amplitudes with $n > 3$.

As an example, we consider the scattering of four identical scalar particles. The lowest-order contact amplitude is just a constant

$$O(p^0): \qquad \mathcal{A}(1,2,3,4) = C_{d=0} \ . \tag{1.40}$$

This corresponds to the well-known $\lambda\phi^4$ theory, described by the following interaction Lagrangian

$$\mathcal{L} \supset C_{d=0}\ \phi^4 \ . \tag{1.41}$$

Higher-order contact amplitudes include terms such as

$$O(p^2): \qquad \mathcal{A}(1,2,3,4) = C_{d=-2}\,(C_1 s_{12} + C_2 s_{13}) \ , \tag{1.42}$$

where C_i are dimensionless constants. This amplitude arises from an irrelevant dimension-6 operator in an effective field theory, such as

$$\mathcal{L} \supset C_{d=-2}\ \phi^2(\partial\phi)^2 \ . \tag{1.43}$$

In Section 2.2 we will explore examples of contact amplitudes within the Standard Model Effective Field Theory.

1.3.2 Factorizable amplitudes

4-point amplitudes can also be constructed by connecting two (contact) 3-point amplitudes via a propagator. Each propagator introduces a factor $1/s_{ij}$, so the amplitude has a simple pole for $s_{ij} = 0$. Generally, 4-point amplitudes exhibit three simple poles at $s = 0$, $t = 0$ and $u = 0$.

The construction of 4-point amplitudes from 3-point amplitudes relies on factorization: in the limit when one of the propagators is on shell, the amplitude has to factorize into the product of two (on-shell) 3-point amplitudes. For instance, for a boson propagator in the s-channel, factorization imposes

$$\lim_{s_{12}\to 0}\ i\mathcal{A}_4(1,2,3,4) = \sum_h i\mathcal{A}_3(1,2,\ell^h)\ \frac{i}{s_{12}}\ i\mathcal{A}_3(-\ell^{-h},3,4) \ , \tag{1.44}$$

where $\ell = p_1 + p_2 = p_3 + p_4$ is the momentum of the internal propagator and the summation runs over the possible polarizations of particle ℓ. Equivalently, Eq. (1.44) can be expressed as

$$\lim_{s_{12}\to 0}\ s_{12}\mathcal{A}_4(1,2,3,4) = -\sum_h \mathcal{A}_3(1,2,\ell)\mathcal{A}_3(\ell,3,4) \ . \tag{1.45}$$

Extending this to a general internal particle, whether fermion or boson, the factorization condition becomes

$$\lim_{s_{12}\to 0} \; s_{12}\mathcal{A}_4(1,2,3,4) = -\sum_h i^{F[\ell]} \; \mathcal{A}_3(1,2,\ell)\mathcal{A}_3(-\ell,3,4) \; , \tag{1.46}$$

where $F[i_1,...,i_n]$ counts the number of fermions and antifermions in the list $i_1,...,i_n$[1]. For poles in t- and u-channels, we also have

$$\lim_{s_{13}\to 0} \; s_{13}\mathcal{A}_4(1,2,3,4) = -\sum_h i^{F[\ell]}(-1)^{n_{23}} \; \mathcal{A}_3(1,3,\ell)\mathcal{A}_3(-\ell,2,4) \; , \tag{1.47}$$

$$\lim_{s_{14}\to 0} \; s_{14}\mathcal{A}_4(1,2,3,4) = -\sum_h i^{F[\ell]}(-1)^{n_{23}}(-1)^{n_{34}} \; \mathcal{A}_3(1,4,\ell)\mathcal{A}_3(-\ell,2,3) \; , \tag{1.48}$$

where $n_{ij} = 1$ if both i and j are fermions, and $n_{ij} = 0$ otherwise. The (-1) factors account for possible fermion exchanges when the particles are reordered.

Several approaches can be employed to construct factorizable 4-point amplitudes. Here, we focus on the "ansatz" method and the momentum shift method.

The "ansatz" method

This method is based on making an ansatz for the amplitude and then verifying that it factorizes properly. For clarity, let us consider scalar QED, which is the theory of a complex scalar ϕ interacting with a photon γ. The 3-point amplitudes in this theory are

$$\mathcal{A}(1_\phi, 2_{\phi^*}, 3^-_\gamma) = C_{d=0}\frac{\langle 23\rangle\,\langle 31\rangle}{\langle 12\rangle} \; , \quad \mathcal{A}(1_\phi, 2_{\phi^*}, 3^+_\gamma) = C_{d=0}\frac{[23]\,[31]}{[12]} \; . \tag{1.49}$$

We want to compute the 4-point amplitude for the scattering of two scalars and two photons[2]. For this process, we must consider the t- and u-channels, as shown in Figure 1.1. To get an ansatz for the amplitude, we start by imposing factorization in the t-channel. According to Eq. (1.47),

$$\lim_{t\to 0} \; \mathcal{A}_4(1_\phi, 2_{\phi^*}, 3^+_\gamma, 4^-_\gamma) = \frac{1}{t}\mathcal{A}_3(1_\phi, 3^+_\gamma, \ell_{\phi^*})\mathcal{A}_3(-\ell_\phi, 2_{\phi^*}, 4^-_\gamma) \; , \tag{1.50}$$

with $\ell = p_1 + p_3 = p_2 + p_4$ the momentum of the internal scalar. Using expressions Eq. (1.49) for the 3-point amplitudes,

$$\lim_{t\to 0} \; \mathcal{A}_4(1_\phi, 2_{\phi^*}, 3^+_\gamma, 4^-_\gamma) = \frac{1}{t}C^2_{d=0}\frac{[\ell 3]\,[31]}{[1\ell]}\frac{\langle 24\rangle\,\langle 4\ell\rangle}{\langle \ell 2\rangle} = -C^2_{d=0}\frac{\langle 14\rangle\,\langle 24\rangle}{\langle 13\rangle\,\langle 23\rangle} \; , \tag{1.51}$$

where in the last step we have used that $[\ell 3]\,\langle 4\ell\rangle = [13]\,\langle 41\rangle$ and $[1\ell]\,\langle \ell 2\rangle = [13]\,\langle 32\rangle$. This is a good ansatz for the amplitude, since it has the right dimensionality and little group weights.

[1] See Appendix A.3 for details on the origin of the $i^{F[\ell]}$ factor.

[2] In Scalar QED this amplitude could get a contribution from the contact interaction $\phi\phi^* A_\mu A^\mu$. However, one can prove that this term gives a vanishing contribution to the on-shell 4-point amplitude [14].

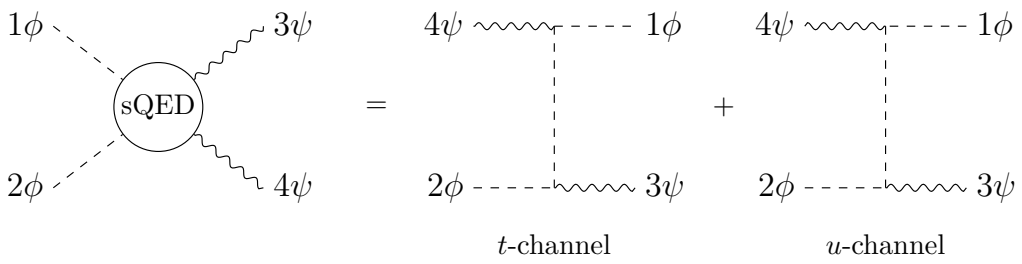

Figure 1.1: *Feynman diagrams for the amplitude* $\mathcal{A}_4(1_\phi, 2_{\phi^*}, 3^+_\gamma, 4^-_\gamma)$ *in sQED at tree level. There are two factorization channels:* t *and* u*.*

The full amplitude will be Eq. (1.51) plus a term that goes to zero when $t \to 0$. Next, we check the factorization in the u-channel. From Eq. (1.48),

$$\begin{aligned}\lim_{u\to 0}\ \mathcal{A}_4(1_\phi, 2_{\phi^*}, 3^+_\gamma, 4^-_\gamma) &= \frac{1}{u}\mathcal{A}_3(1_\phi, 4^-_\gamma, q_{\phi^*})\mathcal{A}_3(-q_\phi, 2_{\phi^*}, 3^+_\gamma) \\ &= \frac{1}{u}C^2_{d=0}\frac{\langle q4\rangle\,\langle 41\rangle}{\langle 1q\rangle}\frac{[23]\,[3q]}{[q2]} = -C^2_{d=0}\frac{\langle 14\rangle\,\langle 24\rangle}{\langle 13\rangle\,\langle 23\rangle}\ ,\end{aligned} \tag{1.52}$$

with $q = p_1 + p_4 = p_2 + p_3$. Again, the full amplitude includes Eq. (1.52) plus a term that vanishes as $u \to 0$. By comparing Eq. (1.51) and Eq. (1.52) we conclude that the amplitude is

$$\mathcal{A}_4(1_\phi, 2_{\phi^*}, 3^+_\gamma, 4^-_\gamma) = -C^2_{d=0}\frac{\langle 14\rangle\,\langle 24\rangle}{\langle 13\rangle\,\langle 23\rangle}\ . \tag{1.53}$$

In this example, deriving the full amplitude by imposing factorization was straightforward, but that is not always true. In order to compute scattering amplitudes in a systematic way for any number of particles, we have to use momentum shifts.

Momentum shifts

The key idea is to build higher-point amplitudes from lower-point amplitudes by means of complex deformations of the external particle momenta. This is done using the analytical properties of on-shell scattering amplitudes.

Let us first introduce the concept of complex momentum shifts [14]. Consider the scattering amplitude $\mathcal{A}_n$ of n massless particles. The on-shell condition requires $p_i^2 = 0$ for $i = 1, ..., n$, and momentum conservation enforces $\sum_{i=1}^n p_i^\mu = 0$. Consider also a set of n complex four-vectors r_i^μ with the following properties:

(a) $\sum_{i=1}^n r_i^\mu = 0$.

(b) $r_i^2 = 0$ and $r_i r_j = 0$ for $i, j = 1, ..., n$.

(c) $r_i p_i = 0$ for each $i = 1, ..., n$.

We define the shifted momenta $\hat{p}_i^\mu$ as

$$\hat{p}_i^\mu \equiv p_i^\mu + z r_i^\mu \ , \qquad z \in \mathbb{C} \ . \tag{1.54}$$

From properties (a), (b) and (c), it is easy to check that the shifted momenta are also on shell ($\hat{p}_i^2 = 0$) and obey momentum conservation ($\sum_{i=1}^n \hat{p}_i^\mu = 0$). For this reason, we can consider the scattering amplitude $\mathcal{A}_n$ in terms of the shifted momenta $\hat{p}_i^\mu$ instead of p_i^μ. We define this shifted amplitude $\hat{\mathcal{A}}_n(z)$ as a function of the complex variable z. The original amplitude is recovered for $\hat{\mathcal{A}}_n(z=0) = \mathcal{A}_n$.

The analytic structure of $\hat{\mathcal{A}}_n(z)$ is easy to determine if $\mathcal{A}_n$ is a tree-level amplitude. In that case, $\mathcal{A}_n$ has simple poles proportional to $1/P_I^2$, where $P_I^\mu = \sum_{i\in I} p_i^\mu$ and $\{p_i^\mu\}_{i\in I}$ is a subset of momenta. The shifted propagators are proportional to $1/\hat{P}_I^2$, with

$$\hat{P}_I^2 = \left(\sum_{i\in I} \hat{p}_i^\mu\right)^2 = P_I^2 + 2z P_I R_I \ , \qquad R_I^\mu = \sum_{i\in I} r_i^\mu \ . \tag{1.55}$$

Notice that $\hat{P}_I^2$ is linear in z, since the terms that should go as z^2 vanish by property (b). It is convenient to write the shifted propagator as

$$\frac{1}{\hat{P}_I^2} = -\frac{z_I}{P_I^2(z - z_I)} \ , \qquad \text{with } z_I = -\frac{P_I^2}{2P_I R_I} \ . \tag{1.56}$$

From this expression, it is easy to see that the only singularities of $\hat{\mathcal{A}}_n(z)$ in the complex plane are simple poles for $z = z_I$. For generic momenta, $z_I \neq 0$ and all the z_I are different.

Now let us consider $\hat{\mathcal{A}}_n(z)/z$ as a function of z with simple poles at $z = 0$ and $z = z_I$. By Cauchy's theorem, the contour integral of $\hat{\mathcal{A}}_n(z)/z$ along a circle surrounding the origin is

$$\oint_{c_0} \frac{\hat{\mathcal{A}}_n(z)}{z} dz = 2\pi i \operatorname*{Res}_{z=0}\left(\frac{\hat{\mathcal{A}}_n(z)}{z}\right) = 2\pi i \hat{\mathcal{A}}_n(z=0) = 2\pi i \mathcal{A}_n \ . \tag{1.57}$$

We can deform the contour c_0 to pick up the other singularities of the function, as shown in Figure 1.2. This leads to

$$\oint_{c_0} \frac{\hat{\mathcal{A}}_n(z)}{z} dz = \left(\sum_I \oint_{c_I} + \oint_{c_\infty}\right) \frac{\hat{\mathcal{A}}_n(z)}{z} dz = -2\pi i \sum_{z_i} \operatorname*{Res}_{z=z_I}\left(\frac{\hat{\mathcal{A}}_n(z)}{z}\right) - 2\pi i B_n \ , \tag{1.58}$$

where B_n is the residue of the pole at infinity, which is equal to the $O(z^0)$ term in the Laurent series of $\hat{\mathcal{A}}_n(z)$ at $z = \infty$. Equating Eq. (1.57) and Eq. (1.58), we obtain

$$\mathcal{A}_n = -\sum_{z_i} \operatorname*{Res}_{z=z_I}\left(\frac{\hat{\mathcal{A}}_n(z)}{z}\right) - B_n \ . \tag{1.59}$$

From Eq. (1.56), the residue of $\hat{\mathcal{A}}_n(z)/z$ at z_I factorizes into two on-shell subamplitudes:

$$\operatorname*{Res}_{z=z_I}\left(\frac{\hat{\mathcal{A}}_n(z)}{z}\right) = -\hat{\mathcal{A}}_L(z_I)\frac{1}{P_I^2}\hat{\mathcal{A}}_R(z_I) \ . \tag{1.60}$$

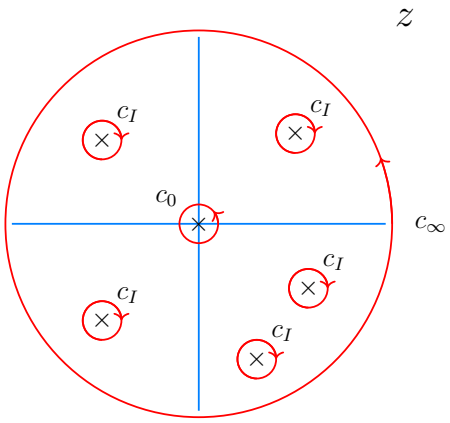

Figure 1.2: *Contours of integration.* c_0 *can be deformed into* $c_I + c_\infty$

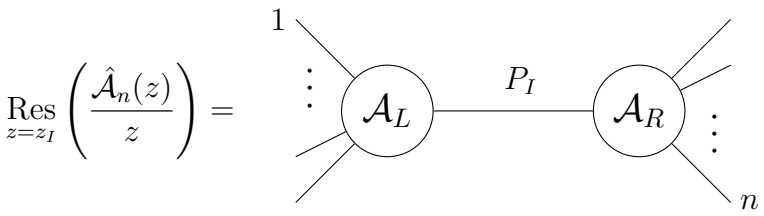

Figure 1.3: *Diagram of the factorization of* $\hat{\mathcal{A}}_n$ *at the pole* $z = z_i$.

This is depicted schematically in Figure 1.3. It looks similar to the usual Feynman diagrams, but remarkably the internal line is now on-shell $P_I^2 = 0$. The subamplitudes $\hat{\mathcal{A}}_L$ and $\hat{\mathcal{A}}_R$ are both scattering amplitudes for $n-1$ particles.

Combining Eq. (1.59) and Eq. (1.60), we obtain

$$\mathcal{A}_n = \sum_{z_I} \hat{\mathcal{A}}_L(z_I) \frac{1}{P_I^2} \hat{\mathcal{A}}_R(z_I) - B_n \ , \tag{1.61}$$

which is an expression for $\mathcal{A}_n$ in terms of lower-point amplitudes $\mathcal{A}_{n-1}$ plus the contribution from the pole at infinity B_n. This term has in general no expression in terms of lower-point amplitudes, so for practical uses of Eq. (1.61) we want it to vanish. To ensure that $B_n = 0$, we must use a momentum shift that satisfies $\hat{\mathcal{A}}_n(z) \to 0$ for $z \to \infty$. This is called a good momentum shift.

For a good momentum shift, Eq. (1.61) leads to the so-called on-shell recursion relations [10, 44]. The main idea is to use lower-point amplitudes as building blocks for higher-point amplitudes. Recursion relations are a powerful tool to compute general n-point amplitudes and have been applied to the context of gauge theories and gravity, among others [45–49]. Some examples of momentum shifts are:

- BCFW shift: This is one of the most relevant momentum shifts. It was first proposed in [10] and is used to obtain the BCFW recursion relations. In this shift, two of the external

momenta –that we label as i and j– are shifted in the following way

$$|\hat{i}\rangle = |i\rangle - z\,|j\rangle \ , \qquad |\hat{i}] = |i] \ , \qquad |\hat{j}\rangle = |j\rangle \ , \qquad |\hat{j}] = |j] + z\,|i] \ . \tag{1.62}$$

This is a $[j,i\rangle$-shift.

- Risager shift: This is a three-line shift that was introduced in [50]. We choose three of the external legs –1,2 and 3– and apply the following deformation,

$$\begin{aligned} |\hat{1}] &= |1] \ , \qquad |\hat{1}\rangle = |1\rangle + z\,[23]\,|\eta\rangle \ , \\ |\hat{2}] &= |2] \ , \qquad |\hat{2}\rangle = |2\rangle + z\,[31]\,|\eta\rangle \ , \\ |\hat{3}] &= |3] \ , \qquad |\hat{3}\rangle = |3\rangle + z\,[12]\,|\eta\rangle \ , \end{aligned} \tag{1.63}$$

with $|\eta\rangle$ a reference spinor that can take any value. Another option for this shift is the complex-conjugate of Eq. (1.63).

We now use momentum shifts to rederive the amplitude Eq. (1.53) that we obtained in the previous section. As shown in Figure 1.1, the scattering of two scalars and two gauge bosons in scalar QED involves the t- and u-channels, so the amplitude has two simple poles for $t=0$ and $u=0$. The shifted amplitude $\hat{\mathcal{A}}_4(z)$ has two simple poles at z_t and z_u. For a good momentum shift, Eq. (1.60) reduces to

$$\begin{aligned} \mathcal{A}_4(1_\phi, 2_{\phi^*}, 3^+_\gamma, 4^-_\gamma) = \hat{\mathcal{A}}_3(1_\phi, 3^+_\gamma, \ell_{\phi^*}; z_t)\frac{1}{t}\hat{\mathcal{A}}_3(-\ell_\phi, 2_{\phi^*}, 4^-_\gamma; z_t) \\ + \hat{\mathcal{A}}_3(1_\phi, 4^-_\gamma, q_{\phi^*}; z_u)\frac{1}{u}\hat{\mathcal{A}}_3(-q_\phi, 2_{\phi^*}, 3^+_\gamma; z_u) \ , \end{aligned} \tag{1.64}$$

with $\ell = p_1 + p_3 = p_2 + p_4$ and $q = p_1 + p_4 = p_2 + p_3$. We have defined $\hat{\mathcal{A}}_n(1,...,n;z_I)$ as the amplitude $\mathcal{A}_n(1,...,n)$ with shifted momenta for $z = z_I$.

The next step is to choose a momentum shift. We will use the BCFW $[4,3\rangle$-shift:

$$|\hat{3}\rangle = |3\rangle - z\,|4\rangle \ , \qquad |\hat{3}] = |3] \ , \qquad |\hat{4}\rangle = |4\rangle \ , \qquad |\hat{4}] = |4] + z\,|3] \ . \tag{1.65}$$

One can check that this is a good shift, since it has the right large-z behavior when applied to Eq. (1.53). The shifted propagators of the amplitude are

$$\hat{t} = (\hat{p}_1 + \hat{p}_3)^2 = \langle \hat{13}\rangle[\hat{13}] = \langle 1|\,(|3\rangle - z\,|4\rangle)\,[13] \ , \tag{1.66}$$

$$\hat{u} = (\hat{p}_1 + \hat{p}_4)^2 = \langle \hat{14}\rangle[\hat{14}] = \langle 14\rangle\,[1|\,(|4] + z\,|3])\ . \tag{1.67}$$

The poles of $\hat{\mathcal{A}}_4(z)$ are the values of z where the propagators go on-shell,

$$0 = \hat{t}|_{z=z_t} = \langle 1|\,(|3\rangle - z_t\,|4\rangle)\,[13] \ , \quad \Longrightarrow \quad z_t = \frac{\langle 13\rangle}{\langle 14\rangle} \ , \tag{1.68}$$

$$0 = \hat{u}|_{z=z_u} = \langle 14\rangle\,[1|\,(|4] + z_u\,|3])\ , \quad \Longrightarrow \quad z_u = -\frac{[14]}{[13]} \ . \tag{1.69}$$

With this, the shifted subamplitudes in Eq. (1.64) are

$$\begin{aligned}\hat{\mathcal{A}}_3(1_\phi,3^+_\gamma,\ell_{\phi^*};z_t)\frac{1}{t}\hat{\mathcal{A}}_3(-\ell_\phi,2_{\phi^*},4^-_\gamma;z_t) &= \frac{C^2_{d=0}}{t}\frac{[\hat{\ell}3][\hat{3}1]}{[\hat{1}\ell]}\frac{\langle\hat{2}4\rangle\langle\hat{4}\ell\rangle}{\langle\hat{\ell}2\rangle} = \frac{C^2_{d=0}}{t}\frac{\langle23\rangle\,\langle41\rangle\,[31]}{\langle32\rangle-\frac{\langle13\rangle}{\langle14\rangle}\langle42\rangle} \\ &= C^2_{d=0}\frac{\langle24\rangle\,\langle14\rangle^2}{\langle12\rangle\,\langle34\rangle\,\langle13\rangle}\ .\end{aligned} \tag{1.70}$$

$$\begin{aligned}\hat{\mathcal{A}}_3(1_\phi,4^-_\gamma,q_{\phi^*};z_u)\frac{1}{u}\hat{\mathcal{A}}_3(-q_\phi,2_{\phi^*},3^+_\gamma;z_u) &= \frac{C^2_{d=0}}{u}\frac{\langle\hat{q}4\rangle\langle\hat{4}1\rangle}{\langle\hat{1}q\rangle}\frac{[\hat{2}3][\hat{3}q]}{[\hat{q}2]} = \frac{C^2_{d=0}}{u}\frac{[23]\,[31]\,\langle41\rangle}{[42]-\frac{[14]}{[13]}[32]} \\ &= C^2_{d=0}\frac{[23]\,[13]^2}{[12]\,[34]\,[14]} = -C^2_{d=0}\frac{\langle24\rangle\,\langle14\rangle}{\langle23\rangle\,\langle13\rangle}\frac{t}{s}\ .\end{aligned} \tag{1.71}$$

Summing Eq. (1.70) and Eq. (1.71) leads to the 4-point amplitude

$$\mathcal{A}_4(1_\phi,2_{\phi^*},3^+_\gamma,4^-_\gamma) = C^2_{d=0}\frac{\langle14\rangle\,\langle24\rangle}{\langle13\rangle\,\langle12\rangle}\left(\frac{\langle14\rangle}{\langle34\rangle}-\frac{\langle13\rangle\,[13]}{\langle23\rangle\,[12]}\right) = -C^2_{d=0}\frac{\langle14\rangle\,\langle24\rangle}{\langle13\rangle\,\langle23\rangle}\ , \tag{1.72}$$

which is equal to Eq. (1.53).

Our derivation relies on the fact that $[4,3\rangle$ is a good momentum shift. This can be proved by applying the shift to $\hat{\mathcal{A}}_4$ in Eq. (1.53) and showing that the amplitude vanishes at large z,

$$\lim_{z\to\infty}\hat{\mathcal{A}}_4 = -C^2_{d=0}\lim_{z\to\infty}\left[\frac{\langle14\rangle\,\langle24\rangle}{(\langle13\rangle-z\,\langle14\rangle)\,(\langle23\rangle-z\,\langle24\rangle)}\right] = 0\ . \tag{1.73}$$

An example of a bad momentum shift is the BCFW $[3,4\rangle$-shift, since it leads to

$$\lim_{z\to\infty}\hat{\mathcal{A}}_4 = -C^2_{d=0}\lim_{z\to\infty}\left[\frac{(\langle14\rangle-z\,\langle13\rangle)\,(\langle24\rangle-z\,\langle23\rangle)}{\langle13\rangle\,\langle23\rangle}\right]\to\infty\ , \tag{1.74}$$

so the pole at infinity gives a non-vanishing contribution to Eq. (1.60). Notice how the only difference between both shifts is the helicity of the shifted particles: $[-,+\rangle$ is a good shift but $[+,-\rangle$ is a bad shift.

A priori, it is a challenging task to choose a good momentum shift to build an amplitude. To determine whether a shift is good or not, we have to study the limit of $\hat{\mathcal{A}}_n(z)$ when $z\to\infty$. However, in the context of recursion relations, we do not know $\mathcal{A}_n$ beforehand. The solution is to do a general study of the large-z behavior of amplitudes in a given theory:

- For example, N. Arkani-Hammed *et al.* used the background field method to study gauge theories in [51]. They concluded that gluon amplitudes in pure Yang-Mills theory are constructible with BCFW shifts for helicity choices $[-,-\rangle$, $[+,+\rangle$ and $[-,+\rangle$, but they are not constructible with a $[+,-\rangle$-shift.

- More recently in [49], C. Cheung *et al.* also applied the background field method to study the constructibility of amplitudes in different theories. They determined the types of momentum shifts that are valid for a collection of theories, including gauge theories with fermions and scalars, supersymmetric theories and the Standard Model.

1.3.3 Generalization to n-point amplitudes

Our discussion of 4-point amplitudes is naturally generalized to n-point amplitudes with $n > 4$. In general we have to consider a contact n-point interaction plus the factorizable terms for all the possible channels,

$$\mathcal{A}_n = \mathcal{A}_n^{\text{contact}} + \sum_i \mathcal{A}_n^i \ , \tag{1.75}$$

where i denotes the different factorization channels. Using momentum shifts, we can compute the factorizable amplitudes $\mathcal{A}_n^i$ from the lower-point amplitudes of the theory: $\mathcal{A}_m$ with $m < n$. The resulting $\mathcal{A}_n$ amplitudes form the basis for higher-point amplitudes: $\mathcal{A}_M$ with $n < M$.

Overall, we have seen how on-shell methods are powerful tools for computing general tree-level n-point amplitudes in a recursive way. Specifying the particle contact and interactions of a theory fixes the on-shell contact amplitudes, which approximately correspond to operators in the Lagrangian approach. Then, these contact amplitudes serve as the fundamental building blocks for constructing higher-point amplitudes.

1.4 Conclusions of the chapter

In this chapter, we have explored the construction of tree-level on-shell amplitudes from first principles, bypassing the need to define a Lagrangian. In particular, we have obtained tree-level amplitudes using locality, Lorentz symmetry and dimensional analysis.

First, we have considered theories for particles of spin-0, -1 and -2. Imposing on-shell kinematics and the correct dependence on polarizations, we have determined all possible 3-point amplitudes. We have identified the amplitudes associated with scalar field theory, non-abelian gauge theory and General Relativity, together with higher-order interactions from effective field theories.

We have introduced the spinor-helicity formalism to streamline the building of 3-point amplitudes for particles of any spin. Considering amplitudes of well-defined helicity, we have used little group covariance to constrain the general structure of 3-point amplitudes, as shown in Eq. (1.32).

Regarding higher-point amplitudes, in general we have contact terms plus factorizable contributions, which contain simple poles associated with propagators. In the limit when one of the propagators goes on shell, the amplitude factorizes into a product of lower-point subamplitudes. The computation of factorizable amplitudes can be systematized with the technique of momentum shifts. This leads to recursion relations that allow us to construct general n-point amplitudes in terms of the fundamental contact amplitudes.

In summary, on-shell amplitude methods provide a practical and efficient framework for studying scattering processes. These methods lay the groundwork for exploring more complex systems, including loop amplitudes in effective field theories, which we develop in subsequent chapters.

Chapter 2

The on-shell Standard Model and Standard Model Effective Field Theory

In this chapter we present the on-shell scattering amplitudes associated with particle interactions in the Standard Model (Section 2.1) and the Standard Model Effective Field Theory (Section 2.2). We primarily follow the approach in [1].

2.1 The on-shell Standard Model

The Standard Model (SM) of particle physics is the theory of electroweak interactions and quantum chromodynamics (QCD). It describes the interactions of elementary fermions and bosons through a non-abelian gauge theory with symmetry group $\mathrm{SU}(3)_c \times \mathrm{SU}(2)_L \times \mathrm{U}(1)_Y$. The particle content of the Standard Model is summarized in Table 2.1.

Gauge bosons (spin 1)	
B	$(\mathbf{1},\mathbf{1})_0$
W	$(\mathbf{1},\mathbf{3})_0$
G	$(\mathbf{8},\mathbf{1})_0$

Fermions (spin 1/2)	
l	$(\mathbf{1},\mathbf{2})_{-1/2}$
e	$(\mathbf{1},\mathbf{1})_{-1}$
q	$(\mathbf{3},\mathbf{2})_{-1/2}$
u	$(\bar{\mathbf{3}},\mathbf{1})_{-1}$
d	$(\bar{\mathbf{3}},\mathbf{1})_{-1}$

Scalars (spin 0)	
H	$(\mathbf{1},\mathbf{2})_{1/2}$

Table 2.1: SM particles and their $\mathrm{SU}(3)_c \times \mathrm{SU}(2)_L \times \mathrm{U}(1)_Y$ representations. We use the following notation: $(\mathrm{SU}(3)_c \text{ representation}, \mathrm{SU}(2)_L \text{ representation})_{\mathrm{U}(1)\text{ hypercharge}}$. For each fermion there are three generations or families, i.e., $l = (l^{(1)}, l^{(2)}, l^{(3)})$, with $\{1,2,3\} = \{e,\mu,\tau\}$.

To compute on-shell scattering amplitudes in the Standard Model, we must specify the interactions between the particles in Table 2.1. In other words, we must define the fundamental contact amplitudes in the theory, which are used to build any n-point amplitude. An important caveat is that the number of contact amplitudes that can theoretically be constructed with

SM particles is infinite. However, since the Standard Model is defined as a renormalizable theory, the only valid amplitudes are those derived from renormalizable interactions in the Lagrangian formalism. These are amplitudes where the coupling constant has a non-negative mass dimension [4]. Other contact amplitudes are not included in the Standard Model and instead they are considered in the context of the Standard Model Effective Field Theory (see Section 2.2).

2.1.1 Contact amplitudes

In this section we list the Standard Model contact amplitudes in the massless limit. Since we require the renormalization of the theory, there are only 3-point and 4-point amplitudes. We begin with those involving gauge bosons. Indices $a, b, ...$ represent the adjoint representation of non-abelian groups, while $i, j, ...$ denote the fundamental representation. We have:

- Three gauge bosons:

$$\mathcal{A}(1_{V_-^a}, 2_{V_-^a}, 3_{V_+^a}) = \frac{g_V}{\sqrt{2}} f^{abc} \frac{\langle 12\rangle^3}{\langle 13\rangle \langle 32\rangle} , \quad \mathcal{A}(1_{V_+^a}, 2_{V_+^a}, 3_{V_-^a}) = \frac{g_V}{\sqrt{2}} f^{abc} \frac{[12]^3}{[13]\,[32]} . \tag{2.1}$$

- One fermion - one antifermion - one gauge boson:

$$\mathcal{A}(1_{\psi^j}, 2_{\bar{\psi}_i}, 3_{V_-^a}) = g_V \frac{\langle 13\rangle^2}{\langle 12\rangle} (T^a)_i^j , \quad \mathcal{A}(1_{\psi^j}, 2_{\bar{\psi}_i}, 3_{V_+^a}) = g_V \frac{[23]^2}{[12]} (T^a)_i^j . \tag{2.2}$$

- Two scalars - one gauge boson:

$$\mathcal{A}(1_{H^j}, 2_{H_i^\dagger}, 3_{V_-^a}) = g_V \frac{\langle 13\rangle \langle 23\rangle}{\langle 21\rangle} (T^a)_i^j , \quad \mathcal{A}(1_{H^j}, 2_{H_i^\dagger}, 3_{V_+^a}) = g_V \frac{[13]\,[23]}{[12]} (T^a)_i^j , \tag{2.3}$$

where g_V is the dimensionless gauge coupling, f^{abc} are the structure constants and T^a are the gauge group generators, normalized so that $\mathrm{Tr}\left[T^a, T^b\right] = \delta^{ab}/2$. We refer to the gauge couplings of $\mathrm{U}(1)_Y$, $\mathrm{SU}(2)_L$ and $\mathrm{SU}(3)_c$ as, respectively, g_1, g_2 and g_3. For $\mathrm{SU}(2)_L$, the structure constants correspond to the Levi-Civita tensor ϵ^{abc} and the generators are $T^a = \sigma^a/2$, with σ^a the Pauli matrices. For $\mathrm{SU}(3)_c$, the structure constants are f^{abc} and the generators are the Gell-Mann matrices λ^a. For the abelian group $\mathrm{U}(1)_Y$ we must replace $(T^a)_i^j \to Y_i \delta_i^j$, with Y_i the hypercharge of particle i.

The relative signs between Eq. (2.2) and Eq. (2.3) are fixed by requiring the proper factorization of 4-point tree-level amplitudes. This is the equivalent of gauge invariance in the Lagrangian approach (see [42]). Finally, note that the first and second amplitudes in Eq. (2.1), Eq. (2.2) and Eq. (2.3) are related by CPT invariance.

There are also Yukawa interactions between fermions and scalars. For one family, we have

$$\mathcal{A}(1_e, 2_{l^i}, 3_{H_j^\dagger}) = y_e \langle 12\rangle \delta_j^i , \qquad \mathcal{A}(1_{\bar{e}}, 2_{\bar{l}_i}, 3_{H^j}) = y_e [12] \delta_i^j , \tag{2.4}$$

$$\mathcal{A}(1_{d_A}, 2_{q_B^i}, 3_{H_j^\dagger}) = y_d \langle 12\rangle \delta_j^i \delta_{AB} , \qquad \mathcal{A}(1_{\bar{d}_A}, 2_{\bar{q}_{i,B}}, 3_{H^j}) = y_d [12] \delta_i^j \delta_{AB} , \tag{2.5}$$

$$\mathcal{A}(1_{u_A}, 2_{q_B^i}, 3_{H^j}) = y_u \langle 12\rangle \epsilon^{ij} \delta_{AB} , \qquad \mathcal{A}(1_{\bar{u}_A}, 2_{\bar{q}_{i,B}}, 3_{H_j^\dagger}) = y_u [12] \epsilon_{ij} \delta_{AB} , \tag{2.6}$$

with y_e, y_d and y_u the dimensionless Yukawa couplings, which can be taken as real for a single fermion family as we will consider here. The generalization to three families is straightforward. Note that we have used $i, j, ...$ for the $\mathrm{SU}(2)_L$ indices and $A, B, ...$ for the $\mathrm{SU}(3)_c$ color indices[1].

Finally, the only non-vanishing 4-point contact amplitude involves four scalars:

$$\mathcal{A}(1_{H^k}, 2_{H^l}, 3_{H_i^\dagger}, 4_{H_j^\dagger}) = \lambda \left(\delta_i^k \delta_j^l + \delta_i^l \delta_j^k\right) \ , \tag{2.7}$$

with λ the 4-scalar coupling, which has mass dimension zero.

It is worth mentioning how the helicities of SM contact amplitudes are fixed by dimensional analysis. For example, 3-vector SM amplitudes can only be $\mathcal{A}(1_{V_-^a}, 2_{V_-^a}, 3_{V_+^a})$ and $\mathcal{A}(1_{V_+^a}, 2_{V_+^a}, 3_{V_-^a})$, as given by Eq. (2.1). The all-plus and all-minus helicity choices are absent in the SM and instead they correspond to non-renormalizable interactions. This structure is hidden when looking at the SM amplitude in terms of momenta and polarization vectors, which is

$$\mathcal{A}(1_{V^a}, 2_{V^b}, 3_{V^c}) = C_{d=0} f_{abc} \left[e_1 e_2 (p_1 e_3 - p_2 e_3) + e_2 e_3 (p_2 e_1 - p_3 e_1) + e_3 e_1 (p_3 e_2 - p_1 e_2)\right] \ , \tag{2.8}$$

as we derived in Section 1.1.2. This highlights the convenience of using the helicity basis for on-shell amplitudes.

An important observation is the absence of a 4-vector contact amplitude. In the Yang-Mills Lagrangian, aside from the cubic interaction $V^2\partial V$ there is a quartic term V^4 that is needed to ensure gauge invariance. When considering on-shell amplitudes, however, the cubic term $V^2\partial V$ already captures all the relevant information [14]. Indeed, the 3-vector on-shell amplitude is a gauge-invariant object that can be used to compute gauge-invariant higher-point amplitudes. Thus, there is no need to include an additional 4-vector contact interaction.

2.1.2 Factorizable amplitudes

Following 1.3.2, we can build higher-point factorizable amplitudes by imposing the correct little-group weights and ensuring proper factorization. For example, we list some 4-point SM amplitudes that will be used in Chapters 4, 5 and 6 of this thesis:

$$\mathcal{A}(1_{G_+^a}, 2_{d_A}, 3_{q_B^i}, 4_{H_j^\dagger}) = -y_d g_3 \delta_j^i \lambda_{AB}^a \frac{[41]^2}{[42]\,[43]} = y_d g_3 \delta_j^i \lambda_{AB}^a \frac{\langle 32\rangle^2}{\langle 12\rangle\,\langle 13\rangle} \ , \tag{2.9}$$

with g_3 and λ^a the $\mathrm{SU}(3)_c$ coupling and generators.

$$\mathcal{A}(1_{W_+^a}, 2_e, 3_{l^i}, 4_{H_j^\dagger}) = y_e g_2 (T^a)_j^i \frac{[21]\,[41]}{[24]\,[23]} = y_e g_2 (T^a)_j^i \frac{\langle 23\rangle\,\langle 43\rangle}{\langle 14\rangle\,\langle 13\rangle} \ , \tag{2.10}$$

with g_2 and T^a the $\mathrm{SU}(2)_L$ coupling and generators.

$$\mathcal{A}(1_{B_+}, 2_e, 3_{l^i}, 4_{H_j^\dagger}) = y_e g_1 \delta_j^i \left(Y_l \frac{[21]\,[41]}{[24]\,[23]} - Y_e \frac{[31]\,[41]}{[34]\,[32]}\right) \ , \tag{2.11}$$

[1] To simplify the notation, we write both covariant and contravariant $\mathrm{SU}(3)_c$ indices as subindices.

with g_1 the $\mathrm{U}(1)_Y$ coupling.

$$\mathcal{A}(1_{B_+}, 2_{H^i}, 3_{W^a_-}, 4_{H^\dagger_j}) = g_1 g_2 Y_H (T^a)^i_j \frac{\langle 23\rangle \langle 43\rangle}{\langle 21\rangle \langle 41\rangle} \ . \tag{2.12}$$

$$\mathcal{A}(1_{B_+}, 2_{l^i}, 3_{W^a_-}, 4_{\bar{l}_j}) = g_1 g_2 Y_l (T^a)^i_j \frac{\langle 23\rangle^2}{\langle 21\rangle \langle 14\rangle} \ . \tag{2.13}$$

We will also require the following 5-point amplitude

$$\mathcal{A}(1_{W^a_+}, 2_{W^b_+}, 3_e, 4_{l^i}, 5_{H^\dagger_j}) = y_e g_2^2 \left((T^a T^b)^i_j \frac{\langle 54\rangle}{\langle 25\rangle \langle 41\rangle} - (T^b T^a)^i_j \frac{\langle 35\rangle}{\langle 32\rangle \langle 51\rangle} \right) \frac{\langle 34\rangle}{\langle 12\rangle} \ . \tag{2.14}$$

By complex-conjugating the above expressions, we obtain the amplitudes for opposite helicities and interchanging particles with antiparticles.

Note that all amplitudes in Eq. (2.9-2.13) have total helicity $h = 0$. Moreover, nearly all 4-point SM amplitudes have $h = 0$, as was pointed out in [52]. The only exception are the $\mathcal{A}(1_e, 2_{l^i}, 3_{u_A}, 4_{q^i_B})$ and $\mathcal{A}(1_d, 2_{q^i}, 3_{u_A}, 4_{q^i_B})$ amplitudes for the scattering of four fermions. These amplitude are proportional to the Yukawa couplings $y_e y_u$ and $y_d y_u$ and have total helicity $h = -2$. In Section 3.4.1, we will use these properties to derive helicity selection rules for the mixing of higher-dimension operators in effective field theories.

2.1.3 Lagrangian formulation

For clarity, let us see the equivalence between our on-shell amplitudes and the usual Lagrangian formulation. The contact amplitudes in Section 2.1.1 can be obtained from the Standard Model Lagrangian[2],

$$\begin{aligned}\mathcal{L}_{\rm SM} = &-\frac{1}{4} W^I_{\mu\nu} W_I^{\mu\nu} - \frac{1}{4} B_{\mu\nu} B^{\mu\nu} - \frac{1}{4} G^a_{\mu\nu} G_a^{\mu\nu} + \sum_{\psi = L_L, e_R, Q_L, u_R, d_R} \left(\bar{\psi} i \gamma^\mu D_\mu \psi\right) \\ &+ \left(D_\mu H\right)^\dagger D^\mu H - \lambda \left(|H|^2 - \frac{v^2}{2} \right)^2 - y_e \left(H^\dagger \bar{e}_R L_L + \bar{L}_L e_R H \right) \\ &- y_d \left(H^\dagger \bar{d}_R Q_L + \bar{Q}_L d_R H \right) - y_u \left(\tilde{H}^\dagger \bar{u}_R Q_L + \bar{Q}_L u_R \tilde{H} \right) \ ,\end{aligned} \tag{2.15}$$

where we have defined $\tilde{H}_i = \epsilon_{ij} H^*_j$, with ϵ_{ij} the totally antisymmetric Levi-Civita tensor and H_j the Higgs doublet. The field-strengths for the gauge fields G^a_μ, W^I_μ and B_μ are

$$G^a_{\mu\nu} = \partial_\mu G^a_\nu - \partial_\mu G^a_\nu + g_3 f^{abc} G^b_\mu G^c_\nu / \sqrt{2} \ , \tag{2.16}$$

$$W^a_{\mu\nu} = \partial_\mu W^a_\nu - \partial_\mu W^a_\nu + g_2 \epsilon^{abc} W^b_\mu W^c_\nu / \sqrt{2} \ , \tag{2.17}$$

$$B_{\mu\nu} = \partial_\mu B_\nu - \partial_\mu B_\nu \ , \tag{2.18}$$

[2]Further details on the Standard Model Lagrangian can be found in standard textbooks on particle physics, such as [4, 53].

where g_2, g_3 are the gauge couplings, and ϵ^{abc}, f^{abc} are the structure constants for the $\mathrm{SU}(2)_L$ and SU(3) gauge groups. The covariant derivative D_μ is given by

$$D_\mu = \partial_\mu - i\frac{g_3}{\sqrt{2}}\lambda^a G^a_\mu - i\frac{g_2}{\sqrt{2}}T^a W^a_\mu - i\frac{g_1}{\sqrt{2}}Y_i B_\mu \ , \tag{2.19}$$

where λ^a and T^a are, respectively, the $\mathrm{SU}(3)_c$ and $\mathrm{SU}(2)_L$ generators and Y_i denotes the hypercharge. The SU(N) generators are normalized so that $\mathrm{Tr}\left[T^a, T^b\right] = \delta^{ab}/2$.

In Eq. (2.15), fermion interactions are expressed in terms of 4-component Dirac spinors. For our purposes and for comparison with Table 2.1, it is convenient to use 2-component Weyl spinors instead. Since we are considering massless fermions, we can write

$$L_L = \begin{pmatrix} l \\ 0 \end{pmatrix} \ , \qquad Q_L = \begin{pmatrix} q \\ 0 \end{pmatrix} \ , \qquad \bar{e}_R = (e, 0) \ , \qquad \bar{d}_R = (d, 0) \ , \qquad \bar{u}_R = (u, 0) \ , \tag{2.20}$$

where l, q, e, d and u are left-handed Weyl spinors with helicity $h = -1/2$. Additional details on the two-component spinor notation can be found in Appendix A.2.

2.2 The on-shell Standard Model Effective Field Theory

The Standard Model can be understood as the low-energy approximation of a more complex theory, whose characteristic energy scale Λ is well above the electroweak scale. At low energies, one can integrate out the heavy degrees of freedom of the complete theory and generate an Effective Field Theory (EFT). This EFT consists of an infinite tower of effective interactions expressed in terms of the lighter degrees of freedom of the theory.

For the case of the Standard Model EFT (SMEFT), one has to consider all the possible (non-renormalizable) interactions of the particles in Table 2.1 and write down the corresponding contact amplitudes. It is convenient to organize the contact amplitudes in terms of the mass dimension of their coupling constants. Couplings with negative mass dimensions come from dimensionless constants suppressed by the energy scale Λ. The greater the negative mass dimension, the more suppressed the interaction. To make this dependence explicit, from now on we adopt the following notation for coupling constants C_d,

$$C_d \ \longrightarrow \ C\Lambda^d \ , \tag{2.21}$$

where C is dimensionless and $[\Lambda] = 1$.

The framework of the SMEFT is particularly useful for parameterizing potential new physics –beyond the Standard Model– in a model-independent manner. Non-renormalizable SMEFT interactions describe deviations from the SM in a systematic way, allowing for a structured analysis of experimental data. We will see an example of this in Chapter 5, where we use the SMEFT to study the phenomenology of lepton flavor violation.

As discussed in Section 2.1, the Standard Model encompasses interactions with couplings of non-negative mass dimension. In contrast, the SMEFT describes interactions among SM

particles with couplings of negative dimension. Then, the basic building blocks of the SMEFT are contact amplitudes with some factors of $1/\Lambda$.

In recent years, on-shell amplitude methods have been widely applied to the study of EFTs and in particular to the task of building a complete basis of interactions for generic theories, including the SMEFT. Some examples include [32, 54–64]. Here we present a simplified discussion, considering only the kinematic structure of the amplitudes and not their color and flavor indices. Using the terminology from [13], these are called "color-stripped" amplitudes.

2.2.1 Contact amplitudes

In the context of the SMEFT, the largest corrections to the Standard Model are expected to be the interactions with the least powers of $1/\Lambda$. This discussion focuses on amplitudes at order $1/\Lambda$ and $1/\Lambda^2$, for any number of particles n and total helicity h. As explained in Section 1.3.1, we can build contact amplitudes using dimensional analysis, locality and little group covariance. Remember that the mass dimension of an amplitude $\mathcal{A}_n$ obeys

$$[\mathcal{A}_n] = 4 - n \ , \tag{2.22}$$

with n the number of scattered particles. Thus, for EFT contact amplitudes at order $1/\Lambda^m$, the mass dimension of the kinematic piece of the amplitude is $4 - n + m$. Knowing this, we can write down the building blocks of the SMEFT.

Order $1/\Lambda$

Table 2.2 summarizes the possible contact amplitudes at order $1/\Lambda$. For each $\mathcal{A}_n$, we express the allowed kinematic factors in terms of angle and square spinor products. Each kinematic factor corresponds to an amplitude with a certain helicity h. Amplitudes with $n > 5$ are not present because they would have negative powers of momenta, which is ruled out by locality. Note also that $\langle..\rangle\,[..]$ (with $h = 0$) is not a valid spinor structure for $n = 3$, since 3-point amplitudes cannot have a mix of angle and square spinors (see Section 1.2).

	$[\mathcal{A}_n]$	[kinematic factor]	Possible spinor structures
$n = 3$	1	2	$\langle..\rangle^2$, $[..]^2$ $(h = \pm 2)$
$n = 4$	0	1	$\langle..\rangle$, $[..]$ $(h = \pm 1)$
$n = 5$	-1	0	1 $(h = 0)$

Table 2.2: Allowed spinor structures for contact amplitudes at order $1/\Lambda$.

Taking into account the spinor structures in Table 2.2, we can build the following amplitudes:

- $n = 3$: There are two possible amplitudes with $h = -2$,

$$\mathcal{A}_{V^2H}(1_{V_-}, 2_{V_-}, 3_H) = \frac{C_{V^2H}}{\Lambda} \langle 12\rangle^2 \ , \tag{2.23}$$

$$\mathcal{A}_{V\psi^2}(1_{V_-}, 2_\psi, 3_\psi) = \frac{C_{V\psi^2}}{\Lambda} \langle 12\rangle \langle 13\rangle \ . \tag{2.24}$$

- $n = 4$: There is one $h = -1$ amplitude,

$$\mathcal{A}_{\psi^2H^2}(1_\psi, 2_\psi, 3_H, 4_H) = \frac{C_{\psi^2H^2}}{\Lambda} \langle 12\rangle \ . \tag{2.25}$$

- $n = 5$: There is one $h = 0$ amplitude,

$$\mathcal{A}_{H^5}(1_\phi, 2_\phi, 3_\phi, 4_\phi, 5_\phi) = \frac{C_{H^5}}{\Lambda} \ . \tag{2.26}$$

However, for the SM particles listed in Table 2.1, most of these amplitudes are forbidden due to the SM charges. In fact, there is only one contact amplitude in the SMEFT at order $1/\Lambda$, up to complex-conjugation,

$$\mathcal{A}_{\psi^2H^2}(1_\psi, 2_\psi, 3_H, 4_H) = \frac{C_{\psi^2H^2}}{\Lambda} \langle 12\rangle \ , \tag{2.27}$$

where ψ is a lepton. Note that this amplitude violates lepton number conservation by two units.

Order $1/\Lambda^2$

The possible amplitudes at order $1/\Lambda^2$ are shown in Table 2.3. In this case locality allows for amplitudes up to $n = 6$. The structures $\langle..\rangle^2 [..]$ and $\langle..\rangle [..]^2$ are not present in $n = 3$ because they mix square and angle spinor products.

	$[\mathcal{A}_n]$	[kinematic factor]	Possible spinor structure
$n = 3$	1	3	$\langle..\rangle^3$, $[..]^3$ $(h = \pm 3)$
$n = 4$	0	2	$\langle..\rangle^2$, $[..]^2$ $(h = \pm 2)$; $\langle..\rangle [..]$ $(h = 0)$
$n = 5$	-1	1	$\langle..\rangle$, $[..]$ $(h = \pm 1)$
$n = 6$	-2	0	1 $(h = 0)$

Table 2.3: Allowed spinor structures for contact amplitudes at order $1/\Lambda^2$.

Within the SMEFT, we have the following amplitudes:

- $n = 3$: There is one possible amplitude,

$$\mathcal{A}_{V^3}(1_{V_-^a}, 2_{V_-^b}, 3_{V_-^c}) = \frac{C_{V^3}}{\Lambda^2} f^{abc} \langle 12\rangle \langle 23\rangle \langle 31\rangle \ . \tag{2.28}$$

- $n = 4$: There are three distinct amplitudes for $h = -2$,

$$\mathcal{A}_{V^2H^2}(1_{V_-}, 2_{V_-}, 3_H, 4_{H^\dagger}) = \frac{C_{V^2H^2}}{\Lambda^2} \langle 12\rangle^2 \ , \tag{2.29}$$

$$\mathcal{A}_{V\psi^2H}(1_{V_-}, 2_\psi, 3_\psi, 4_{H^\dagger}) = \frac{C_{V\psi^2H}}{\Lambda^2} \langle 12\rangle \langle 13\rangle \ , \tag{2.30}$$

$$\mathcal{A}_{\psi^4}(1_\psi, 2_\psi, 3_\psi, 4_\psi) = \left(C_{\psi^4} \langle 12\rangle \langle 34\rangle + C'_{\psi^4} \langle 13\rangle \langle 24\rangle\right) \frac{1}{\Lambda^2} \ . \tag{2.31}$$

Additionally, there are three amplitudes for $h = 0$,

$$\mathcal{A}_{\Box H^4}(1_H, 2_H, 3_{H^\dagger}, 4_{H^\dagger}) = \left(C_{\Box H^4} \langle 12\rangle [12] + C'_{\Box H^4} \langle 13\rangle [13]\right) \frac{1}{\Lambda^2} \ , \tag{2.32}$$

$$\mathcal{A}_{\psi\bar{\psi}H^2}(1_\psi, 2_{\bar{\psi}}, 3_H, 4_{H^\dagger}) = \frac{C_{\psi\bar{\psi}H^2}}{\Lambda^2} \langle 13\rangle [23] \ , \tag{2.33}$$

$$\mathcal{A}_{\psi^2\bar{\psi}^2}(1_\psi, 2_\psi, 3_{\bar{\psi}}, 4_{\bar{\psi}}) = \frac{C_{\psi^2\bar{\psi}^2}}{\Lambda^2} \langle 12\rangle [34] \ . \tag{2.34}$$

- $n = 5$: Only one $h = -1$ amplitude exists,

$$\mathcal{A}_{\psi^2H^3}(1_\psi, 2_\psi, 3_H, 4_H, 5_{H^\dagger}) = \frac{C_{\psi^2H^3}}{\Lambda^2} \langle 12\rangle \ . \tag{2.35}$$

- $n = 6$: Only one $h = 0$ amplitude exists,

$$\mathcal{A}_{H^6}(1_H, 2_H, 3_H, 4_{H^\dagger}, 5_{H^\dagger}, 6_{H^\dagger}) = \frac{C_{H^6}}{\Lambda^2} \ . \tag{2.36}$$

2.2.2 Lagrangian formulation

In the context of an EFT, contact amplitudes are directly equivalent to effective operators in the Lagrangian approach. In this language, the effective Lagrangian can be thought of as an expansion in effective operators of some high-energy theory with energy scale Λ. For the SMEFT, we can write

$$\mathcal{L}_{\text{SMEFT}} = \mathcal{L}_{\text{SM}} + \frac{1}{\Lambda} \sum_{\mathcal{O}_5} C_{\mathcal{O}_5} \mathcal{O}_5 + \frac{1}{\Lambda^2} \sum_{\mathcal{O}_6} C_{\mathcal{O}_6} \mathcal{O}_6 + \dots \ , \tag{2.37}$$

where $\mathcal{O}_n$ are operators of mass dimension n for $n > 4$, also known as higher-dimension operators. The dimensionless coefficients $C_{\mathcal{O}_n}$ in front of the operators are called Wilson coefficients.

Amplitudes at order $1/\Lambda$ correspond to dimension-5 operators. In the SMEFT, the only amplitude at this order is given in Eq. (2.27). It corresponds to the following interaction term:

$$\mathcal{L} \supset \frac{C_{\psi^2H^2}}{\Lambda} \left(\overline{L_L^c}^k L_L^i\right) \epsilon_{ij}\epsilon_{km} H^j H^m \tag{2.38}$$

which generates the Majorana neutrino masses after spontaneous symmetry breaking. We define $L_L^c \equiv C\bar{L}_L^T$, where C is the charge conjugation matrix satisfying $C\gamma^\mu C^{-1} = -(\gamma^\mu)^T$.

At the next order $1/\Lambda^2$ we find dimension-6 operators. It can be shown that there are 59 linearly independent operators of dimension 6 in the SMEFT [65], not counting hermitian conjugations and fermion generation indices. For instance, the 3-point amplitude in Eq. (2.28) corresponds to the following operators:

$$\mathcal{L} \supset f^{abc} V_\nu^{a,\mu} V_\rho^{b,\nu} V_\mu^{c,\rho} \ , \quad \mathcal{L} \supset f^{abc} \widetilde{V}_\nu^{a,\mu} V_\rho^{b,\nu} V_\mu^{c,\rho} \ . \tag{2.39}$$

Appendix B provides a comprehensive list of all dimension-6 operators in the Warsaw basis [65] and the exact relation between those operators and the on-shell amplitudes of the previous section.

2.3 Conclusions of the chapter

In this chapter, we have studied the Standard Model (SM) and the Standard Model Effective Field Theory (SMEFT) through the framework of on-shell scattering amplitudes. In particular, we have explored how these theories are defined by their particle content (Table 2.1) and the contact on-shell amplitudes describing particle interactions.

For the SM, we have presented the contact amplitudes corresponding to renormalizable interactions, which serve as the theory's building blocks. We have found that only certain helicity choices are allowed for some contact amplitudes. This feature is easily observed when working with on-shell amplitudes in the helicity basis, but is obscured in the traditional Lagrangian approach.

For the SMEFT, we have classified contact amplitudes based on their suppression by powers of the new physics scale Λ. We have explicitly built all color-stripped amplitudes at orders $1/\Lambda$ and $1/\Lambda^2$, which correspond to dimension-5 and dimension-6 operators.

We have emphasized the power and efficiency of the on-shell formalism in analyzing both SM interactions and extensions via effective field theories. This provides the foundation for the on-shell renormalization methods discussed in Chapter 3.

Chapter 3

SMEFT renormalization: the on-shell way

In this chapter we apply on-shell amplitude methods to the computation of anomalous dimensions in effective field theories, focusing on the SMEFT at order $1/\Lambda^2$. We include some of the main results from [1].

Until now we have only considered tree-level scattering, so the next step is introducing loops. Within perturbative quantum field theory, tree-level amplitudes receive radiative corrections from loop processes. These corrections are suppressed by a factor $1/16\pi^2$ for each loop, meaning that higher-order terms correspond to diagrams with more loops. Any loop diagram involves an integral over the loop momentum k^μ, which can diverge in the ultraviolet region, when $k \to \infty$. Through a process known as renormalization, these divergences are addressed by absorbing them into redefinitions of physical parameters, so that all the observable quantities are finite. The subject of renormalization is covered in every textbook on quantum field theory, see for example [4, 53, 66].

A feature of renormalization is that it induces the running of coupling constants with the energy scale. In a theory with effective operators $\mathcal{O}_i$, the running of their corresponding Wilson coefficients $C_{\mathcal{O}_i}$ is given by the anomalous dimension γ_i, defined as

$$\gamma_i \equiv \frac{d\, C_{\mathcal{O}_i}}{d \ln \mu} = \sum_j \gamma_{ij}\, C_{\mathcal{O}_j} \ , \tag{3.1}$$

with μ the renormalization scale. Operators of the same dimension mix with each other, so we can write γ_i as a sum of other couplings $C_{\mathcal{O}_j}$ times a coefficient γ_{ij}, which constitutes the anomalous dimension matrix for the mixing of $\mathcal{O}_j$ into $\mathcal{O}_i$.

At the phenomenological level, the computation of γ_i in the SMEFT is essential for understanding which higher-dimension operators contribute to a particular physical observable. The corresponding Wilson coefficients can be constrained by comparing the theoretical predictions with experimental measurements. This serves as an excellent tool for searching for new physics beyond the Standard Model. We will see some applications of this in the context of several lepton flavor violating processes in Chapter 5.

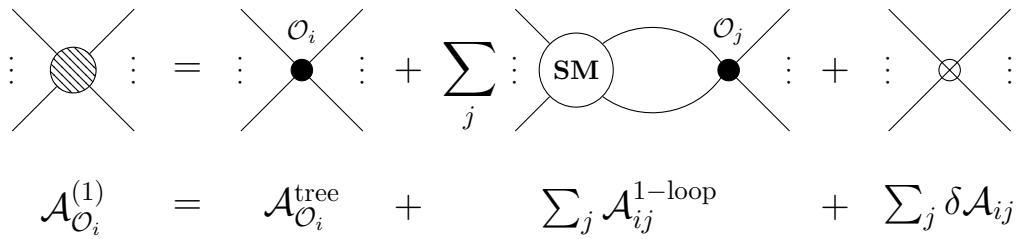

Figure 3.1: *Diagrams for the 1-loop amplitude* $\mathcal{A}^{(1)}_{\mathcal{O}_i}$. $\mathcal{A}_{\mathcal{O}_i}$ *is the tree-level contact amplitude associated with the operator* $\mathcal{O}_i$. $\mathcal{A}^{1\text{-loop}}_{ij}$ *is the 1-loop amplitude generated by an insertion of the* $\mathcal{A}_{\mathcal{O}_j}$ *contact interaction.* $\delta\mathcal{A}_{ij}$ *are the counterterms.*

Our discussion is organized as follows: Section 3.1 presents the basics of renormalization. In Section 3.2, we use on-shell amplitude techniques to derive three different methods to compute anomalous dimensions for mixings at order $1/\Lambda^2$. The effect of IR divergences is analyzed in Section 3.3. Section 3.4 includes additional remarks regarding topics such as helicity selection rules, mixings at order $1/\Lambda$ and 2-loop renormalizations. Finally, we conclude in Section 3.5.

3.1 Review of renormalization

Let us consider a 4-point tree-level contact amplitude $\mathcal{A}_{\mathcal{O}_i}$ corresponding to the operator $\mathcal{O}_i$. An amplitude with the same external legs can be generated at one loop, as shown in the third diagram of Figure 3.1. One vertex corresponds to the contact interaction $\mathcal{A}_{\mathcal{O}_j}$ associated with the operator $\mathcal{O}_j$, while the other vertex corresponds to marginal interactions. We will call this amplitude $\mathcal{A}^{1\text{-loop}}_{ij}$, and we are interested in the cases where dim $(\mathcal{O}_j)$ = dim $(\mathcal{O}_i)$. The full 1-loop amplitude $\mathcal{A}^{(1)}_{\mathcal{O}_i}$ is equal to

$$\mathcal{A}^{(1)}_{\mathcal{O}_i} = \mathcal{A}_{\mathcal{O}_i} + \sum_j \mathcal{A}^{1\text{-loop}}_{ij} + \sum_j \delta\mathcal{A}_{ij} \ , \tag{3.2}$$

where the summation over j is a summation over all possible $\mathcal{A}_{\mathcal{O}_j}$ that generate $\mathcal{A}_{\mathcal{O}_i}$ at one loop. $\delta\mathcal{A}_{ij}$ is a counterterm that must be introduced to cancel the ultraviolet divergence of the loop amplitude. This expression is depicted in Figure 3.1.

The next step is to consider the Passarino-Veltman (PV) decomposition of $\mathcal{A}^{1\text{-loop}}_{ij}$. Any 1-loop amplitude has a decomposition given by [67]

$$\mathcal{A}^{1\text{-loop}} = \sum_a C^{(a)}_2 I^{(a)}_2 + \sum_b C^{(b)}_3 I^{(b)}_3 + \sum_c C^{(c)}_4 I^{(c)}_4 + R \ , \tag{3.3}$$

where I_m are master scalar integrals with m propagators and the coefficients C_m are rational functions of the kinematic variables $\langle ij\rangle$ and $[ij]$. The master integrals are defined as

$$I_m = (-1)^m \tilde{\mu}^{4-D} \int \frac{d^D\ell}{i(2\pi)^D} \frac{1}{\ell^2(\ell-P_1)^2(\ell-P_1-P_2)^2\cdots(\ell-\sum_{n=1}^{m-1}P_n)^2} \ , \tag{3.4}$$

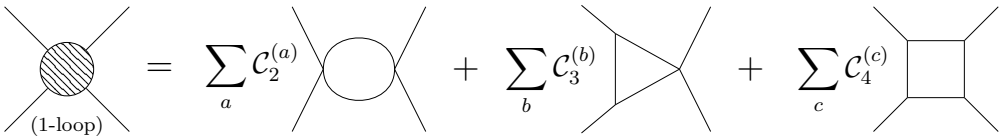

Figure 3.2: *Passarino-Veltman decomposition of a 1-loop amplitude. Any 1-loop amplitude can be written as a sum of master integrals I_2, I_3 and I_4 times some coefficients. $C_2^{(a)}$ correspond to bubbles, $C_3^{(b)}$ to triangles and $C_4^{(c)}$ to boxes.*

where P_n are sums of external momenta. We have used dimensional regularization with $D = 4 - 2\epsilon$, and $\tilde{\mu}$ is some emerging energy scale. The first three pieces in Eq. (3.3) are called, respectively, bubbles, triangles and boxes due to the topology of the master integrals. The last term R corresponds to rational functions of the kinematic invariants, and it will play no role in our discussion. A diagrammatic example of the Passarino-Veltman decomposition is shown in Figure 3.2.

One can check that I_2 is UV divergent, while I_3 and I_4 are UV finite. Indeed, the regularized bubble integral is given by

$$I_2^{(a)} = \frac{1}{16\pi^2}\left[\frac{1}{\epsilon} + \ln\left(\frac{\tilde{\mu}^2}{-P_a^2}\right) + \text{ finite terms}\right] , \tag{3.5}$$

with P_a the sum of external momenta entering the bubble. Notice how the UV divergent term $1/\epsilon$ is accompanied by a logarithm of the energy scale $\tilde{\mu}$, as is customary in dimensional regularization.

Using the PV decomposition, the 1-loop amplitude from Eq. (3.2) can be written as

$$\mathcal{A}_{ij}^{\text{1-loop}} = \frac{1}{16\pi^2}\sum_a C_2^{(a)}\left[\frac{1}{\epsilon} + \ln\left(\frac{\tilde{\mu}^2}{-P_a^2}\right) + \text{ finite terms}\right] , \tag{3.6}$$

where the summation goes over all the bubble integrals with an insertion of $\mathcal{A}_{\mathcal{O}_j}$ that generate an amplitude proportional to $\mathcal{A}_{\mathcal{O}_i}$.

Although $\mathcal{A}_{ij}^{\text{1-loop}}$ is UV divergent, the full physical amplitude $\mathcal{A}_{\mathcal{O}_i}^{(1)}$ must be finite. For that reason we must add a counterterm $\delta\mathcal{A}_{ij}$ that cancels the divergence of $\mathcal{A}_{ij}^{\text{1-loop}}$. There are several ways to define the counterterm, but for clarity we choose $\delta\mathcal{A}$ such that $\mathcal{A}_{\mathcal{O}_i}^{(1)} = \mathcal{A}_{\mathcal{O}_i}$ at momentum $P_a^2 = -\mu^2$. Using this prescription, the counterterm can be written as

$$\delta\mathcal{A}_{ij} = -\frac{1}{16\pi^2}\sum_a C_2^{(a)}\left[\frac{1}{\epsilon} + \ln\left(\frac{\tilde{\mu}^2}{\mu^2}\right) + \text{ finite terms}\right] , \tag{3.7}$$

with μ some arbitrary energy scale. It is convenient to choose $\mu \sim \tilde{\mu}$, so that logarithms of $\tilde{\mu}/\mu$ are small. Finally, the renormalized amplitude is

$$\mathcal{A}_{\mathcal{O}_i}^{(1)} = \mathcal{A}_{\mathcal{O}_i} + \frac{1}{16\pi^2}\sum_a C_2^{(a)} \ln\left(\frac{\mu^2}{-P_a^2}\right) . \tag{3.8}$$

This amplitude must obey the Callan-Symanzik equation [68, 69],

$$\left[\mu\frac{\partial}{\partial\mu}+\sum_{\lambda}\beta_{\lambda}^{(1)}\frac{\partial}{\partial\lambda}+\gamma_{i}^{(1)}\right]\mathcal{A}_{\mathcal{O}_i}^{(1)}=0\ , \tag{3.9}$$

where $\beta_{\lambda}^{(1)}$ is the 1-loop beta function for the marginal coupling λ and γ_i is the 1-loop anomalous dimension associated with $\mathcal{A}_{\mathcal{O}_i}$. At first order, the anomalous dimension is related to the counterterm $\delta\mathcal{A}_{ij}$ by [66]

$$\gamma_i\mathcal{A}_{\mathcal{O}_i}=-\mu\frac{\partial}{\partial\mu}\sum_j C_{\mathcal{O}_i}\delta\mathcal{A}_{ij}\ . \tag{3.10}$$

Using our result Eq. (3.7) for the counterterm, we have

$$-\mu\frac{\partial}{\partial\mu}C_{\mathcal{O}_i}\delta\mathcal{A}_{ij}=-\frac{C_{\mathcal{O}_i}}{8\pi^2}\sum_a C_2^{(a)}\ . \tag{3.11}$$

Naively we could just associate this quantity to the anomalous dimension, but that would not be accurate. First, we have to take into account a subtlety involving "massless" bubble integrals, which are those $I_2^{(a)}$ with $P_a^2=0$. Massless bubbles do not contribute to the PV expansion because they are dimensionless and vanish. This comes from a cancellation between IR and UV divergences in dimensional regularization when we set $\mu=\mu_{UV}=\mu_{\rm IR}$, so the logarithm $\ln(\mu_{UV}/\mu_{\rm IR})$ is zero. The terms proportional to $\ln(\mu_{UV})$ in massless bubbles must be included in the calculation since they give an extra contribution to γ_i. To account for these extra terms, we must compute the IR divergences of the amplitude and subtract them. Doing that, Eq. (3.10) becomes

$$\gamma_i^{(1)}\mathcal{A}_{\mathcal{O}_i}=-\sum_j\left(\frac{C_{\mathcal{O}_i}}{8\pi^2}\sum_a C_2^{(a)}-\gamma_{\rm IR}^{ij}\mathcal{A}_{\mathcal{O}_i}\right)\ . \tag{3.12}$$

Equivalently, we can write

$$\gamma_i^{(1)}\mathcal{A}_{\mathcal{O}_i}=\sum_j\gamma_{ij}^{(1)}C_{\mathcal{O}_j}\mathcal{A}_{\mathcal{O}_i}\ ,\quad\text{with}\quad\gamma_{ij}^{(1)}\mathcal{A}_{\mathcal{O}_i}=\frac{C_{\mathcal{O}_i}}{C_{\mathcal{O}_j}}\sum_a\frac{C_2^{(a)}}{8\pi^2}-\gamma_{\rm IR}^{ij}\frac{\mathcal{A}_{\mathcal{O}_i}}{C_{\mathcal{O}_j}}\ , \tag{3.13}$$

where we have used the definition of the anomalous dimension matrix γ_{ij} in Eq. (3.1).

The term $\gamma_{\rm IR}^{ij}$ includes the contributions from IR divergences, which are also proportional to the tree-level amplitude. The anomalous dimension gets simplified in cases where IR divergences are absent. For example, $\gamma_{\rm IR}^{ij}=0$ for the renormalization of $\mathcal{A}_{\mathcal{O}_i}$ by another amplitude $\mathcal{A}_{\mathcal{O}_j}$ with different number of particles, helicities or species. Other examples are renormalizations where both $\mathcal{A}_{\mathcal{O}_i}$ and $\mathcal{A}_{\mathcal{O}_j}$ are 4-point contact amplitudes, since massless topologies are absent in those theories. We will first focus on the case where $\gamma_{\rm IR}^{ij}=0$ and leave the discussion of IR divergences for Section 3.3.

3.2 Renormalization with on-shell amplitude methods

From Eq. (3.13) we see that, in cases where IR divergences are absent, the 1-loop anomalous dimension $\gamma_{ij}^{(1)}$ can be computed solely from the bubble coefficients C_2. One of the most efficient ways of obtaining these coefficients is by using the so-called generalized unitarity method [11, 12]. This method allows us to reconstruct loop amplitudes without explicitly carrying out loop integrals by applying unitarity cuts.

3.2.1 Generalized unitarity method

Here we briefly introduce the basics of generalized unitarity. More details can be found in [11, 12, 14]. A unitarity m-cut is the operation of "cutting" a loop amplitude by putting m propagators on shell. As a prescription, we use the Cutkosky rule [70] of replacing the propagator $(\ell - P)^{-2}$ by a delta function $\delta^+((\ell - P)^2)$, where the $+$ superscript indicates that we select the positive energy solution. After putting the particles on shell, we have to integrate over the possible four-momenta of the cut propagators. Up to normalization, the m-cut of an amplitude $\mathcal{A}$ is

$$\text{Cut}_m[\mathcal{A}] \sim \prod_i \int d^4\ell_i \; \delta^+((\ell_i - P_i)^2) \; \delta^4(*) \; \mathcal{A}_i \; , \tag{3.14}$$

with $i = 1, ..., m$. ℓ_i are the four-momenta of the cut propagators and $\mathcal{A}_i$ are the remaining subamplitudes after the cut. $\delta^4(*)$ imposes momentum conservation at each subamplitude.

The generalized unitarity method is the procedure of building a loop amplitude from its unitarity cuts. The advantage of this method is that, in general, cutting a loop amplitude is easier than computing the amplitude itself. This is because the unitarity cut of an amplitude is equal to a product of lower-loop subamplitudes, which are simpler to compute, integrated over a phase-space. In order to see how this works, let us write down again the PV expansion of a 1-loop amplitude,

$$\mathcal{A}^{\text{1-loop}} = \sum_a C_2^{(a)} I_2^{(a)} + \sum_b C_3^{(b)} I_3^{(b)} + \sum_c C_4^{(c)} I_4^{(c)} + R \; . \tag{3.15}$$

Up to rational terms, the amplitude is completely determined by its coefficients C_m, which can be obtained from unitarity cuts. At one loop, the computation of unitarity cuts is remarkably simple, since we only have to do a phase-space integration of a product of tree-level amplitudes. The usual procedure for reconstructing $\mathcal{A}^{\text{1-loop}}$ is the following:

- From the definition of the master integrals I_m, it is trivial to see that $\text{Cut}_n[I_m] = 0$ for $n > m$, since there are not enough propagators to cut. This implies that $\text{Cut}_4[\mathcal{A}^{\text{1-loop}}]$ only gets contributions from boxes. Thus, we can obtain all the box coefficients $C_4^{(c)}$ by computing all possible 4-cuts of the 1-loop amplitude.

- Next, we consider 3-cuts of the amplitude. The triangle coefficients $C_3^{(b)}$ cannot be obtained as easily as $C_4^{(c)}$, because $\text{Cut}_3[\mathcal{A}^{\text{1-loop}}]$ includes contributions from both box and triangle integrals. However, since we have previously determined the box coefficients with 4-cuts, the $C_3^{(b)}$ coefficients can be unambiguously determined from all possible 3-cuts.

- Finally, $\text{Cut}_2[\mathcal{A}^{\text{1-loop}}]$ gets contributions from all the integrals: bubbles, triangles and boxes. Once we have obtained the box and triangle coefficients, we can determine all the possible $C_2^{(a)}$ from the 2-cuts of the amplitude.

Finally, let us briefly comment on the rational terms R of the 1-loop amplitude. These terms are not included in the generalized unitarity method, since they cannot be obtained from any unitarity cuts. There are several ways to compute R, but they are usually quite involved and go beyond the scope of this work. For a discussion on this topic, see [71–73]. Luckily for us, rational terms can be altogether ignored in our analysis, since they do not contribute to the anomalous dimensions in Eq. (3.13).

The generalized unitarity method gives us a recipe to systematically obtain the C_2 coefficients of a 1-loop amplitude. If we apply it to the amplitude $\mathcal{A}_{ij}^{\text{1-loop}}$ in Eq. (3.2), we can calculate the 1-loop anomalous dimensions $\gamma_{ij}^{(1)}$ (modulo IR divergences). This is a valid procedure. However, it can be quite cumbersome to obtain all the box and triangle coefficients in order to determine the bubble ones. Ideally, we would like to bypass the computation of C_4 and C_3 to derive the C_2 coefficients directly. We will present three different methods for achieving this in the following subsections.

3.2.2 Method I: γ_{ij} from amplitude 2-cuts

As we have just seen, there is generally no one-to-one correspondence between 2-cuts of a 1-loop amplitude and the bubble coefficients C_2, because 2-cuts receive additional contributions from triangle and box integrals. However, we will show that for amplitudes at order $1/\Lambda^2$ in the SMEFT, the bubble coefficients can be obtained directly from 2-cuts. First we present the final expression for the 1-loop anomalous dimensions, which we will prove later. For amplitudes without IR divergences at order $1/\Lambda^2$, Eq. (3.13) can be rewritten as [1]

$$\gamma_{ij}\mathcal{A}_{\mathcal{O}_i}(1,2,...,n) = \\ -\frac{1}{4\pi^3}\frac{C_{\mathcal{O}_i}}{C_{\mathcal{O}_j}}\int d\text{LIPS}\sum_{\substack{\text{ext. legs}\\ \text{distrib.}}}\sum_{\ell_1,\ell_2}\sigma_{\ell_1\ell_2}\widehat{\mathcal{A}}_{\mathcal{O}_j}(...,\ell_1,\ell_2)\times\mathcal{A}_{\text{SM}}(-\ell_2,-\ell_1,...)\,, \tag{3.16}$$

with no summation over i,j. In the right-hand side (RHS) we have a summation over the 2-cuts of the amplitude $\mathcal{A}_{ij}^{\text{1-loop}}$. For each cut, we must identify the tree-level subamplitudes $\widehat{\mathcal{A}}_{\mathcal{O}_j}$ and $\mathcal{A}_4$. $\widehat{\mathcal{A}}_{\mathcal{O}_j}$ is an $m\geq 4$-point amplitude that contains the contact amplitude $\mathcal{A}_{\mathcal{O}_j}$, of order $1/\Lambda^2$. $\mathcal{A}_{\text{SM}}$ is an $m'\geq 4$-point amplitude of order Λ^0, i.e., containing only relevant and marginal couplings. Clearly, $n=m+m'-4$. The dots ... in the arguments of $\widehat{\mathcal{A}}_{\mathcal{O}_j}$ and $\mathcal{A}_4$ correspond to the external legs $(1,2,...,n)$, that are distributed between the two subamplitudes[1]. There is a summation over the possible distributions of the external legs, which is equivalent to a summation over the possible 2-cuts of the amplitude. Notice the absence of 3-point subamplitudes in Eq. (3.16), since they would lead to massless bubbles that vanish in dimensional regularization. This reduces the number of 2-cuts that we must compute and simplifies the γ_{ij} calculation.

[1] If the order of the external particles in the RHS of Eq. (3.16) is different than the order in the left-hand side (LHS), a minus sign must be included for each pair of exchanged fermions.

The integral in the RHS of Eq. (3.16) spans the Lorentz-Invariant Phase Space (LIPS) of the cut momenta ℓ_1 and ℓ_2. It is defined as

$$\int d\text{LIPS} = \int d^4\ell_1 d^4\ell_2\, \delta^+(\ell_1^2)\delta^+(\ell_2^2)\delta^{(4)}(*)\,, \tag{3.17}$$

where $\delta^4(*)$ imposes momentum conservation at both subamplitudes. The integral is normalized so that $\int d\text{LIPS} = \pi/2$. Eq. (3.16) includes a sum $\sum_{\ell_1,\ell_2}$ over all the possible internal states with momentum ℓ_1 and ℓ_2. A symmetry factor $1/2$ must be included when the two internal particles are indistinguishable. Since we are using an all-incoming notation for the amplitudes, the internal states have negative momenta in one of the subamplitudes. They also carry helicity and all other quantum numbers with an opposite sign. The factor $\sigma_{\ell_1\ell_2}$ is defined as $\sigma_{\ell_1\ell_2} = i^{F[\ell_1,\ell_2]}$, where $F[\ell_1,\ell_2]$ counts the number of fermions in the list $\{\ell_1,\ell_2\}$. This term arises from our conventions on fermion ordering, as we detail in Appendix A.3.

Eq. (3.16) has a surprisingly simple structure because the triangle and box contributions to the 2-cut cancel out at order $1/\Lambda^2$. In Appendix C we prove this cancellation explicitly for the cases where $n_i - n_j \equiv \Delta n < 2$. The main idea is the following: we are considering processes without IR divergences. These IR divergences can only arise from triangle and box integrals, so they must cancel each other. This cancellation ensures that the total contribution of triangles and boxes to the 2-cuts is also zero.

The proof of Eq. (3.16) for a generic Δn is more complex. We will use the results of [26], where the authors derived an expression for the anomalous dimensions in terms of unitarity cuts of form factors. In our particular case, their expression reads

$$\gamma_{ij}\, F_{\mathcal{O}_i}(1,2,...,n) = -\frac{1}{4\pi^3}\int d\text{LIPS} \sum_{\substack{\text{ext. legs}\\ \text{distrib.}}} \sum_{\ell_1,\ell_2} \sigma_{\ell_1\ell_2}\widehat{F}_{\mathcal{O}_j}(...,\ell_1,\ell_2)\times \mathcal{A}_{\text{SM}}(-\ell_2,-\ell_1,...)\ , \tag{3.18}$$

where γ_{ij} is the anomalous dimension for the mixing of the form factor $F_{\mathcal{O}_j}$ into $F_{\mathcal{O}_i}$. Form factors are matrix elements between an operator and on-shell states, defined as

$$F_{\mathcal{O}_i}(1,2,...,n) \equiv \langle 0|\mathcal{O}_i|p_1,p_2,...p_n\rangle\ , \tag{3.19}$$

with non-zero total momentum $p_1+p_2+...+p_n \equiv Q \neq 0$. In Eq. (3.18), $\widehat{F}_{\mathcal{O}_j}$ is a $m \geq 3$-point form factor, which contains the contact form factor $F_{\mathcal{O}_j}$. Note that, contrary to what happened in Eq. (3.16), there are contributions from 3-point form factors. This is because, for $Q \neq 0$, these terms are not 2-cuts of massless bubbles, and thus they do not vanish.

We postpone the derivation of Eq. (3.18) to Section 3.2.4, but for the moment we will use it to prove the validity of Eq. (3.16). In the limit $Q \to 0$, form factors and amplitudes obey the following relation

$$\frac{C_{\mathcal{O}_i}}{\Lambda^2} F_{\mathcal{O}_i}(1,2,...,n) \to \mathcal{A}_{\mathcal{O}_i}(1,2,...,n)\ . \tag{3.20}$$

In this limit, it is easy to see that Eq. (3.18) matches Eq. (3.16), except for the presence of 2-cuts involving 3-point form factors. As we mentioned before, there are no terms with 3-point

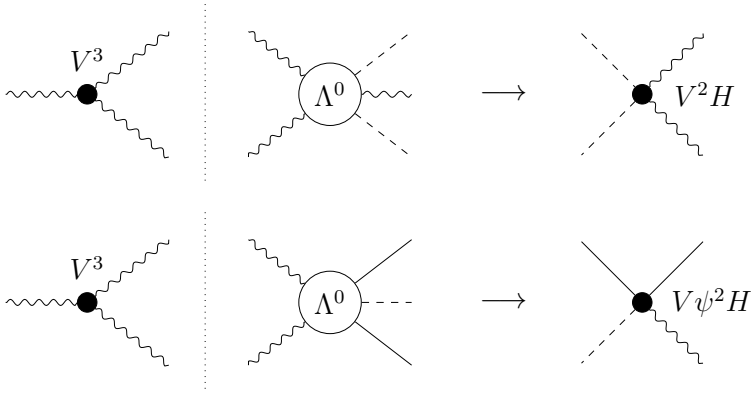

Figure 3.3: *Diagrams for the 1-loop renormalization of $F_{V^2H^2}$ and $F_{V\psi^2H}$ by F_{V^3}. These are the only mixings involving 3-point form factors at order $1/\Lambda^2$.*

subamplitudes in Eq. (3.16) because they vanish. In order to prove Eq. (3.16), we have to check that terms with 3-point form factors also vanish in Eq. (3.18). This is not generally true[2], but we are only interested in amplitudes at order $1/\Lambda^2$ in the SMEFT.

Recalling the contact amplitudes from Section 2.2.1, the only 3-point form factor at order $1/\Lambda^2$ is the one involving three vector bosons, namely F_{V^3}. This form factor contributes to the renormalization of two other form factors: $F_{V^2H^2}$ and $F_{V\psi^2H}$, via the 2-cuts shown in Figure 3.3. To complete the proof of Eq. (3.16) we must show that those cuts vanish. Indeed, since $\Delta n = 1$ for both renormalizations, we can use the result in Appendix C. The 2-cuts of boxes and triangles cancel each other, so the overall 2-cut only picks up the bubble terms. For 3-point factors in the limit $Q \to 0$, this is the 2-cut of a massless bubble integral, which is zero[3]. We conclude that Eq. (3.16) is correct.

Several examples of the usage of Eq. (3.16) can be found in Chapter 4. There, we compute the 1-loop anomalous dimension for mixings of dipole amplitudes in the SMEFT.

3.2.3 Method II: γ_{ij} from momentum deformation

In addition to Eq. (3.16), there is a more general procedure to compute the bubble coefficients from 2-cuts. This method was presented in [74] and it uses the technology of momentum deformations or shifts, which we introduced in Section 1.3.2.

The main idea is the following: the 2-cut of a 1-loop amplitude generally receives contributions from bubbles, triangles and boxes. Given the definition of the master integrals I_n, the terms coming from triangles and boxes have simple poles at the propagators, whereas those coming from bubbles have no discontinuities. Thanks to this distinction, it is possible to disentangle the bubble contributions by performing a complex momentum shift of the internal (cut)

[2]See, for example, the computation of the QCD beta function in [74].

[3]See Section 4.4.3 for an explicit calculation of the renormalization of $F_{V\psi^2H}$ by F_{V^3}.

particles. Consider the following BCFW shift,

$$\begin{aligned} |\ell_1\rangle &\to |\ell_1\rangle + z\,|\ell_2\rangle \ , \\ |\ell_2] &\to |\ell_2] + z\,|\ell_1] \ , \end{aligned} \tag{3.21}$$

with the rest of the spinors unchanged. ℓ_1, ℓ_2 are the momenta of the cut particles and z is a complex number. If we apply this deformation to Eq. (3.16), the subamplitudes become a complex function of z. Then, we can use complex analysis to extract the bubble coefficients. The first step is to rewrite the integrand in Eq. (3.16) using Cauchy's integral formula,

$$\begin{aligned} &\widehat{\mathcal{A}}_{\mathcal{O}_j}(..., -\ell_1, -\ell_2) \times \mathcal{A}_{\rm SM}(\ell_2, \ell_1, ...) = \\ &\qquad \frac{1}{2\pi i}\int_{c_0} \frac{dz}{z} \widehat{\mathcal{A}}_{\mathcal{O}_j}(..., \ell_1(z), \ell_2(z)) \times \mathcal{A}_{\rm SM}(-\ell_2(z), -\ell_1(z), ...) \ . \end{aligned} \tag{3.22}$$

In the RHS, the integral is along the contour c_0, which is a circle around the origin. Observe that $z = 0$ in the LHS, so the momenta are unshifted. We can deform the integration contour as we did in Figure 1.2, so that $\int_{c_0} dz = \int_{c_I} dz + \int_{c_\infty} dz$. The discontinuities captured by c_I are simple poles coming from triangle and box integrals. If we remove these contributions, we are only left with the pole at infinity captured by c_∞. It was shown in [74] that this term is associated with the bubble coefficients, so finally the anomalous dimension is given by

$$\begin{aligned} &\gamma_{ij}\mathcal{A}_{\mathcal{O}_i}(1, 2, ..., n) = \\ &\quad i\frac{C_{\mathcal{O}_i}}{C_{\mathcal{O}_j}} \int \frac{d\text{LIPS}}{8\pi^4} \sum_{\substack{\text{ext. legs} \\ \text{distrib.}}} \sum_{\ell_1,\ell_2} \sigma_{\ell_1\ell_2} \int_{c_\infty} \frac{dz}{z} \widehat{\mathcal{A}}_{\mathcal{O}_j}(..., \ell_1(z), \ell_2(z)) \times \mathcal{A}_{\rm SM}(-\ell_2(z), -\ell_1(z), ...) \ . \end{aligned} \tag{3.23}$$

One can check that performing the integral along c_∞ is equivalent to extracting the constant term in a Laurent series around ∞ for the function $\widehat{\mathcal{A}}_{\mathcal{O}_j}(z) \times \mathcal{A}_{\rm SM}(z)$.

Let us compare equations Eq. (3.23) and Eq. (3.16). The contour integral in Eq. (3.23) removes the contributions of triangles and boxes to each individual 2-cut, whereas in Eq. (3.16) those terms only cancel out in the final result. Then, using the results of Appendix C, we can distinguish between two cases:

- Renormalizations with $\Delta n = 0$: There are no contributions from triangles and boxes in the 2-cuts, so Eq. (3.23) is unnecessary. Each individual 2-cut is the same in both Eq. (3.16) and Eq. (3.23).

- Renormalizations with $\Delta n \geq 1$: The 2-cuts are generally contaminated by triangles and boxes, so the computations with Eq. (3.16) and Eq. (3.23) are different. Although Eq. (3.23) appears more complex, removing the triangles and boxes significantly simplifies the structure of the 2-cuts. The final result, of course, has to be the same.

For an explicit calculation of the anomalous dimension matrix using this method, see Sections 4.1.2 and 4.4.2.

3.2.4 Method III: γ_{ij} from unitarity cuts of form factors

In this section we will explain the derivation of Eq. (3.18), which was used to prove Eq. (3.16). Up until now, we have considered the renormalization scale dependence associated with the divergences of the 1-loop amplitude, i.e., the fact that $1/\epsilon_{UV}$ poles are always accompanied by $\ln \mu^2$ in dimensional regularization. We now present an alternative method for obtaining the anomalous dimensions, based on the fact that the renormalization parameters are also encoded in the logarithms of the amplitude. This comes from the observation that, by dimensional analysis, logarithms of momenta $\ln s_{ij}$ must be balanced with logarithms of the renormalization scale $\ln \mu^2$.

This strategy was first proposed in [26] by S. Caron-Huot and M. Wildhem, who developed a formalism to relate the anomalous dimensions with phase-space integrations of lower-point on-shell amplitudes and form factors. Here we will derive Eq. (3.18) using their approach. Additional details can be found in the original paper. For a slightly different derivation, see [28].

The main idea is to consider the Callan-Symanzik equation, or Renormalization Group Equation (RGE) that is satisfied by a form factor. Then, we can compute the anomalous dimension associated with that form factor, which is included in the RGE. First, we restate the definition of a form factor

$$F_{\mathcal{O}_i}(1,...,n) \equiv \langle 0|\mathcal{O}_i|p_1,...,p_n\rangle \ , \tag{3.24}$$

with $|p_1,...,p_n\rangle$ a multiparticle asymptotic state and $\mathcal{O}_i$ a higher-dimension operator. After renormalization, form factors depend on the energy scale μ and satisfy the renormalization group equation,

$$\left[\mu\frac{\partial}{\partial\mu} + \sum_\lambda \beta_\lambda \frac{\partial}{\partial\lambda} + \sum_j \left(\gamma_{ij} - \gamma^i_{\rm IR}\delta_{ij}\right)\right] F_{\mathcal{O}_i}(1,...,n;\mu) = 0 \ , \tag{3.25}$$

where γ_{ij} is the anomalous dimension matrix, $\gamma^i_{\rm IR}$ is the IR anomalous dimension and β_λ is the beta function of the λ coupling.

By Lorentz invariance, form factors are functions of the momentum invariants $s_{ab} = 2p_a p_b$ and schematically we can write $F_{\mathcal{O}_i}(s_{ab} + i\epsilon)$. Using the Feynman prescription, we must add a factor $+i\epsilon$ to the invariants, with $\epsilon > 0$ a small parameter. The analyticity of the form factor implies

$$F^*_{\mathcal{O}_i}(s_{ab} - i\epsilon) = F_{\mathcal{O}_i}(s_{ab} + i\epsilon) \ . \tag{3.26}$$

This becomes evident in perturbation theory, where the complex conjugation of $F_{\mathcal{O}_i}$ involves replacing the time-ordered propagators $(s_{ab} + i\epsilon)^{-1}$ with anti-time-ordered propagators $(s_{ab} - i\epsilon)^{-1}$. Formally, it corresponds to a counter-clockwise rotation in the complex s_{ab} plane. This operation is generated by the dilatation operator D, which is defined as

$$D = \sum_{a=1}^{n} p_a^\mu \frac{\partial}{\partial p_a^\mu} \ . \tag{3.27}$$

The action of $e^{i\alpha D}$ on the different p_a is a rotation in the complex plane with phase α. Acting on the form factor, we have

$$F(p_1,...,p_n) \quad \to \quad e^{i\alpha D}F(p_1,...,p_n) = F(p_1e^{i\alpha},...,p_ne^{i\alpha}) \ . \tag{3.28}$$

And clearly the s_{ab} are rotated with a phase 2α. For $\alpha = \pi$, the invariants are rotated back to their original values, but on the opposite side of the cut. They go precisely from $s_{ab} + i\epsilon$ to $s_{ab} - i\epsilon$. Knowing this, Eq. (3.26) can be rewritten as

$$e^{-i\pi D}F^*_{\mathcal{O}_i}(s_{ab} + i\epsilon) = F_{\mathcal{O}_i}(s_{ab} + i\epsilon) \ . \tag{3.29}$$

The next step is to relate the form factor and the S-matrix with a version of the optical theorem. By unitarity, $SS^\dagger = 1$. The form factor is a small perturbation of the S-matrix $\delta S = i\mathcal{F}$, with $\mathcal{F}$ denoting the operator with matrix elements F. In terms of the form factor, the unitarity condition is $\mathcal{F} = S\mathcal{F}^\dagger S$. The corresponding matrix elements obey

$$F = SF^* \ . \tag{3.30}$$

Combining Eq. (3.29) and Eq. (3.30) yields

$$e^{-i\pi D}F^* = SF^* \ . \tag{3.31}$$

As pointed out in [26], the dilatation operator is related to the renormalization scale μ in dimensional regularization. The form factor can only depend on dimensionless ratios s_{ij}/μ^2, so we can replace the terms $p_a\partial_{p_a}$ by derivatives of μ, leading to $D \simeq -\mu\partial_\mu$. Then the Callan-Symanzik equation in Eq. (3.25) becomes

$$DF_{\mathcal{O}_i} = \left[\sum_\lambda \beta_\lambda \frac{\partial}{\partial\lambda} + \sum_j \left(\gamma_{ij} - \gamma^i_{\rm IR}\delta_{ij}\right)\right] F_{\mathcal{O}_i}(1,...,n;\mu) = 0 \ . \tag{3.32}$$

This expression is further simplified when $F_{\mathcal{O}_i}$ is a contact (or minimal) form factor. In that case the β-function term vanishes because the form factor does not contain any of the λ couplings of the theory.

Combining Eq. (3.32) and Eq. (3.31), we can finally relate the anomalous dimension γ and the S-matrix. On the LHS of Eq. (3.31), we insert Eq. (3.32) and expand the exponential in powers of D. We will focus on the leading non-trivial order of this expansion. On the RHS of Eq. (3.31), we rewrite the S-matrix as $S = \mathbb{I} + i\mathcal{M}$ with $\mathbb{I}$ the identity and $\mathcal{M}$ some perturbation. For a minimal form factor, this leads to

$$\sum_j \left(\gamma^{(1)}_{ij} - \gamma^{i,(1)}_{\rm IR}\delta_{ij}\right) \langle 0|\mathcal{O}_i|p_1,...p_n\rangle^{(0)} = -\frac{1}{\pi}\sum_j \langle 0|\mathcal{M}\otimes\mathcal{O}_j|p_1,...p_n\rangle^{(0)} \ , \tag{3.33}$$

where $\langle 0|\mathcal{O}_i|p_1,...p_n\rangle^{(0)}$ is the tree-level form factor $F_{\mathcal{O}_i}$ and $\gamma^{(1)}_{ij}, \gamma^{i,(1)}_{\rm IR}$ are respectively the anomalous dimension and IR anomalous dimension at leading order. The superscript (1) refers to the leading single $\ln\mu^2$ in the form factor, which usually appears at 1-loop, but not always.

On the RHS of Eq. (3.33), the convolution $\otimes$ corresponds to an insertion of a complete set of intermediate states, followed by a phase-space integral. This is precisely a unitarity cut of the loop form factor.

To derive Eq. (3.18) we focus on the case where the leading single $\ln \mu^2$ appears at one loop, and thus Eq. (3.33) gives us the 1-loop anomalous dimension[4]. The term $\langle 0|\mathcal{M} \otimes \mathcal{O}_j|p_1, ...p_n\rangle^{(0)}$ is then a 2-cut. After inserting the particle internal states with momentum ℓ_1, ℓ_2, we have a product of a tree-level subamplitude $\mathcal{A}_{\rm SM}$ and a tree-level form factor $\widehat{F}_{\mathcal{O}_j}$ integrated over a phase space. Overall, we can write

$$\begin{aligned}\langle 0|\mathcal{M} \otimes \mathcal{O}_j|p_1, ...p_n\rangle^{(0)} = \\ -\frac{1}{4\pi^2}\int d\text{LIPS} \sum_{\substack{\text{ext. legs}\\ \text{distrib.}}} \sum_{\ell_1,\ell_2} \sigma_{\ell_1\ell_2} \widehat{F}_{\mathcal{O}_j}(..., \ell_1, \ell_2) \times \mathcal{A}_{\rm SM}(-\ell_2, -\ell_1, ...) \ ,\end{aligned} \tag{3.34}$$

with dLIPS and $\sigma_{\ell_1\ell_2}$ as defined in Section 3.2.2. Inserting this expression into Eq. (3.33) for the case of no IR divergences, we obtain

$$\gamma_{ij}\, F_{\mathcal{O}_i}(1, 2, ..., n) = -\frac{1}{4\pi^3}\int d\text{LIPS} \sum_{\substack{\text{ext. legs}\\ \text{distrib.}}} \sum_{\ell_1,\ell_2} \sigma_{\ell_1\ell_2} \widehat{F}_{\mathcal{O}_j}(..., \ell_1, \ell_2) \times \mathcal{A}_{\rm SM}(-\ell_2, -\ell_1, ...) \ , \tag{3.35}$$

which is precisely Eq. (3.18) that we wanted to prove. See Chapters 4 and 5 for some examples of this formula's usage.

3.3 IR divergences

Here we expand our study of on-shell renormalization methods for mixings involving non-zero IR divergences. Following [2], we consider the generalization of Eq. (3.16) in the presence of both soft and collinear singularities. Similar analyses of 1-loop IR divergences in the context of on-shell amplitudes can be found in [26, 28, 29, 74]. See also [75] for a 2-loop extension.

Our starting point is the Passarino-Veltmann decomposition of 1-loop amplitudes, given by Eq. (3.3). For clarity, we consider the case where $\mathcal{A}_{\rm loop}$ is a 4-point amplitude. From the definition of the master integrals I_m in Eq. (3.4), we see that only bubbles and triangles can have IR divergences. The IR-divergent part of the amplitude is

$$\mathcal{A}^{\rm IR}_{\rm loop} = \sum_a \hat{C}^{(a)}_2 I^{(a)}_2 + \sum_b \hat{C}^{(b)}_3 I^{(b)}_3 \ . \tag{3.36}$$

Subtracting these IR-divergent terms from the full amplitude $\mathcal{A}_{\rm loop}$, we obtain

$$\mathcal{A}_{\rm loop} - \mathcal{A}^{\rm IR}_{\rm loop} = \sum_a \left[C^{(a)}_2 - \hat{C}^{(a)}_2\right] I^{(a)}_2 + \sum_b \left[C^{(b)}_3 - \hat{C}^{(b)}_3\right] I^{(b)}_3 + \sum_c C^{(c)}_4 I^{(c)}_4 + R \ , \tag{3.37}$$

[4] We will discuss the computation of the 2-loop anomalous dimension in Section 3.4.5.

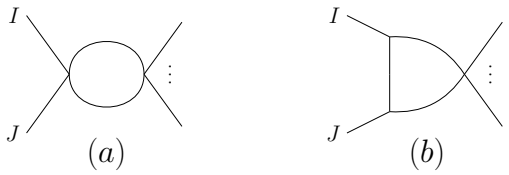

Figure 3.4: *Diagrams of the bubble (a) and triangle (b) topologies that contribute to* $\mathcal{A}^{\rm IR}_{\rm loop}$ *in gauge and gravity theories.*

which is IR-finite. As we saw in Section 3.1, the 1-loop anomalous dimension can be extracted from the UV-divergent part of the amplitude. This corresponds to a sum over the IR-finite bubble terms, namely

$$\gamma_i \mathcal{A}_{\mathcal{O}_i} = -2\mathcal{A}^{\rm UV}_{\rm loop} = -\frac{1}{8\pi^2}\sum_a \left[C_2^{(a)} - \hat{C}_2^{(a)}\right] \ . \tag{3.38}$$

The bubble coefficients can be obtained with the generalized unitarity method. In this case, it is enough to compute the 2-cut of Eq. (3.37),

$$\text{cut}^{(a)}\left[\mathcal{A}_{\rm loop} - \mathcal{A}^{\rm IR}_{\rm loop}\right] = -\frac{C_2^{(a)} - \hat{C}_2^{(a)}}{8\pi^2} + \text{cut}^{(a)}\left[\sum_b C_3^{(b)}|_{\rm reg}\ I_3^{(b)} + \sum_c C_4^{(c)} I_4^{(c)}\right] \ , \tag{3.39}$$

with $C_3|_{\rm reg} = C_3 - \hat{C}_3$. The second term in the RHS is a 2-cut of triangles and boxes, which is generally non-zero. However, as we prove in Appendix C, those terms cancel out for IR-finite amplitudes when we sum over all possible 2-cuts[5]. Thus, we find

$$\sum_a \text{cut}^{(a)}\left[\mathcal{A}_{\rm loop} - \mathcal{A}^{\rm IR}_{\rm loop}\right] = -\frac{1}{8\pi^2}\sum_a \left[C_2^{(a)} - \hat{C}_2^{(a)}\right] = \gamma_i \mathcal{A}_{\mathcal{O}_i} \ , \tag{3.40}$$

which reduces to Eq. (3.16) when $\mathcal{A}^{\rm IR}_{\rm loop} = 0$.

The explicit form of $\mathcal{A}^{\rm IR}_{\rm loop}$ depends on the type of interaction. For instance, the general expression for 1-loop amplitudes in a gauge theory can be found in [76, 77]. Considering the PV decomposition, the bubble coefficients related to collinear IR divergences are

$$\hat{C}_2^{(ij)} = -8\pi^2 \gamma^{(i)}_{\rm coll} \frac{\boldsymbol{T}_i \cdot \boldsymbol{T}_j}{\boldsymbol{T}_i^2} \mathcal{A}_{\rm tree} + (i \leftrightarrow j) \ , \tag{3.41}$$

where the indices i, j refer to two external legs of the corresponding bubble diagram, as is shown in Figure 3.4 (a). T_i are the gauge group generators in the appropriate representation for particle i. Following the color-space formalism [76], we leave the color and flavor indices implicit. Writing them explicitly, we have

$$\mathcal{A}_{\rm tree} \to \mathcal{A}^{abcd}_{\rm tree} \quad \text{and} \quad \boldsymbol{T}_i \to (T_i^A)^{a'}_{a} \ , \tag{3.42}$$

[5]The proof in Appendix C can be adapted to our case by replacing $C_3 \to C_3|_{\rm reg}$.

where the dot product of generators is defined as $\boldsymbol{T}_i \cdot \boldsymbol{T}_j \equiv \boldsymbol{T}_i^A \boldsymbol{T}_j^A$. To recover Eq. (3.40), we sum over all 2-cuts $\text{cut}^{(ij)}$ with $i < j$. Taking into account that $\sum_j \boldsymbol{T}_j \mathcal{A}_{\text{tree}} = 0$ due to color and flavor conservation, we find

$$-\sum_{i<j} \text{cut}^{(ij)} \left[\mathcal{A}^{\text{IR}}_{\text{loop}}\right] |_{\text{bubble}} = \frac{1}{8\pi^2} \sum_{i<j} \hat{C}_2^{(ij)} = \sum_i \gamma^{(i)}_{\text{coll}} \mathcal{A}_{\text{tree}} = \gamma_{\text{coll}} \mathcal{A}_{\text{tree}} \ . \tag{3.43}$$

Comparing this result to Eq. (3.16), we conclude that, for amplitudes with collinear IR divergences, the anomalous dimension gets an additional contribution given by

$$\Delta\gamma_i \, \frac{\mathcal{A}_{\mathcal{O}_i}(1,2,3,4)}{C_{\mathcal{O}_i}} = \gamma_{\text{coll}} \, \mathcal{A}_{\mathcal{O}_i}(1,2,3,4) \ . \tag{3.44}$$

We recall that $\gamma_i = \sum_j \gamma_{ij} C_{\mathcal{O}_j}$. The collinear correction is always diagonal in the amplitude space, meaning that it is proportional to the tree amplitude $\mathcal{A}_{\mathcal{O}_i}$. γ_{coll} depends only on the external legs, so we can write $\gamma_{\text{coll}} = \sum_{n=1}^{4} \gamma^{(n)}_{\text{coll}}$. The particular expressions $\gamma^{(n)}_{\text{coll}}$ for different particles are found for instance in [28, 29].

We must also consider soft IR divergences, which are present in the triangle terms of $\mathcal{A}^{\text{IR}}_{\text{loop}}$. For a gauge theory, the corresponding coefficients are

$$\hat{C}_3^{(ij)} = -g^2 s_{ij} \ \boldsymbol{T}_i \cdot \boldsymbol{T}_j \ \mathcal{A}_{\text{tree}} \ , \tag{3.45}$$

where g is the gauge coupling and i, j are two external legs of the triangle diagram in Figure 3.4 (b). As we mentioned before, the $\hat{C}_3$ coefficients do not contribute to γ_i when we sum over all possible 2-cuts. Nevertheless, their presence in the individual cuts leads to divergences that must be regulated. In particular, the 2-cut contribution is

$$\text{cut}^{(ij)} \left[\mathcal{A}^{\text{IR}}_{\text{loop}}\right] |_{\text{triangle}} = \hat{C}_3^{(ij)} \text{cut}[I_3^{(ij)}] = \frac{1}{4\pi^3} \, g^2 \, \boldsymbol{T}_i \cdot \boldsymbol{T}_j \mathcal{A}_{\text{tree}} \int d\text{LIPS} \frac{1}{s^2_{\theta'/2}} \ . \tag{3.46}$$

Alternatively, we can express the last integral as $\int c^{-2}_{\theta'/2}$, which is equal to $\int s^{-2}_{\theta'/2}$ if we replace $\theta' \to (\pi - \theta')$. We can also express it as $2\int s^{-2}_{\theta'}$ by symmetrization over the interval $[0, \pi]$.

Eq. (3.46) shows that, if we use Eq. (3.16) for mixings with soft IR divergences, the dLIPS integral will not be finite. This occurs because one of the subamplitudes $\mathcal{A}_{L,R}$ is singular for some angle θ. We distinguish three different cases:

- $\mathcal{A}_{L,R} \sim s^{-2}_{\theta/2}$ is singular in the limit $\theta \to 0$.
- $\mathcal{A}_{L,R} \sim c^{-2}_{\theta/2}$ is singular in the limit $\theta \to \pi$. By reordering the amplitude legs, we can always rewrite $\mathcal{A}_{L,R} \sim s^{-2}_{\theta/2}$. Thus, this case can be excluded from our analysis.
- $\mathcal{A}_{L,R} \sim s^{-2}_{\theta}$ is singular for both $\theta \to 0$ and $\theta \to \pi$. This occurs when the two cut particles ℓ_1 and ℓ_2 are identical.

Using Eq. (3.46), the anomalous dimension in Eq. (3.16) must be corrected by adding

$$\Delta\gamma_i \, \frac{\mathcal{A}_{\mathcal{O}_i}(1^a,2^b,3^c,4^d)}{C_{\mathcal{O}_i}} = -\frac{1}{4\pi^3}\left[(\boldsymbol{T}^{12}_{\text{soft}})^{a\,b}_{\hat{a}\,\hat{b}}\mathcal{A}_R(1^{\hat{a}},2^{\hat{b}},3^c,4^d)\int d\text{LIPS}_{12}\,\frac{1}{s^2_{\theta'/2}}\right.$$
$$\left. + (\boldsymbol{T}^{34}_{\text{soft}})^{c\,d}_{\hat{c}\,\hat{d}}\,\mathcal{A}_L(1^a,2^b,3^{\hat{c}},4^{\hat{d}})\int d\text{LIPS}_{34}\,\frac{1}{s^2_{\theta'/2}}\right] + (2\leftrightarrow 3) + (2\leftrightarrow 4)\ , \tag{3.47}$$

where $d\text{LIPS}_{ij}$ is an integral over the phase space for the $i'j'$ state. We generally denote the color and flavor of the external particles with $abcd$ indices, and we have defined the soft operator $\boldsymbol{T}^{ij}_{\text{soft}} = g^2\ \boldsymbol{T}_i\cdot\boldsymbol{T}_j$. For QED, it gets simplified to $\boldsymbol{T}^{ij}_{\text{soft}} = e^2 q_i q_j$, with q_i the charge of particle i. Note that $\Delta\gamma_i$ acts as a regulator for the angular divergences in Eq. (3.16), so the overall contribution from each cut is finite.

Finally, let us comment on the treatment of IR divergences in gravity. The PV structure of $\mathcal{A}^{\text{IR}}_{\text{loop}}$ is the same as in gauge theories, so our analysis holds. It suffices to make the replacement $\gamma_{\text{coll}} = 0$ and $\boldsymbol{T}^{ij}_{\text{soft}} = -2s_{ij}/M_P^2$ [78].

3.4 Additional remarks

3.4.1 Helicity selection rules

One of the most interesting applications of Eq. (3.16) is the study of certain patterns in the anomalous dimension matrix, which are often obscured in the traditional Feynman diagram approach. The presence of unexpected zeroes in the anomalous dimension matrix was observed in the first calculations of 1-loop mixings between dimension-6 operators in the SMEFT, see [19–25, 79]. Non-renormalization theorems were derived to explain these cancellations, employing helicity arguments [52] and supersymmetry [80]. These results were extended to higher-order loop mixings in [30]. Further non-renormalization theorems for general EFTs were obtained using angular momentum conservation in [81], and also for gravity in [31][6].

In this context, on-shell amplitude methods have been particularly helpful for the derivation of helicity selection rules [52] that tell us which are the allowed renormalizations for a given operator. The effects of these selection rules for tree-level and 1-loop amplitudes were studied in [83]. Here we follow [1] to obtain helicity selection rules using our results from Section 3.2.

From Eq. (3.16), it trivially follows that

$$n_i = \hat{n}_j + n_{\text{SM}} - 4\ , \tag{3.48}$$
$$h_i = \hat{h}_j + h_{\text{SM}}\ , \tag{3.49}$$

where $n_i, \hat{n}_j$ and n_{SM} are respectively the number of particles in the amplitudes $\mathcal{A}_{\mathcal{O}_i}$, $\widehat{\mathcal{A}}_{\mathcal{O}_j}$ and $\mathcal{A}_{\text{SM}}$. The corresponding helicities are $h_i, \hat{h}_j$ and h_{SM}. As mentioned in Section 3.2.2, the SM

[6] Non-renormalization theorems for the anomalous dimension matrix can be extended to non-linear mixings in the anomalous dimension tensor. See for example [82].

n								
	6				H^6			
	5			$\bar{\psi}^2H^3$		ψ^2H^3		
	4		$\bar{V}^2H^2$ $\bar{V}\bar{\psi}^2H$ $\bar{\psi}^4$		H^4D^2 $\psi^2\bar{\psi}^2$ $\psi\bar{\psi}H^2D$		V^2H^2 $V\psi^2H$ ψ^4	
	3	$\bar{V}^3$						V^3
		-3	-2	-1	0	1	2	3
					h			

Table 3.1: Contact interactions at order $1/\Lambda^2$ in the SMEFT, classified according to their number of particles n and total helicity h. The gray area shows the interactions that can renormalize $V\psi^2H$ according to the helicity selection rule $\Delta n \geq |\Delta h|$.

subamplitude has $n_{\rm SM} \geq 4$. Also, since $\widehat{\mathcal{A}}_{\mathcal{O}_j}$ is in general a non-minimal amplitude, it obeys $\hat{n}_j \geq n_j$. Thus, from Eq. (3.48), it follows that

$$\Delta n = n_i - n_j \geq 0 \ , \tag{3.50}$$

which tells us that $C_{\mathcal{O}_j}$ can only contribute to the 1-loop renormalization of $C_{\mathcal{O}_i}$ if $\mathcal{A}_{\mathcal{O}_j}$ has the same number of legs or less than $\mathcal{A}_{\mathcal{O}_i}$[7]. The next ingredient we need is the observation made in [52] that most $n = 4$ SM amplitudes have total helicity $h = 0$. The $n \geq 4$ amplitudes made from those building blocks obey $n_{\rm SM} \geq |h_{\rm SM}| + 4$. Combining this expression with Eqs. (3.48, 3.49) leads to the following helicity selection rule:

$$\Delta n \geq |\Delta h| \ . \tag{3.51}$$

This expression is a non-renormalization theorem that gives us some vanishing entries of the 1-loop anomalous dimension matrix. Let us see an example with SMEFT operators at order $1/\Lambda^2$. Table 3.1 shows the different classes of contact interactions, classified in terms of their number of particles n and the helicity h. A dipole amplitude of class $V\psi^2H$ can only be renormalized by amplitudes that obey the condition Eq. (3.51). Graphically, this corresponds to the gray area in Table 3.1, which includes $V^2\psi^2, V\psi^2H, \psi^4$ and V^3. We know that the rest of the renormalizations are zero without the need to compute them.

The only exceptions to the selection rule Eq. (3.51) are renormalizations involving a SM subamplitude with $n = 4$ and $|h_{\rm SM}| > 0$. There is just one amplitude satisfying these conditions: the 4-fermion amplitude with $h = \pm 2$, which contains two Yukawa couplings $y_e y_u$. At order $1/\Lambda^2$ in the SMEFT this exception allows the renormalization between $\psi^2\bar{\psi}^2$ and ψ^4, and also between $\bar{\psi}^2H^3$ and ψ^2H^3.

We will apply the helicity selection rules to the calculation of anomalous dimensions in Chapters 4 and 5.

[7] See [30] for an extension of this result to higher loop orders.

3.4.2 Mixings with several amplitudes

Eq. (3.16) can be applied to cases where the renormalized amplitude $\mathcal{A}$ includes several Wilson coefficients. For example, we can have the contact amplitude $\mathcal{A}_{\mathcal{O}_i}$ plus some non-minimal amplitude $\widehat{\mathcal{A}}_{\mathcal{O}_k}$ with an insertion of $\mathcal{A}_{\mathcal{O}_k}$ and the same external legs as $\mathcal{A}_{\mathcal{O}_i}$. To account for these mixings, we modify the LHS of Eq. (3.16) as follows:

$$\gamma_{ij}\mathcal{A}_{\mathcal{O}_i} \quad \Longrightarrow \quad \gamma_{ij}\mathcal{A}_{\mathcal{O}_i} + \sum_k \gamma_{kj}\widehat{\mathcal{A}}_{\mathcal{O}_k} \ . \tag{3.52}$$

For the SMEFT at order $1/\Lambda^2$, the following cases arise:

- $\mathcal{A}(1_{V_-}, 2_{V_-}, 3_H, 4_{H^\dagger})$ includes the contact amplitude $\mathcal{A}_{V^2H^2}$ and also a non-minimal amplitude with an insertion of $\mathcal{A}_{V^3}$.
- $\mathcal{A}(1_\psi, 2_\psi, 3_H, 4_H, 5_{H^\dagger})$ includes the contact amplitude $\mathcal{A}_{\psi^2H^3}$ and also several non-minimal amplitudes containing $\mathcal{A}_{V\psi^2H}$, $\mathcal{A}_{\psi\bar{\psi}H^2}$ and $\mathcal{A}_{\Box H^4}$.
- $\mathcal{A}(1_H, 2_H, 3_H, 4_{H^\dagger}, 5_{H^\dagger}, 6_{H^\dagger})$ includes the contact amplitude $\mathcal{A}_{H^6}$ plus non-minimal interactions involving $\mathcal{A}_{V^3}$, $\mathcal{A}_{V^2H^2}$ and $\mathcal{A}_{\Box H^4}$.

Note that the different amplitudes $\mathcal{A}_{\mathcal{O}_i}$ and $\widehat{\mathcal{A}}_{\mathcal{O}_k}$ have different kinematic structures, so we can easily disentangle the contributions to the anomalous dimensions γ_{ij} and γ_{kj}. For instance, the amplitude $\mathcal{A}(1_{V_-}, 2_{V_-}, 3_H, 4_{H^\dagger})$ includes two different terms

$$\mathcal{A}_{V^2H^2}(1_{V_-^a}, 2_{V_-^b}, 3_H, 4_{H^\dagger}) = \frac{C_{V^2H^2}}{\Lambda^2}\langle 12\rangle^2\,\delta^{ab} \ , \tag{3.53}$$

$$\widehat{\mathcal{A}}_{V^3}(1_{V_-^a}, 2_{V_-^b}, 3_H, 4_{H^\dagger}) = \frac{C_{V^3}f^{abc}T^c}{\Lambda^2}\left[\frac{\langle 13\rangle\langle 42\rangle\langle 12\rangle}{\langle 34\rangle} - \frac{\langle 23\rangle\langle 14\rangle\langle 12\rangle}{\langle 34\rangle}\right] \ . \tag{3.54}$$

When applying Eq. (3.16) to the renormalization of $\mathcal{A}(1_{V_-}, 2_{V_-}, 3_H, 4_{H^\dagger})$, some terms in the RHS will have the spinor structure of $\mathcal{A}_{V^2H^2}$ and other terms will have the structure of $\widehat{\mathcal{A}}_{V^3}$. Thus we can easily separate contributions to the different anomalous dimensions.

Another possibility is to have an amplitude $\mathcal{A}$ that includes several independent coefficients $C_{\mathcal{O}_i}$ with the same kinematic structure but a different flavor structure. In such cases, we have to project Eq. (3.16) onto a basis of invariant tensors under Lorentz and the global symmetries. Then it is straightforward to identify the contribution to the anomalous dimensions of the different coefficients.

3.4.3 Lorentz-Invariant Phase Space integration

There are several ways to perform the phase-space integration dLIPS. Here we adopt the method described in [26], where the internal momenta are parameterized in terms of a subset of the external momenta. The integral over the phase-space is then transformed into a solid angle integration. The exact form of the parameterization depends on the number of internal particles. In this work we will need the 2-particle and 3-particle cases.

- Two internal particles. We must write the internal spinors ℓ_1, ℓ_2 in terms of two momenta p_a, p_b that are a linear combination of the external momenta and satisfy $p_a + p_b = \ell_1 + \ell_2$. The parameterization is

$$\begin{aligned} |\ell_1\rangle &= c_\theta \, |a\rangle - s_\theta e^{i\phi} \, |b\rangle \ , \\ |\ell_2\rangle &= s_\theta e^{-i\phi} \, |a\rangle + c_\theta \, |b\rangle \ , \end{aligned} \tag{3.55}$$

with $s_\theta \equiv \sin\theta$ and $c_\theta \equiv \cos\theta$. The expressions for the square spinors $|\ell_1], |\ell_2]$ are obtained by complex-conjugating Eq. (3.55). θ and ϕ are the angles that describe the spinors ℓ_1, ℓ_2 in terms of a rotation of p_a, p_b. The dLIPS integration becomes a solid angle integration,

$$\frac{2}{\pi} \int d\text{LIPS} \equiv \int_0^{2\pi} \frac{d\phi}{2\pi} \int_0^{\pi/2} d\theta \, 2 s_\theta c_\theta \ . \tag{3.56}$$

The simplest scenario occurs when we can directly identify p_a and p_b with the momenta of external particles. For example, if we have a 4-point SM subamplitude $\mathcal{A}_{\text{SM}}(p_1, p_2, -\ell_1, -\ell_2)$ we can simply chose $p_a = p_1$ and $p_b = p_2$. Instead, if we have a 5-point SM amplitude $\mathcal{A}_{\text{SM}}(p_1, p_2, p_3, -\ell_1, -\ell_2)$, we must define

$$p_a = p_1 \frac{s_{123}}{s_{12} + s_{13}} \ , \qquad p_b = p_2 + p_3 - p_1 \frac{s_{23}}{s_{12} + s_{13}} \ , \tag{3.57}$$

with $s_{123} = (p_1 + p_2 + p_3)^2$. One can check that this satisfies $p_a + p_b = p_1 + p_2 + p_3 = \ell_1 + \ell_2$. The corresponding spinors are

$$|a\rangle = |1\rangle \sqrt{\frac{s_{123}}{s_{12} + s_{13}}} \ , \qquad |b\rangle = \left([12] \, |2\rangle + [13] \, |3\rangle \right) \sqrt{\frac{1}{s_{12} + s_{13}}} \ . \tag{3.58}$$

- Three internal particles: This scenario corresponds to 3-cuts of 2-loop amplitudes. Again, the internal spinors ℓ_1, ℓ_2, ℓ_3 are expressed in terms of some p_a, p_b, p_c made from the external spinors with $p_a + p_b + p_c = \ell_1 + \ell_2 + \ell_3$. In particular, we have

$$\begin{aligned} |\ell_1\rangle &= c_{\theta_2} \, |a\rangle - e^{i\phi} c_{\theta_1} s_{\theta_2} \, |b\rangle \ , \\ |\ell_2\rangle &= s_{\theta_2} c_{\theta_3} \, |a\rangle + e^{i\phi} \left(c_{\theta_1} c_{\theta_2} c_{\theta_3} - e^{i\rho} s_{\theta_1} s_{\theta_3} \right) |b\rangle \ , \\ |\ell_3\rangle &= s_{\theta_2} s_{\theta_3} \, |a\rangle + e^{i\phi} \left(c_{\theta_1} c_{\theta_2} s_{\theta_3} + e^{i\rho} s_{\theta_1} c_{\theta_3} \right) |b\rangle \ . \end{aligned} \tag{3.59}$$

The corresponding phase-space integration is given by

$$\int d\text{LIPS} \equiv \frac{s_{ab}}{(16\pi^2)^2} \int d\mu \ , \tag{3.60}$$

where $s_{ab} = (p_a + p_b)^2$ and we have defined

$$\int d\mu \equiv \int_0^{\frac{\pi}{2}} 2 s_{\theta_1} c_{\theta_1} d\theta_1 \int_0^{\frac{\pi}{2}} 4 s_{\theta_2}^3 c_{\theta_2} d\theta_2 \int_0^{\frac{\pi}{2}} 2 s_{\theta_3} c_{\theta_3} d\theta_3 \int_0^{2\pi} \frac{d\rho}{2\pi} \int_0^{2\pi} \frac{d\phi}{2\pi} \ , \tag{3.61}$$

which satisfies $\int d\mu = 1$. Throughout this work, we will only use this parameterization in cases where we have a 5-point SM amplitude $\mathcal{A}_{\text{SM}}(p_1, p_2, -\ell_1, -\ell_2, -\ell_3)$, and thus we can choose $p_a = p_1$ and $p_b = p_2$.

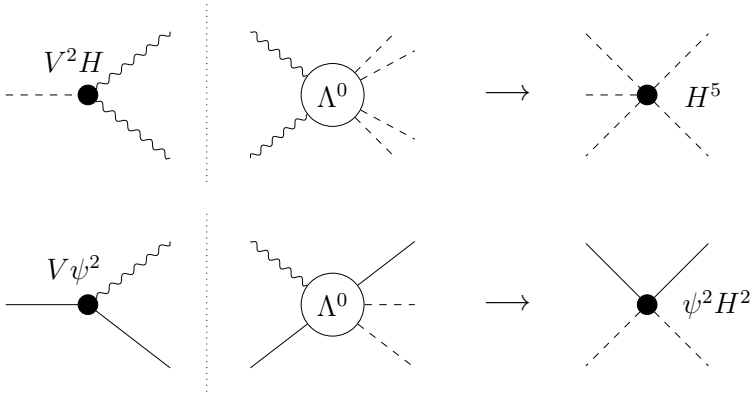

Figure 3.5: *Diagrams for the 1-loop renormalization of F_{H^5} by F_{V^2H}, and $F_{\psi^2H^2}$ by $F_{V\psi^2}$. These are the only mixings involving 3-point form factors at order $1/\Lambda$.*

3.4.4 Renormalization at order $1/\Lambda$

Up until now, we have focused on renormalizations at order $1/\Lambda^2$, but one can prove that Eq. (3.16) is also valid when $\mathcal{A}_{\mathcal{O}_i}, \mathcal{A}_{\mathcal{O}_j}$ are amplitudes of order $1/\Lambda$. The proof goes as follows: we start with Eq. (3.18), which is valid for any form factor, and then we verify that it reduces to Eq. (3.16) in the limit $Q \to 0$. Similarly to the $1/\Lambda^2$ case, we must ensure that there are no additional contributions coming from the 3-point form factors in Eq. (3.18).

As listed in Section 2.2.1, there are two 3-point form factors at order $1/\Lambda$: F_{V^2H} and $F_{V\psi^2}$. The only possible extra terms in Eq. (3.18) come from the renormalization of F_{H^5} by F_{V^2H}, and the renormalization of $F_{\psi^2H^2}$ by $F_{V\psi^2}$. The corresponding 2-cuts are illustrated in Figure 3.5. The explicit computation of those 2-cuts leads to integrals like the ones in Figure C.2. By the arguments in Appendix C, the absence of IR divergences implies that the total contribution of triangles and boxes to Eq. (3.16) vanishes. This ensures the validity of Eq. (3.16) at order $1/\Lambda$.

3.4.5 2-loop anomalous dimensions

We conclude this section with a brief discussion on the anomalous dimension matrix at higher loop orders. Formulas Eq. (3.16) and Eq. (3.23) are based on the observation that bubble coefficients can be derived from 2-cuts, together with Eq. (3.13) that relates the 1-loop anomalous dimension to the bubble coefficients. This derivation does not have a natural extension to higher-order mixings, since it relies on the Passarino-Veltman decomposition of 1-loop amplitudes and the fact that only bubble integrals are UV divergent. There is no analog for this at two loops.

The formalism of form factor renormalization, however, is a robust framework for studying higher loop orders. The formula $e^{-i\pi D}F^* = SF^*$ gives an exact relation between the renormalization coefficients and the S-matrix. Expanding this expression yields a formula for the anomalous dimension at various orders, expressed in terms of unitarity cuts. Let us comment on the two classes of 2-loop anomalous dimensions that we can compute:

- "Easy" 2-loop renormalizations. As we mentioned before, Eq. (3.33) provides the anomalous dimension associated with the leading single logarithm $\ln \mu^2$ in the form factor. If a renormalization is forbidden at one loop, the leading logarithm comes at two loops and we can use Eq. (3.33) to compute the 2-loop anomalous dimension. Now the convolution $\langle 0|\mathcal{M} \otimes \mathcal{O}_j|p_1, ...p_n\rangle$ includes three types of terms, which are diagrammatically shown in Figure 3.6. We have 2-cuts of a 1-loop form factor and a tree-level amplitude, 2-cuts of a tree-level form factor and a 1-loop amplitude, and 3-cuts of a tree-level form factor and a tree-level amplitude.

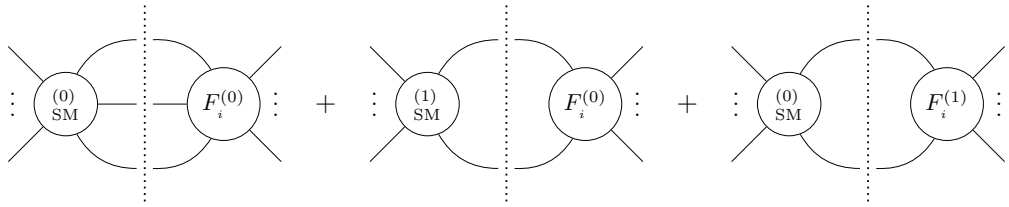

Figure 3.6: *Diagrams illustrating the three classes of contributions to the 2-loop anomalous dimensions.*

- General 2-loop renormalizations. If there is mixing at one loop, the computation of the 2-loop anomalous dimension becomes significantly more complex. We must expand Eq. (3.31) at the next-to-leading order, so instead of Eq. (3.33) we have

$$\begin{aligned}&\left[\Delta\gamma_{ij}^{(1)} + \delta_{ij}\beta_\lambda^{(1)}\partial_\lambda\right] F_{\mathcal{O}_j}^{(1)} + \left[\Delta\gamma_{ij}^{(2)} + \delta_{ij}\beta_\lambda^{(2)}\partial_\lambda\right] F_{\mathcal{O}_j}^{(0)} \\ &\quad - i\pi\frac{1}{2}\left[\Delta\gamma_{ik}^{(1)} + \delta_{ik}\beta_\lambda^{(1)}\partial_\lambda\right]\left[\Delta\gamma_{kj}^{(1)} + \delta_{kj}\beta_\lambda^{(1)}\partial_\lambda\right] F_{\mathcal{O}_j}^{(0)} = -\frac{1}{\pi}(\mathcal{M}F_{\mathcal{O}_i})^{(2)} \,,\end{aligned} \tag{3.62}$$

  where we have defined $\Delta\gamma_{ij} = \gamma_{ij} - \delta_{ij}\gamma_{\rm IR}^i$, and $(\mathcal{M}F_{\mathcal{O}_i})^{(2)}$ includes the 3 classes of unitarity cuts in Figure 3.6. Now we have an expression involving both 1-loop and 2-loop terms, so the extraction of $\gamma_{ij}^{(2)}$ becomes more intricate.

We will see an example of an "easy" 2-loop computation in Chapter 5. The analysis of general 2-loop renormalization goes beyond the scope of this work, but more details can be found in [30].

3.5 Conclusions of the chapter

In this chapter we have studied the renormalization of effective field theories using on-shell amplitude methods. We have seen that the 1-loop anomalous dimensions γ_i for a Wilson coefficient $C_{\mathcal{O}_i}$ depends only on the bubble coefficients C_2 from the Passarino-Veltman decomposition of the 1-loop amplitude, modulo IR divergences. The bubble coefficients can be obtained using the generalized unitarity method, which allows us to reconstruct amplitudes by performing a series of unitarity cuts on their loops. We have explained three different ways to extract the anomalous dimensions directly from 2-cuts:

- Method I relates γ_{ij} to 2-cuts of the loop amplitude, as given by Eq. (3.16) that was derived in our paper [1]. This expression is only valid for renormalizations where 2-cuts receive no contributions from triangle and box integrals. As we have shown, that is precisely the case of the SMEFT at orders $1/\Lambda^2$ and $1/\Lambda$.

- Method II is based in the more general formula Eq. (3.23), which was obtained in [74]. The idea is to perform a BCFW deformation of the internal cut momenta and use Cauchy's theorem to eliminate the simple poles associated with triangle and box integrals, leaving only the bubble terms.

- Method III allows us to obtain the anomalous dimensions using 2-cuts of on-shell form factors, following Eq. (3.35) from [26]. This method makes use of the fact that logarithms of the renormalization scale $\ln \mu^2$ must be accompanied by logarithms of the momenta $\ln s_{ij}$ to ensure the correct dimensions.

It is particularly remarkable that method I gives us the anomalous dimensions from a product of two tree-level on-shell amplitudes integrated over a phase space. This is significantly simpler than the usual approach of computing the loop amplitude with Feynman diagrams.

The simplicity of Eq. (3.16) also allows us to derive helicity selection rules that indicate which operator mixings are allowed or forbidden. In particular, we find that $\mathcal{A}_{\mathcal{O}_j}$ can only renormalize $\mathcal{A}_{\mathcal{O}_i}$ if they satisfy $\Delta n \geq |\Delta h|$, with $\Delta n = n_i - n_j$ and $\Delta h = h_i - h_j$. This selection rule explains several unexpected zeroes in the anomalous dimension matrix.

We have primarily focused on 1-loop renormalizations, but we have discussed how to extend this procedure to higher loop orders. Methods I and II are based on the PV decomposition of 1-loop amplitudes, which does not have an analog at higher orders. In contrast, method III offers a natural extension to two or more loops.

Throughout this chapter, we have mostly focused on mixings with $\gamma^{ij}_{\text{IR}} = 0$. We have presented the basic treatment of soft and collinear IR divergences in Section 3.3.

Our results highlight the power of on-shell amplitude methods in simplifying and systematizing computations in effective field theories, while also providing new insights into the structure and properties of anomalous dimension matrices.

Chapter 4

Applications of renormalization I: 1-loop anomalous dimension of dipole operators

In this chapter we show an example of the computation of 1-loop anomalous dimensions in the SMEFT using on-shell techniques. In particular, we apply methods I, II and III from Chapter 3 to the 1-loop renormalization of the $\mathrm{SU}(2)_L$ dipole amplitude. This covers the results of [1]. A similar computation was done in [28].

The contact on-shell amplitude associated with the dipole interaction $V\psi^2 H$ at order $1/\Lambda^2$ is given by Eq. (2.30). For concreteness, we focus on the SMEFT amplitude $W^a_- H^\dagger le$. Here, W^a_- is an $\mathrm{SU}(2)_L$ gauge boson with helicity $h=-1$, H is the Higgs doublet and e, l are, respectively, a lepton singlet and doublet with $h=-1/2$. At tree-level, the amplitude is given by

$$\mathcal{A}_{WHle}(1_e, 2_{l^j}, 3_{W^a_-}, 4_{H^\dagger_i}) = \frac{C_{WHle}}{\Lambda^2} \langle 31\rangle \langle 32\rangle (T^a)^j_i \ , \tag{4.1}$$

where C_{WHle} is a dimensionless Wilson coefficient and $T^a = \sigma^a/2$, with σ^a the Pauli matrices. Figure 4.1 shows the contact amplitude diagrammatically.

At the loop level, the coupling C_{WHle} acquires an energy scale dependence that is given by the anomalous dimension γ_{WHle}, as per Eq. (3.1). We will focus on the leading corrections to C_{WHle}, which come from other Wilson coefficients that mix at one loop. In principle, one should consider all the possible 1-loop diagrams that generate an amplitude proportional to $\mathcal{A}_{WHle}$. However, thanks to the helicity selection rule described in Section 3.4.1, we know that mixings not obeying the condition $\Delta n \geq |\Delta h|$ vanish. The remaining contributions correspond to the classes of operators in the gray area of Table 3.1: $V^2H^2, V\psi^2 H, \psi^4$ and V^3. With this information, we can compute the full 1-loop anomalous dimension for $\mathcal{A}_{WHle}$, up to self-renormalization.

In Sections 4.1 to 4.4, we perform the explicit calculation of the 1-loop mixings of ψ^4, $V\psi^2 H$, V^2H^2 and V^3 into the dipole amplitude $\mathcal{A}_{WHle}$. In Section 4.5 we compare the obtained result with previous literature. In Section 4.6 we comment on some interesting features of the on-shell procedure. Finally, the conclusions are presented in Section 4.7.

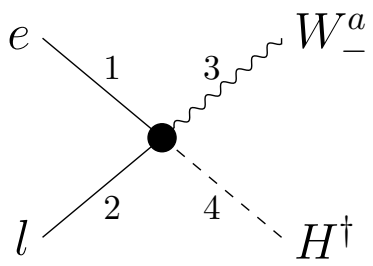

Figure 4.1: *Diagram for the contact (or minimal) 4-point amplitude* $\mathcal{A}_{WHle}(1_e, 2_{l^j}, 3_{W^a_-}, 4_{H^\dagger_i})$.

4.1 1-loop mixing $\psi^4 \to V\psi^2 H$

The first contribution we consider is the 1-loop mixing with ψ^4. The contact on-shell amplitude associated with ψ^4 at order $1/\Lambda^2$ is given by Eq. (2.31). In the SMEFT, there are two independent amplitudes that can generate $\mathcal{A}_{WHle}$ at the 1-loop level, namely:

$$\mathcal{A}_{luqe}(1_e, 2_{l^i}, 3_u, 4_{q^j}) = \frac{C_{luqe}}{\Lambda^2} \langle 14\rangle \langle 32\rangle \epsilon^{ij} \ , \tag{4.2}$$

$$\mathcal{A}_{lequ}(1_e, 2_{l^i}, 3_u, 4_{q^j}) = \frac{C_{lequ}}{\Lambda^2} \langle 12\rangle \langle 34\rangle \epsilon^{ij} \ . \tag{4.3}$$

A third possible amplitude, $\mathcal{A} \sim \langle 13\rangle \langle 24\rangle$, can be reduced to $\mathcal{A}_{luqe}$ and $\mathcal{A}_{lequ}$ using the Schouten identity. By the properties of the spinor product, it is straightforward to see that Eq. (4.3) is antisymmetric under $1 \leftrightarrow 2$, whereas the dipole amplitude Eq. (4.1) is symmetric under that exchange. This implies that C_{lequ} cannot contribute to the renormalization of C_{WHle}, so we only have to consider the mixing with C_{luqe}.

There is, naturally, freedom in the choice of the amplitude basis. For example, in the Warsaw basis [65] we have the operators $\mathcal{O}^{(1)}_{lequ} = (\bar{L}^j_L e_R)\epsilon_{jk}(\bar{Q}^k_L u_R)$ and $\mathcal{O}^{(3)}_{lequ} = (\bar{L}^j_L \sigma_{\mu\nu} e_R)\epsilon_{jk}(\bar{Q}^k_L \sigma^{\mu\nu} u_R)$, which are associated to the contact amplitudes $\langle 12\rangle \langle 34\rangle$ and $(2\langle 14\rangle \langle 32\rangle - \langle 12\rangle \langle 34\rangle)$. However, the choice of basis Eq. (4.2), Eq. (4.3) is a natural choice when working with on-shell amplitudes, since $\langle 14\rangle \langle 32\rangle$ and $\langle 12\rangle \langle 34\rangle$ are the simplest spinor structures we can build.

Let us compute the 1-loop mixing of C_{luqe} into C_{WHle} with the three different methods described in Chapter 3.

4.1.1 Method I: $\gamma_{\{WHle,luqe\}}$ from amplitude 2-cuts

First, we use Eq. (3.16) that was derived in Section 3.2.2. The only contribution to the anomalous dimension corresponds to the 2-cut in Figure 4.2, so we can write

$$\begin{aligned}\gamma_{\{WHle,luqe\}} \frac{C_{luqe}}{C_{WHle}} &\mathcal{A}_{WHle}(1_e, 2_l, 3_{W^a_-}, 4_{H^\dagger}) \\ &= \frac{1}{4\pi^3} \int d\text{LIPS}\, \mathcal{A}_{luqe}(1_e, 2_l, 3'_u, 4'_q) \times \mathcal{A}_{\text{SM}}(-4'_{\bar{q}}, -3'_{\bar{u}}, 3_{W^a_-}, 4_{H^\dagger}) \ ,\end{aligned} \tag{4.4}$$

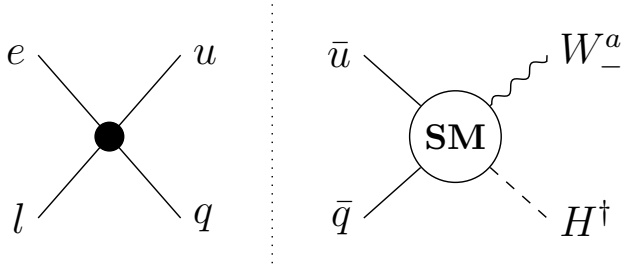

Figure 4.2: *Diagram of the 2-cut relevant for the renormalization of* $\mathcal{A}_{WHle}$ *by* $\mathcal{A}_{lequ}$.

where $\mathcal{A}_{WHle}$ and $\mathcal{A}_{luqe}$ are given by Eq. (4.1) and Eq. (4.2), and $\mathcal{A}_{\rm SM}$ is the Standard Model amplitude in Eq. (2.10). The internal spinor momenta p'_3, p'_4 satisfy $p'_3+p'_4 = p_3+p_4 = -p_1-p_2$. Expressing the amplitudes in terms of spinor-helicity variables, Eq. (4.4) becomes

$$\gamma_{\{WHle,luqe\}} \frac{\langle 31\rangle \langle 32\rangle \; T^a}{\Lambda^2} = -\frac{y_u g_2 N_c}{4\pi^3} T^a \int d\text{LIPS} \, \frac{\langle 23'\rangle \langle 4'1\rangle}{\Lambda^2} \times \frac{\langle 34\rangle \langle 33'\rangle}{\langle 43'\rangle \langle 3'4'\rangle} \; . \tag{4.5}$$

The next step is to perform the phase-space integration as described in Section 3.4.3. We parameterize the internal spinors $|3'\rangle$, $|4'\rangle$ in terms of the external spinors $|3\rangle$, $|4\rangle$, leading to

$$\begin{aligned} |3'\rangle &= c_\theta \, |3\rangle - s_\theta e^{i\phi} \, |4\rangle \; , \\ |4'\rangle &= s_\theta e^{-i\phi} \, |3\rangle + c_\theta \, |4\rangle \; . \end{aligned} \tag{4.6}$$

The dLIPS integral corresponds to a solid angle integration, as given by Eq. (3.56). With this replacement, the phase-space integral in the RHS of Eq. (4.5) becomes

$$\begin{aligned} &\int d\text{LIPS} \, \frac{\langle 23'\rangle \langle 4'1\rangle \langle 34\rangle \langle 33'\rangle}{\langle 43'\rangle \langle 3'4'\rangle} \\ &\quad = \frac{\pi}{2} \int_0^{2\pi} \frac{d\phi}{2\pi} \int_0^{\pi/2} d\theta \; 2 s_\theta c_\theta \; \frac{s_\theta e^{i\phi}}{c_\theta} \left(c_\theta \langle 23\rangle - s_\theta e^{i\phi} \langle 24\rangle \right) \left(s_\theta e^{-i\phi} \langle 31\rangle + c_\theta \langle 41\rangle \right) \\ &\quad = -\pi \langle 31\rangle \langle 32\rangle \int_0^{\pi/2} d\theta \; s_\theta^3 c_\theta = -\frac{\pi}{4} \langle 31\rangle \langle 32\rangle \; . \end{aligned} \tag{4.7}$$

Notice how the ϕ integration projects the amplitude product to $\langle 31\rangle \langle 32\rangle$, which is the spinor structure of $\mathcal{A}_{WHle}$. Going back to Eq. (4.5), we can finally obtain the anomalous dimension

$$\gamma_{\{WHle,luqe\}} = \frac{y_u g_2 N_c}{16\pi^2} \; . \tag{4.8}$$

Following Eq. (3.1), the total 1-loop anomalous dimension is $\gamma_{WHle} = \sum_j \gamma_{\{WHle,j\}} \cdot C_{\mathcal{O}_j}$, where $\gamma_{\{WHle,j\}}$ represents the mixing between C_{WHle} and $C_{\mathcal{O}_j}$. Then Eq. (4.8) can also be written as

$$\gamma_{WHle} \supset \frac{y_u g_2 N_c}{16\pi^2} C_{luqe} \; . \tag{4.9}$$

As a final remark, notice that the choice of parameterization in Eq. (4.6) is not unique. We can interchange the spinors $3 \leftrightarrow 4$ and $3' \leftrightarrow 4'$, and we can also write the internal spinors in terms of the momenta p_1, p_2 instead of p_3, p_4. The dLIPS integral can be more or less complicated depending on the parameterization, but the final result remains the same.

4.1.2 Method II: $\gamma_{\{WHle,luqe\}}$ from momentum deformation

We can compute the anomalous dimension using the method of momentum deformation from Section 3.2.3. Using Eq. (3.23) for the mixing of $\mathcal{A}_{luqe}$ into $\mathcal{A}_{WHle}$, we obtain:

$$\begin{aligned}&\gamma_{\{WHle,luqe\}}\frac{C_{luqe}}{C_{WHle}}\mathcal{A}_{WHle}(1_e,2_l,3_{W_-^a},4_{H^\dagger})\\&\quad=\frac{-i}{8\pi^4}\int d\text{LIPS}\int_{\mathcal{C}}\frac{dz}{z}\,\mathcal{A}_{luqe}(1_e,2_l,3'_u(z),4'_q(z))\times\mathcal{A}_{\text{SM}}(-4'_{\bar{q}}(z),-3'_{\bar{u}}(z),3_{W_-^a},4_{H^\dagger})\ ,\end{aligned}\tag{4.10}$$

where the internal momenta are shifted as follows:

$$\begin{aligned}&|4'\rangle\to|4'\rangle+z\,|3'\rangle\ ,\qquad&&|3'\rangle\to|3'\rangle\ ,\\&|3']\to|3']+z\,|4']\ ,\qquad&&|4']\to|4']\ .\end{aligned}\tag{4.11}$$

Now we must perform the contour z integral before the phase-space integration. The product of the shifted subamplitudes in the RHS of Eq. (4.10) is

$$\frac{\langle23'\rangle\,\langle4'1\rangle\,\langle34\rangle\,\langle33'\rangle}{\langle43'\rangle\,\langle3'4'\rangle}\to\frac{\langle23'\rangle\,(\langle4'1\rangle+z\,\langle3'1\rangle)\,\langle34\rangle\,\langle33'\rangle}{\langle43'\rangle\,\langle3'4'\rangle}\ .\tag{4.12}$$

We have a contour integral with the following structure

$$\int_{\mathcal{C}}\frac{dz}{z}\,(a+zb)=2\pi i a\ ,\tag{4.13}$$

where a and b are real constants. As noted earlier, the result of the integral is the z-independent coefficient of the Lauren series of the integrand at $z=\infty$ (times $2\pi i$). Then we have

$$\int_{\mathcal{C}}\frac{dz}{z}\frac{\langle23'\rangle\,(\langle4'1\rangle+z\,\langle3'1\rangle)\,\langle34\rangle\,\langle33'\rangle}{\langle43'\rangle\,\langle3'4'\rangle}=2\pi i\,\frac{\langle23'\rangle\,\langle4'1\rangle\,\langle34\rangle\,\langle33'\rangle}{\langle43'\rangle\,\langle3'4'\rangle}\ .\tag{4.14}$$

We can see how the z integration has not changed the kinematic structure of the amplitude product. The phase integration in Eq. (4.10) matches that in Eq. (4.7), leading to the anomalous dimension in Eq. (4.8). This is an example of how Eq. (3.23) coincides with Eq. (3.16) for renormalizations with $\Delta n=0$. Indeed, the contour integration in Eq. (3.23) removes the contributions from triangles and boxes to the 2-cuts, but in our case those contributions were already zero.

Notice how our choice of the BCFW shift made the contour integration very simple. We can choose the other possible BCFW shift, interchanging $3\leftrightarrow4$ in Eq. (4.11). In that case, instead of Eq. (4.13) we obtain the following contour integral

$$\int_{\mathcal{C}}\frac{dz}{z}\frac{(a+zb)\,(c+zd)}{(e+zf)}=2\pi i\,\frac{adf+bcf-bde}{f^2}\ .\tag{4.15}$$

While it is not immediately apparent that both shift choices are equivalent, we know they must be. Indeed, if we write a,b,c,d,e,f in terms of the corresponding spinor products and simplify the expression using the Schouten identity, we obtain the same result as in Eq. (4.14).

4.1.3 Method III: $\gamma_{\{WHle,luqe\}}$ from form factor unitarity cuts

We can also compute the anomalous dimension using form factor renormalization, as described in Section 3.2.4. Applying Eq. (3.35) to the mixing of F_{luqe} and F_{WHle}, we obtain:

$$\begin{aligned}&\gamma_{\{WHle,luqe\}} F_{WHle}(1_e, 2_l, 3_{W_-^a}, 4_{H^\dagger}) \\ &\qquad = \frac{1}{4\pi^3} \int d\text{LIPS}\, F_{luqe}(1_e, 2_l, 3'_u, 4'_q) \times A_{\text{SM}}(-4'_{\bar{q}}, -3'_{\bar{u}}, 3_{W_-^a}, 4_{H^\dagger}) \ .\end{aligned} \tag{4.16}$$

Again, the contribution comes solely from the 2-cut in Figure 4.2. Expressing the equation in terms of spinor-helicity variables leads to

$$\gamma_{\{WHle,luqe\}} \frac{\langle 31\rangle \langle 32\rangle \ T^a}{\Lambda^2} = -\frac{y_u g_2 N_c}{4\pi^3} T^a \int d\text{LIPS}\, \frac{\langle 23'\rangle \langle 4'1\rangle}{\Lambda^2} \times \frac{\langle 34\rangle \langle 33'\rangle}{\langle 43'\rangle \langle 3'4'\rangle} \ . \tag{4.17}$$

This is similar to Eq. (4.5), except that now the form factors have $p_1+p_2+p_3+p_4 = Q \neq 0$ and $p_1+p_2+p'_3+p'_4 = Q \neq 0$[1]. For the phase-space integral, our previous choice of parameterization was Eq. (4.6), which imposes momentum conservation in the SM amplitude $p'_3 + p'_4 = p_3 + p_4$. However, we did not use momentum conservation in the amplitude $\mathcal{A}_{luqe}$. This means our computation is also valid for the form factors in Eq. (4.17)[2]. Proceeding as before and taking the limit $Q \to 0$ at the end of the calculation yields Eq. (4.8) once more. This is a check that, as we proved in Section 3.2.2, Eq. (3.16) and Eq. (3.35) coincide at this order.

4.2 1-loop mixing $V\psi^2 H \to V\psi^2 H$

We now examine the mixings of $WHle$ with other dipoles. Excluding self-renormalization, the only SMEFT amplitude of class $V\psi^2 H$ that can generate $WHle$ at one loop is:

$$\mathcal{A}_{BHle}(1_e, 2_{l^j}, 3_{B_-}, 4_{H_i^\dagger}) = \frac{C_{BHle}}{\Lambda^2} \langle 31\rangle \langle 32\rangle \, \delta_i^j \ . \tag{4.18}$$

The calculation can be done using any of the three methods we have previously described. In this case, method I is the most convenient one. Since $\Delta n = 0$, there is no advantage in using method II. Moreover, as F_{BHle} is a 4-point form factor, method III involves essentially the same computations as method I. For these reasons, we focus on method I. There are two contributions to Eq. (3.16), corresponding to the 2-cuts in Figure 4.3. We can write:

$$\begin{aligned}&\gamma_{\{WHle,BHle\}} \frac{C_{BHle}}{C_{WHle}} \mathcal{A}_{WHle}(1_e, 2_l, 3_{W_-^a}, 4_{H^\dagger}) \\ &\qquad = \frac{1}{4\pi^3} \int d\text{LIPS}\, \mathcal{A}_{BHle}(1_e, 2_l, 3'_{B_-}, 4'_{H^\dagger}) \times \mathcal{A}_{\text{SM}}(-3'_{B_+}, -4'_H, 3_{W_-^a}, 4_{H^\dagger}) \\ &\qquad\quad + \frac{1}{4\pi^3} \int d\text{LIPS}\, \mathcal{A}_{BHle}(1_e, 2'_l, 3'_{B_-}, 4_{H^\dagger}) \times \mathcal{A}_{\text{SM}}(-3'_{B_+}, -2'_{\bar{l}}, 3_{W_-^a}, 2_l) \ .\end{aligned} \tag{4.19}$$

[1] In Eq. (4.4) we had $p_1 + p_2 + p_3 + p_4 = 0$ and $p_1 + p_2 + p'_3 + p'_4 = 0$ for the amplitudes $\mathcal{A}_{WHle}$ and $\mathcal{A}_{luqe}$.

[2] The choice of parameterization of the internal spinors in terms of p_1, p_2 is not valid in this case, since it imposes $p_1 + p_2 + p'_3 + p'_4 = 0$, which is not true.

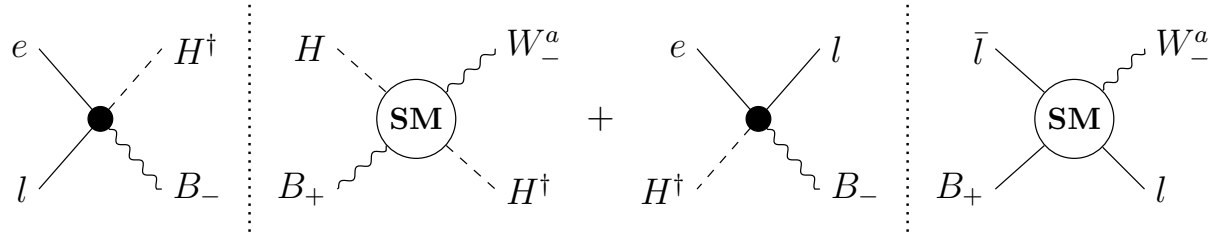

Figure 4.3: *Diagrams illustrating the two 2-cuts contributing to the renormalization of* $\mathcal{A}_{WHle}$ *by* $\mathcal{A}_{BHle}$.

Using Eqs. (4.1, 4.18) for the $1/\Lambda^2$ amplitudes and Eqs. (2.12, 2.13) for the SM amplitudes, we have

$$\begin{aligned}\gamma_{\{WHle,BHle\}}\frac{\langle 31\rangle\,\langle 32\rangle\;T^a}{\Lambda^2} = \frac{g_1 g_2 Y_H}{4\pi^3}T^a\int d\text{LIPS}\,\frac{\langle 3'1\rangle\,\langle 3'2\rangle}{\Lambda^2}\times\frac{\langle 4'3\rangle\,\langle 43\rangle}{\langle 4'3'\rangle\,\langle 43'\rangle}\\ -\frac{g_1 g_2 Y_l}{4\pi^3}T^a\int d\text{LIPS}\,\frac{\langle 3'1\rangle\,\langle 3'2'\rangle}{\Lambda^2}\times\frac{\langle 23\rangle^2}{\langle 23'\rangle\,\langle 3'2'\rangle}\;.\end{aligned} \tag{4.20}$$

After performing the two phase-space integrations, we find:

$$\gamma_{\{WHle,BHle\}} = \frac{g_1 g_2 Y_H}{4\pi^2}\int_0^{\pi/2} d\theta c_\theta^3 s_\theta + \frac{g_1 g_2 Y_l}{4\pi^2}\int_0^{\pi/2} d\theta s_\theta c_\theta = \frac{g_1 g_2}{16\pi^2}\left(Y_H + 2Y_l\right)\;. \tag{4.21}$$

Given that the hypercharges satisfy $Y_H = Y_l + Y_e$, we can finally write

$$\gamma_{\{WHle,BHle\}} = \frac{g_1 g_2}{16\pi^2}\left(3Y_l + Y_e\right)\;. \tag{4.22}$$

4.3 1-loop mixing $V^2H^2 \to V\psi^2 H$

Next, we examine the mixings involving $V\psi^2 H$. There are two different SMEFT amplitudes of this class that generate $WHle$ at one loop:

$$\mathcal{A}_{W^2H^2}(1_{W_-^a}, 2_{W_-^a}, 3_{H^j}, 4_{H_i^\dagger}) = \frac{C_{W^2H^2}}{\Lambda^2}\langle 12\rangle^2\,\delta_i^j\;, \tag{4.23}$$

$$\mathcal{A}_{WBH^2}(1_{W_-^a}, 2_{B_-}, 3_{H^j}, 4_{H_i^\dagger}) = \frac{C_{WBH^2}}{\Lambda^2}\langle 12\rangle^2\,(T^a)_i^j\;. \tag{4.24}$$

Again, we use method I to obtain the anomalous dimension matrix. For the mixing with W^2H^2, the only contribution to Eq. (3.16) is given by the 2-cut in Figure 4.4, which is

$$\begin{aligned}\gamma_{\{WHle,W^2H^2\}}\frac{C_{W^2H^2}}{C_{WHle}}&\mathcal{A}_{WHle}(1_e, 2_l, 3_{W_-^a}, 4_{H^\dagger})\\ &= \frac{1}{4\pi^3}\int d\text{LIPS}\,\mathcal{A}_{W^2H^2}(3_{W_-^a}, 4_{H^\dagger}, 1'_{W_-^a}, 2'_H)\times\mathcal{A}_{\text{SM}}(-1'^a_{W_+}, -2'_{H^\dagger}, 1_e, 2_l)\;.\end{aligned} \tag{4.25}$$

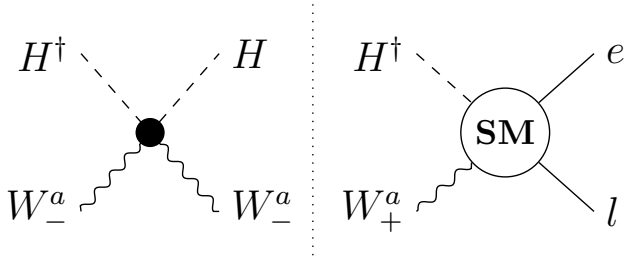

Figure 4.4: *Diagram of the 2-cut contributing to the renormalization of* $\mathcal{A}_{WHle}$ *by* $\mathcal{A}_{W^2H^2}$.

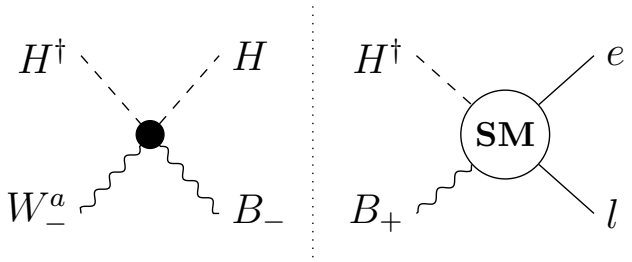

Figure 4.5: *Diagram of the 2-cut contributing to the renormalization of* $\mathcal{A}_{WHle}$ *by* $\mathcal{A}_{WBH^2}$.

Thus, the anomalous dimension is

$$\gamma_{\{WHle,W^2H^2\}} = \frac{y_e g_2}{4\pi^3}\frac{1}{\langle 31\rangle\langle 32\rangle}\int d\text{LIPS}\,\frac{\langle 31'\rangle^2\langle 2'2\rangle\langle 12\rangle}{\langle 1'2'\rangle\langle 1'2\rangle} = -\frac{y_e g_2}{2\pi^2}\int_0^{\pi/2} d\theta\, s_\theta^3 c_\theta = -\frac{y_e g_2}{8\pi^2}\ . \quad (4.26)$$

For the remaining amplitude $\mathcal{A}_{WBH^2}$, there is again one single 2-cut contribution to Eq. (3.16), as shown in Figure 4.5. The anomalous dimension is given by

$$\begin{aligned}&\gamma_{\{WHle,WBH^2\}}\frac{C_{WBH^2}}{C_{WHle}}\mathcal{A}_{WHle}(1_e,2_l,3_{W_-^a},4_{H^\dagger})\\ &\qquad = \frac{1}{4\pi^3}\int d\text{LIPS}\,\mathcal{A}_{WBH^2}(3_{W_-^a},4_{H^\dagger},1'_{B_-},2'_H)\times\mathcal{A}_{\text{SM}}(-1'_{B_+},-2'_{H^\dagger},1_e,2_l)\ ,\end{aligned} \quad (4.27)$$

and finally we obtain

$$\begin{aligned}\gamma_{\{WHle,WBH^2\}} &= \frac{y_e g_1}{4\pi^3}\frac{1}{\langle 31\rangle\langle 32\rangle}\int d\text{LIPS}\,\langle 31'\rangle^2\left(Y_l\frac{\langle 2'2\rangle\langle 12\rangle}{\langle 1'2'\rangle\langle 1'2\rangle} - Y_e\frac{\langle 2'1\rangle\langle 21\rangle}{\langle 1'2'\rangle\langle 1'1\rangle}\right)\\ &= -\frac{y_e g_1}{2\pi^2}\int_0^{\pi/2} d\theta\,\left(Y_l s_\theta^3 c_\theta - Y_e s_\theta c_\theta^3\right) = -\frac{y_e g_1}{8\pi^2}\left(Y_l - Y_e\right)\ .\end{aligned} \quad (4.28)$$

4.4 1-loop mixing $V^3 \to V\psi^2 H$

The remaining mixing corresponds to amplitudes of class V^3. The only SMEFT amplitude that can generate $WHle$ at one loop is

$$\mathcal{A}_{W^3}(1_{W_-^a},2_{W_-^b},3_{W_-^c}) = \frac{iC_{W^3}}{\Lambda^2}\langle 12\rangle\langle 23\rangle\langle 31\rangle f^{abc}\ . \quad (4.29)$$

Notice that this is the first time we are encountering a $\Delta n = 1$ mixing and a 3-point $1/\Lambda^2$ amplitude, so it is interesting to compute the anomalous dimension using the three different methods explained in Chapter 3.

4.4.1 Method I: $\gamma_{\{WHle,W^3\}}$ from amplitude 2-cuts

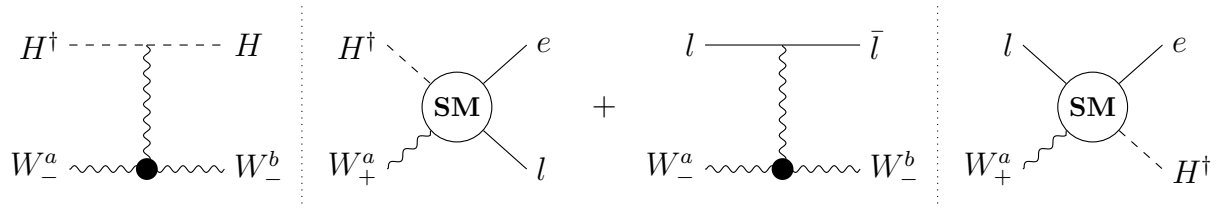

(a) (b)

Figure 4.6: *Diagrams of the 2-cuts that contribute to the renormalization of $\mathcal{A}_{WHle}$ by $\mathcal{A}_{W^3}$.*

In this case there are two contributions to the anomalous dimension, given by the 2-cuts in Figure 4.6. Eq. (3.16) becomes

$$\begin{aligned}\gamma_{\{WHle,W^3\}}\frac{C_{W^3}}{C_{WHle}}&\mathcal{A}_{WHle}(1_e,2_l,3_{W_-^a},4_{H^\dagger})\\ &=\frac{1}{4\pi^3}\int d\text{LIPS}\,\hat{\mathcal{A}}_{W^3}(3_{W_-^a},4_{H^\dagger},1'_H,2'_{W_-^b})\times\mathcal{A}_{\text{SM}}(-1'_{H^\dagger},-2'_{W_+^b},1_e,2_l)\\ &\quad+\frac{1}{4\pi^3}\int d\text{LIPS}\,\hat{\mathcal{A}}_{W^3}(3_{W_-^a},2_l,1'_{\bar{l}},4'_{W_-^b})\times\mathcal{A}_{\text{SM}}(-1'_l,-4'_{W_+^b},1_e,4_{H^\dagger})\,,\end{aligned}\tag{4.30}$$

where $\hat{\mathcal{A}}_{W^3}$ is a non-minimal (or factorizable) amplitude that includes the $\mathcal{A}_{W^3}$ contact amplitude Eq. (4.29). These amplitudes can be computed using the strategies outlined in Section 1.3.2. For example, we can use the ansatz method and impose proper factorization and crossing $a \leftrightarrow b$. Ultimately, we obtain

$$\hat{\mathcal{A}}_{W^3}(3_{W_-^a},4_{H_i^\dagger},1'_{H^j},2'_{W_-^b})=\frac{ig_2C_{W^3}f^{abc}(T^c)_i^j}{2\Lambda^2}\left[\frac{\langle 31'\rangle\langle 42'\rangle\langle 32'\rangle}{\langle 1'4\rangle}-\frac{\langle 2'1'\rangle\langle 34\rangle\langle 32'\rangle}{\langle 1'4\rangle}\right]\,,\tag{4.31}$$

$$\hat{\mathcal{A}}_{W^3}(3_{W_-^a},2_{l^j},1'_{\bar{l}_i},4'_{W_-^b})=\frac{ig_2C_{W^3}f^{abc}(T^c)_i^j}{\Lambda^2}\frac{\langle 34'\rangle\langle 32\rangle\langle 24'\rangle}{\langle 1'2\rangle}\,.\tag{4.32}$$

Using these expressions, together with Eq. (2.10) for the SM amplitudes, the RHS of Eq. (4.30) can be written as

$$\begin{aligned}&rT^a\int d\text{LIPS}\,\langle 12\rangle\left[\frac{\langle 32'\rangle}{2}\left(\frac{\langle 31'\rangle}{\langle 2'1'\rangle}+\frac{\langle 23\rangle}{\langle 2'2\rangle}\right)+\langle 43\rangle\left(\frac{\langle 31'\rangle}{\langle 41'\rangle}+\frac{\langle 32\rangle\langle 1'2'\rangle}{\langle 41'\rangle\langle 2'2\rangle}\right)\right]\\ &+rT^a\int d\text{LIPS}\,\langle 23\rangle\left[\langle 34'\rangle\left(\frac{\langle 11'\rangle}{\langle 4'1'\rangle}+\frac{\langle 41\rangle}{\langle 4'4\rangle}\right)+\langle 21\rangle\left(\frac{\langle 31'\rangle}{\langle 21'\rangle}+\frac{\langle 34\rangle\langle 1'4'\rangle}{\langle 21'\rangle\langle 4'4\rangle}\right)\right]\,,\end{aligned}\tag{4.33}$$

with $r = -\frac{g_2^2 y_e C_{W^3}}{4\pi^3\Lambda^2}$. We have rearranged the spinor-helicity variables with the Schouten identity and we have used that $f^{abc}T^bT^c = iNT^a/2$ for an SU(N) group. Next, we must perform the phase-space integration. In the first line of Eq. (4.33) we parameterize $|1'\rangle, |2'\rangle$ in terms of $|1\rangle, |2\rangle$. In the second line we parameterize $|1'\rangle, |4'\rangle$ in terms of $|1\rangle, |4\rangle$. This leads to

$$\begin{aligned} & rT^a \left[-\frac{1}{2}\langle 31\rangle\langle 32\rangle + \int d\text{LIPS}\ \langle 12\rangle\langle 43\rangle \frac{\langle 31\rangle s_\theta e^{-i\phi} - \langle 32\rangle \frac{s_\theta^2}{c_\theta}}{\langle 41\rangle s_\theta e^{-i\phi} + \langle 42\rangle c_\theta} \right] \\ & + rT^a \left[\frac{1}{2}\langle 31\rangle\langle 32\rangle + \int d\text{LIPS}\ \langle 23\rangle\langle 21\rangle \frac{\langle 31\rangle s_\theta e^{-i\phi} - \langle 34\rangle \frac{s_\theta^2}{c_\theta}}{\langle 21\rangle s_\theta e^{-i\phi} + \langle 24\rangle c_\theta} \right] . \end{aligned} \tag{4.34}$$

In both lines, the second term contains a polynomial of $e^{i\phi}$ in the denominator, which makes the dLIPS integration more involved. The ϕ integral is equivalent to a contour integral of $z = e^{i\phi}$ along a unit circle, which can be computed with Cauchy's theorem. In our case we have

$$\int_0^{2\pi} \frac{d\phi}{2\pi} \frac{ae^{-i\phi}+b}{ce^{-i\phi}+d} = \frac{1}{2\pi i}\oint \frac{dz}{z}\frac{a+bz}{c+dz} = \frac{a}{c} + \left(\frac{b}{d}-\frac{a}{c}\right)\Theta\left(1-\left|\frac{c}{d}\right|\right) , \tag{4.35}$$

where we have added the contributions from the poles at $z=0$ and $z=-c/d$. The Θ function ensures that we only include the residue at $z=-c/d$ when the pole falls inside the unit circle. If c/d depends on the θ angle, the Θ function changes the integration limits of the $d\theta$ integral. For example, one of the terms in Eq. (4.34) is

$$\begin{aligned} \frac{2}{\pi}\int d\text{LIPS}\ \frac{\langle 31\rangle s_\theta e^{-i\phi} - \langle 32\rangle \frac{s_\theta^2}{c_\theta}}{\langle 41\rangle s_\theta e^{-i\phi} + \langle 42\rangle c_\theta} &= \frac{\langle 31\rangle}{\langle 41\rangle} - \int_0^{\arctan\sqrt{\frac{s_{24}}{s_{14}}}} d\theta 2 s_\theta c_\theta \left(\frac{\langle 32\rangle s_\theta^2}{\langle 42\rangle c_\theta^2} + \frac{\langle 31\rangle}{\langle 41\rangle}\right) \\ &= \frac{\langle 31\rangle}{\langle 41\rangle} + \frac{\langle 34\rangle\langle 21\rangle}{\langle 41\rangle\langle 42\rangle}\frac{s_{24}}{s_{24}+s_{14}} + \frac{\langle 32\rangle}{\langle 42\rangle}\ln\left(\frac{s_{14}}{s_{24}+s_{14}}\right) , \end{aligned} \tag{4.36}$$

where the integration limit $\theta \leq \arctan\left(\sqrt{s_{24}/s_{14}}\right)$ comes from the $\Theta\left(1-\left|\frac{\langle 41\rangle s_\theta}{\langle 42\rangle c_\theta}\right|\right)$ function. The remaining integral in Eq. (4.34) can be computed in a similar manner. Finally, the anomalous dimension is

$$\gamma_{\{WHle,W^3\}} = \frac{g_2^2 y_e}{8\pi^2}\left[\frac{1}{2} - \frac{s_{12}}{s_{24}}\ln\left(\frac{s_{14}}{s_{14}+s_{24}}\right)\right] - \frac{g_2^2 y_e}{8\pi^2}\left[\frac{1}{2} + \frac{s_{12}}{s_{24}}\ln\left(\frac{s_{12}}{s_{24}+s_{12}}\right)\right] . \tag{4.37}$$

Notice that the individual 2-cuts (a) and (b) in Figure 4.6 contain logarithms, which arise from the presence of triangles and boxes. As explained in Section 3.2.3, this is something we expect for renormalizations with $\Delta n = 1$ instead of $\Delta n = 0$. Logarithms are expected to cancel when summing over all 2-cuts in Eq. (3.16). Indeed, using the condition $s_{12}+s_{14}+s_{24}=0$, Eq. (4.37) becomes

$$\gamma_{\{WHle,W^3\}} = \frac{g_2^2 y_e}{8\pi^2}\left[\frac{1}{2} - \frac{s_{12}}{s_{24}}\ln\left(\frac{s_{14}}{-s_{12}}\right)\right] - \frac{g_2^2 y_e}{8\pi^2}\left[\frac{1}{2} + \frac{s_{12}}{s_{24}}\ln\left(\frac{s_{12}}{-s_{14}}\right)\right] = 0 , \tag{4.38}$$

where the logarithms from (a) and (b) cancel out as expected. In this case, surprisingly, the non-logarithmic terms also cancel and the anomalous dimension is zero.

As a final remark, the coefficients in front of the logarithms in Eq. (4.37) are related to the box coefficients of the amplitude $\mathcal{A}_{ij}^{1-\text{loop}}$ for the mixing $\mathcal{A}_{W^3} \to \mathcal{A}_{WHle}$. In Appendix C.2, we show how those coefficients can be computed directly from 4-cuts of $\mathcal{A}_{ij}^{1-\text{loop}}$.

4.4.2 Method II: $\gamma_{\{WHle,W^3\}}$ from momentum deformation

The computation of $\gamma_{\{WHle,W^3\}}$ can be simplified using Eq. (3.23), which eliminates the contributions from triangles and boxes in the individual cuts before the dLIPS integration. For the 2-cut (a) in Figure 4.6, we perform the following BCFW shift

$$\begin{aligned} |1'\rangle &\to |1'\rangle + z\,|2'\rangle \ , \qquad & |2'\rangle &\to |2'\rangle \ , \\ |2'] &\to |2'] + z\,|1'] \ , \qquad & |1'] &\to |1'] \ . \end{aligned} \tag{4.39}$$

Next, we perform the z integration to extract the pole at infinity, yielding

$$\begin{aligned} &\int_{\mathcal{C}} \frac{dz}{z} \langle 12\rangle \left[\frac{\langle 32'\rangle}{2} \left(\frac{\langle 31'\rangle + z\,\langle 32'\rangle}{\langle 2'1'\rangle} + \frac{\langle 23\rangle}{\langle 2'2\rangle} \right) + \langle 43\rangle \frac{\left(\langle 31'\rangle + z\,\langle 32'\rangle + \frac{\langle 32\rangle \langle 1'2'\rangle}{\langle 2'2\rangle} \right)}{\langle 41'\rangle + z\,\langle 42'\rangle} \right] \\ &\qquad = \langle 12\rangle \left[\frac{\langle 32'\rangle}{2} \left(\frac{\langle 31'\rangle}{\langle 2'1'\rangle} + \frac{\langle 23\rangle}{\langle 2'2\rangle} \right) + \frac{\langle 43\rangle\,\langle 32'\rangle}{\langle 42'\rangle} \right] \end{aligned} \tag{4.40}$$

We can proceed similarly with the other 2-cut (b). Using Eq. (3.23), the anomalous dimension is given by

$$\begin{aligned} &\gamma_{\{WHle,W^3\}} \frac{C_{W^3}}{C_{WHle}} \mathcal{A}_{WHle}(1_e, 2_l, 3_{W_-^a}, 4_{H^\dagger}) \\ &\qquad = rT^a \int d\text{LIPS}\ \langle 12\rangle \left[\frac{\langle 32'\rangle}{2} \left(\frac{\langle 31'\rangle}{\langle 2'1'\rangle} + \frac{\langle 23\rangle}{\langle 2'2\rangle} \right) + \frac{\langle 43\rangle\,\langle 32'\rangle}{\langle 42'\rangle} \right] \\ &\qquad\quad + rT^a \int d\text{LIPS}\ \langle 23\rangle \left[\langle 34'\rangle \left(\frac{\langle 11'\rangle}{\langle 4'1'\rangle} + \frac{\langle 41\rangle}{\langle 4'4\rangle} \right) + \frac{\langle 21\rangle\,\langle 34'\rangle}{\langle 24'\rangle} \right] . \end{aligned} \tag{4.41}$$

The RHS of this expression should be compared with Eq. (4.33), derived from Eq. (3.16). The first term of every line remains the same, whereas the second term has changed with the z integration. Naturally, both formulas for the anomalous dimension must coincide. Indeed, performing the phase space integration of Eq. (4.41) yields

$$\gamma_{\{WHle,W^3\}} = \frac{g_2^2 y_e}{8\pi^2} \left[\frac{1}{2} + \frac{s_{12}}{s_{14}} \left(1 + \frac{s_{12}}{s_{24}+s_{14}} \right) \right] + \frac{g_2^2 y_e}{8\pi^2} \left[\frac{1}{2} + \frac{s_{14}}{s_{24}+s_{12}} \right] = 0 \ , \tag{4.42}$$

which is zero since $s_{12} + s_{14} + s_{24} = 0$. Notice that we obtain the same terms as in Eq. (4.38) except for the logarithms, which have been removed with the momentum deformation. This shows the effectiveness of Eq. (3.23) for mixings with $\Delta n = 1$.

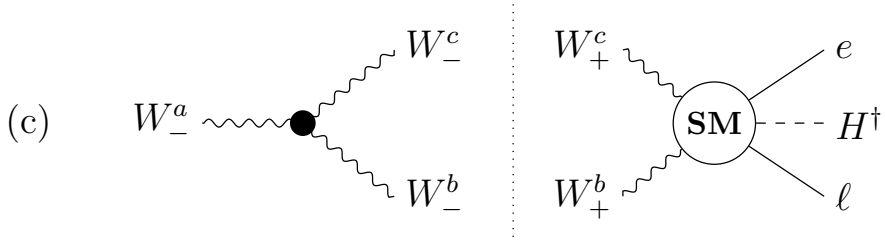

Figure 4.7: *Diagram of the extra 2-cut that contributes to the renormalization of F_{WHle} by F_{W^3}.*

4.4.3 Method III: $\gamma_{\{WHle,W^3\}}$ from form factor unitarity cuts

We can also apply form factor renormalization to the mixing $W^3 \to WHle$. Using Eq. (3.35), there are three contributions to the anomalous dimension. Two of them correspond to the 2-cuts (a) and (b), previously shown in Figure 4.6. However, now we must also consider the 2-cut (c) in Figure 4.7. The overall expression can be written as

$$\begin{aligned}
&\gamma_{\{WHle,luqe\}} F_{WHle}(1_e, 2_l, 3_{W^a_-}, 4_{H^\dagger}) \\
&\quad = \frac{1}{4\pi^3}\int d\text{LIPS}\, \hat{F}_{W^3}(3_{W^a_-}, 4_{H^\dagger}, 1'_H, 2'_{W^b_-}) \times A_{\text{SM}}(-1'_{H^\dagger}, -2'_{W^b_+}, 1_e, 2_l) \\
&\qquad + \frac{1}{4\pi^3}\int d\text{LIPS}\, \hat{F}_{W^3}(3_{W^a_-}, 2_l, 1'_l, 4'_{W^b_-}) \times A_{\text{SM}}(-1'_l, -4'_{W^b_+}, 1_e, 4_{H^\dagger}) \\
&\qquad + \frac{1}{4\pi^3}\int d\text{LIPS}\, F_{W^3}(3_{W^a_-}, 1'_{W^b_-}, 2'_{W^c_-}) \times A_{\text{SM}}(-1'_{W^b_+}, -2'_{W^c_+}, 1_e, 2_l, 4_{H^\dagger}) \ ,
\end{aligned} \tag{4.43}$$

where the last line corresponds to the 2-cut (c). This term does not appear in Eq. (4.30) because the on-shell 3-point amplitude vanishes, but we must include it when working with form factors. The contributions from cuts (a) and (b) have already been computed in the previous subsection,

$$\begin{aligned}
\gamma_{\{WHle,W^3\}} \supset\ & \frac{g_2^2 y_e}{8\pi^2}\left\{\frac{1}{2} + \frac{\langle 12\rangle\langle 43\rangle}{\langle 14\rangle\langle 32\rangle}\frac{s_{14}}{s_{24}+s_{14}} + \frac{\langle 12\rangle\langle 43\rangle}{\langle 24\rangle\langle 31\rangle}\left[\frac{s_{24}}{s_{24}+s_{14}} + \ln\left(\frac{s_{14}}{s_{14}+s_{24}}\right)\right]\right\} \\
& + \frac{g_2^2 y_e}{8\pi^2}\left\{\frac{1}{2} - \frac{s_{24}}{s_{24}+s_{12}} + \frac{\langle 12\rangle\langle 43\rangle}{\langle 24\rangle\langle 31\rangle}\left[\frac{s_{24}}{s_{24}+s_{12}} + \ln\left(\frac{s_{12}}{s_{24}+s_{12}}\right)\right]\right\} \ .
\end{aligned} \tag{4.44}$$

Notice that now $p_1+p_2+p_3+p_4 = Q^2 \neq 0$, so we cannot simplify this expression into Eq. (4.37) as we did before. The remaining cut (c) requires the phase-space integration of the minimal form factor F_{W^3} and the 5-point SM amplitude Eq. (2.14),

$$\int d\text{LIPS}\ \langle 31'\rangle\langle 2'3\rangle\langle 12\rangle\left(\frac{\langle 42\rangle}{\langle 2'4\rangle\langle 21'\rangle} + \frac{\langle 14\rangle}{\langle 12'\rangle\langle 41'\rangle}\right) \ . \tag{4.45}$$

To solve the integral, we parameterize $|1'\rangle, |2'\rangle$ as explained in Section 3.4.3. Since we have a 5-point SM amplitude, we define two spinors which are a linear combination of the external $|1\rangle, |2\rangle, |4\rangle$. Following Eq. (3.58), this is

$$|a\rangle = |1\rangle\sqrt{\frac{s_{124}}{s_{12}+s_{14}}} \ , \qquad |b\rangle = \left([12]\,|2\rangle + [14]\,|4\rangle\right)\sqrt{\frac{1}{s_{12}+s_{14}}} \ . \tag{4.46}$$

Then we can use Eq. (3.55) to write the internal spinors as

$$\begin{aligned}|1'\rangle &= c_\theta\,|a\rangle - s_\theta e^{i\phi}\,|b\rangle = \sqrt{\frac{1}{s_{12}+s_{14}}}\left[c_\theta\,|1\rangle\sqrt{s_{124}} - s_\theta e^{i\phi}\left([12]\,|2\rangle + [14]\,|4\rangle\right)\right]\,,\\ |2'\rangle &= s_\theta e^{-i\phi}\,|a\rangle + c_\theta\,|b\rangle = \sqrt{\frac{1}{s_{12}+s_{14}}}\left[s_\theta e^{-i\phi}\,|1\rangle\sqrt{s_{124}} + c_\theta\left([12]\,|2\rangle + [14]\,|4\rangle\right)\right]\,.\end{aligned} \tag{4.47}$$

After performing the phase-space integration, the contribution from cut (c) is

$$\begin{aligned}\gamma_{\{WHle,W^3\}} \supset -\frac{g_2^2 y_e}{8\pi^2}\Bigg\{1 - \frac{s_{24}}{s_{24}+s_{12}} + \frac{\langle 12\rangle\,\langle 43\rangle}{\langle 14\rangle\,\langle 32\rangle}\frac{s_{14}}{s_{24}+s_{14}}\\ + \frac{\langle 12\rangle\,\langle 43\rangle}{\langle 24\rangle\,\langle 31\rangle}\left[\frac{s_{24}}{s_{24}+s_{12}} + \frac{s_{24}}{s_{24}+s_{14}} + \ln\left(\frac{s_{12}s_{14}}{(s_{24}+s_{12})(s_{14}+s_{24})}\right)\right]\Bigg\}\,.\end{aligned} \tag{4.48}$$

The anomalous dimension is obtained by summing the three cuts, ultimately yielding $\gamma_{\{WHle,W^3\}} = 0$. Notice that the additional terms in Eq. (4.44) that we could not simplify because $Q^2 \neq 0$ are exactly canceled by the cut involving the 3-point form factor. Indeed, both Eq. (3.16) and Eq. (3.35) give the same result as expected. This is demonstrated by taking the limit $Q^2 \to 0$ of Eq. (4.43). The contributions from (a) and (b) reduce to Eq. (4.42), while the contribution from (c) goes smoothly to zero.

4.5 Comparison with the literature

Our results can be compared with previous computations of the 1-loop anomalous dimension matrix for dimension-six operators in the SMEFT. A review of the existing calculations, predominantly performed using the Feynman approach, is provided in the introduction.

Throughout this chapter we have examined the renormalization of the $\mathrm{SU}(2)_L$ dipole amplitude $\mathcal{A}_{WHle}$ by other $1/\Lambda^2$ amplitudes. In order to relate this to previous literature, we must establish the correspondence between our amplitude basis and some dimension-6 operator basis. This correspondence is presented in Appendix B, where we list the on-shell amplitudes associated with SMEFT operators in the Warsaw basis [65]. In particular, our calculation should be compared to the 1-loop anomalous dimensions of C_{eW}, the Wilson coefficient of the dipole operator $\mathcal{O}_{eW} = \bar{L}_L\sigma^a\sigma^{\mu\nu}e_R H W^a_{\mu\nu}$. Indeed, we find that our results successfully reproduce those in [20, 21, 84]. This demonstrates the utility of on-shell techniques in verifying calculations performed using other methods.

4.6 Additional observations

We have successfully computed the 1-loop anomalous dimension of the $WHle$ dipole using on-shell amplitude methods. At this point, it is pertinent to discuss some notable features of this procedure:

- We observe that, even if two mixings appear different at the level of Feynman diagrams, they can exhibit remarkable similarity when analyzed using on-shell methods. For example, the mixings $luqe \to WHle$ and $W^2H^2 \to WHle$ are reduced to the same angular integral,

$$\gamma_{\{WHle,luqe\}} = \frac{y_u g_2 N_c}{4\pi^2} \int_0^{\pi/2} d\theta \, s_\theta^3 c_\theta = \frac{y_u g_2 N_c}{16\pi^2} \ , \tag{4.49}$$

$$\gamma_{\{WHle,W^2H^2\}} = -\frac{y_e g_2}{2\pi^2} \int_0^{\pi/2} d\theta \, s_\theta^3 c_\theta = -\frac{y_e g_2}{8\pi^2} \ . \tag{4.50}$$

  This similarity arises from the helicity structure of the on-shell subamplitudes, which remains obscured in the Feynman diagram approach.

- The mixings of the dipole with ψ^4 and V^2H^2 involve only a variant of the same SM amplitude $\mathcal{A}_{\rm SM}(1_{V_+^a}, 2_{H^\dagger}, 3_\psi, 4_\psi)$. More broadly, let us consider the subset of $1/\Lambda^2$ amplitudes with $n = 4, h = -2$, as given in Eqs. (2.29, 2.30, 2.31). The anomalous dimension matrix for this subset is

$$\begin{pmatrix} \gamma_{V\psi^2H} \\ \gamma_{\psi^4} \\ \gamma_{V^2H^2} \end{pmatrix}_{\substack{n=4 \\ h=-2}} = \begin{pmatrix} \gamma_{\{V\psi^2H,V\psi^2H\}} & \gamma_{\{V\psi^2H,\psi^4\}} & \gamma_{\{V\psi^2H,V^2H^2\}} \\ \gamma_{\{\psi^4,V\psi^2\phi\}} & \gamma_{\{\psi^4,\psi^4\}} & \gamma_{\{\psi^4,V^2H^2\}} \\ \gamma_{\{V^2H^2,V\psi^2H\}} & \gamma_{\{V^2H^2,\psi^4\}} & \gamma_{\{V^2H^2,V^2H^2\}} \end{pmatrix} \begin{pmatrix} C_{V\psi^2H} \\ C_{\psi^4} \\ C_{V^2H^2} \end{pmatrix} \ . \tag{4.51}$$

  Using Eq. (3.16), we can check that all the non-diagonal mixings require uniquely the Λ^0 amplitude $\mathcal{A}(1_{V_+^a}, 2_{H^\dagger}, 3_\psi, 4_\psi)$. Similarly, for the subset of $1/\Lambda^2$ amplitudes with $n = 4, h = 0$ in Eqs. (2.32, 2.33, 2.34), the anomalous dimension matrix is

$$\begin{pmatrix} \gamma_{\Box H^4} \\ \gamma_{\psi\bar{\psi}H^2} \\ \gamma_{\psi^2\bar{\psi}^2} \end{pmatrix}_{\substack{n=4 \\ h=0}} = \begin{pmatrix} \gamma_{\{\Box H^4,\Box H^4\}} & \gamma_{\{\Box H^4,\psi\bar{\psi}H^2\}} & \gamma_{\{\Box H^4,\psi^2\bar{\psi}^2\}} \\ \gamma_{\{\psi\bar{\psi}H^2,\Box H^4\}} & \gamma_{\{\psi\bar{\psi}H^2,\psi\bar{\psi}H^2\}} & \gamma_{\{\psi\bar{\psi}H^2,\psi^2\bar{\psi}^2\}} \\ \gamma_{\{\psi^2\bar{\psi}^2,\Box H^4\}} & \gamma_{\{\psi^2\bar{\psi}^2,\psi\bar{\psi}H^2\}} & \gamma_{\{\psi^2\bar{\psi}^2,\psi^2\bar{\psi}^2\}} \end{pmatrix} \begin{pmatrix} C_{\Box H^4} \\ C_{\psi\bar{\psi}H^2} \\ C_{\psi^2\bar{\psi}^2} \end{pmatrix} \ , \tag{4.52}$$

  where now all the non-diagonal mixings involve the Λ^0 amplitude $\mathcal{A}(1_H, 2_{H^\dagger}, 3_\psi, 4_{\bar{\psi}})$. This implies that multiple 1-loop renormalizations can be computed from a single tree-level amplitude, enhancing efficiency.

- As a final remark, on-shell methods possess the convenient property of "recyclability". This property allows new calculations to build upon previous results, avoiding the need to start from scratch. Once we compute some mixing γ_{ij} it is easier to obtain the "inverse" mixing γ_{ji} because it involves the same on-shell amplitudes. As an example, let us consider the "inverse" of Eq. (4.4), which is the contribution of the dipole $\mathcal{A}_{WHle}$ to the 4-fermion amplitudes $\mathcal{A}_{lequ}$ and $\mathcal{A}_{luqe}$. The relevant 2-cut is shown in Figure 4.8.

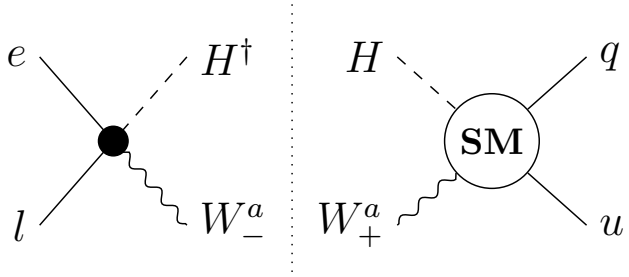

Figure 4.8: *Diagram of the 2-cut relevant for the renormalization of $\mathcal{A}_{lequ}$ and $\mathcal{A}_{luqe}$ by $\mathcal{A}_{WHle}$.*

Using Eq. (3.16), we have

$$\begin{aligned}
&\gamma_{\{lequ,WHle\}}\frac{C_{WHle}}{C_{lequ}}\mathcal{A}_{lequ}(1_e,2_l,3_u,4_q)+\gamma_{\{luqe,WHle\}}\frac{C_{WHle}}{C_{luqe}}\mathcal{A}_{luqe}(1_e,2_l,3_u,4_q)\\
&\quad=\frac{1}{4\pi^3}\int d\text{LIPS}\,\mathcal{A}_{WHle}(1_e,2_l,3'_{W_-^a},4'_{H^\dagger})\times\mathcal{A}_{\text{SM}}(-3'_{W_+^a},-4'_H,3_u,4_q)\\
&\quad=\frac{y_u g_2}{4\pi^3}\frac{C_{WHle}}{\Lambda^2}(T^a)^2\int d\text{LIPS}\,\langle 3'1\rangle\,\langle 3'2\rangle\times\frac{\langle 34\rangle\,\langle 4'4\rangle}{\langle 3'4\rangle\,\langle 3'4'\rangle}\\
&\quad=-\frac{3y_u g_2}{64\pi^2}\frac{C_{WHle}}{\Lambda^2}\left(\langle 31\rangle\,\langle 42\rangle+\langle 32\rangle\,\langle 41\rangle\right)\ ,
\end{aligned}\tag{4.53}$$

with $(T^a)^2=3/4$. Notice that, since $\mathcal{A}_{WHle}$ is symmetric under $1\leftrightarrow 2$, it can only renormalize a linear combination of 4-fermion amplitudes that share this symmetry. This selection rule is obscured when working with Feynman diagrams but becomes evident in the on-shell amplitude approach. Applying the Schouten identity to express Eq. (4.53) in terms of the 4-fermion amplitudes $\mathcal{A}_{luqe}$ and $\mathcal{A}_{lequ}$, we derive

$$\gamma_{\{luqe,WHle\}}=-2\gamma_{\{lequ,WHle\}}=\frac{3y_u g_2}{32\pi^2}\ .\tag{4.54}$$

4.7 Conclusions of the chapter

In this chapter, we have successfully applied on-shell amplitude methods to compute 1-loop renormalizations in the SMEFT, focusing on the $\text{SU}(2)_L$ dipole amplitude $\mathcal{A}_{WHle}$. This procedure offers an efficient alternative to traditional Feynman diagram loop calculations.

We have obtained the full 1-loop anomalous dimension matrix for C_{WHle}, excluding self-renormalization. We have computed the mixings of $\mathcal{A}_{WHle}$ with interactions of classes ψ^4, $V\psi^2H$, V^2H^2 and V^3, using the three methods described in Chapter 3. The simplest one is method I, which allows us to compute the anomalous dimension from a product of two tree-level amplitudes integrated over a phase space. This integral can be reduced to an angular integral, which often becomes trivial, showcasing the remarkable simplicity of the on-shell approach.

Regarding the other methods, we have demonstrated how method II of momentum deformation is primarily helpful for mixings with $\Delta n=1$, where the individual 2-cuts of method I

receive logarithmic contributions from triangle and box integrals. Such contributions are eliminated by shifting the internal momenta into the complex plane and applying Cauchy's theorem. We have also seen how method III includes additional contributions from 2-cuts involving 3-point form factors, which vanish for method I. Nevertheless, all three methods give the same result.

We have checked that our results for the anomalous dimensions associated with $\mathcal{A}_{WHle}$ match those obtained using Feynman diagram techniques in previous studies. In particular, we have considered the renormalization of the dipole operator $\mathcal{O}_{eW} = \bar{L}_L \sigma^a \sigma^{\mu\nu} e_R H W^a_{\mu\nu}$. This validates the use of on-shell methods as a robust computational tool in the SMEFT.

Our calculation has provided several insights into the power of on-shell methods. Amplitude symmetries and helicity structures are naturally embedded in the on-shell framework, simplifying the identification of non-zero contributions to the anomalous dimensions. Mixings that seem distinct in the Feynman diagram approach often reduce to similar angular integrals when analyzed on-shell, highlighting structural simplifications.

The studied methods are highly efficient because, once we have computed some on-shell amplitude, we can reuse it in related renormalizations. For example, the mixing $\mathcal{A}_{\mathcal{O}_i} \to \mathcal{A}_{\mathcal{O}_j}$ requires the same amplitudes as the inverse mixing $\mathcal{A}_{\mathcal{O}_j} \to \mathcal{A}_{\mathcal{O}_i}$. Additionally, we have seen that all 1-loop mixings between operators with the same n and h involve a single SM amplitude.

In conclusion, we have tested the advantages and versatility of on-shell amplitudes for SMEFT renormalization calculations. The considered methods offer an efficient procedure for computing anomalous dimensions, complementing other techniques.

Chapter 5

Applications of renormalization II: Lepton Flavor Violation

In this chapter we consider a phenomenological application of on-shell renormalization techniques. Following [3], we analyze Lepton Flavor Violating (LFV) muon decays, which are some of the most promising probes for new physics at the TeV scale. Using on-shell amplitude methods, we study the mixing of SMEFT higher-dimension operators into several LFV observables up to two loops.

The chapter is organized as follows: In Section 5.1 we highlight the role of LFV processes in searches for new physics. In Section 5.2 we perform a systematic analysis of $\mu \to e\gamma$, $\mu \to eee$ and $\mu N \to eN$ at tree level in the SMEFT and discuss the obtained energy bounds. In Section 5.3 we identify which operators contribute to the LFV processes at the 1-loop and 2-loop levels. In Section 5.4 we use on-shell amplitude methods to obtain the relevant anomalous dimension mixings up to two loops. We present the new energy bounds, including loop effects, in Section 5.5. As an example, we show the impact of our analysis in two different BSM models in Section 5.6. We summarize the main conclusion from this work in Section 5.7.

5.1 LFV processes as probes for BSM physics

Within the Standard Model, the number of leptons of different species $L_{e,\mu,\tau}$ is conserved in all interactions. This symmetry is considered accidental because it is not preserved by higher-dimension operators made of SM fields. Therefore, LFV processes are excellent tools for testing the SM and exploring new physics.

Considering the SMEFT expansion in powers of $1/\Lambda$ (see Section 2.2.2), the total lepton number $L = L_e + L_\mu + L_\tau$ is already not preserved at the first order $1/\Lambda$. The dimension-5 operator $\mathcal{O}_{\psi^2 H^2}$ in Eq. (2.38), which is responsible for neutrino masses, breaks lepton number by two units $\Delta L = 2$. The effects of this operator, however, are primarily relevant to neutrino physics. Indeed, since neutrino masses are so small ($m_\nu < 0.8$ eV [17]), the ratio between the Wilson coefficient $C_{\psi^2 H^2}$ and the scale of new physics Λ is expected to be small as well. Consequently, contributions of order $C_{\psi^2 H^2}/\Lambda$ to other observables are negligible.

At the next order $1/\Lambda^2$, dimension-6 operators generate LFV interactions involving charged leptons. This kind of interaction is yet to be observed experimentally, despite being predicted in the vast majority of BSM models. Here we will focus on LFV processes that violate the relative lepton numbers $L_{e,\mu,\tau}$ while preserving the total lepton number L. These processes are one of the most promising indirect probes for new physics [85], since they generically get sizable contributions from BSM effects. Moreover, dimension-6 operators that preserve total lepton number are much less suppressed than dimension-5 operators, so that they can have a larger impact on LFV observables.

For concreteness, we consider LFV processes with $\Delta L_e = \Delta L_\mu = 1$. In this category, the most competitive experimental searches are:

- $\mu \to e\gamma$: muon decay into an electron plus a photon. Currently the leading sensitivity is $\mathrm{BR}(\mu \to e\gamma) \leq 4.2 \cdot 10^{-13}$, which comes from the MEG experiment [86]. The MEG II [87] experiment is projected to continue the search for this decay and aims to achieve a sensitivity of $6 \cdot 10^{-14}$.

- $\mu \to eee$: muon decay into three electrons. The current limit was set by the SINDRUM collaboration [88] and is given by $\mathrm{BR}(\mu \to eee) \leq 10^{-12}$. The best future prospect comes from the Mu3e experiment [89], which has a target sensitivity of 10^{-16}.

- $\mu N \to eN$: muon-to-electron conversion in nuclei. The current bound on the conversion rate is $\mathrm{R}(\mu N \to eN) \leq 7 \cdot 10^{-13}$, as measured in the SINDRUM-II experiment [90]. This sensitivity is expected to improve in the future Mu2e experiment [91], reaching $8 \cdot 10^{-17}$.

These three processes are particularly interesting for BSM searches because their branching ratios in the SM are extremely small, very far from the present and future experimental sensitivities. Therefore they are very clean observables for new physics. Moreover, the searches of all three processes are expected to improve their sensitivities in the next decade [92]. Other processes with $\Delta L_e = \Delta L_\mu = 1$ include the following LFV decays:

- $h \to e\mu$ and $Z \to e\mu$, which get indirect constraints at the LHC. The current sensitivities are $\mathrm{BR}(h \to e\mu) \leq 4.4 \cdot 10^{-5}$ [93] and $\mathrm{BR}(Z \to e\mu) \leq 2.6 \cdot 10^{-7}$ [94].

- Meson decays such as $J/\psi \to \mu e$ (measured at BESIII [95]), $K_L^0 \to \mu e$ (measured at BNL E871 [96]) and $B^0 \to \mu e$ (measured at LHCb [97]). See [85] for an extensive list. We will not consider these decays in our study because they are quite constrained by other non-LFV processes.

Table 5.1 summarizes the present and future sensitivities for the LFV processes discussed in this work. Our aim is to systematically analyze $\mu \to e\gamma$, $\mu \to eee$ and $\mu N \to eN$ in a model-independent way, following the EFT approach. We will characterize the BSM contributions to the different processes using dimension-6 operators in the SMEFT. Then we will use the experimental constraints on the processes to bound the new physics energy scale Λ.

	BR($\mu \to e\gamma$)	BR($\mu \to eee$)	R($\mu N \to eN$)	BR($h \to \mu e$)	BR($Z \to \mu e$)
Current	$4.2 \cdot 10^{-13}$ [86]	$1 \cdot 10^{-12}$ [88]	$7 \cdot 10^{-13}$ [90]	$4.4 \cdot 10^{-5}$ [93]	$2.6 \cdot 10^{-7}$ [94]
Future	$6.0 \cdot 10^{-14}$ [87]	$1 \cdot 10^{-16}$ [89]	$8 \cdot 10^{-17}$ [91]		

Table 5.1: Current and near future upper bounds on $\Delta L_e = \Delta L_\mu = 1$ processes.

Previously there have been several analyses on LFV muon decays with dimension-6 operators, see for example [98–104][1]. As a novelty, in [3] we were the first to include the effects of renormalization group 2-loop mixing into the dipole operators. This allows us to bound certain Wilson coefficients that only enter the LFV observables at two loops. Our study is motivated by the next generation of LFV experiments, which will reach such high precision that it requires an EFT analysis at the 2-loop level. The calculation of anomalous dimensions up to two loops is greatly simplified thanks to on-shell amplitude methods (see [1, 26, 28–31]). See Chapter 3 for more details on this topic.

5.2 LFV experimental constraints at tree level

As mentioned in Section 2.2, the SMEFT can be used to parameterize the effects of BSM physics in a model-independent way. Here, we perform a systematic analysis of three LFV processes ($\mu \to e\gamma$, $\mu \to eee$ and $\mu N \to eN$) up to two loops, using dimension-6 operators. The goal is to understand which operators are probed by a measurement of the LFV branching ratios. Then, using the experimental sensitivities in Table 5.1, we derive bounds on the new physics scale Λ.

The general procedure goes as follows: for a given LFV process, we consider the corresponding effective Lagrangian and identify which SMEFT operators generate the effective coefficients. In this section we focus on the leading contributions, which come from Wilson coefficients that appear at tree level. In Section 5.3 we will consider higher-order contributions from operators that mix with the tree-level ones via loops.

5.2.1 Dimension-6 operator basis

The first step is to establish our choice of dimension-6 operator basis for studying the LFV processes $\mu \to e\gamma$, $\mu \to eee$ and $\mu N \to eN$. Since these processes have $\Delta L_e = \Delta L_\mu = 1$, we are interested in operators involving both μ and e. Such operators are classified in terms of their particle content as follows:

- $V\psi^2 H$:

$$\mathcal{L}_6 \supset \frac{C_{DW}^{\mu e}}{\sqrt{2}} \frac{y_\mu g_2}{\Lambda^2} \bar{L}_L^{(2)} \sigma^a \sigma^{\mu\nu} e_R^{(1)} H W_{\mu\nu}^a + \frac{C_{DB}^{\mu e}}{\sqrt{2}} \frac{y_\mu g_1}{\Lambda^2} \bar{L}_L^{(2)} \sigma^{\mu\nu} e_R^{(1)} H B_{\mu\nu} + (\mu \leftrightarrow e) + \text{h.c.} \,. \tag{5.1}$$

[1] There are similar studies for LFV processes involving τ leptons, such as [105–108].

- $\psi^2 H^3$:

$$\mathcal{L}_6 \supset C_y^{\mu e}\frac{y_\mu}{\Lambda^2}\left(H^\dagger H\right)\left(\bar{L}_L^{(2)}e_R^{(1)}H\right) + (\mu \leftrightarrow e) + \text{h.c.}\ . \tag{5.2}$$

- $\psi^2 H^2$:

$$\begin{aligned}\mathcal{L}_6 \supset\ & \frac{C_L^{\mu e}}{\Lambda^2}(H^\dagger i\overleftrightarrow{D}_\mu H)(\bar{L}_L^{(2)}\gamma^\mu L_L^{(1)}) + \frac{C_{L3}^{\mu e}}{\Lambda^2}(H^\dagger i\overleftrightarrow{D}^a_\mu H)(\bar{L}_L^{(2)}\sigma^a\gamma^\mu L_L^{(1)}) \\ & + \frac{C_R^{\mu e}}{\Lambda^2}(H^\dagger i\overleftrightarrow{D}_\mu H)(\bar{e}_R^{(2)}\gamma^\mu e_R^{(1)}) + +(\mu \leftrightarrow e)\ .\end{aligned} \tag{5.3}$$

- $\psi^2\bar{\psi}^2$:

$$\begin{aligned}\mathcal{L}_6 \supset\ & \frac{C_{LL}^{\mu e f f}}{\Lambda^2}(\bar{L}_L^{(2)}\gamma_\mu L_L^{(1)})(\bar{F}_L\gamma^\mu F_L) + \frac{C_{LL3}^{\mu e f f}}{\Lambda^2}(\bar{L}_L^{(2)}\sigma^a\gamma_\mu L_L^{(1)})(\bar{F}_L\sigma^a\gamma^\mu F_L) \\ & + \frac{C_{RR}^{\mu e f f}}{\Lambda^2}(\bar{e}_R^{(2)}\gamma_\mu e_R^{(1)})(\bar{f}_R\gamma^\mu f_R) + \frac{C_{LR}^{\mu e f f}}{\Lambda^2}(\bar{L}_L^{(2)}\gamma_\mu L_L^{(1)})(\bar{f}_R\gamma^\mu f_R) \\ & + \frac{C_{RL}^{\mu e f f}}{\Lambda^2}(\bar{e}_R^{(2)}\gamma^\mu e_R^{(1)})(\bar{F}_L\gamma_\mu F_L) + C_{LR}^{\mu lle}\frac{y_\mu}{\Lambda^2}(\bar{L}_L^{(2)}\gamma_\mu L_L)(\bar{e}_R\gamma^\mu e_R^{(1)}) \\ & + C_{LR}^{\mu qqe}\frac{y_\mu}{\Lambda^2}(\bar{L}_L^{(2)}\gamma_\mu Q_L)(\bar{d}_R\gamma^\mu e_R^{(1)}) + (\mu \leftrightarrow e) + \text{h.c.}\ .\end{aligned} \tag{5.4}$$

- ψ^4:

$$\mathcal{L}_6 \supset C_{LuQe}^{\mu eqq}\frac{y_\mu}{\Lambda^2}(\bar{L}_L^{(2)}u_R)(\epsilon\bar{Q}_L e_R^{(1)}) + C_{LeQu}^{\mu eqq}\frac{y_\mu}{\Lambda^2}(\bar{L}_L^{(2)}e_R^{(1)})(\epsilon\bar{Q}_L u_R) + (\mu \leftrightarrow e) + \text{h.c.}\ . \tag{5.5}$$

We write explicitly the flavor indices $1 = e, 2 = \mu$ for the lepton fields L_L, e_R in LFV transitions. We also specify the fermion types in the Wilson coefficients, with ℓ, q and f respectively referring to any lepton, quark and fermion. $F_L = L_L, Q_L$ is a general SM left-handed $\mathrm{SU}(2)_L$ doublet, while $f_R = e_R, u_R, d_R$ is a general right-handed singlet. For operators with $\bar{L}_L^{(2)}e_R^{(1)}$ or $L_L^{(1)}e_R^{(2)}$, we have factored out a muon Yukawa coupling y_μ due to the chirality flip. Therefore we must keep y_μ fixed when exchanging $\mu \leftrightarrow e$. Additionally, we have included a gauge coupling g_1, g_2 in the dipoles Eq. (5.1), because we expect them to be generated by a gauge theory even above the energy scale Λ.

Our choice of operators mostly corresponds to the Warsaw basis[2], replacing $\mathcal{O}_{lequ}^{(3)}$ by $\mathcal{O}_{LuQe}$ according to Eq. (B.1) and rewriting $\mathcal{O}_{ledq}$ with the Fierz identity,

$$\mathcal{O}_{ledq} = (\bar{L}_L e_R)(\bar{d}_R Q_L) = -\frac{1}{2}(\bar{L}_L\gamma_\mu Q_L)(\bar{d}_R\gamma^\mu e_R)\ . \tag{5.6}$$

[2]See [65] for the original paper. The complete basis and its corresponding on-shell amplitudes are listed in Appendix B.

We have also changed the operator labels to simplify our notation.

As a final remark, it is enlightening to rewrite Eq. (5.3) in the unitary gauge. We parameterize the Higgs doublet H as

$$H(x) = \frac{1}{\sqrt{2}} e^{iT^a \xi^a(x)/v} \begin{pmatrix} 0 \\ v + h(x) \end{pmatrix} , \tag{5.7}$$

where v is the vacuum expectation value, $h(x)$ is the physical Higgs and $\xi^a(x)$ are Goldstone bosons. $H(x)$ is invariant under local gauge transformations $H(x) \to H(x) e^{iT^a \alpha^a(x)}$. In particular we can choose $\alpha(x)$ so that the Goldstone bosons ξ^a are removed from $H(x)$. This is the so-called unitary gauge, which corresponds to

$$H(x) = \frac{1}{\sqrt{2}} \begin{pmatrix} 0 \\ v + h(x) \end{pmatrix} . \tag{5.8}$$

Using this gauge and writing explicitly the $\mathrm{SU}(2)_L$ doublet $L_L = \begin{pmatrix} \nu \\ e_L \end{pmatrix}$, Eq. (5.3) becomes

$$\begin{aligned} -\frac{g(v+h)^2}{2c_{\theta_W}} \Bigg[& \frac{C_R^{\mu e}}{\Lambda^2} Z_\mu \bar{e}_R^{(2)} \gamma^\mu e_R^{(1)} + \frac{C_L^{\mu e} + C_{L3}^{\mu e}}{\Lambda^2} \left(Z_\mu \bar{e}_L^{(2)} \gamma^\mu e_L^{(1)} - \frac{c_{\theta_W}}{\sqrt{2}} [W_\mu^+ \bar{\nu}^{(2)} \gamma^\mu e_L^{(1)} + \text{h.c.}] \right) \\ & + \frac{C_L^{\mu e} - C_{L3}^{\mu e}}{\Lambda^2} \left(Z_\mu \bar{\nu}^{(2)} \gamma^\mu \nu^{(1)} + \frac{c_{\theta_W}}{\sqrt{2}} [W_\mu^+ \bar{\nu}^{(2)} \gamma^\mu e_L^{(1)} + \text{h.c.}] \right) \Bigg] + (\mu \leftrightarrow e) , \end{aligned} \tag{5.9}$$

where θ_W is the Weinberg angle and we have rewritten the gauge boson fields $W_\mu^{1,2,3}$ and B_μ in terms of $W_\mu^\pm, Z_\mu$ and A_μ, according to

$$W^\pm = \tfrac{1}{\sqrt{2}} (W^1 \mp i W^2) , \tag{5.10}$$

$$Z_\mu = c_{\theta_W} W_\mu^3 - s_{\theta_W} B_\mu , \tag{5.11}$$

$$A_\mu = c_{\theta_W} B_\mu + s_{\theta_W} W_\mu^3 . \tag{5.12}$$

From Eq. (5.9) we see how the Wilson coefficients $C_{L,L3,R}^{\mu e}$ generate the tree-level LFV interactions $W^\pm \mu e$, $W^\pm h \mu e$, $Z \mu e$ and $Z h \mu e$. However, as explained in [24], BSM theories with custodial symmetry and $L \leftrightarrow R$ parity must have $C_L + C_{L3} = 0$. This cancellation sets to zero the $Z\mu e$ and $Zh\mu e$ interactions, and we are only left with LFV couplings involving neutrinos, which are difficult to detect. This means we cannot derive strong bounds on the combination $C_L + C_{L3}$ from direct measurements such as $W \to \mu \bar{\nu}_e, W \to e \bar{\nu}_\mu$ or $Z \to \nu_\mu \bar{\nu}_e$. Instead, we can obtain better bounds by considering the loop effects of these operators in other LFV observables, like $\mu \to e\gamma$. We will see this in detail in Section 5.3.1.

After establishing our basis of dimension-6 operators, we proceed to study how the different Wilson coefficients enter several LFV observables.

5.2.2 $\mu \to e\gamma$

The $\mu \to e\gamma$ decay arises from the following effective Lagrangian

$$\mathcal{L} = -\frac{4G_F}{\sqrt{2}} m_\mu \left[d_{\mu e} \bar{\mu}_L \sigma^{\mu\nu} e_R F_{\mu\nu} + d_{e\mu} \bar{e}_L \sigma^{\mu\nu} \mu_R F_{\mu\nu} \right] + \text{h.c.} \,, \tag{5.13}$$

where G_F is the Fermi constant and $d_{\mu e, e\mu}$ are the dipole coefficients. Note that we use the fields $e_{L,R}$ and $\mu_{L,R}$, which are related to $e_R^{(1,2)}$ and $L_L^{(1,2)}$ by

$$e_R^{(1)} = e_R \,, \qquad e_R^{(2)} = \mu_R \,, \qquad L_L^{(1)} = \begin{pmatrix} \nu_e \\ e_L \end{pmatrix} \,, \qquad L_L^{(2)} = \begin{pmatrix} \nu_\mu \\ \mu_L \end{pmatrix} \,. \tag{5.14}$$

From Eq. (5.13), we derive the branching ratio [109]

$$\text{BR}(\mu \to e\gamma) = 384\pi^2 \left(|d_{\mu e}|^2 + |d_{e\mu}|^2 \right) \,. \tag{5.15}$$

The large numerical factor can be understood because $\mu \to e\gamma$ is a two-body process, while the dominant channel $\mu \to e\bar{\nu}_e\nu_\mu$ is a three-body one. The experimental constraint on this decay, together with the projected future sensitivity, are shown in Table 5.1. Notice that the dipole coefficients are running couplings, which should be evaluated at the muon mass in Eq. (5.15).

We are interested in the SMEFT operators contributing to this LFV muon decay, since they can be constrained with the experimental measurements of $\text{BR}(\mu \to e\gamma)$. The leading contribution comes from the Wilson coefficients that generate $d_{\mu e, e\mu}$ at tree level. In this case we only have the dipoles $C_{DW,DB}^{\mu e, e\mu}$ from Eq. (5.1), which lead to

$$d_{\mu e} = \frac{v^2 g_2 s_{\theta_W}}{2\Lambda^2} \left(C_{DW}^{\mu e} - C_{DB}^{\mu e} \right) \,, \tag{5.16}$$

and analogously for $d_{e\mu}$ if we interchange $\mu \leftrightarrow e$. Substituting into Eq. (5.15), the current and future experimental bounds on $\text{BR}(\mu \to e\gamma)$ lead to the following constraints

$$\frac{1}{\Lambda^2} \sqrt{|C_{DW}^{\mu e} - C_{DB}^{\mu e}|^2 + |C_{DW}^{e\mu} - C_{DB}^{e\mu}|^2} \lesssim \begin{cases} 1/(951 \text{ TeV})^2 & \text{(current)} \\ 1/(1547 \text{ TeV})^2 & \text{(future)} \end{cases} \,. \tag{5.17}$$

Assuming $(C_{DW}^{\mu e} - C_{DB}^{\mu e}) \sim (C_{DW}^{e\mu} - C_{DB}^{e\mu}) \sim 1$, we find $\Lambda \gtrsim 951$ TeV for the current bounds and $\Lambda \gtrsim 1547$ TeV for the future ones.

5.2.3 $\mu \to eee$

The next LFV process we consider is the $\mu \to eee$ muon decay, which is generated by the effective Lagrangian

$$\begin{aligned} \mathcal{L} = -\frac{4G_F}{\sqrt{2}} \Big[& g_1 (\bar{\mu}_R e_L)(\bar{e}_R e_L) + g_2 (\bar{\mu}_L e_R)(\bar{e}_L e_R) + g_3 (\bar{\mu}_R \gamma_\mu e_R)(\bar{e}_R \gamma_\mu e_R) \\ & + g_4 (\bar{\mu}_L \gamma^\mu e_L)(\bar{e}_L \gamma_\mu e_L) + g_5 (\bar{\mu}_R \gamma^\mu e_R)(\bar{e}_L \gamma_\mu e_L) + g_6 (\bar{\mu}_L \gamma^\mu e_L)(\bar{e}_R \gamma_\mu e_R) \Big] + \text{h.c.} \,, \end{aligned} \tag{5.18}$$

plus the dipole terms in Eq. (5.13). The corresponding branching ratio is given by [109]

$$\begin{aligned}\mathrm{BR}\left(\mu\to eee\right) = 2\left(|g_3|^2+|g_4|^2\right)+|g_5|^2+|g_6|^2+32e^2\left[\ln\left(\frac{m_\mu^2}{m_e^2}\right)-\frac{11}{4}\right]\left(|d_{\mu e}|^2+|d_{e\mu}|^2\right)\\ +8e\,\mathrm{Re}\left(d_{e\mu}^* g_6^* + d_{\mu e} g_5^*\right)+16e\mathrm{Re}\left(d_{e\mu}^* g_4^* + d_{\mu e} g_3^*\right)+\frac{1}{8}\left(|\tilde{g}_1|^2+|\tilde{g}_2|^2\right)\ ,\end{aligned} \tag{5.19}$$

which has to be compared with the experimental values of Table 5.1. Let us see which dimension-6 SMEFT operators contribute to this branching ratio at tree level. We have already seen the expression for the dipoles $d_{\mu e,e\mu}$ in Eq. (5.16), whereas the g_i can be written in terms of the following Wilson coefficients

$$\begin{aligned} g_3 &= -\frac{v^2}{2\Lambda^2}\left(C_{RR}^{\mu eee}+2s_{\theta_W}^2 C_R^{\mu e}\right)\ , \quad g_4 = -\frac{v^2}{2\Lambda^2}\left(C_{LL}^{\mu eee}-(1-2s_{\theta_W}^2)\left(C_L^{\mu e}+C_{L3}^{\mu e}\right)\right)\ ,\\ g_5 &= -\frac{v^2}{2\Lambda^2}\left(C_{RL}^{\mu eee}-(1-2s_{\theta_W}^2)C_R^{\mu e}\right)\ , \quad g_6 = -\frac{v^2}{2\Lambda^2}\left(C_{LR}^{\mu eee}+2s_{\theta_W}^2\left(C_L^{\mu e}+C_{L3}^{\mu e}\right)\right)\ .\end{aligned} \tag{5.20}$$

The remaining $\tilde{g}_1$ and $\tilde{g}_2$ are zero in this order, since they are only generated by dimension-8 operators. The coefficients in Eq. (5.20) receive contributions from the $\psi^2\bar{\psi}^2$ operators $\mathcal{O}_{LL,RR,LR,RL}^{\mu eee}$, and also from the $\psi\bar{\psi}H^2$ operators $\mathcal{O}_{L,L3,R}^{\mu e}$. Notice that only the combination $C_L^{\mu e}+C_{L3}^{\mu e}$ appears, since $\mu\to eee$ is induced through the $Z\mu e$ coupling in the unitary gauge (see Eq. (5.9)).

Considering the experimental sensitivity for $\mu\to eee$, we can obtain energy bounds associated with the different operators. For simplicity, we assume that all Wilson coefficients are set to zero except for one C_i that is fixed to 1, so there are no interference effects. The bounds on Λ for the different operators are shown in Table 5.2.

5.2.4 $\mu N\to eN$

The remaining process we cover is the $\mu\to e$ conversion in nuclei. It arises from the following Lagrangian:

$$\begin{aligned}\mathcal{L} = -\frac{4G_F}{\sqrt{2}}\Big[&g_{L,V}^u(\bar{\mu}_L\gamma^\mu e_L)(\bar{u}\gamma_\mu u)+g_{R,V}^u(\bar{\mu}_R\gamma^\mu e_R)(\bar{u}\gamma_\mu u)\\ &+g_{L,S}^u(\bar{\mu}_L e_R)(\bar{u}u)+g_{R,S}^u(\bar{\mu}_R e_L)(\bar{u}u)+(u\to d)\Big]+\mathrm{h.c.}\ ,\end{aligned} \tag{5.21}$$

defined at the nuclei scale. We must also include the dipole terms in Eq. (5.13), which can lead to $\mu N\to eN$ through photon splitting into quarks. The rate for the process is given by [110]

$$\begin{aligned}\mathrm{R}(\mu N\to eN) = \frac{2G_F^2}{\omega_{capture}}\Big(&\left|D\ d_{\mu e}+g_{L,V}^{(p)}V^{(p)}+g_{L,V}^{(n)}V^{(n)}+g_{L,S}^{(p)}S^{(p)}+g_{L,S}^{(n)}S^{(n)}\right|^2\\ &+\left|D\ d_{e\mu}^*+g_{R,V}^{(p)}V^{(p)}+g_{R,V}^{(n)}V^{(n)}+g_{R,S}^{(p)}S^{(p)}+g_{R,S}^{(n)}S^{(n)}\right|^2\Big)\ ,\end{aligned} \tag{5.22}$$

where $\omega_{capture}$ is the muon nuclear capture rate and D, $V^{(p,n)}$, $S^{(p,n)}$ are overlap integrals defined in [110]. We also define the g coefficients as

$$\begin{aligned} g^{(p)}_{L/R,V} &= 2g^u_{L/R,V} + g^d_{L/R,V}, \qquad g^{(n)}_{L/R,V} = g^u_{L/R,V} + 2g^d_{L/R,V} \ , \\ g^{(p)}_{L/R,S} &= \sum_{q=u,d} G^{(q,p)}_S g^q_{L/R,S}, \qquad g^{(n)}_{L/R,S} = \sum_{q=u,d} G^{(q,n)}_S g^q_{L/R,S} \ , \end{aligned} \tag{5.23}$$

with $G^{(u,p)}_S \simeq G^{(d,n)}_S \simeq 5.1$, $G^{(d,p)}_S \simeq G^{(u,n)}_S \simeq 4.3$ and we have neglected the contribution from the s quark. The experimental measurement of Eq. (5.22) is shown in Table 5.1.

Proceeding as before, we write the effective couplings from Eq. (5.23) in terms of the Wilson coefficients that enter at tree level. For the up sector, we have

$$\begin{aligned} g^u_{L,S} &= \frac{v^2}{2\Lambda^2} y_\mu C^{\mu euu}_{LeQu} \ , \qquad g^u_{R,S} = \frac{v^2}{2\Lambda^2} y_\mu C^{e\mu uu}_{LeQu} \ , \\ g^u_{L,V} &= -\frac{v^2}{4\Lambda^2}\left[(C^{\mu euu}_{LL} + C^{\mu euu}_{LR}) + 2g^u_Z \left(C^{\mu e}_L + C^{\mu e}_{L3}\right) \right] , \\ g^u_{R,V} &= -\frac{v^2}{4\Lambda^2}\left[(C^{\mu euu}_{RL} + C^{\mu euu}_{RR}) + 2g^u_Z C^{\mu e}_R \right] , \end{aligned} \tag{5.24}$$

with $g^u_Z = (\frac{1}{2} - \frac{4}{3} s^2_{\theta_W})$. For the down sector,

$$\begin{aligned} g^d_{L,S} &= \frac{v^2}{\Lambda^2} y_\mu C^{\mu dde}_{LR} \ , \qquad g^d_{R,S} = \frac{v^2}{\Lambda^2} y_\mu C^{edd\mu}_{LR} \ , \\ g^d_{L,V} &= -\frac{v^2}{4\Lambda^2}\left[(C^{\mu edd}_{LL} + C^{\mu edd}_{LR}) + 2g^d_Z \left(C^{\mu e}_L + C^{\mu e}_{L3}\right) \right] , \\ g^d_{R,V} &= -\frac{v^2}{4\Lambda^2}\left[(C^{\mu edd}_{RL} + C^{\mu edd}_{RR}) + 2g^d_Z C^{\mu e}_R \right] , \end{aligned} \tag{5.25}$$

with $g^d_Z = (-\frac{1}{2} + \frac{2}{3} s^2_{\theta_W})$. The operators entering $\mu N \to eN$ at tree level are similar to those entering $\mu \to eee$, replacing the μeee four-fermion operators with μeuu and μedd. The only new ingredients are the ψ^4 operators $\mathcal{O}^{\mu euu}_{LeQu}$ and $\mathcal{O}^{e\mu uu}_{LeQu}$, which were not present in Eq. (5.20).

Table 5.2 summarizes the energy bounds obtained from Wilson coefficients that enter $\mathrm{R}(\mu N \to eN)$ at tree level, considering the current and future experimental sensitivities.

5.2.5 Discussion on tree-level LFV bounds

The tree-level energy bounds for the LFV processes $\mu \to e\gamma$, $\mu \to eee$ and $\mu N \to eN$ are listed in Table 5.2. For each entry, the present bounds are on the first row and the future bounds are in parenthesis on the second row. Our aim in this subsection is to identify which bounds can be significantly improved by considering loop mixings into the tree-level Wilson coefficients.

For current experiments, the most competitive bound is $\Lambda \gtrsim 951$ TeV, which comes from the dipoles $C^{\mu e, e\mu}_{DW,DB}$ in $\mu \to e\gamma$. Renormalization effects from other Wilson coefficients C_i into $(C_{DW} - C_{DB})$ are thus expected to provide strong constraints on C_i/Λ as well. At the 1-loop level, these effects are of order

$$\Delta(C_{DW} - C_{DB}) \sim C_i/16\pi^2 \qquad \Rightarrow \qquad C_i/\Lambda^2 \lesssim 1/(75 \text{ TeV})^2 \ . \tag{5.26}$$

	$\mu \to e\gamma$	$\mu \to eee$	$\mu N \to eN$	$h \to \mu e$	$Z \to \mu e$
$C_{DB}^{\mu e} - C_{DW}^{\mu e}$	951 TeV (1547 TeV)	218 TeV (2183 TeV)	208 TeV (1812 TeV)		
$C_R^{\mu e}$		160 TeV (1602 TeV)	225 TeV (1535 TeV)		
$C_L^{\mu e} + C_{L3}^{\mu e}$		164 TeV (1642 TeV)	225 TeV (1535 TeV)		5 TeV
$C_{LL(RR),LR(RL)}^{\mu eee}$		207,174 TeV (2070,1740 TeV)			
$C_{LL,RR,LR}^{\mu euu}$			352 TeV (2693 TeV)		
$C_{LL,RR,LR}^{\mu edd}$			376 TeV (2725 TeV)		
$C_{LR}^{\mu dde}$			18 TeV (164 TeV)		
$C_y^{\mu e}$				0.3 TeV	

Table 5.2: Present (future) tree-level lower bounds on Λ, coming from the different dimension-6 operators entering $\mu \to e\gamma$, $\mu \to eee$ and $\mu N \to eN$.

At the 2-loop level, we have

$$\Delta(C_{DW} - C_{DB}) \sim C_i/\left(16\pi^2\right)^2 \qquad \Rightarrow \qquad C_i/\Lambda^2 \lesssim 1/(6 \text{ TeV})^2 \ . \tag{5.27}$$

The estimated bounds are sizable even for 2-loop effects, so in our study we must include mixings into the dipoles $C_{DW,DB}^{\mu e, e\mu}$ up to two loops. The Wilson coefficients $C_{DW} - C_{DB}$ also enter the processes $\mu \to eee$ and $\mu N \to eN$ at tree level, but the current energy bounds are less competitive, around $\Lambda \gtrsim 200$ TeV. This is expected to change with the next generation of LFV experiments, since the projected sensitivities lead to an improvement by one order of magnitude on the bounds, reaching $\Lambda \gtrsim 2000$ TeV. Therefore we expect the bounds from $\mu \to eee$ and $\mu N \to eN$ to dominate over $\mu \to e\gamma$ in the future.

We must also consider the energy bounds coming from four-fermion operators entering $\mu \to eee$ and $\mu N \to eN$ at tree level, which are in the range $\Lambda \gtrsim 170 - 370$ TeV. These constraints are projected to improve around an order of magnitude in the near future, becoming comparable to the dipole bounds. For this reason, we should consider the loop mixing of other Wilson coefficients into $C_{LL,RR,LR,RL}^{\mu eee}$, $C_{LL,RR,LR}^{\mu euu}$ and $C_{LL,RR,LR}^{\mu edd}$. As an example, the current bounds for 1-loop mixings with $C_{LL}^{\mu eee}$ are of order

$$\Delta C_{LL}^{\mu eee} \sim C_i/16\pi^2 \qquad \Rightarrow \qquad C_i/\Lambda^2 \lesssim 1/(16 \text{ TeV})^2 \ . \tag{5.28}$$

And we expect to reach $\Lambda \gtrsim 160$ TeV in the future. In Section 5.3.2 we will see that it is not necessary to consider 2-loop effects to four-fermion operators, since all relevant mixings already occur at the 1-loop level and no new operators enter at two loops.

Another set of operators entering our LFV processes at tree level are the fermion-scalar operators $\mathcal{O}^{\mu e}_{L,L3,R}$. In this case the present energy bounds are $\Lambda \gtrsim 160$ TeV for $\mu \to eee$ and $\Lambda \gtrsim 225$ TeV for $\mu N \to eN$, which are again expected to improve about an order of magnitude in future experiments. For a complete analysis, we must consider the effects of 1-loop mixing of other Wilson coefficients into $C^{\mu e}_{R,L,L3}$. As we explained before, only the combination $C^{\mu e}_L + C^{\mu e}_{L3}$ appears at tree level, so we need to include the orthogonal combination $C^{\mu e}_L - C^{\mu e}_{L3}$ at one loop. The corresponding bounds are approximately

$$\Delta\left(C^{\mu e}_L + C^{\mu e}_{L3}\right) \sim C_i/16\pi^2 \qquad \Rightarrow \qquad C_i/\Lambda^2 \lesssim 1/(15\text{ TeV})^2\,, \tag{5.29}$$

that again will increase to $\Lambda \gtrsim 120$ TeV in the near future. The combination $C^{\mu e}_L - C^{\mu e}_{L3}$ can also be probed at tree level by LFV processes involving neutrinos, but the bounds are much worse. Notice that the $\mathcal{O}^{\mu e}_{R,L,L3}$ operators also receive direct constraints from the decay $Z \to \mu e$, whose branching ratio is given by [100]

$$\text{BR}(Z \to \mu e) = \frac{m_Z^3 v^2}{12\pi\Gamma_Z \Lambda^4}\left[|C^{\mu e}_R|^2 + |C^{\mu e}_L + C^{\mu e}_{L3}|^2 + \frac{y_\mu^2 g_2^2}{4}\left(|C^{\mu e}_{eZ}|^2 + |C^{e\mu}_{eZ}|^2\right)\right], \tag{5.30}$$

where we have defined $C_{DZ} = \frac{s^2_{\theta_W}}{c_{\theta_W}} C_{DB} + c_{\theta_W} C_{DW}$ and $\Gamma_Z = 2.5\,\text{GeV}$ is the decay width of the Z boson [17]. The experimental sensitivity for this decay is shown in Table 5.1. The associated energy bounds for $C^{\mu e}_R$ and $C^{\mu e}_L + C^{\mu e}_{L3}$ are roughly $\Lambda \gtrsim 5$ TeV, much less competitive than the $\mu \to eee$ and $\mu N \to eN$ constraints.

Finally, it is worth mentioning the operator $\mathcal{O}^{\mu e}_y$, which enters the Higgs decay $h \to \mu e$ at tree level. The corresponding branching ratio is [100]

$$\text{BR}\left(h \to \mu e\right) = \frac{m_H m_\mu^2 v^2}{8\pi\Gamma_H \Lambda^4}\left(\left|C^{\mu e}_y\right|^2 + \left|C^{e\mu}_y\right|^2\right)\,, \tag{5.31}$$

where $\Gamma_H = 0.013$ GeV is the Higgs decay width [17]. The current sensitivity for this decay (see Table 5.1) results in a weak energy bound of $\Lambda \gtrsim 0.3$ TeV. According to the estimate in Eq. (5.27), we expect stronger bounds on $C^{\mu e}_y$ from the 2-loop mixing into $\mu \to e\gamma$.

We have summarized the loop effects that are potentially relevant to study the LFV processes $\mu \to e\gamma$, $\mu \to eee$ and $\mu N \to eN$. In the next section, we will analyze which operators can enter the different observables via loops.

5.3 Loop mixings

In addition to operators entering LFV processes at tree level, we must also consider contributions from loop mixings. There are several effects that should be taken into account:

(i) Finite matching contributions from a new physics scale Λ.

(*ii*) Renormalization Group (RG) mixing from Λ to the electroweak scale $\sim m_W$.

(*iii*) Finite threshold corrections arising from integrating out the W, Z, H bosons and the heavy SM fermions.

(*iv*) RG mixing from the electroweak scale m_W to m_μ, which is the energy scale of the LFV processes we are studying.

We are mainly interested in determining which higher-dimension operators give rise to the different observables. For this reason, we will neglect altogether the contributions from (*iv*). The RG mixing between m_W and m_μ does not add new Wilson coefficients and instead it only modifies the energy bounds slightly. For example, using the results of [103], we expect corrections of at most $\sim 10\%$ in the bounds on Table 5.2. It would be interesting to include the complete RG mixing in the calculation, but that is beyond the scope of this work.

At the loop level, the UV matching (*i*) and the SM IR matching (*iii*) give rise to finite contributions to the tree-level coefficients. The UV corrections from (*i*) depend on the particular model for physics at the Λ scale. This means they could (partially) cancel against the IR corrections from (*iii*). In Section 5.6.1 we will see some examples of this cancellation. Instead of model-dependent corrections, we will focus on the contributions from the RG running of Wilson coefficients between Λ and the electroweak scale (*ii*). This type of corrections are accompanied by logarithms $\ln(\Lambda/m_W)$, which cannot cancel against the finite contributions of (*i*) and (*iii*).

We will consider the leading RG mixing of dimension-6 operators up to two loops. At one loop, we have contributions proportional to

$$\frac{C_i}{16\pi^2}\ln(\Lambda/m_W)\ . \tag{5.32}$$

Operators that mix at two loops can be classified according to a logarithmic expansion. The leading ones are 2-loop double-log contributions proportional to

$$\frac{C_iC_j}{(16\pi^2)^2}\ln^2(\Lambda/m_W) \quad i\neq j\ , \tag{5.33}$$

which arise from two-step 1-loop mixings of the type $O_i \overset{\text{1-loop}}{\longrightarrow} O_j \overset{\text{1-loop}}{\longrightarrow} O_k$. The next order corresponds to direct 2-loop mixings $O_i \overset{\text{2-loop}}{\longrightarrow} O_k$, which are proportional to

$$\frac{C_i}{(16\pi^2)^2}\ln(\Lambda/m_W)\ . \tag{5.34}$$

These are the three types of loop mixings that we will incorporate into our analysis. The next step is identifying the order in which the different Wilson coefficients enter the LFV observables.

5.3.1 $\mu \to e\gamma$

The only coefficients entering the branching ratio Eq. (5.15) at tree level are $C_{DW,DB}^{\mu e,e\mu}$. As stated earlier, we are interested in the leading RG mixing of SMEFT dimension-6 operators into the dipole coefficients up to two loops. To identify the possible 1-loop mixings, we will use the helicity selection rule derived in 3.4.1, which states that an operator $\mathcal{O}_j$ can only mix with another operator $\mathcal{O}_i$ if their number of particles n and helicities h satisfy $\Delta n \geq |\Delta h|$, with $\Delta n = n_i - n_j$ and $\Delta h = h_i - h_j$. The relevant mixings are discussed below.

- 1-loop mixing: According to the helicity selection rule, dipole operators $V\psi^2 H$ are only renormalized at one loop by operators of classes $V\psi^2 H, \psi^4, V^2H^2$ and V^3 (see Table 3.1). Moreover, the LFV dipoles can only mix with LFV higher-dimension operators, since the SM interactions preserve lepton flavor. This excludes operators of classes V^2H^2 and V^3. Regarding other dipoles $V\psi^2 H$, in Eq. (5.16) we see that only the combination $C_{DW}^{\mu e} - C_{DB}^{\mu e}$ contributes at tree level, so the orthogonal combination $C_{DW}^{\mu e} + C_{DB}^{\mu e}$ appears at one loop. Finally, we have the ψ^4 operators $\mathcal{O}_{LeQu}$ and $\mathcal{O}_{LuQe}$. We can check that $\mathcal{O}_{LeQu}^{\mu eqq}$ does not mix with $\mathcal{O}_{DW,DB}^{\mu e}$, since the leptons $\bar{L}^{(2)}e^{(1)}$ are external to the loop calculation and do not have the dipole structure. This leaves us only with the operator $\mathcal{O}_{LuQe}^{\mu eqq}$.

- 2-loop double log mixing: These are 1-loop mixings with the operators that generate $C_{DW,DB}^{\mu e,e\mu}$ at one loop. In our case, there are no new operators that mix at one loop with $C_{DW}^{\mu e} + C_{DB}^{\mu e}$ and we only have to consider mixings with $\mathcal{O}_{LuQe}^{\mu eqq}$. Using the helicity selection rule again, the only new operator is $\mathcal{O}_{LeQu}^{\mu eqq}$. In this case, however, there is an additional mixing $\psi^2\bar{\psi}^2 \to \psi^4$, which comes from the exception to the selection rule. Thus we also have operators of class $\psi^2\bar{\psi}^2$ entering $d_{\mu e}$ at this order, namely $\mathcal{O}_{LL,RR,LR,RL,LL3}^{\mu eqq}$.

- 2-loop single log mixing: These are direct 2-loop mixings into the dipoles, including operators of classes $\psi^2H^3, \psi^2\bar{\psi}^2$ and $\psi\bar{\psi}H^2$. For ψ^2H^3 we have the operator $\mathcal{O}_y^{\mu e}$. For $\psi^2\bar{\psi}^2$ we have $\mathcal{O}_{LL,RR,LR,RL,LL3}^{\mu e\ell\ell}$ where ℓ are leptons. Finally, for $\psi\bar{\psi}H^2$ we have $\mathcal{O}_{L,L3,R}^{\mu e}$.

	Tree level	1-loop	2-loop double log	2-loop single log
$\mu \to e\gamma$	$C_{DB}^{\mu e} - C_{DW}^{\mu e}$	$C_{DB}^{\mu e} + C_{DW}^{\mu e}$ $C_{LuQe}^{\mu eqq}$	$C_{LeQu}^{\mu eqq}$ $C_{LL,RR,LR,RL,LL3}^{\mu eqq}$	$C_y^{\mu e}$ $C_{L,L3,R}^{\mu e}$ $C_{LL,RR,LR,RL,LL3}^{\mu e\ell\ell}$

Table 5.3: Wilson coefficients entering BR($\mu \to e\gamma$) up to two loops.

Table 5.3 summarizes the Wilson coefficients that enter the process $\mu \to e\gamma$ at different orders. For simplicity, we are only writing the coefficients that enter $d_{\mu e}$, but the coefficients for $d_{e\mu}$ can be easily obtained by interchanging $\mu \leftrightarrow e$ in the table. The flavor indices qq ($\ell\ell$) indicate that the operators include any quark (lepton) species. For practical purposes, however, we are interested in the operators that produce the strongest bounds. For example, loops with $C_{luqe}^{\mu eqq}$ have a Yukawa coupling y_q, so the largest contribution comes from the coefficient $C_{luqe}^{\mu ett}$. We will comment on the obtained bounds in Section 5.5.

5.3.2 $\mu \to eee$

The tree-level contributions to this process include the operators $\mathcal{O}^{\mu e,\mu e}_{DW,DB}$, $\mathcal{O}^{\mu eee}_{LL,RR,LR,RL}$ and $\mathcal{O}^{\mu e}_{R,L,L3}$. Aside from the $\mathcal{O}^{\mu e,e\mu}_{DB,DW}$ mixings that we have just covered, we have:

- 1-loop mixing: From helicity selection rules, the operators of classes $\psi^2\bar{\psi}^2$ and $\psi\bar{\psi}H^2$ that appear in Eq. (5.20) can only mix with other LFV operators of the same classes. In our case this includes the mixing with the combination $C^{\mu e}_L - C^{\mu e}_{L3}$, orthogonal to $C^{\mu e}_L + C^{\mu e}_{L3}$, and also mixings with other four-fermion operators $\mathcal{O}^{\mu eff}_{LL,LL3,RR,LR,RL}$, with f any fermion.
- 2-loop mixing: No new operators enter the g_i coefficients in this order.

Table 5.4 shows the Wilson coefficients that we must consider for the process $\mu \to eee$. See Section 5.5 for a discussion on the obtained energy bounds.

	Tree level	1-loop	2-loop double log	2-loop single log
$\mu \to eee$	$C^{\mu e}_{DB} - C^{\mu e}_{DW}$ $C^{\mu e}_R$ $C^{\mu e}_L + C^{\mu e}_{L3}$ $C^{\mu eee}_{LL,RR,LR,RL}$	$C^{\mu e}_{DB} + C^{\mu e}_{DW}$ $C^{\mu e}_L - C^{\mu e}_{L3}$ $C^{\mu eqq}_{LuQe}$ $C^{\mu eff}_{LL,LL3,RR,LR,RL}$	$C^{\mu eqq}_{LeQu}$ $C^{\mu eqq}_{LL,LL3,RR,LR,RL}$	$C^{\mu e}_y$

Table 5.4: Wilson coefficients entering BR($\mu \to eee$) up to two loops.

5.3.3 $\mu N \to eN$

The analysis of the loop contributions to R($\mu N \to eN$) is very similar to that of BR ($\mu \to eee$). The only new type of operator that appears at tree level is $\mathcal{O}^{\mu euu}_{LeQu}$, which mixes with $\mathcal{O}^{\mu euu}_{LuQe}$ at one loop. Nevertheless we will not include these operators in our study, since they also receive significant corrections at the QCD scale [111]. Table 5.5 summarizes the contributions to the $\mu N \to eN$ process. The corresponding energy bounds are presented in Section 5.5.

	Tree level	1-loop	2-loop double log	2-loop single log
$\mu N \to eN$	$C^{\mu e}_{DB} - C^{\mu e}_{DW}$ $C^{\mu e}_R$ $C^{\mu e}_L + C^{\mu e}_{L3}$ $C^{\mu euu}_{LL,RR,LR,RL}$ $C^{\mu edd}_{LL,RR,LR,RL}$ $C^{\mu dde}_{LR}$	$C^{\mu e}_{DB} + C^{\mu e}_{DW}$ $C^{\mu e}_L - C^{\mu e}_{L3}$ $C^{\mu eqq}_{LuQe}$ $C^{\mu eff}_{LL,LL3,RR,LR,RL}$	$C^{\mu eqq}_{LeQu}$	$C^{\mu e}_y$

Table 5.5: Wilson coefficients entering R($\mu N \to eN$) up to two loops.

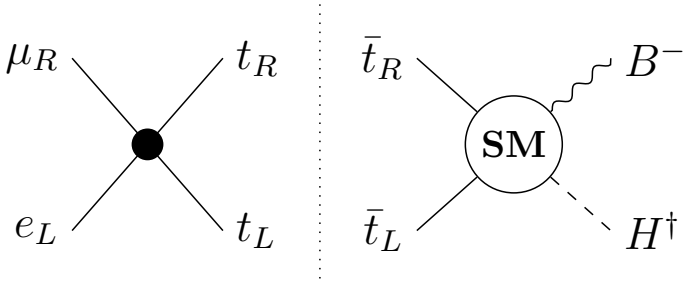

Figure 5.1: *Diagram of the 2-cut relevant for the renormalization of F_{DB} by F_{luqe}.*

5.4 RG mixings: the on-shell way

Now that we have identified which dimension-6 operators enter the different LFV processes, the next step is to compute the anomalous dimension matrix for the corresponding mixings. This can be done in several ways, but we will focus on the on-shell amplitude methods described in Chapter 3. Through this subsection we apply those methods to mixings that are relevant for LFV experiments, up to two loops.

5.4.1 1-loop mixings

The Wilson coefficients entering the different LFV processes are listed in Tables 5.3, 5.4 and 5.5. Our goal is to compute the RG mixing of those coefficients into the tree-level ones. As an example, we calculate the mixing of $C^{\mu ett}_{LuQe}$ into the dipoles.

The mixing $C^{\mu ett}_{LuQe} \to C^{\mu e}_{DW,DB}$ can be computed using the on-shell methods explained in Chapter 3. We use the method of form factor renormalization in Section 3.2.4, since it is the only one that is easily extended to 2-loop calculations. The contact form factors for the dipoles in Eq. (5.1) are

$$F^{\mu e}_{DB}(1_e, 2_{l^j}, 3_{B_-}, 4_{H_i^\dagger}) = 2y_\mu g_1 \langle 31\rangle \langle 32\rangle \delta_i^j \ , \tag{5.35}$$

$$F^{\mu e}_{BW}(1_e, 2_{l^j}, 3_{W^a_-}, 4_{H_i^\dagger}) = 4y_\mu g_2 \langle 31\rangle \langle 32\rangle (T^a)_i^j \ . \tag{5.36}$$

We are interested in the 1-loop mixing with

$$F^{\mu ett}_{LuQe}(1_e, 2_{l_i}, 3_u, 4_{q_j}) = y_\mu \langle 14\rangle \langle 32\rangle \epsilon_{ij} \ . \tag{5.37}$$

Using Eq. (3.35), the only contribution to the anomalous dimension $\gamma^{\mu e}_{\{DB,LuQe\}}$ is given by the 2-cut in Figure 5.1. We can write

$$\begin{aligned}&\gamma^{\mu e}_{\{DB,LuQe\}} F^{\mu e}_{DB}(1_e, 2_l, 3_{B_-}, 4_{H^\dagger}) \\ &\qquad = \frac{1}{4\pi^3}\int d\text{LIPS}\, F^{\mu ett}_{LuQe}(1_e, 2_l, 3'_u, 4'_q) \times \mathcal{A}^{tt}_{\text{SM}}(-4'_{\bar{q}}, -3'_{\bar{u}}, 3_{B_-}, 4_{H^\dagger}) \ ,\end{aligned} \tag{5.38}$$

where $\mathcal{A}^{tt}_{\text{SM}}$ is the SM on-shell amplitude in Eq. (2.11). In terms of spinor-helicity variables, this expression becomes

$$\gamma^{\mu e}_{\{DB,LuQe\}} \langle 31\rangle \langle 32\rangle = \frac{y_t N_c}{8\pi^3}\int d\text{LIPS}\ \langle 14'\rangle \langle 3'2\rangle \left(Y_q \frac{\langle 3'3\rangle \langle 43\rangle}{\langle 3'4\rangle \langle 3'4'\rangle} - Y_t \frac{\langle 4'3\rangle \langle 43\rangle}{\langle 4'4\rangle \langle 4'3'\rangle} \right) \ . \tag{5.39}$$

For the phase-space integral, we parameterize the internal spinors as explained in Section 3.4.3. In particular, we use

$$\begin{aligned} |3'\rangle &= c_\theta\,|3\rangle - s_\theta e^{i\phi}\,|4\rangle \ , \\ |4'\rangle &= s_\theta e^{-i\phi}\,|3\rangle + c_\theta\,|4\rangle \ . \end{aligned} \tag{5.40}$$

After performing the angular integrals, we obtain the anomalous dimension

$$\gamma^{\mu e}_{\{DB,LuQe\}} = -\frac{y_t N_c}{32\pi^2}\left(Y_q - Y_t\right) \ . \tag{5.41}$$

The mixing of C_{LuQe} with the other dipole C_{DW} was already computed in Section 4.1. The corresponding anomalous dimension is

$$\gamma^{\mu e}_{\{DW,LuQe\}} = \frac{y_t N_c}{64\pi^2} \ . \tag{5.42}$$

Let us summarize the mixings $C^{\mu ett}_{LuQe} \to C^{\mu e}_{DW,DB}$ in the following matrix

$$\begin{pmatrix} \gamma_{C^{\mu e}_{DB}} \\ \gamma_{C^{\mu e}_{DW}} \end{pmatrix} = \frac{N_c y_t}{32\pi^2} \begin{pmatrix} -1 \\ \frac{1}{2} \end{pmatrix} C^{\mu ett}_{LuQe} \ . \tag{5.43}$$

The mixings $C^{e\mu tt}_{LuQe} \to C^{e\mu}_{DW,DB}$ are obtained in an analogous way, leading to

$$\begin{pmatrix} \gamma_{C^{e\mu}_{DB}} \\ \gamma_{C^{e\mu}_{DW}} \end{pmatrix} = \frac{N_c y_t}{32\pi^2} \begin{pmatrix} -1 \\ \frac{1}{2} \end{pmatrix} C^{e\mu tt}_{LuQe} \ . \tag{5.44}$$

We can repeat the same procedure with the other mixings. The relevant 1-loop anomalous dimensions are listed in Appendix D.1.

5.4.2 2-loop mixings

To illustrate the power of on-shell amplitude methods at higher loop orders, we calculate the 2-loop mixing $\psi\bar{\psi}H^2 \to V\psi^2 H$. As explained in Section 3.4.5, this kind of computation can be done with the form factor renormalization method. Since we are considering the leading order mixing for each coefficient, we can use Eq. (3.33) for the calculation. In this case, the 2-loop anomalous dimension gets contributions from both 2-cuts and 3-cuts, as shown in Figure 3.6.

The 2-loop anomalous dimension for $\psi\bar{\psi}H^2 \to V\psi^2 H$ has several contributions proportional to y_u^2, λ^4 and g^2. We only consider the leading ones: those involving the top Yukawa y_t^2 and the quartic coupling λ^4. We will see that only 3-cuts contribute to these mixings due to helicity selection rules.

$C_{L,L3,R} \to C_{DW,DB}$ - Top Yukawa y_t^2 contributions

Contributions proportional to $N_c y_t^2$ are expected to be the dominant ones. Let us start with the mixing $C_L^{e\mu} \to C_{DB}^{e\mu}$. Using Eq. (3.33), the 2-loop anomalous dimension can be obtained from three types of unitarity cuts:

- 2-cut of a tree-level SM amplitude and a 1-loop form factor. The only potential contribution is shown in Figure 5.2. The SM amplitude $\mathcal{A}^{\text{tree}}(1_e, 2'_l, 3_{B_-}, 4'_H)$ vanishes on shell for the all-negative helicity configuration. Therefore the 2-cut is zero as well.

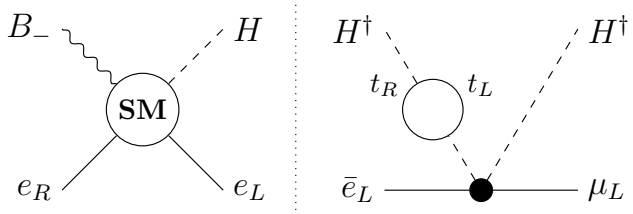

Figure 5.2: *Diagram for the 2-cut of a tree-level SM amplitude and a 1-loop form factor. This cut is zero because the SM amplitude with all-negative helicity vanishes.*

- 2-cut of a 1-loop SM amplitude and a tree-level form factor. Figure 5.3 shows the only potential cut of this type. The SM amplitude $\mathcal{A}^{1-\text{loop}}(1_e, 2_l, 3_{B_-}, 4_H)$ is obtained from a sum of diagrams where the B boson is attached to the different particles in the LHS of the cut, as can also be seen in Figure 5.3. Contributions where the B is attached to the lepton fermion line are zero because the diagrams factorize into an all-negative on-shell tree-level amplitude (which vanishes) and a 1-loop dressing for the Higgs boson. For the remaining terms, the sum of diagrams can be written as $\langle 12' \rangle f(3, 4')$, with f a function that only depends on the spinors 3 and $4'$. However, using only $\langle 34' \rangle$ and $[4'3]$, it is impossible to build a function $f(3, 4')$ so that $\mathcal{A} \sim \langle 12' \rangle f(3, 4')$ satisfies little group covariance. For this reason, we conclude that the 1-loop amplitude vanishes.

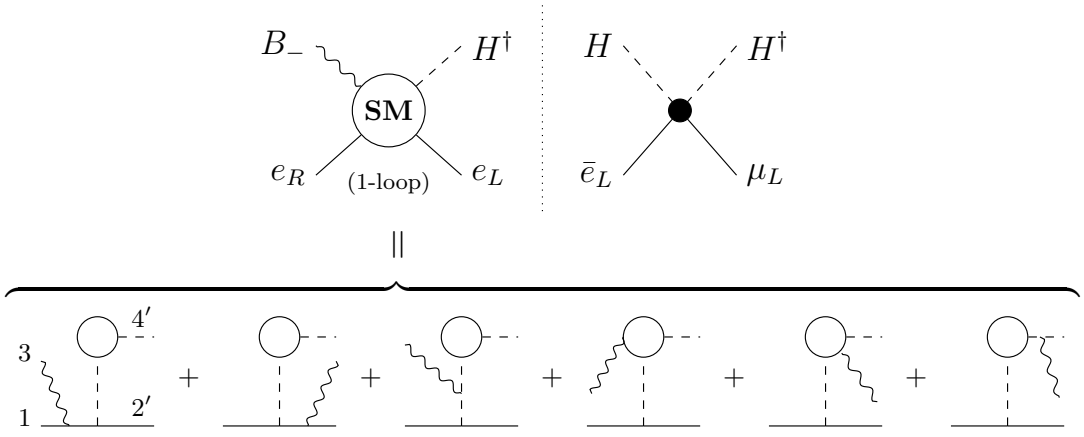

Figure 5.3: *Diagram for the 2-cut of a 1-loop SM amplitude and a tree-level form factor. This cut is zero because the 1-loop SM amplitude vanishes.*

- 3-cut of a tree-level SM amplitude and a tree-level form factor. The only non-vanishing contribution to the RG mixing is given by the 3-cut in Figure 5.4. Below we perform the explicit calculation of the anomalous dimensions.

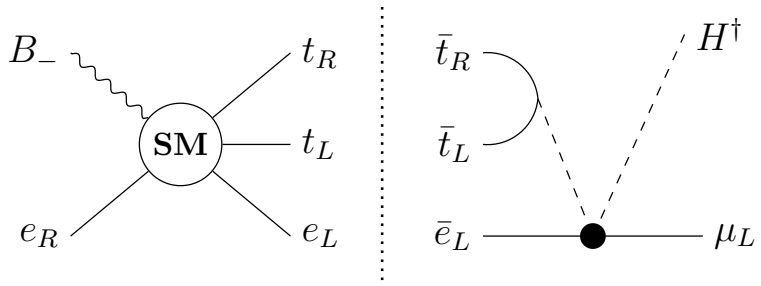

Figure 5.4: *Diagram for the 3-cut contributing to the mixing of $F_L^{e\mu}$ into $F_{DB}^{e\mu}$ at order y_t^2.*

From Eq. (3.33), we have

$$\begin{aligned}&\gamma^{e\mu}_{\{DB,L\}} F^{e\mu}_{DB}(1_e, 2_{l^j_\mu}, 3_{B_-}, 4_{H_i^\dagger}) \\ &\quad = -\frac{(-i)^3 N_c}{(16\pi^2)^2} s_{13} \int d\mu\ \widehat{F}^{e\mu}_L(2_{l^j_\mu}, 4_{H_i^\dagger}, x_{\bar{l}_{e,n}}, y_{\bar{l}_{t,k}}, z_{\bar{t}}) \times \mathcal{A}_{\rm SM}(-z_t, -y_{l^k_t}, -x_{l^n_e}, 1_e, 3_{B_-})\ ,\end{aligned} \tag{5.45}$$

with $\int d\mu$ as defined in Eq. (3.61). $\widehat{F}^{e\mu}_L$ is a non-minimal form factor and $\mathcal{A}_{\rm SM}$ is a 5-point SM on-shell amplitude. Both of them can be computed using the method of momentum shifts in Section 1.3.2. The form factor is

$$\widehat{F}^{e\mu}_L(2_{l^j_\mu}, 4_{H_i^\dagger}, x_{\bar{l}_{e,n}}, y_{\bar{l}_{t,k}}, z_{\bar{t}}) = 2y_t \frac{\langle 24\rangle\,[4x]}{\langle zy\rangle} \mathcal{A}^j_{ink}\ , \tag{5.46}$$

where $\mathcal{A}^j_{ink} = \epsilon_{ik}\delta^j_n$ is an $\mathrm{SU}(2)_L$ tensor. The SM amplitude is

$$\mathcal{A}_{\rm SM}(-z_t, -y_{l^k_t}, -x_{l^n_e}, 1_e, 3_{B_-}) = iy_t y_e \left(Y_H \frac{\langle 1z\rangle}{[3x][y3]} - Y_{\mu_R} \frac{\langle yz\rangle}{[3x][31]} + Y_{t_R} \frac{\langle 1x\rangle}{[y3][3z]} \right) \mathcal{B}^{kn}\ , \tag{5.47}$$

where $\mathcal{B}^{kn} = g_1 \epsilon^{kn}$. Now we can substitute Eq. (5.46) and Eq. (5.47) into Eq. (5.45) and perform the phase-space integration. Following Section 3.4.3, we parameterize the internal spinors $|x\rangle, |y\rangle, |z\rangle$ as

$$\begin{aligned}|z\rangle &= |1\rangle\, s_{\theta_2} c_{\theta_3} + |3\rangle\, e^{i\phi}(c_{\theta_1} c_{\theta_2} c_{\theta_3} - e^{i\rho} s_{\theta_1} s_{\theta_3})\ , \\ |y\rangle &= |1\rangle\, s_{\theta_2} s_{\theta_3} + |3\rangle\, e^{i\phi}(c_{\theta_1} c_{\theta_2} s_{\theta_3} + e^{i\rho} s_{\theta_1} c_{\theta_3})\ , \\ |x\rangle &= |1\rangle\, c_{\theta_2} - |3\rangle\, e^{i\phi} c_{\theta_1} s_{\theta_2}\ .\end{aligned} \tag{5.48}$$

This leads to the following angular integral

$$\int d\mu \frac{\langle 24\rangle\,[4x]}{\langle zy\rangle} \left(Y_H \frac{\langle 1z\rangle}{[3x][y3]} - Y_{\mu_R} \frac{\langle yz\rangle}{[3x][31]} + Y_{t_R} \frac{\langle 1x\rangle}{[y3][3z]} \right) = \frac{\langle 32\rangle}{[31]} (2Y_H + Y_\mu)\ . \tag{5.49}$$

Finally the anomalous dimension is

$$\gamma^{e\mu}_{\{DB,L\}} = -\frac{2N_c}{(16\pi^2)^2} y_t^2 y_e g_1 \left(2Y_H + Y_{\mu_R}\right) \ . \tag{5.50}$$

We can check that this mixing is actually zero for the SM hypercharges, since $2Y_H + Y_{\mu_R} = 0$.

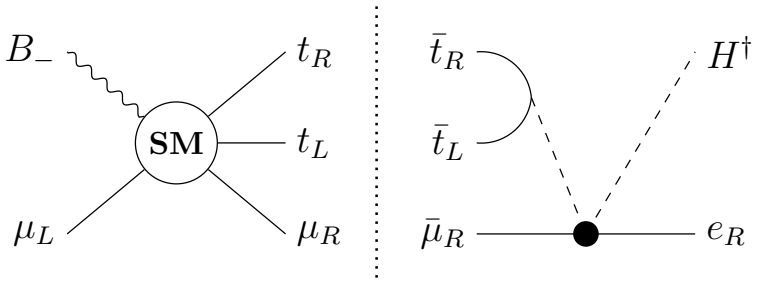

Figure 5.5: *Diagram for the 3-cut contributing to the mixing of $F^{e\mu}_R$ into $F^{e\mu}_{DB}$ at order y_t^2.*

Similarly, we can study the mixing $C^{e\mu}_R \to C^{e\mu}_{DB}$. In this case we only have to consider the 3-cut in Figure 5.5. Then Eq. (3.33) becomes

$$\begin{aligned}&\gamma^{e\mu}_{\{DB,R\}} F^{e\mu}_{DB}(1_e, 2_{l^j_\mu}, 3_{B_-}, 4_{H^\dagger_i}) \\ &\quad = \frac{(-i)^3 N_c}{(16\pi^2)^2} s_{23} \int d\mu \ \widehat{F}^{e\mu}_R(1_e, 4_{H^\dagger_i}, x_{\bar{\mu}}, y_{\bar{l}_{t,k}}, z_{\bar{t}}) \times \mathcal{A}_{\rm SM}(-z_t, -y_{l^k_t}, -x_\mu, 2_{l^j_\mu}, 3_{B_-}) \ .\end{aligned} \tag{5.51}$$

The form factor $\widehat{F}^{e\mu}_R$ and the on-shell amplitude $\mathcal{A}_{\rm SM}$ are given by

$$\widehat{F}^{e\mu}_R(1_e, 4_{H^\dagger_i}, x_{\bar{\mu}}, y_{\bar{l}_{t,k}}, z_{\bar{t}}) = -2y_t \frac{\langle 14\rangle\,[4x]}{\langle zy\rangle} \mathcal{A}_{ik} \ , \tag{5.52}$$

$$\mathcal{A}_{\rm SM}(-z_t, -y_{l^k_t}, -x_\mu, 2_{l^j_\mu}, 3_{B_-}) = -iy_t y_\mu \left(Y_H \frac{\langle zx\rangle}{[23][3y]} + Y_\mu \frac{\langle zy\rangle}{[23][x3]} - Y_e \frac{\langle x2\rangle}{[3y][3z]} \right) \mathcal{B}^{jk} \ , \tag{5.53}$$

where the $\mathrm{SU}(2)_L$ tensors are $\mathcal{A}_{ik} = \epsilon_{ik}$ and $\mathcal{B}^{jk} = g_1 \epsilon^{jk}$. Again, we parameterize the internal spinors in terms of $|2\rangle, |3\rangle$, replacing $1 \to 2$ in Eq. (5.48). The phase-space integral is then

$$\int d\mu \frac{\langle 14\rangle\,[4x]}{\langle zy\rangle} \left(Y_H \frac{\langle zx\rangle}{[23][3y]} + Y_\mu \frac{\langle zy\rangle}{[23][x3]} - Y_e \frac{\langle x2\rangle}{[3y][3z]} \right) = \frac{\langle 13\rangle}{[32]} \left(Y_H - Y_\mu\right) \ . \tag{5.54}$$

The anomalous dimension is

$$\gamma^{e\mu}_{\{DB,R\}} = \frac{2N_c}{(16\pi^2)^2} y_t^2 y_\mu g_1 \left(Y_H - Y_{\mu_R}\right) \ . \tag{5.55}$$

Now it is straightforward to obtain the 2-loop anomalous dimensions for the remaining mixings of $C^{e\mu}_{L,L3,R}$ into the dipoles $C^{e\mu}_{DB,DW}$. Essentially, mixings of $C^{e\mu}_{L,L3}$ involve the form

$\mathcal{A}\times\mathcal{B}$	C_L	C_{L3}	C_R
C_{DB}	$\epsilon_{ik}\delta^j_n \times g_1\epsilon^{kn}$	$\left(2\epsilon_{kn}\delta^j_i - \epsilon_{ik}\delta^j_n\right) \times g_1\epsilon^{kn}$	$\epsilon_{ik} \times g_1\epsilon^{jk}$
C_{DW}	$\epsilon_{ik}\delta^j_n \times g_2(\epsilon\cdot T^a)^{kn}$	$\left(2\epsilon_{kn}\delta^j_i - \epsilon_{ik}\delta^j_n\right) \times g_2(\epsilon\cdot T^a)^{kn}$	$\epsilon_{ik} \times g_2(\epsilon\cdot T^a)^{kj}$

Table 5.6: Expressions of the $\mathrm{SU}(2)_L$ tensors $\mathcal{A}$ and $\mathcal{B}$ that appear in the 2-loop renormalization of $C_{DB,DW}$ by $C_{L,L3,R}$ at order y_t^2.

factor and the amplitude in Eq. (5.46) and Eq. (5.47), whereas mixings of $C_R^{e\mu}$ involve Eq. (5.52) and Eq. (5.53). The flavor structure of the amplitudes and form factors will vary depending on the mixing. The values of the $\mathrm{SU}(2)_L$ tensors $\mathcal{A}$ and $\mathcal{B}$ are listed in Table 5.6. Moreover, for the renormalization of C_{DW} we have to set the hypercharges in the amplitudes Eq. (5.47) and Eq. (5.53) to $Y_e = Y_\mu = Y_t = 0$ and $Y_H = 1$.

With these considerations, we can finally obtain the anomalous dimensions matrix for the subset of operators at order y_t^2,

$$\begin{pmatrix}\gamma_{C_{DB}^{e\mu}}\\ \gamma_{C_{DW}^{e\mu}}\end{pmatrix} = \frac{N_c y_t^2}{(16\pi^2)^2}\begin{pmatrix}0 & 0 & -\frac{3y_e}{2y_\mu}\\ 1 & -1 & \frac{y_e}{2y_\mu}\end{pmatrix}\begin{pmatrix}C_L^{e\mu}\\ C_{L3}^{e\mu}\\ C_R^{e\mu}\end{pmatrix} \approx \frac{N_c y_t^2}{(16\pi^2)^2}\begin{pmatrix}0 & 0 & 0\\ 1 & -1 & 0\end{pmatrix}\begin{pmatrix}C_L^{e\mu}\\ C_{L3}^{e\mu}\\ C_R^{e\mu}\end{pmatrix} \quad , \tag{5.56}$$

where in the last step we have neglected terms of order $\mathcal{O}(y_e/y_\mu) \approx 0$. The mixings of $C_{L,L3,R}^{\mu e}$ into the dipoles $C_{DB,DW}^{\mu e}$ are obtained in an analogous way, interchanging $e \leftrightarrow \mu$ in the amplitudes and form factors. We find

$$\begin{pmatrix}\gamma_{C_{DB}^{\mu e}}\\ \gamma_{C_{DW}^{\mu e}}\end{pmatrix} = \frac{N_c y_t^2}{(16\pi^2)^2}\begin{pmatrix}0 & 0 & -\frac{3}{2}\\ \frac{y_e}{y_\mu} & -\frac{y_e}{y_\mu} & \frac{1}{2}\end{pmatrix}\begin{pmatrix}C_L^{\mu e}\\ C_{L3}^{\mu e}\\ C_R^{\mu e}\end{pmatrix} \approx \frac{N_c y_t^2}{(16\pi^2)^2}\begin{pmatrix}0 & 0 & -\frac{3}{2}\\ 0 & 0 & \frac{1}{2}\end{pmatrix}\begin{pmatrix}C_L^{\mu e}\\ C_{L3}^{\mu e}\\ C_R^{\mu e}\end{pmatrix} \quad . \tag{5.57}$$

Note that there is an accidental cancellation in the renormalization of $C_{DB}^{\mu e,e\mu}$ by C_L and C_{L3}. As we have seen earlier, this entry is proportional to $2Y_H + Y_e$ and vanishes for the SM hypercharges.

$C_{L,L3,R} \to C_{DW,DB}$ - Higgs quartic λ^4 contributions

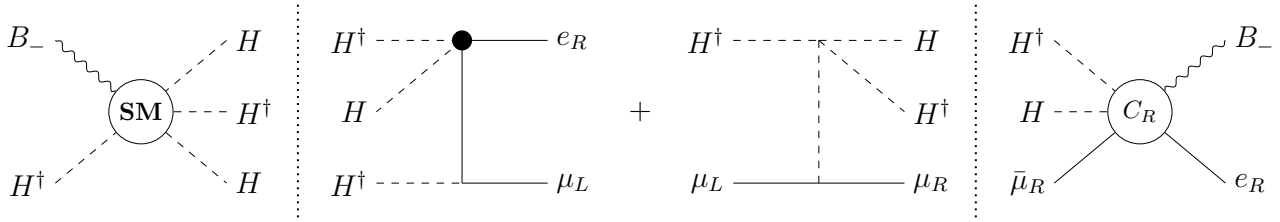

Figure 5.6: *Diagram for the 3-cuts contributing to the mixing of $F_L^{e\mu}$ into $F_{DB}^{e\mu}$ at order λ^4.*

The next mixings to consider are those proportional to the quartic Higgs coupling λ^4. In this case there are no 2-cut contributions to the anomalous dimension. Instead, the 2-loop mixing $C_L^{e\mu} \to C_{DB}^{e\mu}$ is given by the two 3-cuts in Figure 5.6. From Eq. (3.33), we can write

$$\begin{aligned}
&\gamma^{e\mu}_{\{DB,L\}} F^{e\mu}_{DB}(1_e, 2_{l^j_\mu}, 3_{B_-}, 4_{H^\dagger_i}) \\
&\quad = -\frac{i s_{14}}{(16\pi^2)^2} \int d\mu\ \widehat{F}^{e\mu}_L(2_{l^j_\mu}, 3_{B_-}, x_{\bar{l}_{e,m}}, y_{H^l}, z_{H^\dagger_k}) \times \mathcal{A}_{\rm SM}(-z_{H^k}, -y_{H^\dagger_l}, -x_{l^m_e}, 1_e, 4_{H^\dagger_i}) \\
&\quad - \frac{s_{34}}{(16\pi^2)^2} \int \frac{d\mu}{2!}\ \widehat{F}^{e\mu}_L(1_e, 2_{l^j_\mu}, x_{H^\dagger_m}, y_{H^l}, z_{H^\dagger_k}) \times \mathcal{A}_{\rm SM}(-z_{H^k}, -y_{H^\dagger_l}, -x_{H^m}, 3_{B_-}, 4_{H^\dagger_i}) \ ,
\end{aligned} \tag{5.58}$$

where the factor 1/2! in the second cut accounts for the fact that we are cutting two identical Higgs particles. For the first cut, the non-minimal form factor is

$$\widehat{F}^{e\mu}_L(3_{B_-}, 2_{l^j_\mu}, x_{\bar{l}_{e,m}}, y_{H^l}, z_{H^\dagger_k}) = 2\left(Y_H \frac{[zx][yx]\langle 2x\rangle}{[y3][z3]} \mathcal{G}^{jl}_{mk} - Y_e \frac{[zx][yx]\langle yz\rangle}{[x3][32]} \mathcal{G}^{lj}_{km}\right) \ , \tag{5.59}$$

with $\mathcal{G}^{jl}_{mk} = g_1 \delta^j_m \delta^l_k$. The SM amplitude is

$$\mathcal{A}_{\rm SM}(-z_{H^k}, -y_{H^\dagger_l}, -x_{l^m_e}, 1_e, 4_{H^\dagger_i}) = i y_e \frac{\lambda}{2} \frac{1}{[1x]} \mathcal{F}^{km}_{li} \ , \tag{5.60}$$

with $\mathcal{F}^{km}_{li} = \delta^k_i \delta^m_l + \delta^m_i \delta^k_l$. Next, we parameterize the internal spinors x, y, z in terms of $1, 4$ as in Eq. (5.48) and perform the phase-space integral. The contribution of the first cut to the anomalous dimension in Eq. (5.58) is

$$\gamma^{e\mu}_{\{DB,L\}} \supset -\frac{3 y_e \lambda g_1 Y_H}{(16\pi^2)^2} \frac{s_{14}}{s_{13}} \left[1 - 2\frac{s_{12}}{s_{13}} + 2\frac{s_{12}^2}{s_{13}^2} \ln\left(\frac{s_{13}+s_{12}}{s_{12}}\right)\right] \ . \tag{5.61}$$

Regarding the second cut, we have to compute the form factor

$$\begin{aligned}
&\widehat{F}^{e\mu}_L(1_e, 2_{l^j_\mu}, x_{H^\dagger_m}, y_{H^l}, z_{H^\dagger_k}) \\
&\qquad = -y_e \left[\left(2\frac{\langle 2y\rangle [yx]}{[1x]} + \langle 21\rangle\right) \mathcal{D}^{jl}_{mk} + \left(2\frac{\langle 2y\rangle [yz]}{[1z]} + \langle 21\rangle\right) \mathcal{D}^{jl}_{km}\right] \ ,
\end{aligned} \tag{5.62}$$

with $\mathcal{D}^{jl}_{mk} = \delta^l_k \delta^j_m$. We also need to know the SM amplitude

$$\begin{aligned}
&\mathcal{A}_{\rm SM}(-z_{H^k}, -y_{H^\dagger_l}, -x_{H^m}, 3_{B_-}, 4_{H^\dagger_i}) \\
&\qquad = \frac{\lambda}{2} Y_H \left(\frac{[z4]}{[z3][43]} \mathcal{C}^{km}_{li} + \frac{[xy]}{[x3][y3]} \mathcal{C}^{mk}_{il} + \mathcal{C}^{mk}_{li} \frac{[zy]}{[z3][y3]} + \mathcal{C}^{km}_{il} \frac{[x4]}{[x3][43]}\right) \ ,
\end{aligned} \tag{5.63}$$

with $\mathcal{C}^{km}_{li} = g_1 \delta^k_i \delta^m_l$. After the phase-space integration, the contribution from the second cut is

$$\gamma^{e\mu}_{\{DB,L\}} \supset -\frac{6 y_e \lambda g_1 Y_H}{(16\pi^2)^2} \frac{s_{12}}{s_{13}} \left[\frac{1}{2} + \frac{s_{14}}{s_{13}} - \left(\frac{s_{14}}{s_{13}} + \frac{s_{14}^2}{s_{13}^2}\right) \ln\left(\frac{s_{13}+s_{14}}{s_{14}}\right)\right] \ . \tag{5.64}$$

Notice that both Eq. (5.61) and Eq. (5.64) contain logarithmic terms. When we add both cuts, however, non-local terms cancel out and the anomalous dimension is

$$\gamma^{e\mu}_{\{DB,L\}} = \frac{3y_e\lambda g_1 Y_H}{(16\pi^2)^2} \ . \tag{5.65}$$

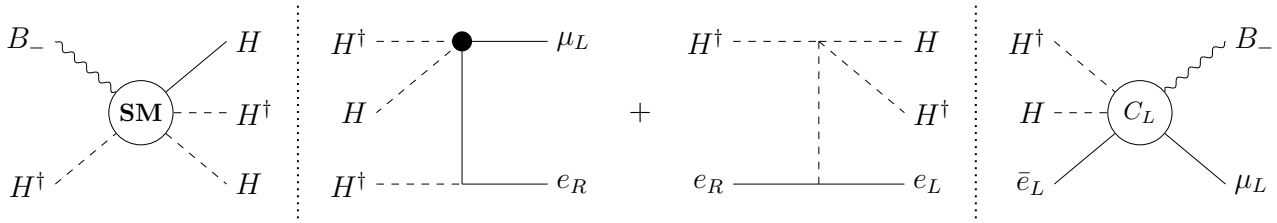

Figure 5.7: *Diagram for the 3-cut contributing to the mixing of $F_R^{e\mu}$ into $F_{DB}^{e\mu}$ at order λ^4.*

Next we focus on the mixing $C_R^{e\mu} \to C_{DB}^{e\mu}$. Figure 5.7 shows the two 3-cuts that contribute to the anomalous dimension, which can be written as

$$\begin{aligned}
&\gamma^{e\mu}_{\{DB,R\}} F^{e\mu}_{DB}(1_e, 2_{l^j_\mu}, 3_{B_-}, 4_{H^\dagger_i}) \\
&\quad = -\frac{is_{13}}{(16\pi^2)^2}\int d\mu\ \widehat{F}^{e\mu}_R(1_e, 3_{B_-}, x_{\bar{\mu}}, y_{H^l}, z_{H^\dagger_k}) \times \mathcal{A}_{\rm SM}(-z_{H^k}, -y_{H^\dagger_l}, -x_\mu, 2_{l^j_\mu}, 4_{H^\dagger_i}) \\
&\quad - \frac{s_{34}}{(16\pi^2)^2}\int \frac{d\mu}{2}\ \widehat{F}^{e\mu}_R(1_e, 2_{l^j_\mu}, x_{H^\dagger_k}, y_{H^l}, z_{H^\dagger_m}) \times \mathcal{A}_{\rm SM}(-z_{H^m}, -y_{H^\dagger_l}, -x_{H^k}, 3_{B_-}, 4_{H^\dagger_i}) \ .
\end{aligned} \tag{5.66}$$

The non-minimal form factor of the first cut is given by

$$\widehat{F}^{e\mu}_R(1_e, 3_{B_-}, x_{\bar{\mu}}, y_{H^l}, z_{H^\dagger_k}) = -2\left(Y_H \frac{[zx][yx]\langle 1x\rangle}{[y3][z3]} + Y_e \frac{[zx][yx]\langle yz\rangle}{[x3][31]}\right)\mathcal{G}^l_k \ , \tag{5.67}$$

with $\mathcal{G}^l_k = g_1\delta^l_k$. The amplitude is

$$\mathcal{A}_{\rm SM}(-z_{H^k}, -y_{H^\dagger_l}, -x_\mu, 2_{l^j_\mu}, 4_{H^\dagger_i}) = iy_\mu \frac{\lambda}{2}\frac{1}{[2x]}\mathcal{F}^{kj}_{li} \ , \tag{5.68}$$

with $\mathcal{F}^{kj}_{li} = \delta^k_i\delta^j_l + \delta^j_i\delta^k_l$. For the second cut, the form factor is

$$\begin{aligned}
\widehat{F}^{e\mu}_R(1_e, 2_{l^j_\mu}, x_{H^\dagger_k}, y_{H^l}, z_{H^\dagger_m}) = -y_\mu \Bigg[&\left(2\frac{\langle 1y\rangle[yz]}{[2z]} + \langle 12\rangle\right)\mathcal{D}^{lj}_{km} \\
&+ \left(2\frac{\langle 1y\rangle[yx]}{[2x]} + \langle 12\rangle\right)\mathcal{D}^{lj}_{mk}\Bigg] \ ,
\end{aligned} \tag{5.69}$$

with $\mathcal{D}^{lj}_{km} = \delta^l_k\delta^j_m$. The SM amplitude is given by Eq. (5.63). As happened in the $C_L^{e\mu} \to C_{DB}^{e\mu}$ mixing, the individual cuts in Eq. (5.66) have logarithmic terms that cancel out when summing both contributions. In the end the anomalous dimension is

$$\gamma^{e\mu}_{\{DB,R\}} = \frac{(3y_\mu\lambda g_1 Y_H}{(16\pi^2)^2} \ . \tag{5.70}$$

Now we can generalize our calculations for other renormalizations $C^{e\mu}_{L,L3,R} \to C^{e\mu}_{DB,DW}$. For mixings with $C^{e\mu}_{L,L3}$ we have to use the amplitudes and form factors in Eq. (5.59), Eq. (5.60), Eq. (5.62) and Eq. (5.63). Table 5.7 summarizes the required $\mathrm{SU}(2)_L$ tensors: $\mathcal{G}$ and $\mathcal{F}$ for the first cut and $\mathcal{D}$ and $\mathcal{C}$ for the second one. In the mixings with the $C^{e\mu}_{DW}$ dipole we also have to set the hypercharges to $Y_e = 0, Y_H = 1$.

$\mathcal{G}\times\mathcal{F}$	C_L	C_{L3}
C_{DB}	$g_1\delta^j_m\delta^l_k \times \left(\delta^k_i\delta^m_l + \delta^m_i\delta^k_l\right)$	$g_1(\sigma^b)^j_m(\sigma^b)^l_k \times \left(\delta^k_i\delta^m_l + \delta^m_i\delta^k_l\right)$
C_{DW}	$g_2\delta^j_m(T^a)^l_k \times \left(\delta^k_i\delta^m_l + \delta^m_i\delta^k_l\right)$	$g_2(\sigma^b)^j_m(\sigma^b)^l_s(T^a)^s_k \times \left(\delta^k_i\delta^m_l + \delta^m_i\delta^k_l\right)$
$\mathcal{D}\times\mathcal{C}$	C_L	C_{L3}
C_{DB}	$\delta^l_k\delta^j_m \times g_1\delta^k_i\delta^m_l$	$(\sigma^b)^l_k(\sigma^b)^j_m \times g_1\delta^k_i\delta^m_l$
C_{DW}	$\delta^l_k\delta^j_m \times g_2(T^a)^k_i\delta^m_l$	$(\sigma^b)^l_k(\sigma^b)^j_m \times g_2(T^a)^k_i\delta^m_l$

Table 5.7: Expressions of the $\mathrm{SU}(2)_L$ tensors that appear in the mixings $C_{L,L3} \to C_{DB,DW}$ at order λ^2. $\mathcal{G}\times\mathcal{F}$ and $\mathcal{D}\times\mathcal{C}$ correspond, respectively, to the first and second cuts in Figure 5.6.

For mixings with $C^{e\mu}_R$, we use the amplitudes and form factors in Eq. (5.67), Eq. (5.68), Eq. (5.69) and Eq. (5.63). The different flavor tensors for both cuts are included in Table 5.7.

$\mathcal{G}\times\mathcal{F}$	C_R	$\mathcal{D}\times\mathcal{C}$	C_R
C_{DB}	$g_1\delta^l_k \times \left(\delta^k_i\delta^j_l + \delta^j_i\delta^k_l\right)$	C_{DB}	$\delta^l_k\delta^j_m \times g_1\delta^k_i\delta^m_l$
C_{DW}	$g_2(T^a)^l_k \times \left(\delta^k_i\delta^j_l + \delta^j_i\delta^k_l\right)$	C_{DW}	$\delta^l_k\delta^j_m \times g_2(T^a)^k_i\delta^m_l$

Table 5.8: Expressions of the $\mathrm{SU}(2)_L$ tensors that appear in the mixing $C_R \to C_{DB,DW}$ at order λ^2. $\mathcal{G}\times\mathcal{F}$ and $\mathcal{D}\times\mathcal{C}$ correspond, respectively, to the first and second cuts in Figure 5.7.

Finally, the anomalous dimension matrix at order λ^4 is

$$\begin{pmatrix}\gamma_{C^{e\mu}_{DB}}\\ \gamma_{C^{e\mu}_{DW}}\end{pmatrix} = \frac{\lambda}{(16\pi^2)^2}\begin{pmatrix}3 & 3 & -\frac{3y_e}{y_\mu}\\ 1 & 3 & \frac{y_e}{y_\mu}\end{pmatrix}\begin{pmatrix}C^{e\mu}_L\\ C^{e\mu}_{L3}\\ C^{e\mu}_R\end{pmatrix} \approx \frac{\lambda}{(16\pi^2)^2}\begin{pmatrix}3 & 3 & 0\\ 1 & 3 & 0\end{pmatrix}\begin{pmatrix}C^{e\mu}_L\\ C^{e\mu}_{L3}\\ C^{e\mu}_R\end{pmatrix} . \tag{5.71}$$

For the other mixings $C^{\mu e}_{L,L3,R} \to C^{e\mu e}_{DB,DW}$, we have

$$\begin{pmatrix}\gamma_{C^{\mu e}_{DB}}\\ \gamma_{C^{\mu e}_{DW}}\end{pmatrix} = \frac{\lambda}{(16\pi^2)^2}\begin{pmatrix}3\frac{y_e}{y_\mu} & 3\frac{y_e}{y_\mu} & 3\\ \frac{y_e}{y_\mu} & 3\frac{y_e}{y_\mu} & 1\end{pmatrix}\begin{pmatrix}C^{\mu e}_L\\ C^{\mu e}_{L3}\\ C^{\mu e}_R\end{pmatrix} \approx \frac{\lambda}{(16\pi^2)^2}\begin{pmatrix}0 & 0 & 3\\ 0 & 0 & 1\end{pmatrix}\begin{pmatrix}C^{\mu e}_L\\ C^{\mu e}_{L3}\\ C^{\mu e}_R\end{pmatrix} . \tag{5.72}$$

5.4.3 Finite corrections at the electroweak scale

Before finishing this section, let us compare our results for the 2-loop RG mixing $C_{L,L3,R} \to C_{DW,DB}$ with some of the finite loop contributions we mentioned in Section 5.3. At the electroweak scale $\sim m_W$, we have to integrate out the heavy particles (W and Z bosons, the Higgs h and the top quark) and match the SM onto the EFT of light fermions and photons. This procedure generates extra finite contributions to the dipole coefficients $d_{\mu e,e\mu}$. There are 1-loop finite corrections proportional to the coefficients $C_{L,L3,R}$ that should be compared to the 2-loop anomalous dimension for the mixing $C_{L,L3,R} \to C_{DW,DB}$. These corrections come from 1-loop diagrams that include the interactions in Eq. (5.9) and involve a Z or W boson. From [98], the contributions to $d_{e\mu}$ are

$$\Delta d_{e\mu}(m_W) = \frac{e}{16\pi^2}\frac{5}{6} C_{L3}^{e\mu}\frac{v^2}{\Lambda^2} \ , \tag{5.73}$$

for the W boson and

$$\begin{aligned} \Delta d_{e\mu}(m_W) &= -\frac{e}{16\pi^2}\frac{1}{3}(C_L^{e\mu} + C_{L3}^{e\mu})\left[\frac{5}{4} - (\frac{1}{4} - s^2_{\theta_W})\right]\frac{v^2}{\Lambda^2} \ , \\ \Delta d_{\mu e}(m_W) &= +\frac{e}{16\pi^2}\frac{1}{3} C_R^{\mu e}\left[\frac{5}{4} + (\frac{1}{4} - s^2_{\theta_W})\right]\frac{v^2}{\Lambda^2} \ , \end{aligned} \tag{5.74}$$

for the Z boson. Note that we have neglected terms proportional to the electron Yukawa y_e. These 1-loop corrections are larger than the 2-loop mixings we have computed. However, since they are finite, they might be canceled against other matching contributions at the new physics scale Λ. The total finite portion of the dipoles is therefore model-dependent. For instance, in certain BSM theories where $C_L^{e\mu} = C_{L3}^{e\mu} \neq 0$, the sum of $\Delta d_{e\mu}(m_W)$ for W and Z is roughly zero, since $s^2_{\theta_W} \approx 1/4$. In Section 5.6 we will see some examples of BSM models that satisfy this condition.

5.5 Energy bounds from anomalous dimension mixings

Once we know the anomalous dimensions for the mixings that contribute to an LFV observable, we can move forward to compute energy bounds for the corresponding Wilson coefficients. As an example, let us consider the 1-loop mixing of the operator $\mathcal{O}_{LuQe}$ into $\mathrm{BR}(\mu \to e\gamma)$. The anomalous dimensions for the mixings $C_{LuQe} \to C_{DW,DB}$ are listed in Eq. (5.43) and Eq. (5.44). For simplicity, we assume that all Wilson coefficients $\mathcal{O}_i$ are zero except for $\mathcal{O}_{LuQe}$. In that case the running couplings $C_{DW,DB}$ obey

$$\frac{\partial}{\partial \ln \mu}\begin{pmatrix} C_{DB}^{\mu e} \\ C_{DW}^{\mu e} \end{pmatrix} = \frac{N_c y_t}{32\pi^2}\begin{pmatrix} -1 \\ \frac{1}{2} \end{pmatrix} C_{LuQe}^{\mu ett} \ . \tag{5.75}$$

In order to compute the RG mixing from the new physics scale Λ to the electroweak scale $\sim m_W$, we integrate from $\mu = \Lambda$ to $\mu = m_W$,

$$\begin{pmatrix} C_{DB}^{\mu e}(m_W) \\ C_{DW}^{\mu e}(m_W) \end{pmatrix} = \frac{N_c y_t}{32\pi^2}\begin{pmatrix} -1 \\ \frac{1}{2} \end{pmatrix} C_{LuQe}^{\mu ett} \ln\left(\frac{m_W}{\Lambda}\right) \ . \tag{5.76}$$

Using Eq. (5.16), the dipole coefficients are

$$\begin{pmatrix} d_{\mu e} \\ d_{e\mu} \end{pmatrix} = \frac{v^2 g s_{\theta_W} N_c y_t}{\Lambda^2} \frac{3}{128\pi^2} \begin{pmatrix} C_{LuQe}^{\mu ett} \\ C_{LuQe}^{e\mu tt} \end{pmatrix} \ln\left(\frac{m_W}{\Lambda}\right) \ . \tag{5.77}$$

Consequently, the branching ratio Eq. (5.15) can be expressed as

$$\mathrm{BR}(\mu \to e\gamma) = 384\pi^2 \left(|C_{LuQe}^{\mu ett}|^2 + |C_{LuQe}^{e\mu tt}|^2\right) \left(\frac{v^2 g s_{\theta_W} N_c y_t}{\Lambda^2} \frac{3}{128\pi^2} \ln\left(\frac{m_W}{\Lambda}\right)\right)^2 \ . \tag{5.78}$$

By setting $|C_{LuQe}^{\mu ett}|^2 + |C_{LuQe}^{e\mu tt}|^2 = 1$ and solving for Λ, we find a lower bound for the energy scale of new physics. In our case we have $\Lambda \gtrsim 304$ TeV for the current sensitivity and $\Lambda \gtrsim 510$ TeV for the future one. We can proceed in the same way for the remaining loop mixings, using the anomalous dimensions listed in Appendix D.

5.5.1 Results

Table 5.9 shows the energy bounds for the operators that contribute to LFV observables, either at tree level or via RG mixing. For each entry, the first row shows the present bounds and the second row shows the future bounds. We use the following color legend:

- Black: tree-level bounds.
- Blue: bounds for coefficients that enter the observables at one loop.
- Red: bounds for coefficients that enter the observables at two loops.
- Purple: bounds for coefficients that enter the observables via a two-step 1-loop mixing.

Notice that blank spaces in the table correspond to bounds that are too small to be competitive against the constraints from other observables. As a reminder, we only include RG mixing effects and have not considered finite loop contributions. Those corrections are potentially large but also model-dependent. In Section 5.6 we show some examples of their cancellation for some particular BSM models.

The main novelty of our analysis is the inclusion of 2-loop RG mixings into the dipoles for $\mu \to e\gamma$. As we explained in Section 5.3, there are three classes of dimension-6 operators whose leading contribution to $C_{DB,DW}^{\mu e}$ arises at two loops:

- $\psi\bar{\psi}H^2$: The most interesting bound corresponds to the combination $C_L^{\mu e} - C_{L3}^{\mu e}$, because it is the only one that does not contribute to the other processes $\mu \to eee$ and $\mu N \to eN$ at tree level. For the current experimental constraints we find $\Lambda \gtrsim 24$ TeV, which is only a factor ~ 2 smaller than the 1-loop bound coming from $\mu N \to eN$. It is quite remarkable that a bound coming from a 2-loop mixing is of the same magnitude as other 1-loop bounds. Moreover, since the three observables lead to similar constraints, the measurement of one of them would suggest that the other two are also experimentally accessible.

	$\mu \to e\gamma$	$\mu \to eee$	$\mu N \to eN$	$h \to \mu e$	$Z \to \mu e$
$C_{DB}^{\mu e} - C_{DW}^{\mu e}$	951 TeV (1547 TeV)	218 TeV (2183 TeV)	208 TeV (1812 TeV)		
$C_{DB}^{\mu e} + C_{DW}^{\mu e}$	127 TeV (214 TeV)	26 TeV (309 TeV)	24 TeV (253 TeV)		
$C_{R}^{\mu e}$	35 TeV (59 TeV)	160 TeV (1602 TeV)	225 TeV (1535 TeV)		
$C_{L}^{\mu e} + C_{L3}^{\mu e}$	4 TeV (7 TeV)	164 TeV (1642 TeV)	225 TeV (1535 TeV)		5 TeV
$C_{L}^{\mu e} - C_{L3}^{\mu e}$	24 TeV (41 TeV)	35 TeV (421 TeV)	50 TeV (395 TeV)		
$C_{LuQe}^{\mu ett}$	304 TeV (510 TeV)	63 TeV (735 TeV)	59 TeV (604 TeV)		
$C_{LeQu}^{\mu ett}$	80 TeV (141 TeV)	14 TeV (209 TeV)	5 TeV (57 TeV)		
$C_{LL(RR),LR(RL)}^{\mu eee}$		207,174 TeV (2070,1740 TeV)			
$C_{LL,RR,LR}^{\mu euu}$			352 TeV (2693 TeV)		
$C_{LL,RR,LR}^{\mu edd}$			376 TeV (2725 TeV)		
$C_{LR}^{\mu dde}$			18 TeV (164 TeV)		
$C_{LL(LR),RR(RL)}^{\mu e\tau\tau,\mu ebb}$		14,16 TeV (174,194 TeV)	22 TeV (200 TeV)		
$C_{LL3}^{\mu e\tau\tau}$		20 TeV (247 TeV)	55 TeV (476 TeV)		
$C_{LL(RL),RR(LR)}^{\mu ett}$	122 TeV (214 TeV)	21 TeV (317 TeV)	22,32 TeV (200,290 TeV)		
$C_{LL3}^{\mu ett}$	230 TeV (401 TeV)	41 TeV (592 TeV)	100 TeV (851 TeV)		
$C_{y}^{\mu e}$	4 TeV (6 TeV)	1 TeV (9 TeV)	1 TeV (7 TeV)	0.3 TeV	

Table 5.9: Present (future) lower bounds on Λ of SMEFT dimension-6 operators from the different LFV processes. We have fixed the Wilson coefficient $C_i = 1$, turning each one by one. We show the bound in black, blue, purple and red depending on whether the coefficients contribute to the observables at tree level, 1-loop single log, 2-loop double log or 2-loop single log order, respectively.

We can also consider the effects of $C_L^{\mu e} + C_{L3}^{\mu e}$ and $C_R^{\mu e}$. In this case, however, the bounds are not competitive against those coming from $\mu \to eee$ and $\mu N \to eN$ at tree level.

- $\psi^2 H^3$: The 2-loop bound for $C_y^{\mu e}$ is $\Lambda \gtrsim 4$ TeV, which is ~ 10 times greater than the tree-level bound from $h \to \mu e$. We can actually use the constraint from $\mu \to e\gamma$ in Eq. (5.31) to determine that $\text{BR}(h \to \mu e) \lesssim 2 \cdot 10^{-8}$, so we do not expect it to be measured at the LHC in the near future.

- $\bar{\psi}^2\psi^2$: We can also obtain bounds on the coefficients $C_{LR}^{\mu\ell\ell e,\mu qqe}$. However, since the anomalous dimensions are proportional to a Yukawa coupling y_ℓ or y_d, the constraints are very weak and we have not included them in the table.

Let us now consider bounds coming from 1-loop mixings. This has been studied in previous works, such as [85, 98–103]. In our case, we were able to simplify the calculations making use of on-shell amplitude methods. According to the helicity selection rule $\Delta n \geq |\Delta h|$, the only LFV operator that can mix with the dipoles at one loop is $\mathcal{O}_{LuQe}$. Since the mixing is proportional to a Yukawa coupling, the largest contribution comes from $C_{LuQe}^{\mu ett}$, which leads to the bound $\Lambda \gtrsim 304$ TeV. Other operators can renormalize $\mathcal{O}_{LuQe}$, entering $\mu \to e\gamma$ via two-step 1-loop mixing. As explained in Section 3.4.1, the helicity selection rules have one exception, so $\bar{\psi}^2\psi^2$ operators involving a y_u Yukawa can mix with $\mathcal{O}_{LuQe}$. Again, the largest bounds correspond to operators involving the top quark. They are even larger than constraints coming from direct 1-loop mixings into $\mu \to eee$ and $\mu N \to eN$.

Finally, the majority of bounds for $\mu \to eee$ and $\mu N \to eN$ arise from 1-loop mixings of four-fermion operators (μeee, μeuu and μedd) with other four-fermion operators μeff. In this case the mixing is not proportional to the Yukawa coupling and instead depends on the particle hypercharges. Notice that Table 5.9 shows the bounds for operators μeff with f a 3rd-family fermion, but we could also include bounds for the 2nd-family ones.

5.6 UV models for LFV

Until now, we have focused on studying RG mixing contributions to the different LFV observables. This analysis has the advantage of being model-independent, but in general we expect to have additional contributions from matching the UV model. We are interested in the impact of the RG running on the observables compared to the finite contributions from a particular BSM scenario. We will focus on two cases: models with extra heavy fermions and models with lepton flavor universality violation.

5.6.1 Heavy vector-like fermions

For these models we assume a new heavy vector-like fermion of mass M, which can be a:

- Singlet (S).

- State of hypercharge $Y_E = -1$ (E).

- $\mathrm{SU}(2)_L$ doublet (D).

These new particles couple to the SM by mixing with the SM fermions through the following interaction Lagrangians,

$$\begin{aligned}\Delta\mathcal{L}_S &= (y_S^{(1)}\bar{L}_L^{(1)} + y_S^{(2)}\bar{L}_L^{(2)})S_R i\sigma_2 H^* + \text{h.c.}\ ,\\ \Delta\mathcal{L}_E &= (y_E^{(1)}\bar{L}_L^{(1)} + y_E^{(2)}\bar{L}_L^{(2)})E_R H + \text{h.c.}\ ,\\ \Delta\mathcal{L}_D &= (y_D^{*(1)}\bar{e}_R^{(1)} + y_D^{*(2)}\bar{e}_R^{(2)})D_L H^\dagger + \text{h.c.}\ .\end{aligned} \tag{5.79}$$

We are interested in the contribution of these particles to the branching ratio $\mathrm{BR}(\mu\to e\gamma)$. As customary in the EFT approach, we integrate out the heavy states at the scale $\Lambda = M$ and match them with the SMEFT Wilson coefficients listed in Section 5.2.1. At tree level, we find

$$\begin{aligned}C_L^{e\mu}(M) &= -C_{L3}^{e\mu}(M) = +\tfrac{1}{4}y_S^{(1)}y_S^{*(2)}\ ,\ \text{for } S\ ,\\ C_L^{e\mu}(M) &= \ \ C_{L3}^{e\mu}(M) = -\tfrac{1}{4}y_E^{(1)}y_E^{*(2)}\ ,\ \text{for } E\ ,\\ C_R^{\mu e}(M) &= -\tfrac{1}{2}y_D^{(1)}y_D^{*(2)}\qquad\qquad\ ,\ \text{for } D\ ,\end{aligned} \tag{5.80}$$

with $C^{\mu e}_{L,L3,R} = (C^{e\mu}_{L,L3,R})^*$. Note that the heavy singlet S generates $C_L^{e\mu}(M) = -C_{L3}^{e\mu}(M)$. Following our discussion in 5.4.3, this implies that the finite contributions to $d_{e\mu}$ from matching at the electroweak scale are approximately zero. We also find

$$\begin{aligned}&C_y^{e\mu}(M) = 0\ , && C_y^{\mu e}(M) = 0\ , && \text{for } S\ ,\\ &C_y^{e\mu}(M) = -y_E^{(1)}y_E^{*(2)}\ , && C_y^{\mu e}(M) = -(y_e/y_\mu)y_E^{(2)}y_E^{*(1)}\approx 0\ , && \text{for } E\ ,\\ &C_y^{\mu e}(M) = -y_D^{(1)}y_D^{*(2)}\ , && C_y^{e\mu}(M) = -(y_e/y_\mu)y_D^{(2)}y_D^{*(1)}\approx 0\ , && \text{for } D\ ,\end{aligned} \tag{5.81}$$

plus the corresponding Hermitian conjugates $(C_y)^*$.

Moving on to the next order, heavy fermions contribute to the dipole coefficients $d_{\mu e,e\mu}$ at one loop. We can extract their values from the $(g-2)$ contributions in [112], leading to

$$\begin{aligned}C_{DW}^{e\mu}(M) - C_{DB}^{e\mu}(M) &= \frac{1}{6}\frac{y_S^{(1)}y_S^{*(2)}}{16\pi^2}\ , && \text{for } S\ ,\\ C_{DW}^{e\mu}(M) - C_{DB}^{e\mu}(M) &= \frac{1}{24}\frac{y_E^{(1)}y_E^{*(2)}}{16\pi^2}\ , && \text{for } E\ ,\\ C_{DW}^{\mu e}(M) - C_{DB}^{\mu e}(M) &= -\frac{1}{24}\frac{y_D^{(1)}y_D^{*(2)}}{16\pi^2}\ , && \text{for } D\ .\end{aligned} \tag{5.82}$$

The remaining coefficients $C^{\mu e}_{DW,DB}$ for S, E, and $C^{e\mu}_{DW,DB}$ for D are negligible as they are proportional to $O(y_e/y_\mu)\approx 0$.

Once we have identified the contributions to the dipoles, we have to do the RG running of the couplings from M to the electroweak scale. As we have seen in Section 5.3.1, the Wilson coefficients in Eq. (5.80) and Eq. (5.81) mix with the dipoles at the 2-loop level. Then, at the electroweak scale, we should match the theory to the EFT of light fermions and photons.

Following Section 5.4.3, this matching leads to one-loop finite contributions to the dipoles $\Delta d_{e\mu}$ given by Eq. (5.73) and Eq. (5.74). Those corrections are proportional to the coefficients $C^{\mu e}_{L,L3,R}$, which in our case correspond to Eq. (5.80). As an example, for the singlet S heavy fermion we obtain

$$\Delta d_{e\mu}(m_W) = -\frac{y_S^{(1)} y_S^{*(2)}}{16\pi^2}\frac{5}{12}\,, \tag{5.83}$$

and the dipole coefficients are given by

$$\begin{aligned} d_{e\mu}(m_W) \simeq \frac{e}{2}\frac{v^2}{M^2}\Bigg[&\Delta d_{e\mu}(m_W) + (C^{e\mu}_{DW}(M) - C^{e\mu}_{DB}(M))\left(1 - N_c y_t^2\,\frac{\ln(M/m_W)}{16\pi^2}\right) \\ &+ \left((-N_c y_t^2 + 2\lambda)\, C_L^{e\mu}(M) + N_c y_t^2 C^{e\mu}_{L3}(M) - \frac{5}{8} g'^2 C_y^{e\mu}(M)\right)\frac{\ln(M/m_W)}{(16\pi^2)^2}\Bigg]\,, \\ d_{\mu e}(m_W) \simeq \frac{e}{2}\frac{v^2}{M^2}\Bigg[&\Delta d_{\mu e}(m_W) + (C^{\mu e}_{DW}(M) - C^{\mu e}_{DB}(M))\left(1 - N_c y_t^2\,\frac{\ln(M/m_W)}{16\pi^2}\right) \\ &+ \left((-2N_c y_t^2 + 2\lambda)\, C_R^{\mu e}(M) - \frac{5}{8} g'^2 C_y^{\mu e}(M)\right)\frac{\ln(M/m_W)}{(16\pi^2)^2}\Bigg]\,. \end{aligned} \tag{5.84}$$

Note that, for simplicity, this analysis does not include the RG running from m_W to m_μ. Substituting Eq. (5.84) into $\mathrm{BR}(\mu \to e\gamma)$ we can finally obtain bounds on the heavy fermion mass M. This allows us to assess the relative significance of 2-loop RG running effects compared to 1-loop matching contributions. For example, in the singlet model, if we set $y_S^{(i)} = 1$, the experimental bound on $\mu \to e\gamma$ leads to $M \gtrsim 43$ TeV. In this case, the RG mixing represents around 20% of $d_{e\mu}$. Proceeding in the same way for the doublet D, we find that $M \gtrsim 54$ TeV, with RG mixing contributing approximately 25% to $d_{\mu e}$. Overall, we observe that higher values of M correspond to a greater relative contribution from RG mixing. For low values of M, the RG running is only relevant in some models where the finite terms cancel.

5.6.2 BSM with lepton universality violations

Other interesting UV completions are theories that feature lepton flavor universality violation. They have been widely studied in recent years to explain some experimental tension in the muon sector (see for example [113]). The main idea is to construct a model in which some BSM particles couple only to SM muons and not to electrons. For example, we can have the effective operator

$$\frac{1}{M^2}(\bar{L}_L^{(2)}\sigma^a\gamma^\mu L_L^{(2)})(\bar{Q}_L^{(i)}\sigma^a\gamma_\mu Q_L^{(i)})\,, \tag{5.85}$$

that is generated by integrating out a heavy vector boson that only couples to muons and one quark family denoted as i. This particle breaks lepton universality, and lepton number is no longer preserved, as the diagonalization of the SM Yukawa matrix y_e leads to a violation of muon number. In particular, the dimension-6 operator $\mathcal{O}^{\mu ett}_{LL3} = (\bar{L}_L^{(2)}\sigma^a\gamma_\mu L_L^{(1)})(\bar{Q}_L^{(3)}\sigma^a\gamma^\mu Q_L^{(3)})$ is

generated with coefficient

$$\frac{C^{\mu ett}_{LL3}}{\Lambda^2} = \frac{U^{21}_{L_L} U^{\dagger\, i3}_{Q_L} U^{i3}_{Q_L}}{M^2} \ , \tag{5.86}$$

where U_{L_L}, U_{Q_L} are the left-handed rotation matrices that diagonalize, respectively, y_e and y_u. If the Yukawa matrices $y_{e,u}$ are roughly symmetric, we can estimate $U^{21}_{L_L} \sim \sqrt{m_e/m_\mu}$ and $U_{Q_L} \sim V_{\rm CKM}$. Using the experimental constraint on $C^{\mu ett}_{LL3}$ from $\mu \to e\gamma$, we obtain the bounds

$$M \gtrsim 0.8 \text{ TeV} \ , \quad \text{for } i = 2 \ ; \qquad\qquad M \gtrsim 60 \text{ TeV} \ , \quad \text{for } i = 3 \ . \tag{5.87}$$

The operator $\mathcal{O}^{\mu\mu bs}_{LL3} = (\bar{L}^{(2)}_L \sigma^a \gamma_\mu L^{(2)}_L)(\bar{Q}^{(2)}_L \sigma^a \gamma^\mu Q^{(3)}_L)$ is also generated from Eq. (5.85) with the coefficient

$$\frac{C^{\mu\mu bs}_{LL3}}{\Lambda^2} = \frac{U^{\dagger\, i2}_{Q_L} U^{i3}_{Q_L}}{M^2} \ . \tag{5.88}$$

Using Eq. (5.87), we can derive bounds on $C^{\mu\mu bs}_{LL3}$, which contributes to the process $b \to s\mu\mu$ at tree level. We find

$$\frac{C^{\mu\mu bs}_{LL3}}{\Lambda^2} \lesssim \frac{1}{(4 \text{ TeV})^2} \ , \text{ for } i = 2 \ , \qquad\qquad \frac{C^{\mu\mu bs}_{LL3}}{\Lambda^2} \lesssim \frac{1}{(290 \text{ TeV})^2} \ , \text{ for } i = 3 \ . \tag{5.89}$$

Following [114], the experimental discrepancy in the measurement of $B \to K\mu\mu$ can be explained if $C^{\mu\mu bs}_{LL3}/\Lambda^2 \sim 1/(56 \text{ TeV})^2$. From Eq. (5.89) we see that $\mu \to e\gamma$ constraints permit $i = 2$ but exclude $i = 3$. This shows an interesting interplay between bounds coming from different observables for some UV models.

5.7 Conclusions of the chapter

In this chapter we have used the SMEFT to analyze several LFV observables with $\Delta L_\mu = \Delta L_e = 1$ in a systematic way. We have focused on the muon decays $\mu \to e\gamma$, $\mu \to eee$ and $\mu N \to eN$, which have the most stringent experimental bounds. The sensitivities of these three processes are expected to improve substantially in the next decade, as summarized in Table 5.1. Given such prospects, we have aimed to analyze the LFV processes up to the 2-loop level.

We have identified the Wilson coefficients entering the LFV observables at tree level and those that mix with them via loops. For this task, we have used helicity selection rules, which tell us the only possible 1-loop mixings. After that, we have shown how to apply on-shell amplitude techniques to compute the necessary anomalous dimensions. Following Chapter 3, we have seen that some loop mixings can be obtained simply from a product of tree-level amplitudes integrated over a phase space.

For the process $\mu \to e\gamma$, helicity selection rules tell us that only the operator $\mathcal{O}_{LuQe}$ can enter the branching ratio at the 1-loop level. Then we have three classes of operators that enter at two loops: $\psi^2 H^2$, $\psi^2 H^3$ and $\bar{\psi}^2 \psi^2$. While the mixings of $\psi^2 H^3$ and $\bar{\psi}^2 \psi^2$ had already been computed in [28, 84], we calculated the mixing with $\psi^2 H^2$ for the first time in [3]. In particular, we obtained the 2-loop anomalous dimension for the renormalization $C_{L,L3,R} \to C_{DB,DW}$ at orders y_t^2 and λ^4, using on-shell methods. For the other two processes $\mu \to eee$ and $\mu N \to eN$, most

of the relevant operators enter the branching ratios at one loop. The only 2-loop contribution corresponds to $\psi^2 H^3$, which enters the processes via 2-loop mixing with the dipole operators.

The main results of our work are summarized in Table 5.9, which shows the bounds on the new physics scale Λ for the Wilson coefficients that enter $\mu \to e\gamma$, $\mu \to eee$ and $\mu N \to eN$, either at tree level or via RG mixing. Remarkably, we note the importance of some 2-loop effects that had not been considered before. Indeed, the bound on $C_L^{\mu e} - C_{L3}^{\mu e}$ from $\mu \to e\gamma$ is comparable to the bounds coming from $\mu \to eee$ and $\mu N \to eN$, which arise via 1-loop mixings. Additionally, the coefficient $C_y^{\mu e}$ only enters the muon decays via 2-loop mixing into the dipoles. The obtained bound is not quite large, but it is still better than the tree-level bound from the Higgs decay $h \to e\mu$. Moreover, the bound on $C_y^{\mu e}$ from $\mu \to e\gamma$ can be used to constrain the branching ratio $\mathrm{BR}(h \to e\mu)$. Doing that, we find that $h \to e\mu$ will not be accessible at colliders in the near future. The interplay between bounds coming from different LFV observables is discussed in Section 5.5.

The effects of 2-loop RG mixing into the dipole coefficients $d_{\mu e, e\mu}$ must be compared with finite contributions arising at one loop. In particular, we must consider corrections from EFT matching at the electroweak scale and from matching with some BSM theory at Λ. The sum of these two pieces depends on the particular UV model we consider. In general it can be larger than the 2-loop RG mixing, but one should perform a case-by-case analysis. As an example, we have computed the full dipole contribution in a theory with additional heavy fermions.

Overall, we have seen that the next generation of LFV precision experiments requires extending the analysis of renormalization effects to higher orders. On-shell amplitude methods can be a valuable tool for this purpose, since they are suitable for computing anomalous dimensions and also allow us to understand patterns behind the operator mixings.

Chapter 6

Applications of renormalization III: Anomalous dimensions from Partial Waves

In this chapter, we revisit our results for the 1-loop renormalization of EFTs, studying the effects of angular momentum decomposition. As we derived in Chapter 3, anomalous dimensions can be computed from a product of on-shell amplitudes integrated over some phase space. Building upon that work, we consider the impact of the partial-wave expansion of amplitudes. We mostly follow the results in [2]. Related analyses include [81, 115].

We aim to gain a deeper understanding of renormalization from angular momentum conservation. By decomposing amplitudes in partial waves, we will compute the anomalous dimension as a sum of products of partial-wave coefficients a^J. This is particularly useful for amplitudes with a finite number of a^J, such as contact interactions in an EFT.

The discussion is organized as follows: In Section 6.1, we derive the main formula to express anomalous dimensions in terms of partial waves. For simplicity, we work with 4-point amplitudes associated with two-to-two scattering. We extend these results to renormalizations featuring infrared divergences, which involve a regularized version of the partial-wave coefficients. In Section 6.2, we explicitly compute anomalous dimensions in several EFTs: the SMEFT, the SO(N) nonlinear sigma model and the EFT of gravity. Finally, we present our conclusions in Section 6.3.

6.1 Partial-wave analysis of anomalous dimensions

First, we derive a formula to calculate anomalous dimensions in terms of partial-wave coefficients. We consider an EFT with contact interactions given by $\mathcal{A}_{\mathcal{O}_i}$. These are the building blocks of the theory, which are classified according to an expansion in E/Λ, with Λ the UV cut-off of the EFT. The Wilson coefficient of the amplitude, denoted as $C_{\mathcal{O}_i}$, is renormalized at the loop level, so it receives an anomalous dimension γ_i. Our goal is to show how angular momentum decomposition can simplify the computation of γ_i.

6.1.1 Renormalization with on-shell amplitude methods

Our starting point is formula Eq. (3.16) for the 1-loop renormalization of amplitudes, which we derived in Section 3.2.2. That expression gives us the anomalous dimension γ_{ij} for the mixing $\mathcal{A}_{\mathcal{O}_j} \to \mathcal{A}_{\mathcal{O}_i}$ in terms of 2-cuts of a loop amplitude when there are no IR divergences. For convenience, we shall consider the full anomalous dimension $\gamma_i = dC_{\mathcal{O}_i}/d\ln\mu = \sum_j \gamma_{ij} C_{\mathcal{O}_j}$ instead of γ_{ij}. If both $\mathcal{A}_{\mathcal{O}_i}$ and $\mathcal{A}_{\mathcal{O}_j}$ are 4-point amplitudes, we can write

$$\gamma_i \frac{\mathcal{A}_{\mathcal{O}_i}(1,2,3,4)}{C_{\mathcal{O}_i}} = \\ -\frac{1}{4\pi^3}\int d\text{LIPS} \sum_{\ell_1,\ell_2} \sigma_{\ell_1\ell_2} \left[\mathcal{A}_L(1,2,\bar{\ell}_2,\bar{\ell}_1)\mathcal{A}_R(\ell_1,\ell_2,3,4)\right] + (2\leftrightarrow 3) + (2\leftrightarrow 4)\ , \tag{6.1}$$

where the subamplitudes $\mathcal{A}_L$, $\mathcal{A}_R$ contain the contact amplitudes $\mathcal{A}_{\mathcal{O}_j}$. We define a weight w corresponding to the order of an amplitude $\mathcal{A} \sim 1/\Lambda^w$, so that $w_i = w_L + w_R$. The three terms in the RHS side correspond to the s-, t- and u- channels[1]. The summation $\sum_{\ell_1,\ell_2}$ is over all possible internal states with momentum ℓ_1, ℓ_2. A bar over a state, such as $\bar{1}$, indicates the opposite momentum sign, helicity, and other quantum numbers relative to the original state. We define $\sigma_{\ell_1,\ell_2} = (-i)^{F[\ell_1,\ell_2]}$, with $F[\ell_1,\ell_2]$ the number of fermions in the list $\{\ell_1,\ell_2\}$[2]. We must also add a factor of $1/2$ when the cut particles are identical.

Eq. (6.1) can be generalized to cases where there is more than one independent amplitude $\mathcal{A}_{\mathcal{O}_i}$ with the same external states. In that case, we must add a summation over all possible $\mathcal{A}_{\mathcal{O}_i}$ in the LHS of Eq. (6.1). Another possibility is to have a non-minimal amplitude $\widehat{\mathcal{A}}_{\mathcal{O}_i}$ instead of the contact one.

6.1.2 Partial-wave decomposition of amplitudes

The next step is to consider the angular-momentum decomposition of a general 4-point amplitude $\mathcal{A}(1_{h_1}, 2_{h_2}, 3_{h_3}, 4_{h_4})$, with h_i the helicity of particle i. For this purpose, it is convenient to specify incoming and outgoing states instead of using the all-incoming notation. For instance, let us consider an s-channel scattering with $1_{h_1}, 2_{h_2} \to 3_{-h_3}, 4_{-h_4}$. The amplitude for this process is related to the all-incoming amplitude as follows:

$$\mathcal{A}(1_{h_1}, 2_{h_2} \to 3_{-h_3}, 4_{-h_4}) \equiv \sigma_{34}\mathcal{A}(1_{h_1}, 2_{h_2}, -4_{h_4}, -3_{h_3})\ , \tag{6.2}$$

where $\sigma_{34} = (-i)^{F[34]}$ as defined earlier. Let us consider the center-of-momentum frame for $1_{h_1}, 2_{h_2} \to 3_{-h_3}, 4_{-h_4}$. We align the z-axis with the momentum of particles 1 and 2, with $\vec{p}_1$ pointing downwards. The direction of the outgoing particles can be parameterized using polar

[1] Note that the particle ordering is 1324 in the t-channel and 1432 in the u-channel. We must add a minus sign for every fermion exchange compared to 1234.

[2] This factor comes from our parameterization of spinors with negative momenta in Eq. (A.26), see Appendix A.3 for more details. Note that $\sigma_{\ell_1,\ell_2} = (-i)^{F[\ell_1,\ell_2]}$ and not $(+i)^{F[\ell_1,\ell_2]}$ because the left subamplitude is the one with negative momenta for the internal states.

coordinates (θ, ϕ). Thus, the scattering amplitude can be written as a function of the angles θ, ϕ and the Mandelstam variable s:

$$\mathcal{A}(1_{h_1}, 2_{h_2} \to 3_{-h_3}, 4_{-h_4}) = \mathcal{A}(s, \theta, \phi) \ . \tag{6.3}$$

Using this parameterization, the spinor-helicity variables associated with the outgoing particles 3 and 4 are:

$$\begin{aligned} |3\rangle &= c_{\theta/2}|1\rangle - s_{\theta/2}e^{-i\phi}|2\rangle \ , & |3] &= c_{\theta/2}|1] - s_{\theta/2}e^{i\phi}|2] \ , \\ |4\rangle &= s_{\theta/2}e^{i\phi}|1\rangle + c_{\theta/2}|2\rangle \ , & |4] &= s_{\theta/2}e^{-i\phi}|1] + c_{\theta/2}|2] \ , \end{aligned} \tag{6.4}$$

which satisfies momentum conservation $p_1 + p_2 = p_3 + p_4$. The Mandelstam variables s, t, u can be expressed as follows

$$s = \langle 12 \rangle [21] \ , \qquad t = -\langle 13 \rangle [31] = -s\,\frac{1 - c_\theta}{2} \ , \qquad u = -\langle 14 \rangle [41] = -s\,\frac{1 + c_\theta}{2} \ . \tag{6.5}$$

With these considerations, we can perform a partial-wave decomposition of the scattering amplitude $\mathcal{A}(s, \theta, \phi)$. It is convenient to use the formalism introduced by M. Jacob and G. C. Wick in [116]. We consider a basis of definite angular momentum quantized along the z-axis, so the amplitude can be written as

$$\mathcal{A}(s, \theta, \phi) = e^{i\phi(h_{12} - h_{43})} \left(\frac{\sqrt{s}}{\Lambda}\right)^w \sum_J n_J \ d^J_{h_{12}h_{43}}(\theta) \ a^J \ , \tag{6.6}$$

where $n_J = 2J + 1$, $h_{12} = h_1 - h_2$, $h_{34} = h_3 - h_4$ and $d^J_{h_{12}h_{43}}(\theta)$ are the Wigner d-functions. We have factored out the Λ dependence of the amplitude, extracting the dimensionless ratio $\sqrt{s}/\Lambda$. More details on the derivation of this formula can be found in Appendix E.

From Eq. (6.5) we find that $c_\theta = (t - u)/s$. This relation allows us to remove the θ dependence in Eq. (6.6) and express the amplitude in a manifestly Lorentz-invariant form. We can also invert the partial-wave decomposition in Eq. (6.6) and find an expression for the a^J coefficients:

$$a^J = \frac{1}{2}\left(\frac{\sqrt{s}}{\Lambda}\right)^{-w} \int_0^\pi d\theta \ s_\theta \ d^J_{h_{12}h_{43}}(\theta) \ \mathcal{A}(s, \theta, \phi = 0) \ , \tag{6.7}$$

where we have used the orthogonality of the Wigner d-functions, as given by Eq. (E.6). Note that we have assumed the existence of well-defined coefficients a^J, which is not always true. For instance, in Section 6.1.4, we will see that a^J are singular for mixings with soft IR divergences.

Thus far, we have considered scattering in the s-channel, but we can proceed analogously for the t- and u- channels. For the t-channel amplitude $\mathcal{A}(1_{h_1}, 3_{h_3} \to 2_{-h_2}, 4_{-h_4})$, the partial-wave decomposition is

$$\mathcal{A}(t, \theta', \phi') = e^{i\phi'(h_{13} - h_{42})} \left(\frac{\sqrt{t}}{\Lambda}\right)^w \sum_J n_J \ d^J_{h_{12}h_{43}}(\theta') \ a^J \ , \tag{6.8}$$

where the polar angles (θ', ϕ') correspond the direction of the outgoing particles 2,4. The relation between θ' and the Mandelstam variables is given by $c_{\theta'} = (s-u)/t$. Similarly, the u-channel amplitude $\mathcal{A}(1_{h_1}, 4_{h_4} \to 2_{-h_2}, 3_{-h_3})$ can be written as

$$\mathcal{A}(u, \theta'', \phi'') = e^{i\phi''(h_{13}-h_{42})} \left(\frac{\sqrt{u}}{\Lambda}\right)^w \sum_J n_J \; d^J_{h_{12}h_{43}}(\theta'') \; a^J \;, \tag{6.9}$$

with (θ'', ϕ'') the polar coordinates for the outgoing 2,3 and $c_{\theta''} = (t-s)/u$.

For all channels, the partial-wave coefficients a^J completely characterize the amplitude $\mathcal{A}(1_{h_1}, 2_{h_2}, 3_{h_3}, 4_{h_4})$. We can choose one channel or another depending on the problem under consideration.

6.1.3 Partial-wave decomposition of the anomalous dimensions

At this stage, we are ready to carry out a partial-wave decomposition of the subamplitudes $\mathcal{A}_L, \mathcal{A}_R$ in Eq. (6.1). We start by considering the s-channel terms, which can be expressed as

$$\sigma_{\ell_1\ell_2}\mathcal{A}_L(1, 2, \bar{\ell}_2, \bar{\ell}_1)\mathcal{A}_R(\ell_1, \ell_2, 3, 4) = \mathcal{A}_L(1, 2 \to \ell_1, \ell_2)\sigma_{34}^{-1}\mathcal{A}_R(\ell_1, \ell_2 \to \bar{4}, \bar{3}) \;, \tag{6.10}$$

where we have rewritten the all-incoming amplitudes according to Eq. (6.2). It is convenient to define polar coordinates for both subamplitudes. For $\mathcal{A}_L(1, 2 \to \ell_1, \ell_2)$, the direction of ℓ_1, ℓ_2 is described by the polar angles (θ', ϕ'). For $\mathcal{A}_R(\ell_1, \ell_2 \to \bar{4}, \bar{3})$, the direction of $\bar{4}, \bar{3}$ is given by (θ, ϕ). Using Eq. (6.6) for the partial-wave decomposition of $\mathcal{A}_L$ and Eq. (E.3) for the decomposition of $\mathcal{A}_R$, Eq. (6.10) leads to

$$\begin{aligned}\mathcal{A}_L(1, 2 \to \ell_1, \ell_2)\sigma_{34}^{-1}\mathcal{A}_R(\ell_1, \ell_2 \to \bar{4}, \bar{3}) = \left(\frac{\sqrt{s}}{\Lambda}\right)^{w_L+w_R} e^{i\phi'(h_{12}-h'_{12})} \sum_{J'} n_{J'} d^{J'}_{h_{12}h'_{12}}(\theta') a_L^{J'} \\ \times \sigma_{34}^{-1} \sum_{J,M} n_J e^{i\phi(M-h_{34})} d^J_{Mh_{34}}(\theta) \; e^{-i\phi'(M-h'_{12})} d^J_{Mh'_{12}}(\theta') a_R^J \;,\end{aligned} \tag{6.11}$$

where $a^J_{L,R}$ are the partial-wave coefficients for $\mathcal{A}_{L,R}$. With this parameterization, the dLIPS integral for the internal spinors ℓ_1, ℓ_2 in Eq. (6.1) corresponds to an angular integration over the (θ', ϕ') coordinates. Specifically, we have $\int d\text{LIPS} = \frac{1}{8}\int_0^\pi d\theta' s_{\theta'} \int_0^{2\pi} d\phi'$. Performing the phase-space integration of Eq. (6.11), we obtain

$$\begin{aligned}\int d\text{LIPS} \; \mathcal{A}_L(1, 2 \to \ell_1, \ell_2)\sigma_{34}^{-1}\mathcal{A}_R(\ell_1, \ell_2 \to \bar{4}, \bar{3}) = \\ \frac{\pi}{2}\sigma_{34}^{-1} \; e^{i\phi(h_{12}-h_{34})} \left(\frac{\sqrt{s}}{\Lambda}\right)^{w_L+w_R} \sum_J n_J \; d^J_{h_{12}h_{34}}(\theta) \; a_L^J a_R^J \;,\end{aligned} \tag{6.12}$$

where again we have used the orthogonality of the Wigner d-functions.

We can proceed in the same way for the second and third terms in the RHS of Eq. (6.1), performing the angular momentum decomposition in the t- and u- channels. Doing that, the

anomalous dimenion is finally given by

$$\gamma_i \frac{\mathcal{A}_{\mathcal{O}_i}}{C_{\mathcal{O}_i}} = -\frac{\sigma_{34}^{-1}}{8\pi^2}\, e^{i\phi(h_{12}-h_{34})} \left(\frac{\sqrt{s}}{\Lambda}\right)^{w_i} \sum_J n_J\, d^J_{h_{12}h_{34}}(\theta) \sum_{\ell_1,\ell_2} a_L^J a_R^J \; + (s \leftrightarrow t) + (s \leftrightarrow u)\ . \quad (6.13)$$

This expression is particularly helpful when there is a finite number of non-zero $a^J_{L,R}$ coefficients. For instance, that is the case when $\mathcal{A}_{\mathcal{O}_i}$ is a contact 4-point amplitude, as the incoming states can only be in a few J configurations. We distinguish two different types of renormalizations:

- If either $\mathcal{A}_L$ or $\mathcal{A}_R$ are contact subamplitudes, their partial-wave decompositions contain a finite number of a^J. Therefore, the J summation in Eq. (6.13) only includes a finite number of terms and the anomalous dimension γ_i can be obtained easily.

- If both $\mathcal{A}_L$ are $\mathcal{A}_R$ non-contact subamplitudes, the summation over J in Eq. (6.13) becomes infinite, making the expression less practical. In that case, there must be a non-trivial cancellation between the different channels, making the overall contribution to the anomalous dimension finite. See Section 6.2.1 for an example of this type of mixing within the SMEFT.

We can also identify some cases where Eq. (6.13) is further simplified:

- If only one kinematic channel contributes to Eq. (6.13), we can expand the amplitude $\mathcal{A}_{\mathcal{O}_i}$ into partial waves in the same channel. For example, if there are only s-channel contributions, we can write

$$\gamma_i \frac{a_i^J}{C_{\mathcal{O}_i}} = -\frac{1}{8\pi^2} \sum_{\ell_1,\ell_2} a_L^J a_R^J\ , \quad (6.14)$$

  where a^J are partial-wave coefficients in the s-channel. If several amplitudes $\mathcal{A}_{\mathcal{O}_i}$ contribute to the LHS of Eq. (6.13), we must add a summation over the i indices in the LHS of Eq. (6.14). This leads to a system of equations for the different γ_i.

- Another interesting scenario occurs when the contributions from different channels in Eq. (6.13) are proportional to a single amplitude $\mathcal{A}_{\mathcal{O}_i}$. In general, the RHS of Eq. (6.13) is only proportional to $\mathcal{A}_{\mathcal{O}_i}$ after summing the three kinematic channels, but that is not always true. If the different channel contributions are parametrically independent from each other, the anomalous dimension satisfies

$$\gamma_i = \gamma_i^s + \gamma_i^t + \gamma_i^u\ , \quad (6.15)$$

  with $\gamma_i^{s,t,u}$ the contribution from the s-, t- and u- channels. For the s-channel, we have

$$\gamma_i^s \frac{\mathcal{A}_{\mathcal{O}_i}}{C_{\mathcal{O}_i}} = -\frac{1}{8\pi^2}\, \sigma_{34}^{-1}\, e^{i\phi(h_{12}-h_{34})} \left(\frac{\sqrt{s}}{\Lambda}\right)^{w_L+w_R} \sum_J n_J\, d^J_{h_{12}h_{34}}(\theta) \sum_{\ell_1,\ell_2} a_L^J a_R^J\ . \quad (6.16)$$

Performing a partial-wave expansion of $\mathcal{A}_{\mathcal{O}_i}$ in the s-channel as well, we obtain

$$\gamma_i^s = -\frac{C_{\mathcal{O}_i}}{8\pi^2} \sum_{\ell_1,\ell_2} \frac{a_L^J a_R^J}{a_i^J} \ . \tag{6.17}$$

In order to compute the other contributions γ_i^t and γ_i^u, we can proceed in the same manner for the t- and u- channels.

In Section 6.2, we will show examples of these simplifications when applying Eq. (6.13) to several EFTs. For the case of the SMEFT, we will demonstrate that several mixings between SMEFT amplitudes at order $1/\Lambda^2$ include partial waves in a single channel, so Eq. (6.14) is valid. For the nonlinear sigma model and gravity, we will see that contributions from different kinematic channels are related by crossing symmetry, so only the s-channel computation is necessary.

6.1.4 IR divergences

Following Section 3.3, we can extend Eq. (6.1) for renormalizations with both collinear and soft IR divergences. For the collinear case, we must add the following term to Eq. (6.1),

$$\Delta\gamma_{\mathcal{O}_i} \frac{\mathcal{A}_{\mathcal{O}_i}(1,2,3,4)}{C_{\mathcal{O}_i}} = \gamma_{\text{coll}} \mathcal{A}_{\mathcal{O}_i}(1,2,3,4) \ . \tag{6.18}$$

The coefficients γ_{coll} depend only on the external legs, so we can write $\gamma_{\text{coll}} = \sum_{n=1}^4 \gamma_{\text{coll}}^{(n)}$. The explicit form of $\gamma_{\text{coll}}^{(n)}$ for different particles can be found in [28, 29].

The treatment of soft IR divergences requires a more detailed approach. These contributions are associated with angular singularities of the subamplitudes $\mathcal{A}_{L,R}$, so the dLIPS integral is not finite. As explained in Section 3.3, $\theta \to 0$ divergences in Eq. (6.1) must be regulated by adding

$$\begin{aligned} \Delta\gamma_i \ \frac{\mathcal{A}_{\mathcal{O}_i}(1^a,2^b,3^c,4^d)}{C_{\mathcal{O}_i}} = -\frac{1}{4\pi^3} \Bigg[& (\boldsymbol{T}^{12}_{\text{soft}})^{a\,b}_{\hat{a}\,\hat{b}} \mathcal{A}_R(1^{\hat{a}},2^{\hat{b}},3^c,4^d) \int d\text{LIPS}_{12} \ \frac{1}{s^2_{\theta'/2}} \\ & + (\boldsymbol{T}^{34}_{\text{soft}})^{c\,d}_{\hat{c}\,\hat{d}} \mathcal{A}_L(1^a,2^b,3^{\hat{c}},4^{\hat{d}}) \int d\text{LIPS}_{34} \ \frac{1}{s^2_{\theta'/2}} \Bigg] + (2 \leftrightarrow 3) + (2 \leftrightarrow 4) \ , \end{aligned} \tag{6.19}$$

where the dLIPS$_{ij}$ integral is over the phase space of the $i'j'$ particle pair. The soft operator $\boldsymbol{T}^{ij}_{\text{soft}}$ acts on the color or flavor indices a, b, c, d, and its explicit form depends on the theory we consider. For instance, the QED operator is given by $\boldsymbol{T}^{ij}_{\text{soft}} = e^2 q_i q_j$, where q_i is the charge of particle i. Similarly, the gravity operator is $\boldsymbol{T}^{ij}_{\text{soft}} = -2s_{ij}/M_P^2$, with M_P the Planck mass.

When the subamplitudes $\mathcal{A}_{L,R}$ have angular singularities, Eq. (6.7) leads to logarithmically divergent partial-wave coefficients $a^J \sim \lim_{\epsilon\to 0} \int_\epsilon^\pi d\theta/\theta \sim \ln\epsilon$. Including the additional terms in Eq. (6.19), we define the regularized coefficients as

$$a^J|_{\text{reg}} = \frac{1}{2} \left(\frac{\sqrt{s}}{\Lambda}\right)^{-w} \int_0^\pi d\theta \, s_\theta \left(d^J_{h_{12}h_{43}}(\theta) \mathcal{A}(1^a_{h_1}, 2^b_{h_2} \to 3^c_{-h_3}, 4^d_{-h_4})|_{\theta,\phi=0} + \frac{(\boldsymbol{T}_{\text{soft}})^{a\,b}_{c\,d}}{s^2_{\theta/2}} \right) \ . \tag{6.20}$$

Now we can generalize Eq. (6.13) for renormalizations with soft IR divergences: we must simply replace the partial-wave coefficients a^J with their regularized version $a^J|_{\rm reg}$. Let us prove this statement. We consider a mixing where the subamplitude $\mathcal{A}_L$ has divergent plane-wave coefficients, whereas $\mathcal{A}_R$ has all a^J finite, as is the case when $\mathcal{A}_R$ represents a contact amplitude. The anomalous dimension is given by Eq. (6.1) plus the regulator in Eq. (6.19). For each individual cut, the dLIPS integral can be written as

$$\begin{aligned}
&\int d\text{LIPS}\left(\sigma_{\ell_1\ell_2}\,\mathcal{A}_L(1,2,\bar{\ell}_2,\bar{\ell}_1)\mathcal{A}_R(\ell_1,\ell_2,3,4)+\frac{\boldsymbol{T}_{\rm soft}}{s^2_{\theta'/2}}\mathcal{A}_R(1,2,3,4)\right)\sigma_{34}\\
&=\frac{\pi}{4}e^{i\phi(h_{12}-h_{34})}\left(\frac{\sqrt{s}}{\Lambda}\right)^{w_R}\sum_J n_J\, d^J_{h_{12}h_{34}}(\theta)\,a^J_R\int_0^\pi d\theta' s_{\theta'}\left(d^J_{h_{12}h'_{12}}(\theta')\mathcal{A}_L(s,\theta',0)+\frac{\boldsymbol{T}_{\rm soft}}{s^2_{\theta'/2}}\right) \qquad (6.21)\\
&=\frac{\pi}{2}e^{i\phi(h_{12}-h_{34})}\left(\frac{\sqrt{s}}{\Lambda}\right)^{w_R+w_L}\sum_J n_J\, d^J_{h_{12}h_{34}}(\theta)\,a^J_R\,a^J_L|_{\rm reg}\ ,
\end{aligned}$$

where the color/flavor indices are implicit. Indeed, we recover the result in Eq. (6.13), replacing the divergent a^J_L by the regularized $a^J_L|_{\rm reg}$. We will see some examples of renormalizations with IR divergences in Sections 6.2.1 and 6.2.3.

Finally, we consider the scenario where $\mathcal{A}_L$ or $\mathcal{A}_R$ diverge for both $\theta\to 0$ and $\theta\to\pi$. In this case, the integral $\int s^{-2}_{\theta'/2}$ must be replaced with $2\int s^{-2}_{\theta'}$ in both Eq. (6.19) and Eq. (6.20). This ensures that the integrands are well-behaved. Moreover, Eq. (6.20) has to be computed only for even J since $a^J=0$ for odd J[3].

6.2 Applications

6.2.1 SMEFT renormalization with partial-waves

As a first application, we revisit the renormalization of $1/\Lambda^2$ amplitudes in the SMEFT, including the cases discussed in Chapter 4. We are interested in computing the anomalous dimensions matrix using the method of partial-wave decomposition in Eq. (6.13), which can provide new insights into the mixing structure. We start by considering all $1/\Lambda^2$ SMEFT amplitudes with $n=4$ and total helicity $h=-2$, namely:

$$\begin{aligned}
\mathcal{A}_{WHle}(1_e,2_{l^j},3_{W^a_-},4_{H^\dagger_i})&=\frac{C_{WHle}}{\Lambda^2}\langle 31\rangle\langle 32\rangle\,(T^a)^j_i\ ,\\
\mathcal{A}_{W^2H^2}(1_{W^a_-},2_{H^j},3_{W^b_-},4_{H^\dagger_i})&=\frac{C_{W^2H^2}}{\Lambda^2}\langle 13\rangle^2\,\delta_{ab}\delta^j_i\ ,\\
\mathcal{A}_{lequ,0}(1_e,2_{l^i},3_u,4_{q^j})&=\frac{C_{lequ,0}}{\Lambda^2}\langle 12\rangle\langle 34\rangle\,\epsilon^{ij}\ ,\\
\mathcal{A}_{lequ,1}(1_e,2_{l^i},3_u,4_{q^j})&=\frac{C_{lequ,1}}{\Lambda^2}\frac{1}{2}\left(\langle 23\rangle\langle 41\rangle+\langle 13\rangle\langle 42\rangle\right)\epsilon^{ij}\ .
\end{aligned}\qquad (6.22)$$

[3]Note that $\mathcal{A}$ is even in $[0,\pi]$, whereas the product $s_\theta\, d^J_{00}(\theta)$ is odd for odd J. Therefore, the coefficient a^J computed with Eq. (6.7) vanishes. Since the amplitude $\mathcal{A}$ diverges for both $\theta\to 0$ and $\theta\to\pi$, we must compute $\int_\epsilon^{\pi-\epsilon} d\theta\, s_\theta\,\mathcal{A}(\theta)d^J_{00}(\theta)$ and then take the limit $\epsilon\to 0$.

	$J=0$	$J=1$	
$\mathcal{A}_{\rm SM}(1_{\bar{\psi}_R}, 2_{\bar{\psi}_{Li}}, 3_{W_-^a}, 4_{H^j})$	0	$\frac{1}{\sqrt{2}}$	$\times\, y_\psi g_2\, (T^a)_i^j$
$\mathcal{A}_{\rm SM}^{I=0}(1_H, 2_{H^\dagger}, 3_{H^\dagger}, 4_H)$	$-\frac{3}{8}$	$-\frac{3}{2}$	$\times\, g_2^2$
$\mathcal{A}_{WHle}(1_e, 2_{l^j}, 3_{W_-^a}, 4_{H_i^\dagger})$	0	$\frac{1}{3\sqrt{2}}$	$\times\, C_{WHle}(T^a)_i^j$
$\mathcal{A}_{eluq,0}(1_e, 2_{l^i}, 3_u, 4_{q^j})$	1	0	$\times\, C_{eluq,0}\, \epsilon^{ij}$
$\mathcal{A}_{eluq,1}(1_e, 2_{l^i}, 3_u, 4_{q^j})$	0	$\frac{1}{6}$	$\times\, C_{eluq,1}\, \epsilon^{ij}$
$\mathcal{A}_{W^2H^2}(1_{W_-^a}, 2_{H^j}, 3_{W_-^b}, 4_{H_i^\dagger})$	0	$\frac{1}{3}$	$\times\, C_{W^2H^2}\delta_{ab}\delta_i^j$
$\mathcal{A}_{B^2H^2}(1_{B_-}, 2_{B_-}, 3_{H^j}, 4_{H_i^\dagger})$	1	0	$\times\, C_{B^2H^2}\delta_i^j$

Table 6.1: Partial-wave coefficients a^J in the s-channel for the different SM and SMEFT amplitudes discussed in the text, up to $J=1$. For $\mathcal{A}_{\rm SM}^{I=0}$, we give the regularized coefficient $a^J|_{\rm reg}$.

Note that we are using mostly the same amplitude basis as in Chapter 4, replacing the four-fermion amplitude $\mathcal{A}_{luqe}$ in Eq. (4.2) by $\mathcal{A}_{lequ,1}$. This basis is convenient because $\mathcal{A}_{lequ,0}$ and $\mathcal{A}_{lequ,1}$ have only one non-vanishing partial-wave coefficient a^J. This is related to their symmetry properties under the exchange $1 \leftrightarrow 2$.

We focus on the renormalization between amplitudes in Eq. (6.22) with different number of fermions n_F. The corresponding anomalous dimensions, which arise from very different Feynman diagrams, showcase a similar structure in the on-shell approach. Indeed, from Eq. (6.1) we see that all those mixings must involve the same type of SM amplitude:

$$\mathcal{A}_{\rm SM}(1_{\bar{e}}, 2_{\bar{l}_i}, 3_{W_-^a}, 4_{H^j}) = y_\psi\ g_2\ (T^a)_i^j \frac{\langle 13\rangle\, \langle 43\rangle}{\langle 14\rangle\, \langle 12\rangle}\ , \tag{6.23}$$

or its complex conjugate. The fermions ψ_L and ψ_R are, respectively, the $\mathrm{SU}(2)_L$ doublet and singlet leptons l and e. We can also have the same amplitude for the up-type quark fields q, u, replacing $H^j \to H_j^\dagger$ and $(T^a)_i^j \to (T^a)_i^{j'} \epsilon_{j'j}$ in Eq. (6.23).

In Section 4.6, we already pointed out that only one SM amplitude is involved in all non-diagonal mixings between amplitudes of classes $V\psi^2 H$, V^2H^2 and ψ^4. Now we can analyze this behavior using angular momentum decomposition. The first step is to notice that all renormalizations between amplitudes in Eq. (6.22) with different n_F include solely the s-channel. The only exception is the renormalization of $\mathcal{A}_{W^2H^2}$ by $\mathcal{A}_{WHle}$, which gets contributions from both the s- and t- channels. However, the t-channel terms can be easily obtained from the s-channel ones by interchanging the external W bosons. Using Eq. (6.7), we compute the partial-wave coefficients for Eq. (6.23) in the s-channel, leading to

$$a_{\rm SM}^{J=0} = 0\ , \qquad a_{\rm SM}^{J\geq 1} = y_\psi g_2 (T^a)_i^j\ \frac{1}{2}\int_0^\pi d\theta s_\theta\ d_{0,1}^J(\theta) \frac{s_{\theta/2}}{c_{\theta/2}} = \frac{y_\psi g_2 (T^a)_i^j}{\sqrt{J(J+1)}}\ . \tag{6.24}$$

Similarly, the a_J coefficients for the $1/\Lambda^2$ amplitudes in Eq. (6.22) are listed in Table 6.1.

Given Eq. (6.13), we see that amplitudes ¡only mix when they have partial waves for the same J. This constitutes an angular momentum selection rule that was first discussed in [81]. Since $\mathcal{A}_{lequ,0}$ only has a $J=0$ component, it cannot mix with $\mathcal{A}_{WHle}$, $\mathcal{A}_{W^2H^2}$ and $\mathcal{A}_{lequ,1}$, which solely include $J=1$. The other amplitudes mix among themselves through the $J=1$ partial wave, so all the mixings involve $a_{\rm SM}^{J=1}$. Using Eq. (6.14), the anomalous dimensions satisfy

$$\begin{pmatrix} \gamma_{WHle}\ C^{-1}_{WHle}\ a^1_{WHle} \\ \gamma_{lequ,1}\ C^{-1}_{lequ,1}\ a^1_{lequ,1} \\ \gamma_{W^2H^2}\ C^{-1}_{W^2H^2}\ a^1_{W^2H^2} \end{pmatrix} = -\frac{\widetilde{a}_{\rm SM}^{J=1}}{8\pi^2} \begin{pmatrix} \times & -N_c y_u & y_e \\ -y_u & \times & 0 \\ y_e & 0 & \times \end{pmatrix} \begin{pmatrix} a^1_{WHle} \\ a^1_{eluq,1} \\ a^1_{W^2H^2} \end{pmatrix} + \text{crossing}\ , \tag{6.25}$$

with $a^J_{\rm SM} \equiv y_\psi \widetilde{a}^J_{\rm SM}$. We are not including diagonal entries since they involve different SM amplitudes. The "crossing" term adds the t-channel contribution to the mixing $\mathcal{A}_{WHle} \to \mathcal{A}_{W^2H^2}$. It can be easily obtained by interchanging the W bosons in $\mathcal{A}_{W^2H^2}$. Remarkably, all non-trivial information about the anomalous dimensions is encoded in the partial-wave coefficients a^J. The matrix in the RHS of Eq. (6.25) includes only color factors, different Yukawa couplings and signs from fermion permutations. Substituting the values of a^J from Table 6.1, we finally obtain

$$\begin{pmatrix} \gamma_{WHle} \\ \gamma_{lequ,1} \\ \gamma_{W^2H^2} \end{pmatrix} = \frac{g_2}{16\pi^2} \begin{pmatrix} \times & N_c y_u & -2y_e \\ \frac{3}{2} y_u & \times & 0 \\ -\frac{1}{2} y_e & 0 & \times \end{pmatrix} \begin{pmatrix} C_{WHle} \\ C_{lequ,1} \\ C_{W^2H^2} \end{pmatrix} \ . \tag{6.26}$$

These results coincide with previous calculations of the anomalous dimension matrix, such as [20, 21]. We also obtained the same γ_{WHle} values in Chapter 4.

The property that several 1-loop mixings involve the same SM amplitude is not exclusive to the subset $\mathcal{A}_{WHle}$, $\mathcal{A}_{W^2H^2}$, $\mathcal{A}_{lequ,1}$. This generally occurs for $1/\Lambda^2$ amplitudes with equal n and h, but different number of fermions n_F. As noted in Section 4.6, another example are the $n=4, h=0$ amplitudes $\mathcal{A}_{\Box H^4}$, $\mathcal{A}_{\psi\bar{\psi}H^2}$ and $\mathcal{A}_{\psi^2\bar{\psi}^2}$. In that case, the non-diagonal mixings involve the $J=1$ partial wave of the SM amplitude $\mathcal{A}(1_H, 2_{H^\dagger}, 3_\psi, 4_{\bar{\psi}})$.

As a final remark, we note that not all mixings are suited for the partial-wave approach. In cases where Eq. (6.13) contains an infinite number of J terms, it is more efficient to use the standard formula Eq. (6.1). An example of this is the renormalization of $\mathcal{A}_{WHle}$ by $\mathcal{A}_{W^3}$ that we computed in Section 4.4. In that case, we have a non-minimal amplitude $\widehat{\mathcal{A}}_{W^3}$ that is expanded into an infinite number of a^J coefficients. The RHS of Eq. (6.13) includes an infinite sum over J corresponding to a logarithm. When summing the contributions from all channels, the different logarithms cancel and we are only left with a term proportional to $\mathcal{A}_{WHle}$. This cancellation is more easily observed if we directly use Eq. (6.1).

Self-renormalization of $\mathcal{A}_{B^2H^2}$

As an example of SMEFT renormalization with non-zero IR divergences, we consider the self-renormalization of

$$\mathcal{A}_{B^2H^2}(1_{B_-}, 2_{B_-}, 3_{H^j}, 4_{H_i^\dagger}) = \frac{C_{B^2H^2}}{\Lambda^2} \langle 12 \rangle^2 \delta_i^j \ . \tag{6.27}$$

For concreteness, we focus on the terms proportional to g_2, which only involve the s-channel. From Eq. (6.1), the anomalous dimension gets contributions from a 2-cut involving the subamplitudes

$$\mathcal{A}_{B^2H^2}(1_{B_-}, 2_{B_-}, -3'_{H^k}, -4'_{H_l^\dagger}) \times \mathcal{A}_{\rm SM}(4'_{H^l}, 3'_{H_k^\dagger}, 3_{H^j}, 4_{H_i^\dagger}) \ . \tag{6.28}$$

At one loop, the SM amplitude can only generate $\mathcal{A}_{B^2H^2}$ through the flavor structure $\delta_i^j \delta_k^l$, which corresponds to SU_L isospin $I = 0$. Thus, we only need to consider the $I = 0$ projection of the amplitude,

$$\mathcal{A}_{\rm SM}^{I=0}(4'_H, 3'_{H^\dagger}, 3_H, 4_{H^\dagger}) = \frac{3}{4}\, g_2^2 \left(\frac{1}{2} + \frac{u}{t}\right) \ . \tag{6.29}$$

The relevant partial-wave coefficients for $\mathcal{A}_{B^2H^2}$ and $\mathcal{A}_{\rm SM}^{I=0}$ are listed in Table 6.1. Since $\mathcal{A}_{B^2H^2}$ only has a $J = 0$ component, its renormalization must involve the $J = 0$ partial wave of $\mathcal{A}_{\rm SM}^{I=0}$. Following Eq. (6.4), we rewrite Eq. (6.29) in polar coordinates and find that it is singular for $\theta \to 0$. For this reason, we must consider the regularized partial-wave coefficients defined in Eq. (6.20). The $I = 0$ projection of the soft operator is

$$\boldsymbol{T}_{\rm soft}^{I=0} = -\frac{3}{4}\, g_2^2 \ . \tag{6.30}$$

Substituting Eq. (6.29) and Eq. (6.30) into Eq. (6.20), the regularized coefficients are

$$a_{\rm SM}^{J=0}|_{\rm reg} = -3g_2^2/8 \ , \qquad a_{\rm SM}^{J\geq 1}|_{\rm reg} = 2H_J \boldsymbol{T}_{\rm soft}^{I=0} \ , \tag{6.31}$$

with H_J the J-th harmonic number. The anomalous dimension is given by Eq. (6.14) plus the contributions from collinear IR divergences in Eq. (6.18),

$$\gamma_{B^2H^2} = -\frac{1}{8\pi^2}\, a_{\rm SM}^{J=0}|_{\rm reg}\, C_{B^2H^2} + \gamma_{\rm coll} C_{B^2H^2} \ . \tag{6.32}$$

From [28, 29], the collinear coefficient is $\gamma_{\rm coll} = 2\gamma_{\rm coll}^H = -3g_2^2/16\pi^2$, so we finally obtain

$$\gamma_{B^2H^2} = -\frac{9}{64\pi^2}\, g_2^2\, C_{B^2H^2} \ . \tag{6.33}$$

This result agrees with the self-renormalization of $C_{B^2H^2}$ that was computed in [21].

Up to this point, we have focused on the SMEFT, but the partial-wave decomposition approach is also helpful for other EFTs. To showcase the power of Eq. (6.13), we consider the renormalization of theories with pions and gravitons.

6.2.2 Nonlinear sigma models

A nonlinear sigma model is a scalar field theory where the scalar field maps a Minkowski spacetime into some nonlinear manifold. Within the context of low-energy QCD, these models were first introduced in [117] to describe the dynamics of Goldstone bosons associated with chiral symmetry breaking. The general framework for nonlinear sigma models was developed

in [118, 119] by Callan, Coleman, Wess and Zumino. This formalism provides a systematic way to construct Lagrangians for theories with spontaneous symmetry breaking.

We can also define the nonlinear sigma model from its interactions. In that sense, we define it as an EFT of real scalars transforming under a given symmetry group, whose corresponding scattering amplitudes satisfy Adler's zero condition [120]. This means the amplitudes must vanish in the soft limit, when some external momenta go to zero.

Here we consider the nonlinear sigma model with unbroken group SO(N), which is a theory of scalars in the fundamental representation of SO(N). The coset associated with the spontaneous symmetry breaking is SO(N+1)/SO(N). In general, it was proven in [74, 121] that one can extract information about the coset structure from the double soft limit of the amplitudes. This corresponds to taking two of the external momenta to zero simultaneously.

The nonlinear sigma model includes an infinite number of tree-level amplitudes that can be classified in a power expansion of E/Λ. We focus on 4-point amplitudes with positive powers of momenta, which automatically satisfy Adler's zero condition. Starting at order E^2/Λ^2, these amplitudes are obtained by imposing SO(N) invariance. After that, we can construct higher-point interactions by requiring factorization. 4-point amplitudes can be considered "building blocks" of the theory, in the sense that they satisfy Adler's zero condition on their own. In contrast, higher-point amplitudes require additional contact interactions to satisfy that condition, as was proved in [122–124][4].

We start by constructing the 4-point amplitudes that act as building blocks of the EFT. Considering a theory with N scalars in the fundamental representation of SO(N), a general 4-point amplitude can be written as[5]

$$\mathcal{A}(1^i, 2^j, 3^k, 4^l) = f_s(t,u)\delta_s + f_t(u,s)\delta_t + f_u(s,t)\delta_u \ , \tag{6.34}$$

where $f_{s,t,u}$ denote generic functions of the Mandelstam variables s,t,u and i,j,k,l are flavor indices for the scalars. We define the flavor SO(N) tensors as

$$\delta_s = \delta_{ij}\delta_{kl} \ , \quad \delta_t = \delta_{ik}\delta_{jl} \ , \quad \delta_u = \delta_{il}\delta_{jk} \ . \tag{6.35}$$

By imposing crossing invariance in Eq. (6.34), we find that $f_{s,t,u}$ must satisfy $f_s = f_t = f_u \equiv f$, where $f(t,u)$ is symmetric under $t \leftrightarrow u$. Therefore, the problem of finding all independent amplitudes at order $(E/\Lambda)^w$ corresponds to finding all linearly independent functions $f(t,u)$ that are polynomials of degree $w/2$ in the momenta and are symmetric in t and u. A possible basis for the f functions at order w is the following:

$$f_{wr}(t,u) \equiv P_r\left(\frac{t-u}{s}\right) s^{w/2} \qquad (w = 2,4,...) \ , \tag{6.36}$$

with $P_r(x)$ the Legendre polynomial of degree r. The variable r takes values $r = 0,2,...,w/2$ if $w/2$ is even and $r = 0,2,...,w/2-1$ if it is odd. To justify that Eq. (6.36) forms a basis,

[4] 4-point amplitudes are not the only building blocks of the nonlinear sigma model. At order E^6/Λ^6 and higher, there are $n > 4$-point amplitudes that satisfy Adler's zero condition by themselves [123, 124]. We do not consider those terms in our analysis.

[5] For SO(4) there is an additional term for the flavor structure ϵ_{ijkl}, which we do not include here.

we consider the functions $\widetilde{f}_{wr}(t,u) = t^{r/2}u^{(w-r)/2} + t^{(w-r)/2}u^{r/2}$ for the same range of r. $\widetilde{f}_{wr}$ is clearly a basis since it includes all polynomials of degree $w/2$ in t, u, and is symmetric under those variables. We also see that $\widetilde{f}_{wr}$ includes the same number of functions as f_{wr}. Given that the Legendre polynomials are linearly independent, we conclude that f_{wr} also forms a basis.

Using the f_{wr} functions, we can write a general expression for 4-point amplitudes in the SO(N) nonlinear sigma model:

$$\mathcal{A}_{wr}(1^i, 2^j, 3^k, 4^l) = \frac{C_{wr}}{F_\pi^w}\left[f_{wr}(t,u)\delta_s + f_{wr}(u,s)\delta_t + f_{wr}(s,t)\delta_u\right] \ , \tag{6.37}$$

with C_{wr} the Wilson coefficients. The pion decay constant F_π, which is defined by fixing $C_{20} = 1$, plays the role of the Λ scale. Let us see some examples of amplitudes on this basis. At $\mathcal{O}(E^2)$, we only have

$$\mathcal{A}_{20}(1^i, 2^j, 3^k, 4^l) = \frac{1}{F_\pi^2}\left(s\delta_s + t\delta_t + u\delta_u\right) \ . \tag{6.38}$$

At order $\mathcal{O}(E^4)$, there are two amplitudes:

$$\begin{aligned}
\mathcal{A}_{40}(1^i, 2^j, 3^k, 4^l) &= \frac{C_{40}}{F_\pi^4}\left(s^2\delta_s + t^2\delta_t + u^2\delta_u\right) \ , \\
\mathcal{A}_{42}(1^i, 2^j, 3^k, 4^l) &= \frac{C_{42}}{2F_\pi^4}\left((t-u)^2 - s^2\right)\delta_s + \text{ crossing} \ .
\end{aligned} \tag{6.39}$$

It is convenient to rewrite Eq. (6.37) in the isospin flavor basis, namely

$$\mathcal{A}_{wr} = \sum_{I=0}^{2} \mathcal{A}^I_{wr}\ \Delta_I \ , \tag{6.40}$$

where the flavor structures Δ_I are

$$\Delta_0 \equiv \frac{\delta_s}{N} \ , \qquad \Delta_1 \equiv \frac{1}{2}\left(\delta_t - \delta_u\right) \ , \qquad \Delta_2 \equiv \frac{1}{2}\left(\delta_t + \delta_u - \frac{2}{N}\delta_s\right) \ . \tag{6.41}$$

For $N = 3$, $\mathcal{A}^I_{wr}$ are amplitudes with definite isospin I. For a general N, $\mathcal{A}^I_{wr}$ corresponds to a specific flavor configuration for the initial and final states. In particular, $I = 0, 1, 2$ are the singlet, antisymmetric and traceless symmetric configurations, respectively. The isospin flavor tensors are orthogonal, satisfying

$$\sum_{i'j'}(\Delta_I)_{iji'j'}(\Delta_{I'})_{i'j'kl} = \delta_{II'}(\Delta_I)_{ijkl} \ . \tag{6.42}$$

Once we have expanded the amplitude $\mathcal{A}_{wr}$ in terms of isospin, we can apply Eq. (6.6) for the partial-wave decomposition. We find

$$\mathcal{A}_{wr} = \left(\frac{s}{F_\pi^2}\right)^{w/2} \sum_{IJ} n_J\ P_J(c_\theta)\ a^{IJ}_{wr}\ \Delta_I \ , \tag{6.43}$$

where we have rewritten the Wigner d-functions in terms of Legendre polynomials, using $d^J_{00}(\theta) = P_J(c_\theta)$. The partial-wave coefficients a^{IJ}_{wr} are obtained by inverting this expression, leading to

$$a^{IJ}_{wr} = \frac{1}{2}\left(\frac{s}{F_\pi^2}\right)^{-w/2} \int_0^\pi d\theta \; s_\theta \; P_J(c_\theta) \; \mathcal{A}^I_{wr} \; . \tag{6.44}$$

Substituting $\mathcal{A}^I_{wr}$ from Eq. (6.37) and Eq. (6.40), we obtain

$$a^{IJ}_{wr} = C_{wr}\left(2\kappa^J_{wr} + \frac{N}{n_J}\delta_{0I} \; \delta_{rJ}\right) \; , \tag{6.45}$$

if the product $I \cdot J$ is an even number, and $a^{IJ}_{wr} = 0$ otherwise. The κ^J_{wr} functions are defined as

$$\kappa^J_{wr} \equiv \frac{(-1)^{w/2+J}[(w/2)!]^2}{(w/2-J)!(w/2+J+1)!} \; {}_4F_3\left(-r, 1+r, -1-J-\frac{w}{2}, J-\frac{w}{2}; 1, -\frac{w}{2}, -\frac{w}{2}; 1\right) \; , \tag{6.46}$$

where ${}_4F_3$ is a generalized hypergeometric function[6]. We can check that $a^{IJ}_{wr} = 0$ for $J > w/2$, so there is a finite number of partial waves contributing to the amplitude $\mathcal{A}_{wr}$.

After establishing the basis of 4-point amplitudes, the next step is to consider renormalization. We denote by γ_{wr} the 1-loop anomalous dimensions of $\mathcal{A}_{wr}$. There are no IR divergences in this case, so we can use Eq. (6.1). The computation of γ_{wr} involves a summation over all relevant cuts involving subamplitudes $\mathcal{A}_{w_L r_L}$ and $\mathcal{A}_{w_R r_R}$. For concreteness, the contribution from each individual cut is $\Delta\gamma_{wr}(w_R, r_R, w_L, r_L)$, so the total anomalous dimension is

$$\gamma_{wr} = \sum_{w_R, r_R, w_L, r_L} \Delta\gamma_{wr}(w_R, r_R, w_L, r_L) \; , \tag{6.47}$$

where the summation is over all $w_{R,L}$ satisfying $w = w_R + w_L$, and all $r_{R,L}$ in the ranges specified under Eq. (6.36). To simplify the notation, from now on we suppress the (w_R, r_R, w_L, r_L) dependence on $\Delta\gamma_{wr}$.

Performing the partial-wave decomposition of the amplitudes as in Eq. (6.13), we find

$$\sum_r \Delta\gamma_{wr}\frac{\mathcal{A}_{wr}}{C_{wr}} = -\left(\frac{s}{F_\pi^2}\right)^{w/2} \sum_{IJ} \frac{n_J \Delta_I}{16\pi^2} a^{IJ}_{w_L r_L} a^{IJ}_{w_R r_R} P_J\left(\frac{t-u}{s}\right) + (s \leftrightarrow t) + (s \leftrightarrow u) \; , \tag{6.48}$$

where the first term corresponds to the s-channel and the other contributions can be obtained by crossing. Since we are considering the isospin basis, the flavor structures Δ_I also change under crossing. The summation over r in the LHS of Eq. (6.48) appears because, in general, a cut involving $\mathcal{A}_{w_L r_L}$ and $\mathcal{A}_{w_R r_R}$ contributes to the anomalous dimensions of all $\mathcal{A}_{wr}$ with $w = w_R + w_L$ and any r.

[6] Alternatively, we can write $\kappa^J_{wr} = \sum_{k=0}^r \frac{(-1)^{w/2+J-k}(r+k)![(w/2-k)!]^2}{[k!]^2(r-k)!(w/2+J+1-k)!(w/2-J-k)!}$.

Now we can solve for $\Delta\gamma_{wr}$. Choosing the particle flavors so that $\delta_s = 1$ and $\delta_t = \delta_u = 0$, and then acting with $\int_0^\pi d\theta s_\theta P_r(c_\theta)$ on both sides of Eq. (6.48), we obtain

$$\Delta\gamma_{wr} = -\frac{C_{w_L r_L} C_{w_R r_R}}{16\pi^2}\left(\frac{N}{n_r}\delta_{r_L r}\delta_{r_R r} + 2\delta_{r_L r}\kappa^r_{w_R r_R} + 2\delta_{r_R r}\,\kappa^r_{w_L r_L} + 4\sum_{J=0}^{\min(\frac{w_L}{2},\frac{w_R}{2})} n_J n_r \kappa^J_{w_L r_L}\kappa^J_{w_R r_R}\kappa^r_{wJ}\right), \tag{6.49}$$

where $n_r = 2r+1$. Notice that the only N-dependent contribution arises from renormalizations with $r_L = r_R = r$. This greatly simplifies the calculation of the anomalous dimension in the large-N limit.

Let us see some examples of the computation of γ_{wr}. For the two $\mathcal{O}(E^4)$ amplitudes in Eq. (6.39), the only possible renormalization involves the $\mathcal{O}(E^2)$ subamplitude in Eq. (6.38). Substituting $w_R = w_L = 2$ and $r_R = r_L = 0$ in Eq. (6.49), the total anomalous dimensions are

$$\gamma_{40} = \frac{\frac{17}{9} - N}{16\pi^2}\,, \qquad \gamma_{42} = -\frac{1}{72\pi^2}\,. \tag{6.50}$$

At the next order, there are two $\mathcal{O}(E^6)$ amplitudes: $\mathcal{A}_{60}$ and $\mathcal{A}_{62}$. Their renormalization involves one subamplitude at $\mathcal{O}(E^4)$ and the other at $\mathcal{O}(E^2)$. We must consider two different cuts: one with $w_L = 2$, $w_R = 4$, $r_L = 0$, $r_R = 0, 2$ and the other one with $w_L = 4$, $w_R = 2$, $r_L = 0, 2$, $r_R = 0$. Summing all the contributions yields

$$\begin{aligned}\gamma_{60} &= C_{40}\,\frac{\frac{11}{36} - N}{8\pi^2} - C_{42}\,\frac{325}{288\pi^2}\,,\\ \gamma_{62} &= -C_{40}\,\frac{5}{288\pi^2} - C_{42}\,\frac{65}{288\pi^2}\,.\end{aligned} \tag{6.51}$$

We can compare these results to previous calculations in chiral perturbation theory. For $N = 3$, the nonlinear sigma model coset satisfies $\mathrm{SO}(4)/\mathrm{SO}(3) \sim \mathrm{SU}(2) \times \mathrm{SU}(2)/\mathrm{SU}(2)$, so we can use the $\pi\pi$ scattering analysis in [125]. Indeed, rewriting their pion amplitudes in our basis Eq. (6.37), the obtained anomalous dimensions agree with our computation.

It is interesting to relate our amplitude analysis of the SO(N) nonlinear sigma model with the Lagrangian description. As discussed in [123, 124], the SO(N+1)-invariant operators of the theory can be expanded in the number of fields, leading to a series of contact interactions. These interactions are equivalent to a set of amplitudes that satisfy Adler's zero condition. Indeed, there is a direct correspondence between our 4-point amplitudes $\mathcal{A}_{wr}$ and some contact operators in the Lagrangian approach. Thus, our renormalization results for the amplitudes are equivalent to the anomalous dimension matrix for the corresponding operators.

6.2.3 Gravity

As a final application, we consider Eq. (6.13) in the context of general EFTs for spin-2 particles (gravitons). On-shell methods are especially convenient for these theories, as they greatly simplify the lengthy calculations from the Lagrangian approach. We start by determining the graviton contact amplitudes, which can be classified in a E/Λ expansion. As explained in Section 1.1.3, there are two possible 3-point amplitudes. At order $\mathcal{O}(E^2)$, we have

$$\mathcal{A}_{\rm GR}(1_{--},2_{--},3_{++}) = \frac{1}{M_P}\left(\frac{\langle 12\rangle^3}{\langle 13\rangle\langle 23\rangle}\right)^2 , \tag{6.52}$$

where the Planck mass M_P plays the role of the Λ scale. This amplitude corresponds to the theory of General Relativity (GR) and can be used to construct higher-point interactions. For example, the tree-level 4-point amplitude in GR is given by

$$\mathcal{A}_{{\rm GR}_{+-}} \equiv \mathcal{A}_{\rm GR}(1_{++},2_{++},3_{--},4_{--}) = \frac{1}{M_P^2}\frac{[12]^4\langle 34\rangle^4}{stu} . \tag{6.53}$$

This amplitude is obtained by requiring the right little group weights and factorization into a product of 3-point subamplitudes $\mathcal{A}_{\rm GR}$. Beyond tree level, a different 4-point GR amplitude can be generated at one loop. As shown in [126], it corresponds to

$$\mathcal{A}_{{\rm GR}_{--}} \equiv \mathcal{A}_{\rm GR}(1_{--},2_{--},3_{--},4_{--}) = \frac{\langle 12\rangle^4\langle 34\rangle^4}{16\pi^2 M_P^4}\frac{r}{s^2} + \text{crossing} = \frac{r\mathcal{T}^2}{16\pi^2 M_P^4}(s^2+t^2+u^2) , \tag{6.54}$$

where $r = (N_F - N_B)/240$ and $N_{F,B}$ counts the number of fermions and bosons inside the loop. We have also defined the kinematic factor $\mathcal{T} \equiv \frac{\langle 12\rangle\langle 34\rangle}{[12][34]}$.

In addition to Eq. (6.52), we can consider higher-order contact amplitudes, which are associated with modified theories of gravity. At order $\mathcal{O}(E^6)$, we have the following 3-point interaction:

$$\mathcal{A}_{R^3}(1_{--},2_{--},3_{--}) = \frac{C_{R^3}}{M_P^5}\langle 12\rangle^2\langle 23\rangle^2\langle 31\rangle^2 , \tag{6.55}$$

with C_{R^3} a massless constant. This term arises from a higher-dimension operator cubic in the Riemann tensor. Moreover, we must consider contact amplitudes for the scattering of $n > 3$ particles. For instance, there are two 4-point amplitudes at order $\mathcal{O}(E^8)$, namely

$$\mathcal{A}_{R^4}(1_{--},2_{--},3_{--},4_{--}) = \frac{C_{R^4}}{M_P^8}\langle 12\rangle^4\langle 34\rangle^4 + \text{crossing} = \frac{C_{R^4}\mathcal{T}^2}{M_P^8}(s^4+t^4+u^4) , \tag{6.56}$$

$$\mathcal{A}'_{R^4}(1_{--},2_{--},3_{++},4_{++}) = \frac{C'_{R^4}}{M_P^8}\langle 12\rangle^4[34]^4 . \tag{6.57}$$

Let us see some examples of the calculation of anomalous dimensions for graviton amplitudes via Eq. (6.13). First, we consider the renormalization of the non-minimal 4-point amplitude

$$\widehat{\mathcal{A}}_{R^3}(1_{--},2_{--},3_{--},4_{--}) = \frac{C_{R^3}}{M_P^6}\mathcal{T}^2 stu , \tag{6.58}$$

	$J=0$	$J=2$	$J=4$	
$\mathcal{A}_{\text{GR}_{+-}}$	0	-6	$-\frac{25}{3}$	
$\mathcal{A}_{\text{GR}_{--}}$	$\frac{5}{3}$	$\frac{1}{15}$	0	$\times \frac{r}{16\pi^2}$
$\widehat{\mathcal{A}}_{R^3}$	$\frac{1}{6}$	$-\frac{1}{30}$	0	$\times C_{R^3}$
$\mathcal{A}_{R^4}$	$\frac{7}{5}$	$\frac{4}{35}$	$\frac{1}{315}$	$\times C_{R^4}$

Table 6.2: Partial-wave coefficients a^J in the s-channel for the different 4-graviton amplitudes defined in the text. For the GR amplitude $\mathcal{A}_{\text{GR}_{+-}}$, we include the regularized coefficients $a^J|_{\text{reg}}$ up to $J=4$.

which includes the contact amplitude $\mathcal{A}_{R^3}$ in Eq. (6.55). One can check that none of the 3-point or 4-point graviton amplitudes can renormalize $\widehat{\mathcal{A}}_{R^3}$ at one loop. As stated in [126], the leading contribution arises at two loops. The formula Eq. (6.13), which was derived for 1-loop mixings, is also valid in this case[7]. The anomalous dimension γ_{R^3} is given by a 2-cut involving the tree-level amplitude $\mathcal{A}_{\text{GR}_{+-}}$ in Eq. (6.53) and the 1-loop amplitude $\mathcal{A}_{\text{GR}_{--}}$ in Eq. (6.54). Since there are IR divergences, we must consider the regularized partial-wave coefficients as explained in Section 6.1.4. Overall, Eq. (6.13) can be written as[8]

$$\gamma_{R^3}\widehat{\mathcal{A}}_{R^3} = -\frac{C_{R^3}}{8\pi^2}\left(\frac{s}{M_P^2}\right)^3 \sum_J n_J\, a^J_{\text{GR}_{--}} a^J_{\text{GR}_{+-}}|_{\text{reg}}\, P_J\left(\frac{t-u}{s}\right) + \text{crossing}\ , \tag{6.59}$$

where $a^J_{\text{GR}_{+-}}|_{\text{reg}}$ are the regularized coefficients in Eq. (6.20). The soft operator is $\boldsymbol{T}_{\text{soft}} = -2s/M_P^2$ and we must replace $\int s_{\theta/2}^{-2} \to 2\int s_\theta^{-2}$ because the internal particles are identical. From Eq. (6.53), this coefficient is given by

$$a^J_{\text{GR}_{+-}}|_{\text{reg}} = -4H_J\ , \tag{6.60}$$

with H_J the J-th harmonic number. The partial-wave coefficients $a^J_{\text{GR}_{--}}$ and $a^J_{\text{GR}_{+-}}|_{\text{reg}}$ for various values of J are listed in Table 6.2. We see that they are only simultaneously non-zero for $J=2$, so the anomalous dimension is

$$\gamma_{R^3}\widehat{\mathcal{A}}_{R^3} = \frac{C_{R^3}}{4\pi^2}\frac{r}{16\pi^2}\frac{s^3}{M_P^6}\, P_2\left(\frac{t-u}{s}\right) + \text{crossing}\ . \tag{6.61}$$

The RHS of this expression must be proportional $\widehat{\mathcal{A}}_{R^3}$ when we sum over the different channels. However, it is more convenient to project both sides of Eq. (6.61) into a specific kinematic configuration such as $t=u=-s/2$. Then, we find that the anomalous dimension is

$$\gamma_{R^3} = \frac{r}{16\pi^4}\left(P_2(0) - \frac{1}{4}P_2(3)\right) = -\frac{60r}{(4\pi)^4}\ . \tag{6.62}$$

[7] One can re-derive Eq. (6.13) for this particular 2-loop mixing. The starting point is Eq. (3.33) for the 2-loop renormalization of form factors, which reduces to Eq. (6.1) in the limit $Q \to 0$.

[8] Note that there are two identical contributions corresponding to different helicity choices for the internal gravitons. This is compensated by the 1/2 symmetrical factor for cutting identical particles.

This result agrees with the previous calculation in [126]. The use of partial waves allows us to understand the momentum dependence in Eq. (6.61), which is determined by the fact that only $J = 2$ states contribute to γ_{R^3}.

We can proceed in a similar manner to compute the anomalous dimension of C_{R^4}. In that case, we must consider the 2-cut involving the tree-level amplitudes $\widehat{\mathcal{A}}_{R^3}$ and $\mathcal{A}_{\text{GR}--}$. Again, the renormalization only involves the $J = 2$ partial waves, so we can write

$$\gamma_{R^4}\mathcal{A}_{R^4} = -C_{R^4}\frac{5}{8\pi^2}\left(\frac{s}{M_P^2}\right)^4 a^{J=2}_{\widehat{R}^3}\; a^{J=2}_{\text{GR}_{+-}}|_{\text{reg}}\; P_2\left(\frac{t-u}{s}\right) + \text{crossing}\ . \tag{6.63}$$

Using the partial-wave coefficients in Table 6.2, we find

$$\gamma_{R^4} = -\frac{C_{R^3}}{8\pi^2}\ . \tag{6.64}$$

Finally, the anomalous dimension of C'_{R^4} is $\gamma'_{R^4} = 0$ because $\mathcal{A}'_{R^4}$ is not renormalized by other amplitudes at one loop.

6.3 Conclusions of the chapter

In this chapter, we have employed angular momentum analysis to study the renormalization of several EFTs. By performing a partial-wave decomposition of scattering amplitudes, we have shown that the anomalous dimensions can be expressed as a sum of products of partial-wave coefficients (see Eq. (6.13)). This sum is finite for mixings involving contact interactions, making the calculation remarkably simple. Our results are naturally extended to include IR divergences, provided that the partial-wave coefficients are regularized as shown in Eq. (6.20).

The use of partial-wave decomposition provides valuable insights into the structure of the anomalous dimension matrix. Some renormalizations only happen through specific angular momenta J, which leads to selection rules such as those in [81]. Moreover, mixings that appear very different at the level of Feynman diagrams may turn out to be quite similar if they involve the same partial-wave coefficients a^J.

We have presented applications of our formula for different EFTs:

- SMEFT: We have observed that only one SM partial wave is involved in mixings between $1/\Lambda^2$ amplitudes with equal n, h and different n_F. We have seen this explicitly for $\mathcal{A}_{WHle}$, $\mathcal{A}_{lequ,1}$ and $\mathcal{A}_{W^2H^2}$.

- SO(N) nonlinear sigma model: We have obtained a general expression for the anomalous dimensions of 4-point amplitudes at all orders in E/Λ.

- EFT of gravity: We have considered the renormalization of $\mathcal{A}_{R^3}$, $\mathcal{A}_{R^4}$ and $\mathcal{A}'_{R^4}$, which arise in modified theories of gravity. Compared to previous calculations [126], the simplicity of the on-shell approach is unmatched.

Beyond angular momentum, decomposing amplitudes according to other conserved quantum numbers can provide additional insights. We have explored this for the case of isospin, both within the SMEFT and nonlinear sigma models. The isospin decomposition introduces additional selection rules because the subamplitudes $\mathcal{A}_{L,R}$ in Eq. (6.1) must have the same isospin as the renormalized amplitude $\mathcal{A}_{\mathcal{O}_i}$.

A possible extension of this work would be to generalize Eq. (6.13) to include higher-point amplitudes and higher loop orders. There are no fundamental obstacles to do this, given that our derivation relies on angular momentum conservation and the expression of γ_i in terms of unitarity cuts.

In summary, the angular momentum analysis presented here provides an efficient tool to study the 1-loop renormalization of EFTs. Thanks to the partial-wave decomposition of amplitudes, we can reveal underlying symmetries that govern operator mixing. This method simplifies practical calculations and offers a deeper perspective on the universal properties of anomalous dimensions.

Appendix A

Conventions and notation

A.1 Spinor-helicity variables

In this appendix we present our conventions for spinor-helicity variables. We mainly follow [127]. Given a massless particle with momentum p^μ, we define the associated spinors $|p\rangle_\alpha$ and $|p]_{\dot\alpha}$, namely "angle" and "square" spinors. $|p\rangle_\alpha$ is a left-handed two-component spinor, which transforms under the $(\frac{1}{2},0)$ representation of the Lorentz group. $|p]_{\dot\alpha}$ is a right-handed two-component spinor that transforms under $(0,\frac{1}{2})$. The momenta written in terms of these spinors are

$$p_{\alpha\dot\alpha} = |p\rangle_\alpha [p|_{\dot\alpha} \ , \tag{A.1}$$

which is a two-by-two matrix given by

$$p_{\alpha\dot\alpha} = p_\mu \sigma^\mu_{\alpha\dot\alpha} = \begin{pmatrix} p_0+p_3 & p_1-ip_2 \\ p_1+ip_2 & p_0-p_3 \end{pmatrix} \ . \tag{A.2}$$

An object like $p_{\alpha\dot\alpha}$, with dotted and undotted spinor indices $\alpha\dot\alpha$, is known as a bi-spinor. The sigma matrix $\sigma^\mu_{\alpha\dot\alpha} = (\mathbb{I}, \vec\sigma)$ is made from the 2×2 identity matrix $\mathbb{I}$ and the three Pauli matrices $\vec\sigma = (\sigma^1,\sigma^2,\sigma^3)$, with

$$\sigma^1 = \begin{pmatrix} 0 & 1 \\ 1 & 0 \end{pmatrix} \ , \qquad \sigma^2 = \begin{pmatrix} 0 & -i \\ i & 0 \end{pmatrix} \ , \qquad \sigma^3 = \begin{pmatrix} 1 & 0 \\ 0 & -1 \end{pmatrix} \ . \tag{A.3}$$

Similarly, we define $\bar\sigma^{\mu,\dot\alpha\alpha} = (\mathbb{I}, -\vec\sigma)$. The 2×2 sigma matrices are related to the Weyl representation of the 4×4 gamma matrices as follows,

$$\gamma^\mu = \begin{pmatrix} 0 & \sigma^\mu_{\alpha\dot\alpha} \\ \bar\sigma^{\mu,\dot\alpha\alpha} & 0 \end{pmatrix} \ . \tag{A.4}$$

The spinor indices of $|p\rangle$ and $|p]$ can be raised and lowered with the antisymmetric tensor ϵ, whose non-vanishing components are

$$\epsilon^{12} = -\epsilon^{21} = \epsilon_{21} = -\epsilon_{12} = 1 \ . \tag{A.5}$$

Spinors with raised and lowered indices are related by

$$|p\rangle_\alpha = \epsilon_{\alpha\beta}\langle p|^\beta, \quad \langle p|^\alpha = \epsilon^{\alpha\beta}|p\rangle_\beta, \quad [p|_{\dot\alpha} = \epsilon_{\dot\alpha\dot\beta}|p]^{\dot\beta}, \quad |p]^{\dot\alpha} = \epsilon^{\dot\alpha\dot\beta}[p|_{\dot\beta} \ . \tag{A.6}$$

Note that $\langle p|^\alpha$ is a left-handed spinor and transforms under $(\frac{1}{2},0)$, just like $|p\rangle_\alpha$. In an analogous way, $|p]^{\dot\alpha}$ is a right-handed spinor that transforms under $(0,\frac{1}{2})$. We can combine spinor products to make objects that transform like Lorentz scalars, vectors and tensors. This is done through the contraction of spinor indices. We choose to contract descending undotted indices ${}^\alpha{}_\alpha$ and ascending dotted indices ${}_{\dot\alpha}{}^{\dot\alpha}$. For example, the contraction of two spinors is given by

$$\langle pq\rangle \equiv \langle p|^\alpha |q\rangle_\alpha \qquad \text{and} \qquad [pq] \equiv [p|_{\dot\alpha}|q]^{\dot\alpha} \ , \tag{A.7}$$

that we call respectively "angle" and "square" brackets. These are the main building blocks of on-shell scattering amplitudes. We can also contract spinors with the sigma matrices $\sigma^\mu_{\alpha\dot\alpha}$ and $\bar\sigma^{\mu,\dot\alpha\alpha}$,

$$\langle i|\sigma^\mu|j] \equiv \langle i|^\alpha \sigma^\mu_{\alpha\dot\alpha}|j]^{\dot\alpha} \qquad \text{and} \qquad [i|\bar\sigma^\mu|j\rangle \equiv \big[i|_{\dot\alpha}\bar\sigma^{\mu,\dot\alpha\alpha}|j\big\rangle_\alpha \ . \tag{A.8}$$

Let us list a few properties of the spinor-helicity variables:

- Spinor products are totally antisymmetric, $\langle ij\rangle = -\langle ji\rangle$ and $[ij] = -[ji]$. In particular this implies that $[ii] = \langle ii\rangle = 0$.

- Schouten identity: since spinors have two components, one can write any spinor $|i\rangle$ as a linear combination of two linearly independent spinors $|j\rangle$ and $|k\rangle$ [14]. Then we have

$$|i\rangle = A|j\rangle + B|k\rangle \ . \tag{A.9}$$

  The coefficients A and B can be obtained by contracting $|i\rangle$ with both $\langle j|$ and $\langle k|$. We find that $A = \langle ki\rangle / \langle kj\rangle$ and $B = \langle ji\rangle / \langle jk\rangle$. Substituting the values of A and B into Eq. (A.9) and contracting $|i\rangle$ with a generic spinor $\langle l|$, we find

$$\langle ij\rangle\langle kl\rangle + \langle il\rangle\langle jk\rangle + \langle ik\rangle\langle lj\rangle = 0 \ , \tag{A.10}$$

  which is known as the Schouten identity.

- Fierz identities: given the definition of the sigma matrices, one can check the following relations

$$\sigma^\mu_{\alpha\dot\alpha}\bar\sigma^{\dot\beta\beta}_\mu = 2\delta^\beta_\alpha\delta^{\dot\beta}_{\dot\alpha} \ , \qquad \sigma^\mu_{\alpha\dot\alpha}\sigma_{\mu\beta\dot\beta} = 2\epsilon_{\alpha\beta}\epsilon_{\dot\alpha\dot\beta} \ , \qquad \bar\sigma^{\mu\dot\alpha\alpha}\sigma_{\mu\beta\dot\beta} = 2\epsilon^{\alpha\beta}\epsilon^{\dot\alpha\dot\beta} \ . \tag{A.11}$$

  They can be used to derive the so-called Fierz identities, namely

$$\langle i|\sigma^\mu|j]\,\langle k|\sigma^\mu|l] = -2\,\langle ik\rangle\,[jl] \ , \tag{A.12}$$
$$[i|\bar\sigma^\mu|j\rangle\,[k|\bar\sigma^\mu|l\rangle = -2\,[ik]\,\langle jl\rangle \ , \tag{A.13}$$
$$\langle i|\sigma^\mu|j]\,[k|\bar\sigma^\mu|l\rangle = -2\,\langle il\rangle\,[jk] \ . \tag{A.14}$$

  From these identities, we obtain the expression for the Mandelstam variables s_{ij} in terms of spinor products,

$$s_{ij} \equiv (p_i+p_j)^2 = 2p_i\cdot p_j = \langle ij\rangle\,[ji] \ . \tag{A.15}$$

In general there is a one-to-one correspondence between any four-vector V^μ and the associated bi-spinor $V_{\alpha\dot{\alpha}}$,

$$V_{\alpha\dot{\alpha}} = V_\mu \sigma^\mu_{\alpha\dot{\alpha}} \ , \qquad V_\mu = \frac{1}{2}\bar{\sigma}^{\mu,\dot{\alpha}\alpha} V_{\alpha\dot{\alpha}} \ . \tag{A.16}$$

Using these expressions for the momenta bi-spinor $p_{\alpha\dot{\alpha}} = |p\rangle_\alpha [p|_{\dot{\alpha}}$, the four-momentum p^μ can be written as

$$p_i^\mu = \frac{1}{2}\,[i|\bar{\sigma}^\mu|i\rangle \ . \tag{A.17}$$

A.2 Two-component spinor notation

The framework of on-shell amplitudes, which involves particles of well-defined helicity, is not suited for the four-component spinor notation. Instead of four-component Dirac spinors, it is more natural to use two-component Weyl spinors, since they transform as irreducible representations of the Lorentz group. Once we know the expression of an operator in terms of two-component spinors, it is straightforward to compute the associated contact on-shell amplitude. Therefore, we must know how to relate Lagrangian operators written in terms of Dirac and Weyl spinors. A generic Dirac spinor ψ can be written in terms of Weyl spinors as

$$\psi = \begin{pmatrix} \psi_{L,\alpha} \\ \psi_R^{\dot{\alpha}} \end{pmatrix} \ , \tag{A.18}$$

with $\psi_{L,\alpha}$ a left-handed two-component spinor and $\psi_R^{\dot{\alpha}}$ a right-handed one. The adjoint Dirac spinor $\bar{\psi}$ is then

$$\bar{\psi} = \psi^\dagger \gamma^0 = \left(\bar{\psi}_{L,\dot{\alpha}}, \bar{\psi}_R^{\alpha}\right) \begin{pmatrix} 0 & \mathbb{I} \\ \mathbb{I} & 0 \end{pmatrix} = \left(\bar{\psi}_R^{\alpha}, \bar{\psi}_{L,\dot{\alpha}}\right) \ , \tag{A.19}$$

where now $\bar{\psi}_{L,\dot{\alpha}}$ is a right-handed Weyl spinor and $\bar{\psi}_R^{\alpha}$ is a left-handed one. We denote the complex-conjugate of a Weyl spinor as $\bar{\psi}_{L,R} \equiv \psi^\dagger_{L,R}$.

Dirac spinors can be used together with the gamma matrices γ^μ to build objects with a well-defined Lorentz structure. These are the so-called covariant bilinears, which have the following expressions in terms of both Dirac and Weyl spinors

$$\begin{aligned}
\text{Scalar} \quad &: \quad \bar{\psi}\psi = \bar{\psi}_R^{\alpha}\psi_{L,\alpha} + \bar{\psi}_{L,\dot{\alpha}}\psi_R^{\dot{\alpha}} \ , \\
\text{Pseudoscalar} \quad &: \quad \bar{\psi}\gamma^5\psi = -\bar{\psi}_R^{\alpha}\psi_{L,\alpha} + \bar{\psi}_{L,\dot{\alpha}}\psi_R^{\dot{\alpha}} \ , \\
\text{Vector} \quad &: \quad \bar{\psi}\gamma^\mu\psi = \bar{\psi}_R^{\alpha}\sigma^\mu_{\alpha\dot{\alpha}}\psi_R^{\dot{\alpha}} + \bar{\psi}_{L,\dot{\alpha}}\bar{\sigma}^{\mu,\dot{\alpha}\alpha}\psi_{L,\alpha} \ , \\
\text{Axial Vector} \quad &: \quad \bar{\psi}\gamma^\mu\gamma^5\psi = \bar{\psi}_R^{\alpha}\sigma^\mu_{\alpha\dot{\alpha}}\psi_R^{\dot{\alpha}} - \bar{\psi}_{L,\dot{\alpha}}\bar{\sigma}^{\mu,\dot{\alpha}\alpha}\psi_{L,\alpha} \ , \\
\text{Tensor} \quad &: \quad \bar{\psi}\widetilde{\sigma}^{\mu\nu}\psi = \bar{\psi}_R^{\alpha}(\sigma^{\mu\nu})^\beta_\alpha\psi_{L,\beta} + \bar{\psi}_{L,\dot{\alpha}}(\bar{\sigma}^{\mu\nu})^{\dot{\alpha}}_{\dot{\beta}}\psi_R^{\dot{\beta}} \ ,
\end{aligned}$$

where we have written γ^μ in terms of σ^μ as in Eq. (A.4). The pseudoscalar and axial vector terms involve the matrix $\gamma^5 = i\gamma^0\gamma^1\gamma^2\gamma^3$, which has the form

$$\gamma^5 = \begin{pmatrix} -\mathbb{I} & 0 \\ 0 & \mathbb{I} \end{pmatrix} \ , \tag{A.20}$$

since we are using the Weyl representation of the gamma matrices. Finally, the tensor bilinear contains the gamma matrix commutator

$$\widetilde{\sigma}^{\mu\nu} = \frac{i}{2}[\gamma^\mu, \gamma^\nu] = \begin{pmatrix} (\sigma^{\mu\nu})^\beta_\alpha & 0 \\ 0 & (\bar{\sigma}^{\mu\nu})^{\dot{\alpha}}_{\dot{\beta}} \end{pmatrix} , \tag{A.21}$$

where $\sigma^{\mu\nu}$ and $\bar{\sigma}^{\mu\nu}$ are 2×2 matrices given by

$$(\sigma^{\mu\nu})^\beta_\alpha \equiv \frac{i}{2}\left(\sigma^\mu_{\alpha\dot{\gamma}}\bar{\sigma}^{\nu\dot{\gamma}\beta} - \sigma^\nu_{\alpha\dot{\gamma}}\bar{\sigma}^{\mu\dot{\gamma}\beta}\right) , \tag{A.22}$$

$$(\bar{\sigma}^{\mu\nu})^{\dot{\alpha}}_{\dot{\beta}} \equiv \frac{i}{2}\left(\bar{\sigma}^{\mu\dot{\alpha}\gamma}\sigma^\nu_{\gamma\dot{\beta}} - \bar{\sigma}^{\nu\dot{\alpha}\gamma}\sigma^\mu_{\gamma\dot{\beta}}\right) . \tag{A.23}$$

Interaction Lagrangians with fermion fields contain some combination of the covariant bilinears, plus potentially scalar and vector fields. If we are using two-component spinor notation, any vector boson V^μ can be related to a bi-spinor $V_{\alpha\dot{\alpha}}$, as given by Eq. (A.16).

A.3 On-shell amplitudes

We consider amplitudes with all states massless and incoming. Outgoing states are related to incoming states with opposite momentum and helicity, interchanging particle $\leftrightarrow$ antiparticle. The wave functions for fermions are given by

$$u_\mp(p) = P_\mp \begin{pmatrix} |p\rangle_\alpha \\ |p]^{\dot{\alpha}} \end{pmatrix} , \qquad \bar{v}_\mp(p) = \begin{pmatrix} \langle p|^\alpha & [p|_{\dot{\alpha}} \end{pmatrix} P_\mp , \tag{A.24}$$

respectively for incoming fermions and antifermions of helicity $h = \mp 1/2$ and momentum p^μ, with $P_\mp = (1 \pm \gamma_5)/2$. The polarization vectors of gauge bosons can be written in terms of spinor-helicity variables, namely

$$\epsilon^+_\mu = \frac{\langle q|\,\sigma_\mu|p]}{\sqrt{2}\,\langle qp\rangle} , \qquad \epsilon^-_\mu = -\frac{\langle p|\,\sigma_\mu|q]}{\sqrt{2}[qp]} , \tag{A.25}$$

for an incoming gauge boson of momentum p^μ and helicity $h = \pm 1$. We have introduced an arbitrary reference momentum $q \neq p$ [13].

Following the conventions in [5], spinors with negative momenta can be related to spinors with positive momenta as follows

$$|-p\rangle_\alpha = i\,|p\rangle_\alpha , \qquad |-p]^{\dot{\alpha}} = i|p]^{\dot{\alpha}} , \tag{A.26}$$

which of course leads to $|-p\rangle\,[-p| = -p$. This convention fixes the factorization of amplitudes that we explained in Section 1.3.2. For instance, if we have a 4-point amplitude with a pole in the s-channel (see Figure A.1), it factorizes as

$$\lim_{s_{12}\to 0} s_{12}\mathcal{A}(1,2,3,4) = i^{F[\ell]}\; i\mathcal{A}_L(1,2,\ell)\; i\mathcal{A}_R(-\ell,3,4) , \tag{A.27}$$

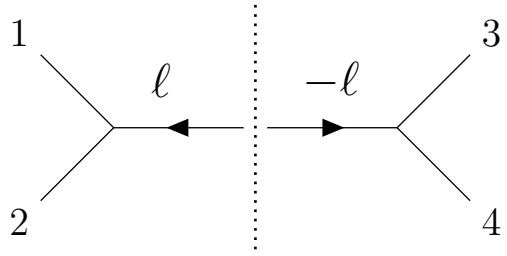

Figure A.1: *Diagram of the factorization of a 4-point amplitude* $\mathcal{A}(1,2,3,4)$ *with a pole in the s-channel into two 3-point subamplitudes.*

where $\ell = p_3 + p_4$ and $F[i_1...i_n]$ counts the number of fermions or antifermions in the list $\{i_1, ..., i_n\}$. Similarly, we can write down the factorization of the amplitude in other channels. If there is a pole in the t-channel, we have

$$\lim_{s_{13}\to 0} s_{13}\mathcal{A}(1,2,3,4) = i^{F[\ell]}(-1)^{n_{23}}\, i\mathcal{A}_L(1,3,\ell)\; i\mathcal{A}_R(-\ell,2,4)\ . \tag{A.28}$$

where $n_{23} = 1$ if both particles 2 and 3 are fermions or antifermions, and $n_{23} = 0$ otherwise. The factor $(-1)^{n_{23}}$ adds a negative sign for fermion exchanges, since we have reordered the particles in the RHS of the expression. We can proceed in the same manner for the factorization in the u-channel.

Let us now focus on the factor $i^{F[\ell]}$ in Eq. (A.27). When we consider the factorization of an amplitude with an internal fermion, one of the subamplitudes includes a factor $u_{\mp}(\ell)$ whereas the other one includes $\bar{v}_{\pm}(-\ell)$. Summing over the possible helicities of the internal fermion leads to

$$u_+(\ell)\bar{v}_-(-\ell) + u_-(\ell)\bar{v}_+(-\ell) = i\sum_h u_h(\ell)\bar{u}_h(\ell) = i\not{\ell}\ , \tag{A.29}$$

where we have used the Dirac slash notation $\not{\ell} = \ell^\mu\gamma_\mu$, with γ_μ the gamma matrices. Factorization gives rise to an extra i compared to the original amplitude, where there is only a factor $\not{\ell}$ from the fermion propagator. This is compensated with the additional i in $i^{F[\ell]}$ when ℓ is a fermion[1]. For the factorization of amplitudes with an internal vector boson, we obtain the following sum over polarizations

$$\epsilon^+_\mu(\ell)\epsilon^-_\nu(-\ell) + \epsilon^-_\mu(\ell)\epsilon^+_\nu(-\ell) = \sum_h \epsilon^h_\mu(\ell)(\epsilon^h_\nu(\ell))^*\ . \tag{A.30}$$

This is precisely the sum over vector polarizations in the propagator of the full amplitude, so there is no need for an additional i factor.

Notice that in Eq. (A.27) the sign of the internal momenta is fixed as shown in Figure A.1. If the momenta has the opposite sign, the factor $i^{F[\ell]}$ must be replaced by $(-i)^{F[\ell]}$, so the amplitude factorization is given by

$$\lim_{s_{12}\to 0} s_{12}\mathcal{A}(1,2,3,4) = (-i)^{F[\ell]}\; i\mathcal{A}_L(1,2,-\ell)\; i\mathcal{A}_R(\ell,3,4)\ . \tag{A.31}$$

[1]In principle we have $i^2 = -1$, but there is an extra minus sign coming from our choice of fermion ordering in Eq. (A.27).

This can be easily understood with an explicit example. Let us consider the 4-point amplitude $\mathcal{A}(1_e, 2_{H^\dagger}, 3_{\bar{e}}, 4_H)$ in a Yukawa theory $\mathcal{L}_y = -y_e H^\dagger e l + \text{h.c.}$, where e and l are Weyl spinors of helicity $h = -1/2$¡. Using Eq. (A.27) and the method of amplitude factorization in Section 1.3.2, the full amplitude can be written as a product of two 3-point subamplitudes,

$$\mathcal{A}(1_e, 2_{H^\dagger}, 3_{\bar{e}}, 4_H) = \frac{i}{s_{12}}\, i\mathcal{A}_L(1_e, 2_{H^\dagger}, \ell)\; i\mathcal{A}_R(-\ell, 3_{\bar{e}}, 4_H)\;, \tag{A.32}$$

where $\ell = p_3 + p_4$. Writing the subamplitudes in terms of spinor-helicity variables, we obtain

$$\mathcal{A}(1_e, 2_{H^\dagger}, 3_{\bar{e}}, 4_H) = -\frac{i y_e^2\, \langle 1\ell\rangle\, [-\ell 3]}{s_{12}} = -\frac{i^2 y_e^2\, \langle 1\ell\rangle\, [\ell 3]}{s_{12}} = y_e^2 \frac{\langle 14\rangle}{\langle 34\rangle}\;. \tag{A.33}$$

On the contrary, if we define the internal momentum with an opposite sign, $\ell = -(p_3 + p_4)$, we must use the factor $(-i)^{F[\ell]}$ to obtain the same result,

$$\begin{aligned}\mathcal{A}(1_e, 2_{H^\dagger}, 3_{\bar{e}}, 4_H) &= \frac{(-i)}{s_{12}}\, i\mathcal{A}_L(1_e, 2_{H^\dagger}, -\ell)\; i\mathcal{A}_R(\ell, 3_{\bar{e}}, 4_H) \\ &= \frac{i y_e^2\, \langle 1{-}\ell\rangle\, [\ell 3]}{s_{12}} = \frac{i^2 y_e^2\, \langle 1\ell\rangle\, [\ell 3]}{s_{12}} = y_e^2 \frac{\langle 14\rangle}{\langle 34\rangle}\;.\end{aligned} \tag{A.34}$$

Finally, our convention Eq. (A.26) for negative momentum spinors also fixes the expression for unitary cuts of loop amplitudes (see Section 3.2.2). Similarly to Eq. (A.27), we must add a factor i for each internal fermion line that goes on shell. For example, the 2-cut of the loop amplitude in Figure A.2 is given by

$$\mathcal{A}(1, 2, ..., i, i{+}1, ..., n) \to \int d\text{LIPS}\; i^{F[\ell_1,\ell_2]} \mathcal{A}_L(1, 2, ..., i, \ell_1, \ell_2)\; \mathcal{A}_R(-\ell_2, -\ell_1, i{+}1, ..., n)\;, \tag{A.35}$$

where the states in the RHS of the equation are ordered following the red dotted line in Figure A.2. This expression can be easily generalized for $n > 2$ unitary cuts.

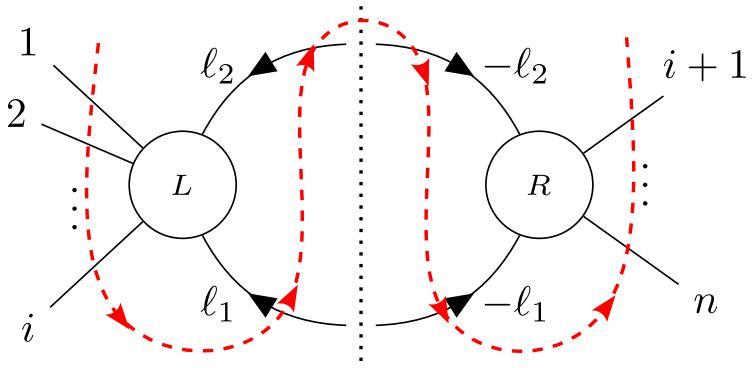

Figure A.2: *Diagram of the 2-cut of a loop amplitude* $\mathcal{A}(1, 2, ..., i, i+1, ..., n)$. *The red dotted line indicates our choice of fermion ordering in Eq. (A.35).*

Appendix B

SMEFT dimension-six operators

The SMEFT includes 59 independent dimension-six operators made from the SM fields and consistent with the SM gauge symmetries. These operators are associated with contact on-shell amplitudes of order $1/\Lambda^2$, belonging to the classes that we listed in Section 2.2.1. To compare our results for the anomalous dimension matrix with the previous literature, we must know the correspondence between dimension-six operators and $1/\Lambda^2$ on-shell amplitudes.

Here we consider the Warsaw basis [65], which is one of the most commonly used SMEFT bases. We will write down the different operators $\mathcal{O}_i$ in terms of Dirac spinors, classified according to their particle content. Then we will compute the contact on-shell amplitudes originated by each operator. In some cases there will be two possible amplitudes for an operator, corresponding to different helicity choices.

For a slightly different $1/\Lambda^2$ SMEFT amplitude basis, see [56].

B.1 Vector boson operators: V^3

$\mathcal{O}_G : f^{abc} G_\nu^{\mu,a} G_\rho^{\nu,b} G_\mu^{\rho,c}$	$\mathcal{A}(1_{G_-^a}, 2_{G_-^b}, 3_{G_-^c}) = i(3!/\sqrt{2})\,\langle 12\rangle\,\langle 23\rangle\,\langle 31\rangle\, f^{abc}$ $\mathcal{A}(1_{G_+^a}, 2_{G_+^b}, 3_{G_+^c}) = -i(3!/\sqrt{2})\,[12]\,[23]\,[31]\, f^{abc}$
$\mathcal{O}_{\widetilde{G}} : f^{abc} \widetilde{G}_\nu^{\mu,a} \widetilde{G}_\rho^{nu,b} \widetilde{G}_\mu^{\rho,c}$	$\mathcal{A}(1_{G_-^a}, 2_{G_-^b}, 3_{G_-^c}) = -(3!/\sqrt{2})\,\langle 12\rangle\,\langle 23\rangle\,\langle 31\rangle\, f^{abc}$ $\mathcal{A}(1_{G_+^a}, 2_{G_+^b}, 3_{G_+^c}) = -(3!/\sqrt{2})\,[12]\,[23]\,[31]\, f^{abc}$
$\mathcal{O}_W : \epsilon^{abc} W_\nu^{a,\mu} W_\rho^{b,\nu} W_\mu^{c,\rho}$	$\mathcal{A}(1_{W_-^a}, 2_{W_-^b}, 3_{W_-^c}) = i(3!/\sqrt{2})\,\langle 12\rangle\,\langle 23\rangle\,\langle 31\rangle\,\epsilon^{abc}$ $\mathcal{A}(1_{W_+^a}, 2_{W_+^b}, 3_{W_+^c}) = -i(3!/\sqrt{2})\,[12]\,[23]\,[31]\,\epsilon^{abc}$
$\mathcal{O}_{\widetilde{W}} : \epsilon^{abc} \widetilde{W}_\nu^{a,\mu} \widetilde{W}_\rho^{b,\nu} \widetilde{W}_\mu^{c,\rho}$	$\mathcal{A}(1_{W_-^a}, 2_{W_-^b}, 3_{W_-^c}) = -(3!/\sqrt{2})\,\langle 12\rangle\,\langle 23\rangle\,\langle 31\rangle\,\epsilon^{abc}$ $\mathcal{A}(1_{W_+^a}, 2_{W_+^b}, 3_{W_+^c}) = -(3!/\sqrt{2})\,[12]\,[23]\,[31]\,\epsilon^{abc}$

Where the dual field-strength tensor is defined as $\widetilde{G}_{\mu\nu} = \epsilon^{\mu\nu\tau\delta} G_{\tau\delta}$, with $\epsilon^{\mu\nu\tau\delta}$ the totally antisymmetric Levi-Civita tensor. The $\mathrm{SU}(3)_c$ and $\mathrm{SU}(2)_L$ structure constants are, respectively, f^{abc} and ϵ^{abc}.

B.2 Scalar operators: H^6 and H^4

$\mathcal{O}_H : \lvert H\rvert^6$	$\mathcal{A}(1_{H^i}, 2_{H^j}, 3_{H^k}, 4_{H_l^\dagger}, 5_{H_m^\dagger}, 6_{H_n^\dagger}) = \mathcal{T}^{ijk}_{lmn}$
$\mathcal{O}_{\Box H} : \lvert H\rvert^2 \Box \lvert H\rvert^2$	$\mathcal{A}(1_{H^i}, 2_{H^j}, 3_{H_k^\dagger}, 4_{H_l^\dagger}) = -2\delta^i_k\delta^j_l s_{13} - 2\delta^i_l\delta^j_k s_{14}$
$\mathcal{O}_{DH} : (H^\dagger D^\mu H)^*(H^\dagger D_\mu H)$	$\mathcal{A}(1_{H^i}, 2_{H^j}, 3_{H_k^\dagger}, 4_{H_l^\dagger}) = \delta^i_k\delta^j_l s_{14} + \delta^i_l\delta^j_k s_{13}$

Where we have defined the fully symmetric tensor $\mathcal{T}^{ijk}_{lmn} = \delta^i_l\delta^j_m\delta^k_n + \delta^i_l\delta^j_m\delta^k_n + \delta^i_l\delta^j_m\delta^k_n + i \leftrightarrow j$.

B.3 Scalar - vector boson operators: H^2V^2

$\mathcal{O}_{HG} : \lvert H\rvert^2\ G^a_{\mu\nu}G^{a,\mu\nu}$	$\mathcal{A}(1_{G^a_-}, 2_{G^b_-}, 3_{H^i}, 4_{H_j^\dagger}) = -2\langle 12\rangle^2\delta^{ab}\delta^i_j$ $\mathcal{A}(1_{G^a_+}, 2_{G^b_+}, 3_{H^i}, 4_{H_j^\dagger}) = -2[12]^2\delta^{ab}\delta^i_j$
$\mathcal{O}_{H\widetilde{G}} : \lvert H\rvert^2\ \widetilde{G}^a_{\mu\nu}G^{a,\mu\nu}$	$\mathcal{A}(1_{G^a_-}, 2_{G^b_-}, 3_{H^i}, 4_{H_j^\dagger}) = -2i\langle 12\rangle^2\delta^{ab}\delta^i_j$ $\mathcal{A}(1_{G^a_+}, 2_{G^b_+}, 3_{H^i}, 4_{H_j^\dagger}) = 2i[12]^2\delta^{ab}\delta^i_j$
$\mathcal{O}_{HW} : \lvert H\rvert^2\ W^a_{\mu\nu}W^{a,\mu\nu}$	$\mathcal{A}(1_{W^a_-}, 2_{W^b_-}, 3_{H^i}, 4_{H_j^\dagger}) = -2\langle 12\rangle^2\delta^{ab}\delta^i_j$ $\mathcal{A}(1_{W^a_+}, 2_{W^b_+}, 3_{H^i}, 4_{H_j^\dagger}) = -2[12]^2\delta^{ab}\delta^i_j$
$\mathcal{O}_{H\widetilde{W}} : \lvert H\rvert^2\ \widetilde{W}^a_{\mu\nu}W^{a,\mu\nu}$	$\mathcal{A}(1_{W^a_-}, 2_{W^b_-}, 3_{H^i}, 4_{H_j^\dagger}) = -2i\langle 12\rangle^2\delta^{ab}\delta^i_j$ $\mathcal{A}(1_{W^a_+}, 2_{W^b_+}, 3_{H^i}, 4_{H_j^\dagger}) = 2i[12]^2\delta^{ab}\delta^i_j$
$\mathcal{O}_{HB} : \lvert H\rvert^2\ B_{\mu\nu}B^{\mu\nu}$	$\mathcal{A}(1_{B_-}, 2_{B_-}, 3_{H^i}, 4_{H_j^\dagger}) = -2\langle 12\rangle^2\delta^i_j$ $\mathcal{A}(1_{B_+}, 2_{B_+}, 3_{H^i}, 4_{H_j^\dagger}) = -2[12]^2\delta^i_j$
$\mathcal{O}_{H\widetilde{B}} : \lvert H\rvert^2\ \widetilde{B}_{\mu\nu}B^{\mu\nu}$	$\mathcal{A}(1_{B_-}, 2_{B_-}, 3_{H^i}, 4_{H_j^\dagger}) = -2i\langle 12\rangle^2\delta^i_j$ $\mathcal{A}(1_{B_+}, 2_{B_+}, 3_{H^i}, 4_{H_j^\dagger}) = 2i[12]^2\delta^i_j$
$\mathcal{O}_{HWB} : (H^\dagger\sigma^a H)\ W^a_{\mu\nu}B^{\mu\nu}$	$\mathcal{A}(1_{W^a_-}, 2_{B_-}, 3_{H^i}, 4_{H_j^\dagger}) = -\langle 12\rangle^2(\sigma^a)^i_j$ $\mathcal{A}(1_{W^a_+}, 2_{B_+}, 3_{H^i}, 4_{H_j^\dagger}) = -[12]^2(\sigma^a)^i_j$
$\mathcal{O}_{H\widetilde{W}B} : (H^\dagger\sigma^a H)\ \widetilde{W}^a_{\mu\nu}B^{\mu\nu}$	$\mathcal{A}(1_{W^a_-}, 2_{B_-}, 3_{H^i}, 4_{H_j^\dagger}) = -i\langle 12\rangle^2(\sigma^a)^i_j$ $\mathcal{A}(1_{W^a_+}, 2_{B_+}, 3_{H^i}, 4_{H_j^\dagger}) = i[12]^2(\sigma^a)^i_j$

B.4 Dipole operators: $V\psi^2 H$

$\mathcal{O}_{eW} : (\bar{L}_L\sigma^{\mu\nu}e_R)\sigma^a H W^a_{\mu\nu} + \text{h.c.}$	$\mathcal{A}(1_e, 2_{l^i}, 3_{W^a_-}, 4_{H^\dagger_j}) = 2\sqrt{2}\,\langle 31\rangle\,\langle 32\rangle\,(\sigma^a)^i_j$ $\mathcal{A}(1_{\bar{e}}, 2_{\bar{l}_i}, 3_{W^a_+}, 4_{H^j}) = 2\sqrt{2}\,[31]\,[32]\,(\sigma^a)^j_i$
$\mathcal{O}_{eB} : (\bar{L}_L\sigma^{\mu\nu}e_R)H B_{\mu\nu} + \text{h.c.}$	$\mathcal{A}(1_e, 2_{l^i}, 3_{B_-}, 4_{H^\dagger_j}) = 2\sqrt{2}\ \langle 31\rangle\,\langle 32\rangle\,\delta^i_j$ $\mathcal{A}(1_{\bar{e}}, 2_{\bar{l}_i}, 3_{B_+}, 4_{H^j}) = 2\sqrt{2}\,[31]\,[32]\,\delta^j_i$
$\mathcal{O}_{uG} : (\bar{Q}_L\sigma^{\mu\nu}\lambda^a u_R)\widetilde{H} G^a_{\mu\nu} + \text{h.c.}$	$\mathcal{A}(1_{u_A}, 2_{q^i_B}, 3_{G^a_-}, 4_{H^j}) = 2\sqrt{2}\,\langle 31\rangle\,\langle 32\rangle\,\epsilon^{ji}\lambda^a_{BA}$ $\mathcal{A}(1_{\bar{u}_A}, 2_{\bar{q}_{i,B}}, 3_{G^a_+}, 4_{H^\dagger_j}) = 2\sqrt{2}\,[31]\,[32]\,\epsilon_{ji}\lambda^a_{BA}$
$\mathcal{O}_{uW} : (\bar{Q}_L\sigma^{\mu\nu}u_R)\sigma^a\widetilde{H} W^a_{\mu\nu} + \text{h.c.}$	$\mathcal{A}(1_{u_A}, 2_{q^i_B}, 3_{W^a_-}, 4_{H^j}) = 2\sqrt{2}\,\langle 31\rangle\,\langle 32\rangle\,\epsilon^{jk}(\sigma^a)^i_k\delta_{AB}$ $\mathcal{A}(1_{\bar{u}_A}, 2_{\bar{q}_{i,B}}, 3_{W^a_+}, 4_{H^\dagger_j}) = 2\sqrt{2}\,[31]\,[32]\,\epsilon_{jk}(\sigma^a)^k_i\delta_{AB}$
$\mathcal{O}_{uB} : (\bar{Q}_L\sigma^{\mu\nu}u_R)\widetilde{H} B_{\mu\nu} + \text{h.c.}$	$\mathcal{A}(1_{u_A}, 2_{q^i_B}, 3_{B_-}, 4_{H^j}) = 2\sqrt{2}\,\langle 31\rangle\,\langle 32\rangle\,\epsilon^{ji}\delta_{AB}$ $\mathcal{A}(1_{\bar{u}_A}, 2_{\bar{q}_{i,B}}, 3_{B_+}, 4_{H^\dagger_j}) = 2\sqrt{2}\,[31]\,[32]\,\epsilon_{ji}\delta_{AB}$
$\mathcal{O}_{dG} : (\bar{Q}_L\sigma^{\mu\nu}\lambda^a d_R)H G^a_{\mu\nu} + \text{h.c.}$	$\mathcal{A}(1_{d_A}, 2_{q^i_B}, 3_{G^a_-}, 4_{H^\dagger_j}) = 2\sqrt{2}\,\langle 31\rangle\,\langle 32\rangle\,\delta^j_i\lambda^a_{BA}$ $\mathcal{A}(1_{\bar{d}_A}, 2_{\bar{q}_{i,B}}, 3_{G^a_+}, 4_{H^j}) = 2\sqrt{2}\,[31]\,[32]\,\delta^j_i\lambda^a_{BA}$
$\mathcal{O}_{dW} : (\bar{Q}_L\sigma^{\mu\nu}d_R)\sigma^a H W^a_{\mu\nu} + \text{h.c.}$	$\mathcal{A}(1_{d_A}, 2_{q^i_B}, 3_{W^a_-}, 4_{H^\dagger_j}) = 2\sqrt{2}\,\langle 31\rangle\,\langle 32\rangle\,(\sigma^a)^i_j\delta_{AB}$ $\mathcal{A}(1_{\bar{d}_A}, 2_{\bar{q}_{i,B}}, 3_{W^a_+}, 4_{H^j}) = 2\sqrt{2}\,[31]\,[32]\,(\sigma^a)^j_i\delta_{AB}$
$\mathcal{O}_{dB} : (\bar{Q}_L\sigma^{\mu\nu}d_R)H B_{\mu\nu} + \text{h.c.}$	$\mathcal{A}(1_{d_A}, 2_{q^i_B}, 3_{B_-}, 4_{H^\dagger_j}) = 2\sqrt{2}\,\langle 31\rangle\,\langle 32\rangle\,\delta^i_j\delta_{AB}$ $\mathcal{A}(1_{\bar{d}_A}, 2_{\bar{q}_{i,B}}, 3_{B_+}, 4_{H^j}) = 2\sqrt{2}\,[31]\,[32]\,\delta^j_i\delta_{AB}$

B.5 Scalar - fermion operators

B.5.1 $H^3\psi^2$

$\mathcal{O}_{eH} : H^\dagger\bar{e}_R L_L\lvert H\rvert^2 + \text{h.c.}$	$\mathcal{A}(1_e, 2_{l^i}, 3_{H^\dagger_j}, 4_{H^k}, 5_{H^\dagger_l}) = -\langle 12\rangle\,\mathcal{T}^{ik}_{jl}$ $\mathcal{A}(1_{\bar{e}}, 2_{\bar{l}_i}, 3_{H^j}, 4_{H^\dagger_k}, 5_{H^l}) = -[12]\,\mathcal{T}^{jl}_{ik}$
$\mathcal{O}_{uH} : \widetilde{H}^\dagger\bar{u}_R Q_L\lvert H\rvert^2 + \text{h.c.}$	$\mathcal{A}(1_{u_A}, 2_{q^i_B}, 3_{H^j}, 4_{H^k}, 5_{H^\dagger_l}) = -\langle 12\rangle\,\epsilon^{in}\mathcal{T}^{jk}_{nl}\delta_{AB}$ $\mathcal{A}(1_{\bar{u}_A}, 2_{\bar{q}_{i,B}}, 3_{H^\dagger_j}, 4_{H^\dagger_k}, 5_{H^l}) = -[12]\,\epsilon_{in}\mathcal{T}^{nl}_{jk}\delta_{AB}$
$\mathcal{O}_{dH} : H^\dagger\bar{d}_R Q_L\lvert H\rvert^2 + \text{h.c.}$	$\mathcal{A}(1_{d_A}, 2_{q^i_B}, 3_{H^\dagger_j}, 4_{H^k}, 5_{H^\dagger_l}) = -\langle 12\rangle\,\mathcal{T}^{ik}_{jl}\delta_{AB}$ $\mathcal{A}(1_{\bar{d}_A}, 2_{\bar{q}_{i,B}}, 3_{H^j}, 4_{H^\dagger_k}, 5_{H^l}) = -[12]\,\mathcal{T}^{jl}_{ik}\delta_{AB}$

With $\mathcal{T}^{ik}_{jl} = \delta^i_j\delta^k_l + \delta^i_l\delta^k_j$.

B.5.2 $H^2\psi^2$

$\mathcal{O}_{HL1} : (H^\dagger i\overleftrightarrow{D}_\mu H)(\bar{L}_L\gamma^\mu L_L) + \text{h.c.}$	$\mathcal{A}(1_{l^i}, 2_{\bar{l}_j}, 3_{H^k}, 4_{H_l^\dagger}) = 2\langle 13\rangle [32]\, \delta^i_j\delta^k_l$
$\mathcal{O}_{HL3} : (H^\dagger i\overleftrightarrow{D}^a_\mu H)(\bar{L}_L\sigma^a\gamma^\mu L_L) + \text{h.c.}$	$\mathcal{A}(1_{l^i}, 2_{\bar{l}_j}, 3_{H^k}, 4_{H_l^\dagger}) = 2\langle 13\rangle [32]\, (\sigma^a)^i_j(\sigma^a)^k_l$
$\mathcal{O}_{He} : (H^\dagger i\overleftrightarrow{D}_\mu H)(\bar{e}_R\gamma^\mu e_R) + \text{h.c.}$	$\mathcal{A}(1_e, 2_{\bar{e}}, 3_{H^i}, 4_{H_j^\dagger}) = 2\langle 13\rangle [32]\, \delta^i_j$
$\mathcal{O}_{HQ1} : (H^\dagger i\overleftrightarrow{D}_\mu H)(\bar{Q}_L\gamma^\mu Q_L) + \text{h.c.}$	$\mathcal{A}(1_{q^i_A}, 2_{\bar{q}_{j,B}}, 3_{H^k}, 4_{H_l^\dagger}) = 2\langle 13\rangle [32]\, \delta^i_j\delta^k_l\delta_{AB}$
$\mathcal{O}_{HQ3} : (H^\dagger i\overleftrightarrow{D}^a_\mu H)(\bar{Q}_L\sigma^a\gamma^\mu Q_L) + \text{h.c.}$	$\mathcal{A}(1_{q^i_A}, 2_{\bar{q}_{j,B}}, 3_{H^k}, 4_{H_l^\dagger}) = 2\langle 13\rangle [32]\, (\sigma^a)^i_j(\sigma^a)^k_l\delta_{AB}$
$\mathcal{O}_{Hu} : (H^\dagger i\overleftrightarrow{D}_\mu H)(\bar{u}_R\gamma^\mu u_R) + \text{h.c.}$	$\mathcal{A}(1_{u_A}, 2_{\bar{u}_B}, 3_{H^i}, 4_{H_j^\dagger}) = 2\langle 13\rangle [32]\, \delta^i_j\delta_{AB}$
$\mathcal{O}_{Hd} : (H^\dagger i\overleftrightarrow{D}_\mu H)(\bar{d}_R\gamma^\mu d_R) + \text{h.c.}$	$\mathcal{A}(1_{d_A}, 2_{\bar{d}_B}, 3_{H^i}, 4_{H_j^\dagger}) = 2\langle 13\rangle [32]\, \delta^i_j\delta_{AB}$
$\mathcal{O}_{Hud} : (\widetilde{H}^\dagger iD_\mu H)(\bar{u}_R\gamma^\mu d_R) + \text{h.c.}$	$\mathcal{A}(1_{u_A}, 2_{\bar{d}_B}, 3_{H^i}, 4_{H^j}) = 2\langle 13\rangle [32]\, \epsilon^{ij}\delta_{AB}$ $\mathcal{A}(1_{\bar{u}_A}, 2_{d_B}, 3_{H_i^\dagger}, 4_{H_j^\dagger}) = -2\langle 23\rangle [31]\, \epsilon_{ij}\delta_{AB}$

B.6 Four fermion operators

B.6.1 $\bar{\psi}^2\psi^2 : \quad \bar{R}R\bar{R}R$

$\mathcal{O}_{ee} : (\bar{e}_R\gamma_\mu e_R)(\bar{e}_R\gamma^\mu e_R)$	$\mathcal{A}(1_e, 2_e, 3_{\bar{e}}, 4_{\bar{e}}) = 2\langle 12\rangle [34]$
$\mathcal{O}_{eu} : (\bar{e}_R\gamma_\mu e_R)(\bar{u}_R\gamma^\mu u_R)$	$\mathcal{A}(1_e, 2_{u_A}, 3_{\bar{e}}, 4_{\bar{u}_B}) = 2\langle 12\rangle [34]\, \delta_{AB}$
$\mathcal{O}_{ed} : (\bar{e}_R\gamma_\mu e_R)(\bar{d}_R\gamma^\mu d_R)$	$\mathcal{A}(1_e, 2_{d_A}, 3_{\bar{e}}, 4_{\bar{d}_B}) = 2\langle 12\rangle [34]\, \delta_{AB}$
$\mathcal{O}_{uu} : (\bar{u}_R\gamma_\mu u_R)(\bar{u}_R\gamma^\mu u_R)$	$\mathcal{A}(1_{u_A}, 2_{u_B}, 3_{\bar{u}_C}, 4_{\bar{u}_D}) = 2\langle 12\rangle [34]\, \mathcal{T}_{AC,BD}$
$\mathcal{O}_{dd} : (\bar{d}_R\gamma_\mu d_R)(\bar{d}_R\gamma^\mu d_R)$	$\mathcal{A}(1_{d_A}, 2_{d_B}, 3_{\bar{d}_C}, 4_{\bar{d}_D}) = 2\langle 12\rangle [34]\, \mathcal{T}_{AC,BD}$
$\mathcal{O}^{(1)}_{ud} : (\bar{u}_R\gamma_\mu u_R)(\bar{d}_R\gamma^\mu d_R)$	$\mathcal{A}(1_{u_A}, 2_{d_B}, 3_{\bar{u}_C}, 4_{\bar{d}_D}) = 2\langle 12\rangle [34]\, \mathcal{T}_{AC,BD}$
$\mathcal{O}^{(8)}_{ud} : (\bar{u}_R\gamma_\mu\lambda^a u_R)(\bar{d}_R\gamma^\mu\lambda^a d_R)$	$\mathcal{A}(1_{u_A}, 2_{d_B}, 3_{\bar{u}_C}, 4_{\bar{d}_D}) = 2\langle 12\rangle [34]\, \widetilde{\mathcal{T}}_{AC,BD}$

Defining $\mathcal{T}_{AC,BD} = \delta_{AC}\delta_{BD} + \delta_{AD}\delta_{BC}$ and $\widetilde{\mathcal{T}}_{AC,BD} = \lambda^a_{AC}\lambda^a_{BD} + \lambda^a_{AD}\lambda^a_{BC}$.

B.6.2 $\bar{\psi}^2\psi^2 : \quad \bar{L}L\bar{L}L$

$\mathcal{O}_{ll} : (\bar{L}_L\gamma_\mu L_L)(\bar{L}_L\gamma^\mu L_L)$	$\mathcal{A}(1_{l^i}, 2_{l^j}, 3_{\bar{l}_k}, 4_{\bar{l}_n}) = 2\langle 12\rangle [34]\, \mathcal{T}^{ij}_{kn}$
$\mathcal{O}^{(1)}_{lq} : (\bar{L}_L\gamma_\mu L_L)(\bar{Q}_L\gamma^\mu Q_L)$	$\mathcal{A}(1_{l^i}, 2_{q^j_A}, 3_{\bar{l}_k}, 4_{\bar{q}_{n,B}}) = 2\langle 12\rangle [34]\, \delta^i_k\delta^j_n\delta_{AB}$
$\mathcal{O}^{(3)}_{lq} : (\bar{L}_L\gamma_\mu\sigma^a L_L)(\bar{Q}_L\gamma^\mu\sigma^a Q_L)$	$\mathcal{A}(1_{l^i}, 2_{q^j_A}, 3_{\bar{l}_k}, 4_{\bar{q}_{n,B}}) = 2\langle 12\rangle [34]\, (\sigma^a)^i_k(\sigma^a)^j_n\delta_{AB}$
$\mathcal{O}^{(1)}_{qq} : (\bar{Q}_L\gamma_\mu Q_L)(\bar{Q}_L\gamma^\mu Q_L)$	$\mathcal{A}(1_{q^i_A}, 2_{q^j_B}, 3_{\bar{q}_{k,C}}, 4_{\bar{q}_{n,D}}) = 2\langle 12\rangle [34]\, \mathcal{T}^{ij}_{kn}\mathcal{T}_{AC,BD}$
$\mathcal{O}^{(3)}_{qq} : (\bar{Q}_L\gamma_\mu\sigma^a Q_L)(\bar{Q}_L\gamma^\mu\sigma^a Q_L)$	$\mathcal{A}(1_{q^i_A}, 2_{q^j_B}, 3_{\bar{q}_{k,C}}, 4_{\bar{q}_{n,D}}) = 2\langle 12\rangle [34]\, \widetilde{\mathcal{T}}^{ij}_{kn}\mathcal{T}_{AC,BD}$

With $\widetilde{\mathcal{T}}^{ij}_{kn} = (\sigma^a)^i_k(\sigma^a)^j_n + (\sigma^a)^j_k(\sigma^a)^i_n$.

B.6.3 $\bar{\psi}^2\psi^2:\quad \bar{L}L\bar{R}R$ and $\bar{L}R\bar{R}L$

$\mathcal{O}_{le}:(\bar{L}_L\gamma_\mu L_L)(\bar{e}_R\gamma^\mu e_R)$	$\mathcal{A}(1_{l^i},2_e,3_{\bar{l}_j},4_{\bar{e}})=2\langle 12\rangle[34]\,\delta^i_j$
$\mathcal{O}_{lu}:(\bar{L}_L\gamma_\mu L_L)(\bar{u}_R\gamma^\mu u_R)$	$\mathcal{A}(1_{l^i},2_{u_A},3_{\bar{l}_j},4_{\bar{u}_B})=2\langle 12\rangle[34]\,\delta^i_j\delta_{AB}$
$\mathcal{O}_{ld}:(\bar{L}_L\gamma_\mu L_L)(\bar{d}_R\gamma^\mu d_R)$	$\mathcal{A}(1_{l^i},2_{d_A},3_{\bar{l}_j},4_{\bar{d}_B})=2\langle 12\rangle[34]\,\delta^i_j\delta_{AB}$
$\mathcal{O}_{qe}:(\bar{Q}_L\gamma_\mu Q_L)(\bar{e}_R\gamma^\mu e_R)$	$\mathcal{A}(1_{q^i_A},2_e,3_{\bar{q}_{j,B}},4_{\bar{e}})=2\langle 12\rangle[34]\,\delta^i_j\delta_{AB}$
$\mathcal{O}^{(1)}_{qu}:(\bar{Q}_L\gamma_\mu Q_L)(\bar{u}_R\gamma^\mu u_R)$	$\mathcal{A}(1_{q^i_A},2_{u_B},3_{\bar{q}_{j,C}},4_{\bar{u}_D})=2\langle 12\rangle[34]\,\delta^i_j\mathcal{T}_{AC,BD}$
$\mathcal{O}^{(8)}_{qu}:(\bar{q}_R\gamma_\mu\lambda^a q_R)(\bar{u}_R\gamma^\mu\lambda^a u_R)$	$\mathcal{A}(1_{q^i_A},2_{u_B},3_{\bar{q}_{j,C}},4_{\bar{u}_D})=2\langle 12\rangle[34]\,\delta^i_j\widetilde{\mathcal{T}}_{AC,BD}$
$\mathcal{O}^{(1)}_{qd}:(\bar{Q}_L\gamma_\mu Q_L)(\bar{d}_R\gamma^\mu d_R)$	$\mathcal{A}(1_{q^i_A},2_{d_B},3_{\bar{q}_{j,C}},4_{\bar{d}_D})=2\langle 12\rangle[34]\,\delta^i_j\mathcal{T}_{AC,BD}$
$\mathcal{O}^{(8)}_{qd}:(\bar{q}_R\gamma_\mu\lambda^a q_R)(\bar{d}_R\gamma^\mu\lambda^a d_R)$	$\mathcal{A}(1_{q^i_A},2_{d_B},3_{\bar{q}_{j,C}},4_{\bar{d}_D})=2\langle 12\rangle[34]\,\delta^i_j\widetilde{\mathcal{T}}_{AC,BD}$
$\mathcal{O}_{ledq}:(\bar{L}_L e_R)(\bar{d}_R Q_L)$	$\mathcal{A}(1_{l^i},2_e,3_{\bar{d}_A},4_{\bar{q}_{j,B}})=\langle 12\rangle[34]\,\delta^i_j\delta_{AB}$ $\mathcal{A}(1_{\bar{l}_i},2_{\bar{e}},3_{d_A},4_{q^j_B})=[12]\langle 34\rangle\,\delta^i_j\delta_{AB}$

B.6.4 $\psi^4:\quad \bar{L}R\bar{L}R$

$\mathcal{O}^{(1)}_{lequ}:(\bar{L}_L e_R)(\epsilon\bar{Q}_L u_R)$	$\mathcal{A}(1_{l^i},2_e,3_{q^j_B},4_{d_A})=\langle 12\rangle\langle 34\rangle\,\epsilon^{ij}\delta_{AB}$ $\mathcal{A}(1_{\bar{l}_i},2_{\bar{e}},3_{\bar{q}_{j,B}},4_{\bar{d}_A})=[12][34]\,\epsilon_{ij}\delta_{AB}$
$\mathcal{O}^{(3)}_{lequ}:(\bar{L}_L\sigma_{\mu\nu}e_R)(\epsilon\bar{Q}_L\sigma^{\mu\nu}u_R)$	$\mathcal{A}(1_{l^i},2_e,3_{q^j_B},4_{d_A})=(2\langle 14\rangle\langle 32\rangle-\langle 12\rangle\langle 34\rangle)\,\epsilon^{ij}\delta_{AB}$ $\mathcal{A}(1_{\bar{l}_i},2_{\bar{e}},3_{\bar{q}_{j,B}},4_{\bar{d}_A})=(2[14][32]-[12][34])\,\epsilon_{ij}\delta_{AB}$
$\mathcal{O}^{(1)}_{quqd}:(\bar{Q}_L u_R)(\epsilon\bar{Q}_L d_R)$	$\mathcal{A}(1_{q^i_A},2_{u_B},3_{q^j_C},4_{d_D})=\langle 12\rangle\langle 34\rangle\,\epsilon^{ij}\mathcal{T}_{AC,BD}$ $\mathcal{A}(1_{\bar{q}_{i,A}},2_{\bar{u}_B},3_{\bar{q}_{j,C}},4_{\bar{d}_D})=[12][34]\,\epsilon_{ij}\mathcal{T}_{AC,BD}$
$\mathcal{O}^{(8)}_{quqd}:(\bar{Q}_L\lambda^a u_R)(\epsilon\bar{Q}_L\lambda^a d_R)$	$\mathcal{A}(1_{q^i_A},2_{u_B},3_{q^j_C},4_{d_D})=\langle 12\rangle\langle 34\rangle\,\epsilon^{ij}\widetilde{\mathcal{T}}_{AC,BD}$ $\mathcal{A}(1_{\bar{q}_{i,A}},2_{\bar{u}_B},3_{\bar{q}_{j,C}},4_{\bar{d}_D})=[12][34]\,\epsilon_{ij}\widetilde{\mathcal{T}}_{AC,BD}$

Since the amplitude associated with $\mathcal{O}^{(3)}_{lequ}$ involves two different spinor structures, it is convenient to replace

$$\mathcal{O}^{(3)}_{lequ}=(\bar{L}_L\sigma_{\mu\nu}e_R)(\epsilon\bar{Q}_L\sigma^{\mu\nu}u_R)\quad\rightarrow\quad\mathcal{O}_{luqe}=(\bar{L}_L u_R)(\epsilon\bar{Q}_L e_R)=\frac{1}{2}\left(\mathcal{O}^{(3)}_{lequ}+\mathcal{O}^{(1)}_{lequ}\right)\,,\quad\text{(B.1)}$$

where the product of $\sigma^{\mu\nu}$ matrices is given by

$$(\sigma^{\mu\nu})^\beta_\alpha(\sigma_{\mu\nu})^\tau_\gamma=2\delta^\tau_\alpha\delta^\beta_\gamma-\delta^\beta_\alpha\delta^\tau_\gamma\,.\quad\text{(B.2)}$$

The new operator $\mathcal{O}_{luqe}$ generates the following on-shell amplitudes

$$\mathcal{A}(1_{l^i},2_e,3_{q^j_B},4_{d_A})=\langle 14\rangle\langle 32\rangle\,\epsilon^{ij}\delta_{AB}\,,\qquad\mathcal{A}(1_{\bar{l}_i},2_{\bar{e}},3_{\bar{q}_{j,B}},4_{\bar{d}_A})=[14][32]\,\epsilon_{ij}\delta_{AB}\,.\quad\text{(B.3)}$$

Appendix C

Cancellation of IR divergences and absence of triangle and box contributions in the sum over 2-cuts

In this appendix we prove the validity of Eq. (3.16) at order $1/\Lambda^2$ for mixings with $\Delta n = n_i - n_j = 0$ and 1. We show how the absence of IR divergences implies that triangle and box contributions cancel in the sum over 2-cuts in Eq. (3.16). This result is only valid for renormalizations with $\gamma_{\rm IR} = 0$.

C.1 Case $\Delta n = 0$

Let us consider the 1-loop mixing between two amplitudes $\mathcal{A}_{\mathcal{O}_i}, \mathcal{A}_{\mathcal{O}_j}$ with the same number of legs. It is easy to see that the PV decomposition of the relevant 1-loop amplitudes only contains bubbles and triangles. Box integrals are trivially absent because there are not enough external legs to build them. The triangle integrals correspond to the diagram Figure C.1. From [128], the master integral I_3 in dimensional regularization is given by

$$I_3^{(IJ)} = \frac{\alpha(\epsilon)\mu^{2\epsilon}}{\epsilon^2}(-s_{IJ})^{-1-\epsilon} \ , \tag{C.1}$$

where $I, J, \ldots$ are the external particles and we have defined

$$\alpha(\epsilon) = \frac{\Gamma(1+\epsilon)\Gamma^2(1-\epsilon)}{\Gamma(1-2\epsilon)(4\pi)^{\frac{D}{2}}} = \frac{1}{16\pi^2} + O(\epsilon) \ . \tag{C.2}$$

The triangle amplitude is UV convergent and the $1/\epsilon^2$ pole in Eq. (C.1) corresponds to an IR divergence. Expanding for small ϵ, we find

$$\alpha(\epsilon)^{-1} I_3^{(IJ)} = -\frac{1}{s_{IJ}}\left(\frac{1}{\epsilon^2} - \frac{1}{\epsilon}\ln\left(\frac{-s_{IJ}}{\mu^2}\right)\right) + O(\epsilon^0) \ . \tag{C.3}$$

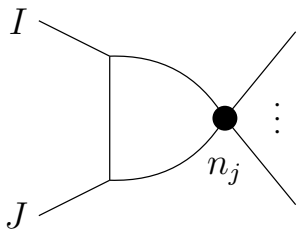

Figure C.1: *Triangle integral for the 1-loop mixing of $\mathcal{A}_{\mathcal{O}_i}$ and $\mathcal{A}_{\mathcal{O}_j}$ with $\Delta n = 0$.*

We know that the IR divergence of the full amplitude is zero by assumption. Bubble integrals are IR convergent, so the sum of triangle IR divergences must vanish. Imposing the cancellation of the $1/\epsilon$ and $1/\epsilon^2$ poles, we obtain the following conditions

$$\sum_{I,J} \frac{C_3^{(IJ)}}{s_{IJ}} = 0 \ , \qquad \sum_{I,J} \frac{C_3^{(IJ)}}{s_{IJ}} \ln(-s_{IJ}) = 0 \ . \tag{C.4}$$

For $n_i = n_j \geq 5$, the second condition can only be satisfied if $C_3^{(IJ)} = 0$ for all I, J. This is because the logarithms are transcendental functions and thus cannot cancel with the C_3 coefficients, which are rational functions of the kinematic variables. We conclude that there are no triangle terms in the PV expansion for this kind of mixing.

Let us see what happens in the cases $n_i = 3, 4$. For $n_i = 3$ all the s_{IJ} are zero, so the triangle integrals are all scaleless and vanish. For $n_i = 4$, some of the s_{IJ} are trivially equal: $s_{12} = s_{34}$, $s_{13} = s_{24}$ and $s_{14} = s_{23}$. The second condition in Eq. (C.4) then allows the solutions $C_3^{(12)} = -C_3^{(34)}$, $C_3^{(13)} = -C_3^{(24)}$ and $C_3^{(14)} = -C_3^{(23)}$. This means we can have nontrivial triangle configurations, but they cancel in pairs,

$$\begin{aligned} C_3^{(12)} I_3^{(12)} + C_3^{(34)} I_3^{(34)} &= 0 \ , \\ C_3^{(13)} I_3^{(13)} + C_3^{(24)} I_3^{(24)} &= 0 \ , \\ C_3^{(14)} I_3^{(14)} + C_3^{(23)} I_3^{(23)} &= 0 \ . \end{aligned} \tag{C.5}$$

In the end the sum of triangle terms in the PV expansion must vanish to cancel the IR divergences. Overall, for any mixing with $n_i = n_J$ we are left with only bubble terms, so no triangle or box coefficients contribute to the 2-cuts in Eq. (3.16).

C.2 Case $\Delta n = 1$

Mixings with $\Delta n = 1$ may include the triangle and box diagrams shown in Figure C.2, where we have only included the topologies associated with IR divergent integrals. (a) corresponds to the triangle integral in Eq. (C.1). Following [128], (b) and (c) are associated with the triangle

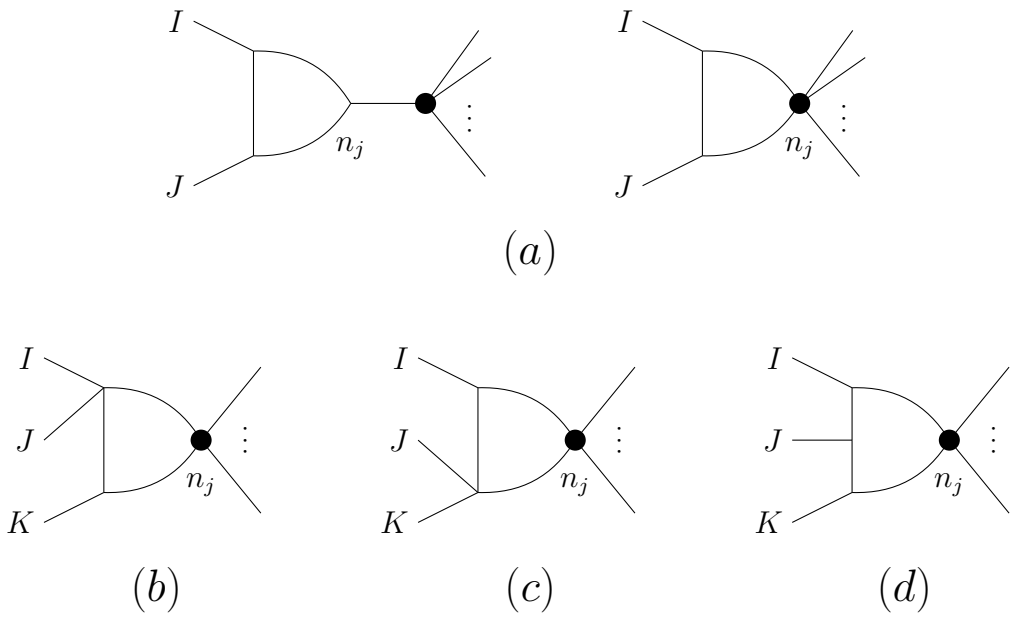

Figure C.2: *IR divergent triangle and box integrals for the 1-loop mixing of $\mathcal{A}_{\mathcal{O}_i}$ and $\mathcal{A}_{\mathcal{O}_j}$ with $\Delta n = 1$.*

integrals

$$
\begin{aligned}
I_3^{(IJ|K)} &= \frac{\alpha(\epsilon)\mu^{2\epsilon}}{\epsilon^2}\frac{(-s_{IJ})^{-\epsilon} - (-s_{IJK})^{-\epsilon}}{(-s_{IJ}) - (-s_{IJK})} \ , \\
I_3^{(I|JK)} &= I_3^{(IJ|K)}(I \leftrightarrow K) \ ,
\end{aligned}
\tag{C.6}
$$

whereas (d) leads to the box integral

$$
I_4^{(IJK)} = \frac{\alpha(\epsilon)\mu^{2\epsilon}}{\epsilon^2}\frac{2}{s_{IJ}s_{JK}}\left[(-s_{IJ})^{-\epsilon} + (-s_{JK})^{-\epsilon} - (-s_{IJK})^{-\epsilon}\right] - \frac{1}{16\pi^2}F_4^{(IJK)} \ , \tag{C.7}
$$

with F_4 given by

$$
F_4^{(IJK)} = \frac{2}{s_{IJ}s_{JK}}\left[\mathrm{Li}_2\left(1 - \frac{s_{IJK}}{s_{IJ}}\right) + \mathrm{Li}_2\left(1 - \frac{s_{IJK}}{s_{JK}}\right) + \frac{1}{2}\ln^2\left(\frac{s_{IJ}}{s_{JK}}\right) + \frac{\pi^2}{6}\right] + O(\epsilon). \tag{C.8}
$$

Expanding these integrals for $\epsilon \to 0$, we can see that they have $1/\epsilon$ and $1/\epsilon^2$ poles, which correspond to IR divergences. Imposing the cancellation of the total IR divergences fixes some relations on the coefficients C_3 and C_4. In this case we do not necessarily have all vanishing coefficients. On the contrary, there can be some nontrivial cancellations between the different triangles and boxes, so the total IR divergence is zero. In particular we have the combination

$$
s_{IJ}s_{JK}I_4^{(IJK)} + s_{IJ}I_3^{(IJ)} + s_{JK}I_3^{(JK)} + (s_{IJ} - s_{IJK})I_3^{(IJ|K)} + (s_{JK} - s_{IJK})I_3^{(I|JK)} \propto s_{IJ}s_{JK}F_4^{(IJK)} \ , \tag{C.9}
$$

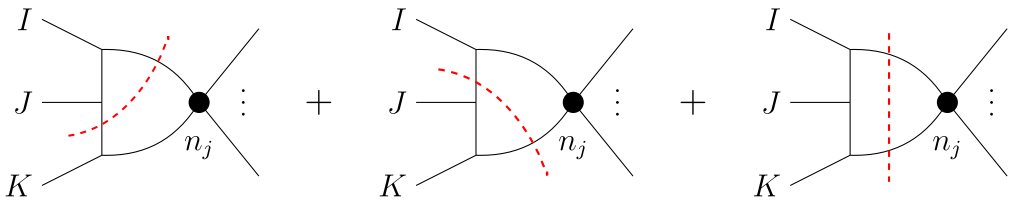

Figure C.3: *Diagram of the possible 2-cuts of the box integral* I_4^{IJK}.

where the ϵ poles cancel. With this combination of triangles and boxes, the total loop amplitude becomes

$$\mathcal{A}^{1-\text{loop}} = \sum_a C_2^{(a)} I_2^{(a)} - \frac{1}{16\pi^2} \sum_c C_4^{(c)} F_4^{(c)} \ , \tag{C.10}$$

which remarkably includes finite contributions from boxes. In order to prove Eq. (3.16), we need to check that these terms do not contribute to the sum over 2-cuts.

The 2-cut of the amplitude can be computed with the Cutkosky rule, as mentioned in Section 3.2.1. We replace the loop propagators ℓ^{-2} and $(\ell - P)^{-2}$ with the delta functions $\delta^+(\ell^2)$ and $\delta^+(\ell^2 - P)$. We choose our normalization so the 2-cut of the I_2 master integral is

$$\text{Cut}_2[I_2^{(a)}] = -\frac{1}{8\pi^2} \ . \tag{C.11}$$

The sum over all possible 2-cuts of the 1-loop amplitude is

$$\sum_{\text{2-cuts}} \text{Cut}_2[\mathcal{A}^{\text{1-loop}}] = \gamma_i \mathcal{A}_{\mathcal{O}_i} - \frac{1}{16\pi^2} \sum_c C_4^{(c)} \sum_{\text{2-cuts}} \text{Cut}_2[F_4^{(c)}] \ , \tag{C.12}$$

where we have used Eq. (3.12) to relate γ_i to the bubble coefficients.

Now we must check that the second term in Eq. (C.12) vanishes. Considering diagram (d) of Figure C.2, there are three possible nonzero 2-cuts of the box integral (see Figure C.3). Applying the Cutkosky rule to the combination in Eq. (C.9), we find

$$\text{Cut}_2^{(IJ)}[F_4^{(IJK)}] = \tfrac{4}{s_{IJ}s_{JK}} \ln\left(\tfrac{s_{IJK}-s_{IJ}}{s_{JK}}\right) \ , \tag{C.13}$$

$$\text{Cut}_2^{(JK)}[F_4^{(IJK)}] = \tfrac{4}{s_{IJ}s_{JK}} \ln\left(\tfrac{s_{IJK}-s_{JK}}{s_{IJ}}\right) \ , \tag{C.14}$$

$$\text{Cut}_2^{(IJK)}[F_4^{(IJK)}] = \tfrac{4}{s_{IJ}s_{JK}} \ln\left(\tfrac{s_{IJ}s_{JK}}{(s_{IJK}-s_{JK})(s_{IJK}-s_{IJ})}\right) \ . \tag{C.15}$$

Now it is easy to see that all three cuts add up to zero, so we have proven Eq. (3.16) for mixings with $\Delta n = 1$. We remark that the individual cuts in Eqs. (C.13)–(C.15) need not be zero. We may find logarithms of the momenta in the different cuts, but they must cancel in the total sum. Note as well that Eq. (C.15) vanishes for $n_i = 4$, since $s_{IJK} = 0$. In that case we only have to consider two 2-cuts.

As a final remark, we refer back to Section 4.4 in the main text, where we calculate the anomalous dimension for the $\Delta n = 1$ renormalization $W^3 \to WHle$. There, we find logarithms in the individual 2-cuts which add up to zero. It is interesting to explore an alternative computation of the logarithm coefficients through a 4-cut. We devote the following section to that.

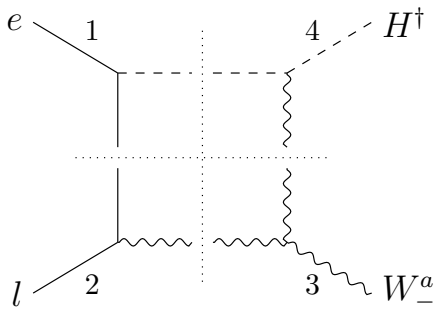

Figure C.4: *4-cut of the 1-loop amplitude for the mixing* $W^3 \to WHle$.

Box contributions from quadruple cuts

The 1-loop amplitude for a $\Delta n = 1$ mixing gets contributions from box integrals, as can be seen in Eq. (C.10). 2-cuts of $\mathcal{A}^{\text{1-loop}}$ include logarithms of the momenta, accompanied by some coefficient C_4. Here we show how the box coefficient can also be computed directly from the 4-cut of the integral. For concreteness, we focus on the renormalization $W^3 \to WHle$, which was covered in Section 4.4. In this case there are two individual 2-cuts, both of which give rise to logarithms, as is shown in Eq. (4.37).

From [74], the box coefficient can be obtained from a 4-cut of the 1-loop integral (see Figure C.4). The C_4 can then be related to a product of 3-point tree-level amplitudes,

$$C_4 = \frac{1}{2}\mathcal{A}_1(p_1, \ell_{41}^+, -\ell_{12}^-)\mathcal{A}_2(p_2, \ell_{12}^-, -\ell_{23}^+)\mathcal{A}_3(p_3, \ell_{23}^+, -\ell_{34}^-)\mathcal{A}_4(p_4, \ell_{34}^-, -\ell_{41}^+) + (- \leftrightarrow +) \ , \quad \text{(C.16)}$$

with $\ell_{ij}^\pm$ the momentum going from vertex i to vertex j. The two terms in this expression correspond to the different possible helicities of the cut particles. For this reason, the two $\ell_{ij}^\pm$ are related by complex-conjugation: $\ell_{ij}^- = (\ell_{ij}^+)^*$. Following [129], the internal momenta can be written as

$$\ell_{12}^+ = \frac{\langle 23\rangle}{\langle 31\rangle}|2]\langle 1| \ , \quad \ell_{12}^- = \frac{[23]}{[31]}|1]\langle 2| \ , \quad \text{(C.17)}$$

and the other $\ell_{ij}^\pm$ are obtained from cyclic permutations of (1234). These momenta satisfy the on-shell condition $(\ell_{ij}^\pm)^2 = 0$ and momentum conservation in the 3-point subamplitudes in Eq. (C.16).

In the case of the 1-loop mixing $\mathcal{A}_{W^3} \to \mathcal{A}_{WHle}$, the only possible 4-cut is shown in Figure C.4. The 3-point amplitudes in Eq. (C.16) are given by

$$\begin{aligned} \mathcal{A}_1 &= iy_e \langle 1\ell_{12}\rangle \ , & \mathcal{A}_3 &= \frac{iC_{W^3}}{\Lambda^2}\langle \ell_{23}3\rangle \langle 3\ell_{34}\rangle \langle \ell_{34}\ell_{23}\rangle f^{abc} \ , \\ \mathcal{A}_2 &= g_2 \frac{[\ell_{12}\ell_{23}]^2}{[\ell_{12}^2]}(T^b)_{kj} \ , & \mathcal{A}_4 &= g_2 \frac{[4\ell_{34}]\,[\ell_{41}\ell_{34}]}{[\ell_{41}4]}(T^c)_{ik} \ , \end{aligned} \quad \text{(C.18)}$$

where we have used Eqs. (2.4, 2.2, 2.3) for the SM amplitudes, and Eq. (2.28) for the $1/\Lambda^2$ amplitude. The product of the four amplitudes can be written as

$$\mathcal{A}_1\mathcal{A}_2\mathcal{A}_3\mathcal{A}_4 = i\frac{g_2^2 y_e C_{W^3}}{\Lambda^2} s_{12}\langle 23\rangle\langle 12\rangle[2|\ell_{23}|3\rangle(T^a)_{ij} \ . \quad \text{(C.19)}$$

Substituting in Eq. (C.16), we find

$$C_4 = -\frac{g_2^2 y_e C_{W^3}}{2\Lambda^2}(T^a)_{ij}\langle 31\rangle\langle 32\rangle\frac{s_{12}^2 s_{23}}{s_{13}} = -\frac{g_2^2 y_e C_{W^3}}{2}\frac{s_{12}^2 s_{23}}{s_{13}}\mathcal{A}_{WHle}\ . \tag{C.20}$$

Now let us consider the 2-cut (a) in Figure 4.6. Using our notation for this appendix, it corresponds to $\text{Cut}_2^{(12)}[F_4^{(123)}]$. Then we can write

$$\text{Cut}^{(12)}[\mathcal{A}^{\text{1-loop}}] = -\frac{C_2^{(12)}}{8\pi^2} - \frac{C_4}{4\pi^2 s_{12}s_{23}}\ln\left(\frac{-s_{12}}{s_{23}}\right)\ . \tag{C.21}$$

Substituting the value of C_4 from Eq. (C.20), we find that the coefficient in front of the logarithm is $\frac{g_2^2 y_e}{8\pi^2}\frac{s_{12}}{s_{24}}$. As we wanted to prove, this agrees with Eq. (4.37).

Appendix D

Anomalous dimensions for LFV observables

In this appendix we present the anomalous dimensions for the Wilson coefficients that enter the LFV observables $\mu \to e\gamma$, $\mu \to eee$ and $\mu N \to eN$ at tree level. We are only interested in the leading order operator mixings up to two loops, which are necessary to obtain bounds on the energy scale of new physics (see Chapter 5).

D.1 One loop

The complete 1-loop anomalous dimension matrix for dimension-six operators in the SMEFT was computed a while ago (see refs. [19–21]). In recent years, it has been revisited with on-shell methods in [28, 29] and in particular [1] that we cover in Chapter 4.

$\mu \to e\gamma$

At tree level, only the combination $C_{DW} - C_{DB}$ enters into $\mu \to e\gamma$. It mixes at one loop with the orthogonal combination of dipole coefficients $C_{DW} + C_{DB}$. Taking into account that

$$\frac{d}{d\ln\mu} C_{DW} = \frac{1}{16\pi^2}\left[\left(g^2\left(-\frac{11}{12}+\frac{1}{4}t_{\theta_W}^2\right)+N_c y_t^2\right)C_{DW} - \frac{1}{2}g^2 t_{\theta_W} C_{DB}\right] , \tag{D.1}$$

$$\frac{d}{d\ln\mu} C_{DB} = \frac{1}{16\pi^2}\left[-\frac{3}{2}g^2 t_{\theta_W} C_{DW} + \left(g^2\left(-\frac{9}{4}+\frac{151}{12}t_{\theta_W}^2\right)+N_c y_t^2\right)C_{DB}\right] , \tag{D.2}$$

the anomalous dimension is

$$\frac{d}{d\ln\mu}(C_{DW} - C_{DB}) = \frac{g^2}{16\pi^2}\left[\frac{2}{3}+\frac{1}{2}t_{\theta_W} - \frac{37}{6}t_{\theta_W}^2\right](C_{DW} + C_{DB}) . \tag{D.3}$$

Additionally, the dipole coefficients are renormalized by the four-fermion operator $\mathcal{O}_{LuQe}$. The calculation for this mixing is detailed in sections 4.1 and 5.4.1, leading to

$$\frac{d}{d\ln\mu}\begin{pmatrix} C_{DB} \\ C_{DW}\end{pmatrix} = \frac{y_u N_c}{16\pi^2}\begin{pmatrix} 5/12 \\ -1/4\end{pmatrix} C_{LuQe} . \tag{D.4}$$

We must also consider the coefficients that mix with the dipoles at the two-loop level with a double log. For this, we need to know the 1-loop anomalous dimensions for $\mathcal{O}_{LuQe}$, which is

$$\begin{aligned}\frac{d}{d\ln\mu}C^{\mu eqq}_{LuQe} =& -\frac{g^2}{16\pi^2}\left(3+5t^2_{\theta_W}\right)C^{\mu eqq}_{LeQu} \\ &+\frac{4y_u}{16\pi^2}\left(C^{\mu euu}_{RR}+\frac{y_e}{y_\mu}C^{\mu eqq}_{LL}-3\frac{y_e}{y_\mu}C^{\mu eqq}_{LL3}+\frac{y_e}{y_\mu}C^{\mu euu}_{LR}+C^{\mu eqq}_{RL}\right)\,,\end{aligned} \tag{D.5}$$

$$\begin{aligned}\frac{d}{d\ln\mu}C^{e\mu qq}_{LuQe} =& -\frac{g^2}{16\pi^2}\left(3+5t^2_{\theta_W}\right)C^{e\mu qq}_{LeQu} \\ &+\frac{4y_u}{16\pi^2}\left(\frac{y_e}{y_\mu}C^{e\mu uu}_{RR}+C^{e\mu qq}_{LL}-3C^{e\mu qq}_{LL3}+C^{e\mu uu}_{LR}+\frac{y_e}{y_\mu}C^{e\mu qq}_{RL}\right)\,,\end{aligned} \tag{D.6}$$

Notice that the terms proportional to a Yukawa coupling correspond to the exception to the helicity selection rule $\Delta n \geq |\Delta h|$, which allows the mixing $\bar{\psi}^2\psi^2 \to \psi^4$.

$\mu \to eee$

Aside from the dipoles, we have to consider the anomalous dimension matrix for $\mathcal{O}^{\mu e}_{L,L3,R}$ and $\mathcal{O}^{\mu eee}_{LL,RR,LR,RL}$. From Eq. (5.20), we see that $C_{L,L3}$ only appear in the combination $C_L + C_{L3}$. Defining

$$C_{L\pm} = C_L \pm C_{L3}\,, \tag{D.7}$$

we are interested in the mixing of C_{L-} into C_{L+}. We have

$$\frac{d}{d\ln\mu}C^{\mu e}_{L} = \frac{g^2}{16\pi^2}\frac{4}{3}t^2_{\theta_W}Y^2_H C^{\mu e}_L\,, \qquad \frac{d}{d\ln\mu}C^{\mu e}_{L3} = -\frac{g^2}{16\pi^2}\frac{17}{3}C^{\mu e}_{L3}\,, \tag{D.8}$$

which leads to

$$\frac{d}{d\ln\mu}C_{L+} = \frac{g^2}{16\pi^2}\left[\frac{17}{6}+\frac{2}{3}t^2_{\theta_W}Y^2_H\right]C_{L-}\,. \tag{D.9}$$

Regarding the four-fermion operators, their 1-loop mixings are given by

$$\begin{aligned}\frac{d}{d\ln\mu}C^{\mu eee}_{LL} =& \frac{g^2}{16\pi^2}\left\{\frac{4}{3}Y_{L_L}t^2_{\theta_W}\left[N_c\left(2Y_{Q_L}C^{\mu eqq}_{LL}+Y_{u_R}C^{\mu euu}_{LR}+Y_{d_R}C^{\mu edd}_{LR}\right)+Y_H C^{\mu e}_L\right]\right. \\ &\left.+\frac{2N_c C^{\mu eqq}_{LL3}}{3}+\frac{C^{\mu e}_{L3}}{3}\right\}\,, \\ \frac{d}{d\ln\mu}C^{\mu eee}_{RR} =& \frac{g^2}{16\pi^2}\frac{4}{3}Y_{e_R}t^2_{\theta_W}\left[N_c\left(2Y_{Q_L}C^{\mu eqq}_{RL}+Y_{u_R}C^{\mu euu}_{RR}+Y_{d_R}C^{\mu edd}_{RR}\right)\right]\,, \\ \frac{d}{d\ln\mu}C^{\mu eee}_{LR} =& \frac{g^2}{16\pi^2}\frac{4}{3}Y_{e_R}t^2_{\theta_W}\left[N_c\left(2Y_{Q_L}C^{\mu eqq}_{LL}+Y_{u_R}C^{\mu euu}_{LR}+Y_{d_R}C^{\mu edd}_{LR}\right)+Y_H C^{\mu e}_L\right]\,, \\ \frac{d}{d\ln\mu}C^{\mu eee}_{RL} =& \frac{g^2}{16\pi^2}\frac{4}{3}Y_{L_L}t^2_{\theta_W}\left[N_c\left(2Y_{Q_L}C^{\mu eqq}_{RL}+Y_{u_R}C^{\mu euu}_{RR}+Y_{d_R}C^{\mu edd}_{RR}\right)\right]\,,\end{aligned} \tag{D.10}$$

where q, u, d belong to the 2nd and 3rd family. For the 1st family, the coefficients are already constrained at tree level by $\mu N \to eN$. In order to go from $C_{L,L3}$ to $C_{L+,L-}$ we use the projection $C_L \to C_{L-}/2$ and $C_{L3} \to -C_{L-}/2$. The mixing with four-fermion coefficients $C^{\mu e\tau\tau}_{LL,LL3,RR,LR,RL}$ instead of $C^{\mu eqq}_{LL,LL3,RR,LR,RL}$ is obtained by replacing $q, d \to \tau$, $N_c \to 1$, $Y_{Q_L} \to Y_{L_L}$, $Y_{d_R} \to Y_{e_R}$ and $Y_{u_R} \to 0$.

$\mu N \to eN$

The anomalous dimension for the four-fermion coefficients $C^{\mu euu}_{LL,RR,LR,RL}$ is obtained by replacing $Y_{L_L} \to Y_{Q_L}$ and $Y_{e_R} \to Y_{u_R}$ in Eq. (D.10). Similarly, for the mixings with $C^{\mu edd}_{LL,RR,LR,RL}$ we must replace $Y_{L_L} \to Y_{Q_L}$ and $Y_{e_R} \to Y_{d_R}$ in that same equation.

D.2 Two loops

In our analysis, we also consider the contribution of LFV operators of classes $\psi^2 H^3$, $\psi^2\bar{\psi}^2$ and $\psi\bar{\psi}H^2$ to the 2-loop anomalous dimension of the dipoles. The 2-loop mixing $C_y \to C_{DW,DB}$ was computed in [28, 84] and is equal to

$$\frac{d}{d\ln\mu}\begin{pmatrix} C_{eB} \\ C_{eW}\end{pmatrix} = \frac{g^3}{(16\pi^2)^2}\cdot\frac{3}{4}\begin{pmatrix} t_W Y_H + 4t_W^3 Y_H^2(Y_L+Y_e) \\ \frac{1}{2} + \frac{2}{3}t_W^2 Y_H(Y_L+Y_e)\end{pmatrix} C_{y_e}\ . \tag{D.11}$$

The mixings $C^{\mu\ell\ell e}_{LR} \to C_{DW,DB}$ and $C^{\mu qqe}_{LR} \to C_{DW,DB}$ were computed in [84], leading to

$$\frac{d}{d\ln\mu}\begin{pmatrix} C_{eB} \\ C_{eW}\end{pmatrix} = \frac{y_d g^3}{(16\pi^2)^2}\frac{N_c}{4}\begin{pmatrix} 3t_W Y_Q + 4t_W^3(Y_L+Y_e)(Y_Q^2+Y_d^2) \\ \frac{1}{2} + 2t_W^2(Y_L+Y_e)Y_Q\end{pmatrix} C_{le\bar{d}q}\ , \tag{D.12}$$

$$\frac{d}{d\ln\mu}\begin{pmatrix} C_{eB} \\ C_{eW}\end{pmatrix} = \frac{y_e g^3}{(16\pi^2)^2}\cdot\frac{1}{4}\begin{pmatrix} 3t_W Y_L + 4t_W^3(Y_L+Y_e)(Y_L^2+Y_e^2) \\ \frac{1}{2} + 2t_W^2(Y_L+Y_e)Y_L\end{pmatrix} C_{le\bar{e}\nu}\ . \tag{D.13}$$

Finally, we have computed the mixing $C_{L,L3,R} \to C_{DW,DB}$ in Section 5.4.2 (see the original paper [3]). The anomalous dimensions at orders y_t^2 and λ^4 are summarized in Eq. (5.56), Eq. (5.57), Eq. (5.71) and Eq. (5.72).

Appendix E

Partial-wave decomposition of amplitudes

In this Appendix we obtain the general formula for the partial-wave decomposition of 4-point amplitudes, following the derivation in [116]. We start considering the scattering process $1,2 \to 3,4$ in the center-of-momentum frame. The direction of the incoming particles 1,2 is defined by the polar angles (ψ, ω), while the direction of the outgoing pair 3,4 is defined by (θ, ϕ). The corresponding scattering amplitude can be written as

$$\begin{aligned}\mathcal{A}(s,\theta,\phi;\psi,\omega) &\equiv \langle \theta\phi; h_3h_4|\mathcal{T}|\psi\omega; h_1h_2\rangle \\ &= \sum_{JJ'MM'} \langle \theta\phi; h_3h_4|J'M'; h_3h_4\rangle \, \langle J'M'; h_3h_4|\mathcal{T}|JM; h_1h_2\rangle \, \langle JM; h_1h_2|\psi\omega; h_1h_2\rangle \ , \end{aligned} \tag{E.1}$$

where $\mathcal{T}$ is related to the S-matrix by $S = 1 + i\mathcal{T}$. We have inserted two complete sets of states, which satisfy $\mathbb{I} = \sum_{J,M} |JM\rangle\langle JM|$ by the completeness of the angular momentum basis. The matrix element is given by

$$\langle J'M'; h_3h_4|\mathcal{T}|JM; h_1h_2\rangle = \delta_{MM'} \ \delta_{JJ'} \left(\frac{\sqrt{s}}{\Lambda}\right)^w a^J \ , \tag{E.2}$$

where a^J is a partial-wave coefficient with angular momentum J. Using this definition, Eq. (E.1) becomes

$$\mathcal{A}(s,\theta,\phi;\psi,\omega) = \left(\frac{\sqrt{s}}{\Lambda}\right)^w \sum_{JM} n_J \ e^{i\phi(M-h_{34})} d^J_{Mh_{34}}(\theta) \ e^{-i\omega(M-h_{12})} d^J_{Mh_{12}}(\psi) \ a^J \ , \tag{E.3}$$

where $n_J = 2J+1$ and $d^J_{Mh}(\theta)$ are the Wigner d-functions, defined as

$$d^J_{Mh_{12}}(\theta) = \frac{e^{i\phi(M-h_{12})}}{\sqrt{n_J}} \langle JM; h_1h_2|\theta\phi; h_1h_2\rangle \ . \tag{E.4}$$

Alternatively, we can write

$$d^J_{MM'}(\theta) = \Big[(J+M)!\,(J-M)!\,(J+M')!\,(J-M')!\Big]^{1/2} \times \sum_S \left[\frac{(-1)^{M'-M+S}\, c_{\theta/2}^{\,2J+M-M'-2S}\, s_{\theta/2}^{\,M'-M+2S}}{(J+M-S)!\,S!\,(M'-M+S)!\,(J-M'-S)!}\right] , \tag{E.5}$$

where the summation includes all values of S that make the factorial arguments non-negative. The Wigner d-functions are orthogonal, satisfying the condition

$$\int_0^\pi d\theta\ s_\theta\ d^J_{MM'}(\theta) d^{J'}_{MM'}(\theta) = \frac{2\delta_{JJ'}}{n_J}\ . \tag{E.6}$$

Finally, we observe that Eq. (E.3) gets simplified by choosing a frame such that $\psi = \omega = 0$, leading to

$$\mathcal{A}(s,\theta,\phi) = e^{i\phi(h_{12}-h_{34})} \left(\frac{\sqrt{s}}{\Lambda}\right)^w \sum_J n_J\ d^J_{h_{12}h_{34}}(\theta)\ a^J\ , \tag{E.7}$$

where we have used that $d^J_{MM'}(0) = \delta_{MM'}$.

Bibliography

[1] P. Baratella, C. Fernandez, and A. Pomarol, Nucl. Phys. B **959**, 115155 (2020), arXiv: 2005.07129.

[2] P. Baratella, C. Fernandez, B. von Harling, and A. Pomarol, JHEP **03**, 287 (2021), arXiv: 2010.13809.

[3] J. Elias Miro, C. Fernandez, M. A. Gumus, and A. Pomarol, JHEP **06**, 126 (2022), arXiv: 2112.12131.

[4] S. Weinberg, *The Quantum theory of fields. Vol. 1: Foundations* (Cambridge University Press, 2005), ISBN 978-0-521-67053-1, 978-0-511-25204-4.

[5] M. L. Mangano and S. J. Parke, Phys. Rept. **200**, 301 (1991), arXiv: hep-th/0509223.

[6] N. Arkani-Hamed and J. Trnka, Journal of High Energy Physics **2014**, 30 (2014).

[7] M. F. Paulos, B. C. van Rees, P. Vieira, and A. Zhiboedov, Nuclear Physics B **902**, 246 (2017).

[8] P. Benincasa and F. Cachazo (2007), arXiv: 0705.4305.

[9] S. J. Parke and T. R. Taylor, Phys. Rev. Lett. **56**, 2459 (1986).

[10] R. Britto, F. Cachazo, B. Feng, and E. Witten, Phys. Rev. Lett. **94**, 181602 (2005), arXiv: hep-th/0501052.

[11] Z. Bern, L. J. Dixon, D. C. Dunbar, and D. A. Kosower, Nucl. Phys. B **425**, 217 (1994), arXiv: hep-ph/9403226.

[12] Z. Bern, L. J. Dixon, D. C. Dunbar, and D. A. Kosower, Nucl. Phys. B **435**, 59 (1995), arXiv: hep-ph/9409265.

[13] L. J. Dixon, in *Theoretical Advanced Study Institute in Elementary Particle Physics: Particle Physics: The Higgs Boson and Beyond* (2014), pp. 31–67, arXiv: 1310.5353.

[14] H. Elvang and Y.-t. Huang (2013), arXiv: 1308.1697.

[15] J. M. Henn and J. C. Plefka, *Scattering Amplitudes in Gauge Theories*, vol. 883 (Springer, Berlin, 2014), ISBN 978-3-642-54021-9.

[16] J. J. M. Carrasco, in *Theoretical Advanced Study Institute in Elementary Particle Physics: Journeys Through the Precision Frontier: Amplitudes for Colliders* (WSP, 2015), pp. 477–557, arXiv: 1506.00974.

[17] S. Navas et al. (Particle Data Group), Phys. Rev. D **110**, 030001 (2024).

[18] W. Buchmuller and D. Wyler, Nucl. Phys. B **268**, 621 (1986).

[19] E. E. Jenkins, A. V. Manohar, and M. Trott, JHEP **10**, 087 (2013), arXiv: 1308.2627.

[20] E. E. Jenkins, A. V. Manohar, and M. Trott, JHEP **01**, 035 (2014), arXiv: 1310.4838.

[21] R. Alonso, E. E. Jenkins, A. V. Manohar, and M. Trott, JHEP **04**, 159 (2014), arXiv: 1312.2014.

[22] C. Grojean, E. E. Jenkins, A. V. Manohar, and M. Trott, JHEP **04**, 016 (2013), arXiv: 1301.2588.

[23] J. Elias-Miró, J. R. Espinosa, E. Masso, and A. Pomarol, JHEP **08**, 033 (2013), arXiv: 1302.5661.

[24] J. Elias-Miro, J. R. Espinosa, E. Masso, and A. Pomarol, JHEP **11**, 066 (2013), arXiv: 1308.1879.

[25] J. Elias-Miró, C. Grojean, R. S. Gupta, and D. Marzocca, JHEP **05**, 019 (2014), arXiv: 1312.2928.

[26] S. Caron-Huot and M. Wilhelm, JHEP **12**, 010 (2016), arXiv: 1607.06448.

[27] Z. Bern, J. Parra-Martinez, and E. Sawyer, Phys. Rev. Lett. **124**, 051601 (2020), arXiv: 1910.05831.

[28] J. Elias Miró, J. Ingoldby, and M. Riembau, JHEP **09**, 163 (2020), arXiv: 2005.06983.

[29] M. Jiang, T. Ma, and J. Shu, JHEP **01**, 101 (2021), arXiv: 2005.10261.

[30] Z. Bern, J. Parra-Martinez, and E. Sawyer, JHEP **10**, 211 (2020), arXiv: 2005.12917.

[31] P. Baratella, D. Haslehner, M. Ruhdorfer, J. Serra, and A. Weiler, JHEP **03**, 156 (2022), arXiv: 2109.06191.

[32] M. Accettulli Huber and S. De Angelis, JHEP **11**, 221 (2021), arXiv: 2108.03669.

[33] C. Cheung, *TASI Lectures on Scattering Amplitudes* (2018), pp. 571–623, arXiv: 1708.03872.

[34] C. Cheung, *Clifford cheung lecture 2 on scattering amplitudes and symmetry*, https://www.youtube.com/watch?v=OJNrq5Qiclw (2023), accessed 21/09/23.

[35] N. Arkani-Hamed, L. Rodina, and J. Trnka, Phys. Rev. Lett. **120**, 231602 (2018), arXiv: 1612.02797.

[36] J. C. Ward, Phys. Rev. **78**, 182 (1950).

[37] Y. Takahashi, Nuovo Cim. **6**, 371 (1957).

[38] W. H. Furry, Phys. Rev. **51**, 125 (1937).

[39] D. Lovelock, J. Math. Phys. **12**, 498 (1971).

[40] Z. Bern, J. J. Carrasco, M. Chiodaroli, H. Johansson, and R. Roiban, J. Phys. A **57**, 333002 (2024), arXiv: 1909.01358.

[41] E. P. Wigner, Annals Math. **40**, 149 (1939).

[42] N. Arkani-Hamed, T.-C. Huang, and Y.-t. Huang, JHEP **11**, 070 (2021), arXiv: 1709.04891.

[43] A. Mardones and J. Zanelli, Class. Quant. Grav. **8**, 1545 (1991).

[44] R. Britto, F. Cachazo, and B. Feng, Nucl. Phys. B **715**, 499 (2005), arXiv: hep-th/0412308.

[45] S. D. Badger, E. W. N. Glover, V. V. Khoze, and P. Svrcek, JHEP **07**, 025 (2005), arXiv: hep-th/0504159.

[46] F. Cachazo and P. Svrcek (2005), arXiv: hep-th/0502160.

[47] A. Brandhuber, P. Heslop, and G. Travaglini, Phys. Rev. D **78**, 125005 (2008), arXiv: 0807.4097.

[48] T. Cohen, H. Elvang, and M. Kiermaier, JHEP **04**, 053 (2011), arXiv: 1010.0257.

[49] C. Cheung, C.-H. Shen, and J. Trnka, JHEP **06**, 118 (2015), arXiv: 1502.05057.

[50] K. Risager, JHEP **12**, 003 (2005), arXiv: hep-th/0508206.

[51] N. Arkani-Hamed and J. Kaplan, JHEP **04**, 076 (2008), arXiv: 0801.2385.

[52] C. Cheung and C.-H. Shen, Phys. Rev. Lett. **115**, 071601 (2015), arXiv: 1505.01844.

[53] C. Itzykson and J. B. Zuber, *Quantum Field Theory*, International Series In Pure and Applied Physics (McGraw-Hill, New York, 1980), ISBN 978-0-486-44568-7.

[54] N. Christensen and B. Field, Phys. Rev. D **98**, 016014 (2018), arXiv: 1802.00448.

[55] Y. Shadmi and Y. Weiss, JHEP **02**, 165 (2019), arXiv: 1809.09644.

[56] T. Ma, J. Shu, and M.-L. Xiao, Chin. Phys. C **47**, 023105 (2023), arXiv: 1902.06752.

[57] N. Christensen, B. Field, A. Moore, and S. Pinto, Phys. Rev. D **101**, 065019 (2020), arXiv: 1909.09164.

[58] B. Bachu and A. Yelleshpur, JHEP **08**, 039 (2020), arXiv: 1912.04334.

[59] R. Aoude and C. S. Machado, JHEP **12**, 058 (2019), arXiv: 1905.11433.

[60] G. Durieux, T. Kitahara, Y. Shadmi, and Y. Weiss, JHEP **01**, 119 (2020), arXiv: 1909.10551.

[61] G. Durieux and C. S. Machado, Phys. Rev. D **101**, 095021 (2020), arXiv: 1912.08827.

[62] G. Durieux, T. Kitahara, C. S. Machado, Y. Shadmi, and Y. Weiss, JHEP **12**, 175 (2020), arXiv: 2008.09652.

[63] H.-L. Li, Z. Ren, M.-L. Xiao, J.-H. Yu, and Y.-H. Zheng, JHEP **04**, 140 (2022), arXiv: 2201.04639.

[64] S. De Angelis, JHEP **08**, 299 (2022), arXiv: 2202.02681.

[65] B. Grzadkowski, M. Iskrzynski, M. Misiak, and J. Rosiek, JHEP **10**, 085 (2010), arXiv: 1008.4884.

[66] M. E. Peskin and D. V. Schroeder, *An Introduction to quantum field theory* (Addison-Wesley, Reading, USA, 1995), ISBN 978-0-201-50397-5, 978-0-429-50355-9, 978-0-429-49417-8.

[67] G. Passarino and M. J. G. Veltman, Nucl. Phys. B **160**, 151 (1979).

[68] C. G. Callan, Jr., Phys. Rev. D **2**, 1541 (1970).

[69] K. Symanzik, Commun. Math. Phys. **18**, 227 (1970).

[70] R. E. Cutkosky, J. Math. Phys. **1**, 429 (1960).

[71] Z. Bern and A. G. Morgan, Nucl. Phys. B **467**, 479 (1996), arXiv: hep-ph/9511336.

[72] Z. Bern, L. J. Dixon, and D. A. Kosower, Ann. Rev. Nucl. Part. Sci. **46**, 109 (1996), arXiv: hep-ph/9602280.

[73] S. D. Badger, JHEP **01**, 049 (2009), arXiv: 0806.4600.

[74] N. Arkani-Hamed, F. Cachazo, and J. Kaplan, JHEP **09**, 016 (2010), arXiv: 0808.1446.

[75] P. Baratella, S. Maggio, M. Stadlbauer, and T. Theil, Eur. Phys. J. C **83**, 751 (2023), arXiv: 2207.08831.

[76] S. Catani, Phys. Lett. B **427**, 161 (1998), arXiv: hep-ph/9802439.

[77] T. Becher and M. Neubert, Phys. Rev. Lett. **102**, 162001 (2009), [Erratum: Phys.Rev.Lett. 111, 199905 (2013)], arXiv: 0901.0722.

[78] D. C. Dunbar and P. S. Norridge, Class. Quant. Grav. **14**, 351 (1997), arXiv: hep-th/9512084.

[79] R. Alonso, E. E. Jenkins, and A. V. Manohar, Phys. Lett. B **739**, 95 (2014), arXiv: 1409.0868.

[80] J. Elias-Miro, J. R. Espinosa, and A. Pomarol, Phys. Lett. B **747**, 272 (2015), arXiv: 1412.7151.

[81] M. Jiang, J. Shu, M.-L. Xiao, and Y.-H. Zheng, Phys. Rev. Lett. **126**, 011601 (2021), arXiv: 2001.04481.

[82] W. Cao, F. Herzog, T. Melia, and J. Roosmale Nepveu, JHEP **08**, 080 (2023), arXiv: 2303.07391.

[83] N. Craig, M. Jiang, Y.-Y. Li, and D. Sutherland, JHEP **08**, 086 (2020), arXiv: 2001.00017.

[84] G. Panico, A. Pomarol, and M. Riembau, JHEP **04**, 090 (2019), arXiv: 1810.09413.

[85] L. Calibbi and G. Signorelli, Riv. Nuovo Cim. **41**, 71 (2018), arXiv: 1709.00294.

[86] A. M. Baldini et al. (MEG), Eur. Phys. J. C **76**, 434 (2016), arXiv: 1605.05081.

[87] A. M. Baldini et al. (MEG II), Eur. Phys. J. C **78**, 380 (2018), arXiv: 1801.04688.

[88] U. Bellgardt et al. (SINDRUM), Nucl. Phys. B **299**, 1 (1988).

[89] A. Blondel et al. (2013), arXiv: 1301.6113.

[90] W. H. Bertl et al. (SINDRUM II), Eur. Phys. J. C **47**, 337 (2006).

[91] L. Bartoszek et al. (Mu2e) (2014), arXiv: 1501.05241.

[92] A. Baldini et al. (2018), arXiv: 1812.06540.

[93] A. Hayrapetyan et al. (CMS), Phys. Rev. D **108**, 072004 (2023), arXiv: 2305.18106.

[94] G. Aad et al. (ATLAS), Phys. Rev. D **108**, 032015 (2023), arXiv: 2204.10783.

[95] M. Ablikim et al. (BESIII), Phys. Rev. D **87**, 112007 (2013), arXiv: 1304.3205.

[96] D. Ambrose et al. (BNL), Phys. Rev. Lett. **81**, 5734 (1998), arXiv: hep-ex/9811038.

[97] R. Aaij et al. (LHCb), JHEP **03**, 078 (2018), arXiv: 1710.04111.

[98] A. Crivellin, S. Najjari, and J. Rosiek, JHEP **04**, 167 (2014), arXiv: 1312.0634.

[99] G. M. Pruna and A. Signer, JHEP **10**, 014 (2014), arXiv: 1408.3565.

[100] G. M. Pruna and A. Signer, EPJ Web Conf. **118**, 01031 (2016), arXiv: 1511.04421.

[101] S. Davidson, Eur. Phys. J. C **76**, 370 (2016), arXiv: 1601.07166.

[102] A. Crivellin, S. Davidson, G. M. Pruna, and A. Signer, JHEP **05**, 117 (2017), arXiv: 1702.03020.

[103] S. Davidson, JHEP **02**, 172 (2021), arXiv: 2010.00317.

[104] M. Ardu and S. Davidson, JHEP **08**, 002 (2021), arXiv: 2103.07212.

[105] A. Celis, V. Cirigliano, and E. Passemar, Phys. Rev. D **89**, 013008 (2014), arXiv: 1309.3564.

[106] A. Celis, V. Cirigliano, and E. Passemar, Phys. Rev. D **89**, 095014 (2014), arXiv: 1403.5781.

[107] T. Husek, K. Monsalvez-Pozo, and J. Portoles, JHEP **01**, 059 (2021), arXiv: 2009.10428.

[108] V. Cirigliano, K. Fuyuto, C. Lee, E. Mereghetti, and B. Yan, JHEP **03**, 256 (2021), arXiv: 2102.06176.

[109] Y. Kuno and Y. Okada, Rev. Mod. Phys. **73**, 151 (2001), arXiv: hep-ph/9909265.

[110] R. Kitano, M. Koike, and Y. Okada, Phys. Rev. D **66**, 096002 (2002), [Erratum: Phys.Rev.D 76, 059902 (2007)], arXiv: hep-ph/0203110.

[111] W. Dekens, E. E. Jenkins, A. V. Manohar, and P. Stoffer, JHEP **01**, 088 (2019), arXiv: 1810.05675.

[112] A. Freitas, J. Lykken, S. Kell, and S. Westhoff, JHEP **05**, 145 (2014), [Erratum: JHEP 09, 155 (2014)], arXiv: 1402.7065.

[113] O. Fischer et al., Eur. Phys. J. C **82**, 665 (2022), arXiv: 2109.06065.

[114] C. Cornella, D. A. Faroughy, J. Fuentes-Martin, G. Isidori, and M. Neubert, JHEP **08**, 050 (2021), arXiv: 2103.16558.

[115] J. Shu, M.-L. Xiao, and Y.-H. Zheng, Phys. Rev. D **107**, 095040 (2023), arXiv: 2111.08019.

[116] M. Jacob and G. C. Wick, Annals Phys. **7**, 404 (1959).

[117] M. Gell-Mann and M. Levy, Nuovo Cim. **16**, 705 (1960).

[118] S. R. Coleman, J. Wess, and B. Zumino, Phys. Rev. **177**, 2239 (1969).

[119] C. G. Callan, Jr., S. R. Coleman, J. Wess, and B. Zumino, Phys. Rev. **177**, 2247 (1969).

[120] S. L. Adler, Phys. Rev. **137**, B1022 (1965).

[121] K. Kampf, J. Novotny, and J. Trnka, JHEP **05**, 032 (2013), arXiv: 1304.3048.

[122] L. Susskind and G. Frye, Phys. Rev. D **1**, 1682 (1970).

[123] I. Low and Z. Yin, JHEP **11**, 078 (2019), arXiv: 1904.12859.

[124] L. Dai, I. Low, T. Mehen, and A. Mohapatra, Phys. Rev. D **102**, 116011 (2020), arXiv: 2009.01819.

[125] J. Bijnens, G. Colangelo, G. Ecker, J. Gasser, and M. E. Sainio, Phys. Lett. B **374**, 210 (1996), arXiv: hep-ph/9511397.

[126] Z. Bern, H.-H. Chi, L. Dixon, and A. Edison, Phys. Rev. D **95**, 046013 (2017), arXiv: 1701.02422.

[127] H. K. Dreiner, H. E. Haber, and S. P. Martin, Phys. Rept. **494**, 1 (2010), arXiv: 0812.1594.

[128] R. Britto, J. Phys. A **44**, 454006 (2011), arXiv: 1012.4493.

[129] H. Johansson, D. A. Kosower, and K. J. Larsen, PoS **LL2012**, 066 (2012), arXiv: 1212.2132.